



TECHNISCHE UNIVERSITÄT MÜNCHEN

TUM School of Medicine and Health

Investigating the role of A20 gene dose in B cell-mediated autoimmunity

Carina Diehl

Vollständiger Abdruck der von der
TUM School of Medicine and Health der Technischen Universität München
zur Erlangung einer Doktorin der Naturwissenschaften (Dr. rer. nat.)
genehmigten Dissertation.

Vorsitz: Prof. Dr. Thomas Korn

Prüfer*innen der Dissertation:

1. Prof. Dr. Marc Schmidt-Supprian
2. Prof. Dr. Matthias Feige

Die Dissertation wurde am 13.06.2023 bei der Fakultät für Medizin der
Technischen Universität München eingereicht und durch die Fakultät für Medizin
am 30.09.2023 angenommen.

ACKNOWLEDGMENTS

First, I want to thank my advisor Prof. Marc Schmidt-Supprian for trusting me with this exciting PhD project and giving me a great amount of freedom to perform my experiments. His incredible knowledge and scientific understanding were truly inspiring and his brilliant ideas guided me along the way. Most importantly, I could always count on his encouragement and moral support, when I was in need.

Particular thanks go to my thesis advisory committee members, PD Dr. med. Peer-Hendrik Kuhn and Prof. Matthias Feige for their precious inputs and encouragement, and to Prof. Thomas Korn for chairing my thesis defense.

During the course of my thesis, I had the pleasure to work together with a number of excellent scientists. I want to thank Rupert Öllinger for performing the RNA sequencing and especially Thomas Engleitner for all the hours we spent on bioinformatic data analysis, for his patience, interest and creative ideas. Furthermore, I want to thank Prof. Maciej Lech for readily performing various pathological analyses over the course of many years as well as Prof. Christoph Daniel, Prof. Katja Steiger and Prof. Martina Rudelius for the histological analysis of organ samples. It was a great pleasure to work together with Ainee Ul Ain Qurrat and Joachim Pircher on the thrombosis assay. Special thanks go to Markus Schick, who helped with injecting a considerable number of bone marrow chimera recipient mice, and to all my dear colleagues who readily supported me with the unforeseen early analysis of the same mice, while I was abroad.

I wish to express my deepest gratitude to all current and former members of the Schmidt-Supprian laboratory. The atmosphere of support and friendship made my work in the lab a pleasure every day. I am very grateful to Maiko Kober for introducing me to the field of immunology and the most crucial laboratory skills, and to Yuanyuan Chu, who mentored and supported me throughout the years. My special thanks go to Valeria Soberón, who guided me along my PhD project with her scientific advice and her friendship. Moreover, I would like to deeply thank Francisco Osorio Barrios, who gave direction to my project with his brilliant ideas and helping hands. I specifically want to thank Sabrina Bortoluzzi, who went the whole PhD journey together with me, for the great scientific and moral support. Special thanks also go to Seren Baygün for her support in the lab and her inspiring warm-heartedness, and to Laura Kraus and Vanessa Gölling for performing experiments during the time I was not in the lab. I also want to thank Tim Ammon and Sabine Helmrath, who made the lab and office a happy place.

I am deeply thankful to Julia Knogler, who performed a great number of assays and mouse analyses for me. I always valued her immense precision and reliability. Furthermore, I received great technical help in the laboratory from Barbara Habermehl, Kasia Jopek, Vera Wanat and Jasmin Schröder, and from Markus Utzt, who supported me during many FACS sorting experiments.

I greatly appreciate the support with genotyping, I received from Momina Hayat and Pankaj Singroul, who also lovingly took care of my baby boy whenever I came by for work. I am very thankful to Monika Mittermeier, who readily assisted me with mouse procedures and colony management during my maternity leave. I want to especially thank Claudia Mugler, who brought sunshine into the lab every day.

I want to thank my students Sophie Levantovsky, Anna Sichler and Eva Prötzl for their sincere interest in the project and for uncountable iGB culture experiments.

I highly appreciate the support from the members of the IMPRS-LS Coordination Office, especially Hans-Jörg Schaeffer and Ingrid Wolf, and I am grateful for all opportunities, the IMPRS Graduate School has offered me to develop my skills and personality.

This work could not have been completed without the unconditional support from my friends and family. This is to them:

Ich schulde meiner lieben Freundin Mimi tiefsten Dank, dass sie seit vielen Jahren an meiner Seite steht. Ich danke Dir, dass Du dich darum gekümmert hast, alles am Laufen zu halten, dass Du mir Essen gebracht und Dich unzählige Male um meine Kinder gekümmert hast, wenn ich es nicht konnte.

Zutiefst dankbar bin ich meinen Eltern, auf die ich mein Leben lang stets zählen konnte. Ihr habt mich in meinen Entscheidungen von Anfang an unterstützt. Ihr habt mir wahnsinnig viel von eurer Zeit geschenkt, so dass ich die Freiheit hatte, diese Doktorarbeit zu Ende zu bringen. Danke Euch, Mama und Papa!

Und danke Dir, liebe Julia, dass du immer für mich da bist.

Ich danke dir viele tausend Mal, Leo, dafür dass Du immer die richtigen Worte findest, dass Du mir Mut gemacht hast, dass Du immer an mich geglaubt hast. Danke für Deine Geduld und Deine Liebe. Ich bin unendlich dankbar für unsere beiden Sonnenscheine, Aaron und Jakob. Ihr hattet einen großen Einfluss auf diese Arbeit, dadurch dass ihr mich einerseits abgelenkt und mich gleichzeitig zur Konzentration gezwungen habt. Danke für das Lächeln und die Freude.

For my family.

Abstract

Haploinsufficiency of A20, a negative regulator of pro-inflammatory NF- κ B signaling, is strongly implicated in various human autoimmune and autoinflammatory disorders. B cells are potent drivers of these pathologies. Still, in mice, the homo- and heterozygous deficiency of A20 in B cells induced only mild autoimmune manifestations. The development of systemic autoimmunity requires the breakdown of a number of checkpoint mechanisms, which can be achieved by the inheritance or acquisition of several disease-predisposing genetic alterations. Next to haploinsufficiency of A20, also enhanced B cell survival can be involved in the initiation of autoimmunity.

Through combination of the haploinsufficiency of A20 with an overexpression of anti-apoptotic BclxL in B cells (B-BclxL^{tg}-A20^{-wt}), I was able to induce the development of a lethal systemic autoimmune disease in mice. The pathology faithfully recapitulated many features of human Systemic Lupus Erythematosus (SLE), including renal immune complex deposition and the development of a secondary antiphospholipid syndrome. The B cell-driven pathology depended on TLR signaling via MyD88 and on the germinal center reaction, which enabled the generation of autoantibodies directed among others against nuclear components. Intriguingly, mice with a full knockout of A20 in their B cells (B-BclxL^{tg}-A20^{-/-}) consistently lacked lethal autoimmunity, despite an enhanced hyperreactivity of BclxL^{tg} A20^{-/-} B cells *in vitro*. Competitive bone marrow chimera experiments indicated the existence of protective mechanisms counteracting the pathological expansion of BclxL^{tg} A20^{-/-} B cells. I was able to identify a T cell checkpoint, which induces the elimination of hyperreactive B cells. In the absence of T cell immune surveillance through CD3 ϵ -knockout, pathogenic BclxL^{tg} B cells malignantly expanded and induced the premature death of mice in direct correlation to the A20 gene dose in their B cells. In the presence of T cells, strongly hyperreactive BclxL^{tg} A20^{-/-} B cells were counter-selected, while less hyperreactive BclxL^{tg} A20^{-wt} B cells were spared, which enabled the development of lethal autoimmunity.

Zusammenfassung

Die Haploinsuffizienz von A20, einem negativen Regulator des pro-inflammatorischen NF- κ B-Signalwegs, tritt häufig in Patienten verschiedener Autoimmun- und autoinflammatorischer Erkrankungen auf. B-Zellen agieren als treibende Kraft hinter diesen Pathologien. In Mausmodellen jedoch induzierte der homo- und heterozygote Verlust von A20 in B-Zellen nur eine sehr schwach ausgeprägte Autoimmunität. Die Entwicklung systemischer Autoimmunkrankheiten erfordert das Versagen einer Reihe von Checkpoint-Mechanismen. Genetische Prädispositionen, welche als Risikofaktoren zur Entwicklung von Autoimmunität beitragen, können erblich bedingt sein oder durch somatische Mutationen im Verlauf des Lebens akkumulieren. Neben der Haploinsuffizienz von A20, ist auch ein erhöhtes Überleben von B-Zellen ein solcher Risikofaktor.

Im Rahmen dieser Doktorarbeit konnte ich durch die Kombination der Haploinsuffizienz von A20 mit einer Überexpression des anti-apoptotischen Proteins BclxL in B-Zellen (B-BclxL^{tg}-A20^{/wt}) die Entwicklung einer tödlichen systemischen Autoimmunerkrankung in Mäusen auslösen. Die Pathologie beinhaltete viele Merkmale der menschlichen Erkrankung Systemischer Lupus Erythematodes (SLE), einschließlich der Ablagerung von Immunkomplexen in den Nieren und der Entwicklung eines sekundären Antiphospholipid-Syndroms. Die von den B-Zellen ausgelöste Pathologie war abhängig von Toll-like-Rezeptor-Signalen (TLR) über das Adapterprotein MyD88 und von der Keimzentrumsreaktion, welche die Bildung von Autoantikörpern ermöglichte, die unter anderem gegen Zellkernkomponenten gerichtet waren. Interessanterweise zeigten jene Mäuse mit einem vollständigen Knockout von A20 in ihren B-Zellen (B-BclxL^{tg}-A20^{-/-}) keine tödliche Autoimmunität, obwohl die intrinsische Hyperreaktivität von BclxL^{tg} A20^{-/-} B-Zellen *in vitro* stark erhöht war. Experimente mit gemischten Knochenmarkschimären wiesen auf die Existenz von Schutzmechanismen hin, welche der pathologischen Expansion von BclxL^{tg} A20^{-/-} *in vivo* B-Zellen entgegenwirken. Ich konnte zeigen, dass T-Zellen eine zentrale Rolle in der Eliminierung hyperreaktiver B-Zellen spielen. In Abwesenheit einer T-Zell-Immunüberwachung, durch den Knockout von CD3 ϵ , expandierten pathogene B-Zellen und verursachten den vorzeitigen Tod von Mäusen in direkter Korrelation mit der A20-Gen dosis in ihren B-Zellen. In Anwesenheit von T-Zellen wurde die Expansion stark hyperreaktiver BclxL^{tg} A20^{-/-} B-Zellen verhindert, während weniger hyperreaktive BclxL^{tg} A20^{/wt} B-Zellen verschont blieben. Dies ermöglichte die Entwicklung der tödlichen Autoimmunpathologie.

Table of Contents

ACKNOWLEDGMENTS.....	I-III
ABSTRACT	IV
ZUSAMMENFASSUNG.....	V
1 INTRODUCTION	1
1.1 Adaptive immunity	1
1.1.1 Generation of high affinity antibodies	1
1.1.1.1 Early B cell development in the bone marrow.....	1
1.1.1.2 Terminal B cell development in the periphery	2
1.1.1.3 The germinal center reaction	4
1.1.1.4 Plasma cell differentiation.....	6
1.1.1.5 B cells as professional antigen-presenting cells	7
1.1.2 Negative selection of autoreactive B cells	8
1.1.3 Natural (auto-)antibodies	9
1.1.4 Relevant aspects of T cell biology	10
1.1.4.1 T cell development and TCR tolerance mechanisms.....	10
1.1.4.2 T cell subsets	10
1.1.4.2.1 Helper T cells.....	11
1.1.4.2.2 Regulatory T cells.....	11
1.1.4.2.3 Cytotoxic T cells.....	12
1.1.4.2.4 T cell exhaustion	13
1.2 Signaling in B cells - a matter of life and death.....	13
1.2.1 Cell death	13
1.2.1.1 Programmed cell death: Apoptosis.....	14
1.2.1.1.1 Intrinsic apoptosis pathway	14
1.2.1.1.2 Fas-mediated apoptosis	14
1.2.1.2 Activation-induced cell death	15
1.2.1.3 Uncontrolled cell death: Oncosis and necrosis	15
1.2.2 Pro-survival signaling by NF- κ B	16
1.2.2.1 B cell receptor signaling.....	17
1.2.2.2 CD40 signaling.....	17
1.2.2.3 Toll like receptor signaling	17
1.2.2.4 BAFF receptors: BAFFR and TACI.....	18
1.2.2.5 Bimodal signal transduction downstream of the TNF receptor	19
1.2.3 The balance of life and death in germinal centers	19
1.3 B cell mediated pathologies.....	20
1.3.1 B cell lymphoma	20
1.3.1.1 Aspects of NF- κ B activation during B cell lymphomagenesis	20
1.3.1.2 T cell immune surveillance of B cell lymphoma	21
1.3.2 Autoimmune diseases	21
1.3.2.1 Organ specific and systemic autoimmune diseases	21
1.3.2.2 Systemic lupus erythematosus (SLE)	22
1.3.2.2.1 SLE pathology	22
1.3.2.2.2 Genetic predisposition of SLE patients.....	24
1.3.2.2.3 SLE mouse models	24
1.3.3 Connection of autoimmunity and B cell lymphomagenesis	25

1.4	Negative regulation of NF- κ B signaling by A20	26
1.4.1	Structure and function of A20	26
1.4.2	A20 knockout and mutation studies	28
1.4.3	A20-deficiency in humans	29
1.5	B cell-specific A20-deficiency.....	31
2	AIM OF THE THESIS.....	32
3	MATERIALS AND METHODS.....	33
3.1	Genetically modified mice	33
3.2	Buffers and media.....	36
3.3	Mouse analysis	37
3.3.1	Preparation of serum	37
3.3.2	Preparation of citrate plasma	37
3.3.3	Organ harvesting and weighing	37
3.3.4	Organ fixation for histology and immunofluorescence	37
3.3.5	Preparation of single cell suspensions	37
3.4	Flow cytometry.....	38
3.4.1	Staining antibodies	38
3.4.2	Staining procedure	40
3.4.3	Sample acquisition and data analysis	41
3.4.4	LEGENDplex assay for the assessment of the serum cytokine concentration	42
3.5	Serum and plasma analyses.....	42
3.5.1	Isotype ELISA	42
3.5.2	Autoantibody ELISA	42
3.5.3	D-Dimer ELISA	43
3.6	Urine analyses	43
3.6.1	Total protein content in urine	43
3.6.2	Albuminuria	43
3.6.3	Blood urea nitrogen (BUN)	44
3.7	Histopathological organ analyses	44
3.7.1	Periodic Acid Schiff staining (PAS)	44
3.7.2	Sirius Red staining	44
3.7.3	IgG immunostainings on kidney sections	45
3.7.4	Kidney immune cell infiltration	45
3.7.5	B cell infiltrations in the salivary glands	45
3.7.6	Histology in lymphoma samples	45
3.8	Sequencing analyses	46
3.8.1	Bulk RNA sequencing	46
3.8.2	Assessment of somatic hypermutation	47
3.8.3	Immunoglobulin heavy- and light-chain amplification for clonality assessment	48
3.9	In vivo analyses.....	48
3.9.1	In vivo T cell depletion	48
3.9.2	In vivo TNF depletion	48
3.9.3	Competitive bone marrow chimeras	49
3.9.4	FeCl ₃ -induced thrombus formation in the Carotis artery	49

3.10	In vitro analyses.....	50
3.10.1	In vitro-derived germinal center B cells (iGB) culture	50
3.10.2	Ex vivo cytokine stimulation	51
3.10.3	TNF stimulation in vitro	51
3.11	Statistical analysis.....	52
4	RESULTS	53
4.1	Analysis of B-BclxL ^{tg} A20-deficient mice.....	53
4.1.1	Enhanced BclxL ^{tg} expression does not protect GCB-like cells from Fas-induced cell death	53
4.1.2	B cell subsets in B-BclxL ^{tg} A20-deficient mice	55
4.1.2.1	Heterozygous loss of A20 cooperates with BclxL ^{tg} expression to drive a strong expansion of GCB cells	59
4.1.2.2	A20-deficiency strongly affects plasmacytic cells in the spleen.....	63
4.1.2.3	Class switching of A20-deficient B cells in vitro	65
4.1.2.4	B cell differentiation in the gut associated lymphoid tissues	66
4.1.2.5	Long lived plasma cells in the bone marrow	68
4.1.3	Antibody production varies greatly between mice with heterozygous and homozygous loss of A20 in B cells	69
4.1.4	B cell activation	70
4.1.5	T cell subsets in B-BclxL transgenic A20-deficient mice	72
4.1.5.1	BclxL ^{tg} A20 ^{-/wt} B cells induce an expansion of most CD4 T cell subsets	73
4.1.5.2	T cell activation	75
4.1.5.3	Effector memory T cell expansion	77
4.1.5.4	T cell exhaustion phenotype	78
4.1.6	Myeloid cells in the spleen	79
4.2	Pathology of B-BclxL ^{tg} -A20 ^{-/wt} mice.....	82
4.2.1	B-BclxL ^{tg} -A20 ^{-/wt} mice develop a lethal autoimmune pathology.....	82
4.2.2	B cell autoreactivity in B-BclxL ^{tg} -A20 ^{-/wt} mice induces a systemic inflammation.....	84
4.2.2.1	Serum cytokine concentration	85
4.2.2.2	Cytokine producing cells	90
4.2.3	Kidney pathology	92
4.2.3.1	Immune complex deposition	92
4.2.3.2	Immune cell infiltration.....	93
4.2.3.3	Glomerular filtration rate.....	96
4.2.4	Heart and liver pathology	97
4.2.5	Thymic B cells and salivary gland infiltration	98
4.2.6	Thrombosis risk	99
4.2.6.1	Development of an antiphospholipid syndrome (APS).....	99
4.2.6.2	Artificial vessel damage assay.....	100
4.3	Mechanisms of the B cell-driven autoimmune pathology in B-BclxL ^{tg} A20 ^{-/wt} mice	102
4.3.1	The B cell-driven autoimmune pathology depends on the signaling via MyD88	102
4.3.2	The role of the germinal center for autoimmune pathology	108
4.3.2.1	Loss of A20 specifically in GCB cells (Cγ1Cre/AIDCre model).....	108
4.3.2.2	The autoimmune pathology depends on the generation of class-switched high-affinity autoantibodies through affinity maturation of autoreactive B cells within the germinal center.....	110

4.4	Homozygous A20 ablation induces contradictory effects in vivo and in vitro	115
4.4.1	Transcriptomics data reveals a high metabolic signature in A20 ^{-/-} B cells	115
4.4.2	Proliferation in the iGB culture	119
4.4.3	BCR stimulation and signaling strength	122
4.4.4	Sensitivity towards TNF-induced apoptosis	124
4.4.4.1	In vivo TNF depletion	124
4.4.4.2	In vitro TNF stimulation	125
4.4.5	Competitive bone marrow transfer reveals a systemic effect counteracting the expansion of BclxL ^{tg} A20 ^{-/-} B cells in vivo	127
4.5	T cell immune surveillance.....	132
4.5.1	In vivo T cell activation	132
4.5.2	Investigating the effects of T cell depletion	133
4.5.2.1	CD8 ⁺ T cell depletion.....	133
4.5.2.2	Depletion of all T cell subsets.....	134
4.5.3	T cell knockout in A20-deficient mice	137
4.5.3.1	BclxL ^{tg} A20 ^{-/-} plasmacytic cells expand in the absence of T cells.....	137
4.5.3.2	The development of autoimmunity in B-BclxL ^{tg} -A20 ^{-/wt} mice is T cell dependent.....	138
4.5.3.3	T cell deficiency allows the lymphoproliferative expansion of A20-deficient B cells	140
4.5.3.4	A20 knockout induces an aberrant surface marker expression on BclxL ^{tg} B cells.....	142
4.5.3.5	Initial characterization of the lymphoproliferative expansions	145
5	DISCUSSION.....	146
5.1	B-BclxL ^{tg} -A20 ^{-/wt} mice as a model for human SLE	147
5.1.1	Similarities between B-BclxL ^{tg} -A20 ^{-/wt} mice and other SLE mouse models	147
5.1.2	The stochastic nature of autoimmunity	149
5.1.3	Why are BclxL ^{tg} A20 ^{-/wt} B cells such potent inducers of systemic autoimmunity?	150
5.1.4	The clinical relevance of heterozygous A20-deficiency	151
5.2	The A20-knockout paradox.....	152
5.2.1	A20 ^{-/-} B cells trigger T cell immune surveillance	153
5.2.2	Initiation of the T cell immune surveillance depends on the extent of B cell hyperactivation	154
5.2.3	Malignant expansion of A20-deficient B cells requires their escape from T cell cytotoxicity	155
	SUPPLEMENTARY FIGURES	157
	SUPPLEMENTARY TABLES	162
	REFERENCES.....	169
	LIST OF FIGURES.....	190
	LIST OF TABLES.....	191

1 Introduction

1.1 Adaptive immunity

Mammals are equipped with an innate immunity comprised of a variety of immune cells with different functions to clear invading pathogens by means of cytotoxicity and phagocytosis, aided by opsonization with antibodies. Patrolling cells capture and present antigen via MHC molecules to inform and alert other, responsive immune cell types. Depending on the pathogen, the effect of the innate immune response may vary.

Adaptive immunity harbors the tremendous benefit of altering the immune cell specificity towards the pathogen to generate the most effective immune reaction. An optimized response is generated depending on the environmental requirements through the development of highly specific antibodies. Furthermore, due to the development of memory B and T cells, the acquired competence for fighting specific pathogens is maintained over a long time and an effective immune reaction can be rapidly initiated again upon repeated appearance of the same antigen.

1.1.1 Generation of high affinity antibodies

One major benefit of adaptive immunity is the generation of antibodies, which can bind to pathogenic antigens with high affinity. This flags pathogens for destruction through complement activation and promotes their phagocytosis and elimination by immune effector cells. Antibodies are secreted by plasma cells, which differentiate from B cells in dependence of extrinsic stimuli. The major steps of B cell maturation towards plasma cells will be summarized in the following chapter.

1.1.1.1 Early B cell development in the bone marrow

Adaptive immunity requires the differentiation of specialized B as well as T cell subsets and the generation of a highly diverse B cell receptor (BCR) and T cell receptor (TCR) repertoire.

In B cells, a large number of BCR specificities is generated during early development in the bone marrow (BM) through a mechanism termed V(D)J recombination, which governs the assembly of immunoglobulin heavy and light chains (Figure 1). Recombined light- and heavy-chain bind to form the final immunoglobulin, which is expressed as membrane bound IgM (μ -heavy chain) isotype on the surface of the immature B cell (1-3).

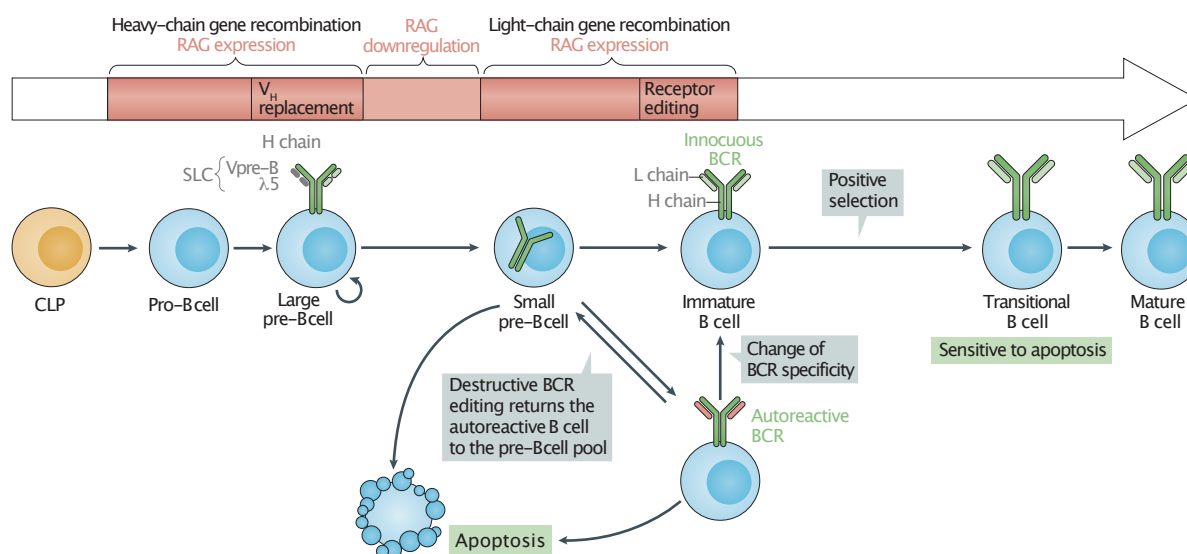


Figure 1. Early B cell development and central tolerance in the bone marrow.

Adapted from Nemazee et al. 2017 (1). Pro-B cells, which are derived from common lymphoid progenitor cells (CLP) initiate heavy chain gene rearrangement through expression of recombination-activating genes (RAG). Productive heavy chain-assembly leads to the association with a surrogate light chain (SLC). Antigen-independent triggering of the pre-BCR promotes progression to large pre-B cells, which downregulate RAG expression and proliferate transiently. At the small pre-B cell stage SLC components are downregulated, RAG is re-expressed directed to the light chain genes. Pairing of heavy on light chain triggers tonic BCR signaling, which promotes positive selection when the BCR is non-autoreactive (innocuous) or receptor editing when the BCR is autoreactive. Positively selected cells enter the transitional B cell stage and are highly sensitive to apoptosis. Persistent failure to generate a functional innocuous BCR induces the deletion of the cell by apoptosis (1).

The IgM forms a complex with the transmembrane proteins Igα and Igβ, thereby producing the functional BCR. Cytoplasmic immunoreceptor tyrosine-based activation motifs (ITAMs) on Igα and Igβ are sites for phosphorylation, which are needed to initiate the intracellular BCR signal transduction (1-3). Upon expression of a successfully rearranged heavy-chain–light-chain complex, the BCR transmits weak tonic signals which drive positive selection of the cell through termination of BCR editing. In case of inefficient expression or pairing of the heavy- and light-chain, tonic BCR signaling is absent and continued light-chain rearrangement persists. In case the BCR recognizes self-antigens, different control mechanisms are applied to remove autoreactivity (1). These will be discussed in detail in chapter 1.1.2.

1.1.1.2 Terminal B cell development in the periphery

B cells, which have acquired a functional non-autoreactive BCR in the BM, can egress to the periphery. Expression of CD62L drives the homing to secondary lymphoid organs like the spleen, lymph nodes (LN) or gut and mucosa associated lymphoid tissues (GALT and MALT) (4). In the transitional stage, the immature B cell starts to co-express the BCR isotype IgD (5). In the periphery, the B cell depends on BCR signaling and signals through the B cell activating factor (BAFF) to sustain survival (1). Depending on the signals the cell encounters, it proceeds to different maturation pathways.

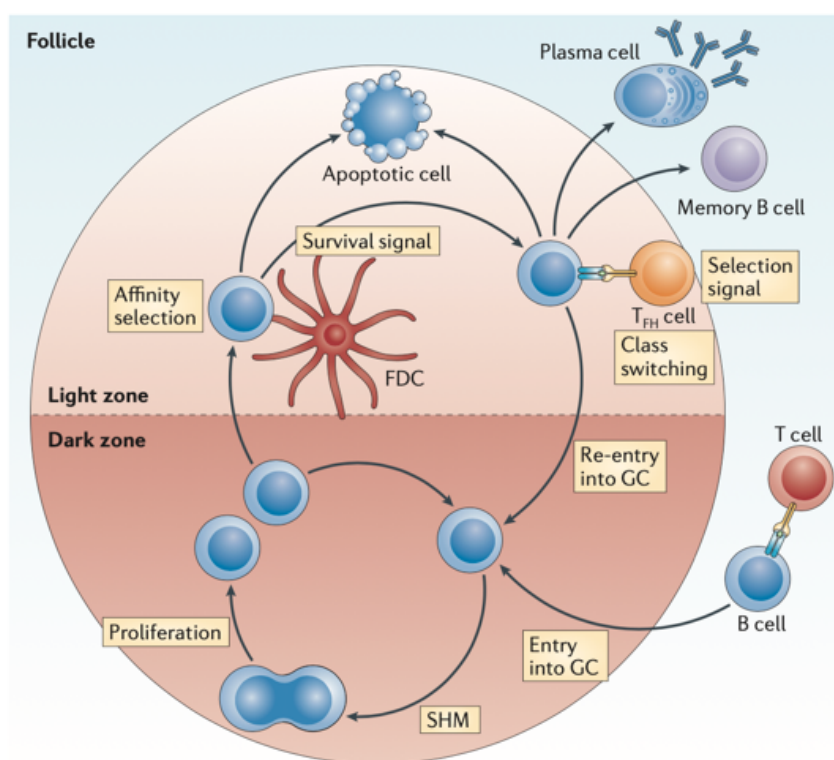
The majority of B cells are of the B2 lineage (CD19⁺ B220⁺) and are generated from transitional B cells, which egress from the BM after successful BCR rearrangement. A distinct subset, however, B1 cells (CD19⁺ B220^{lo}) are independently derived from fetal precursors and sustained through self-renewal. B1 cells are innate-like B cells, which mainly reside in the peritoneal and pleural cavity. They exert T cell independent (TI) immune responses, protecting against mucosal pathogens through recognition of pathogen associated molecular patterns (PAMPs) and danger associated molecular patterns (DAMPs) (6). There are two B1 subclasses, defined by their cell surface CD5 expression: B1a (CD5⁺) cells migrate from the peritoneal cavities toward the spleen where they eventually secrete IgM recognizing restricted microbial regions, while B1b (CD5⁻) can develop into IgA secreting plasma cells at mucosal sites, including the gut, to target commensal bacteria (6, 7). B1 cells can produce natural IgM or IgA antibodies, which are polyreactive low affinity antibodies, generated prior to antigen exposure (7, 8) (see chapter 1.1.3).

Upon migration from the BM to secondary lymphoid organs, B2 lineage cells differentiate into either follicular B (FolB) cells or marginal zone B (MZB) cell precursors, which further develop into mature MZB cells. Both, MZB and FolB cells, are resident in the secondary lymphoid organs but largely differ in their precise localization and function. While FolB cells are localized in the follicles of the spleen and lymph nodes, MZB cells reside in the marginal zone, an area between white pulp and the vascularized red pulp of the spleen (9). MZB cell differentiation depends on BCR signals through low-affinity antigen binding as well as BAFF-BAFFR (BAFF receptor)-induced signal transduction events (9). Furthermore, MZB differentiation is driven through Notch2 activation by the DL1 ligand, expressed on red pulp endothelial cells, which additionally induces migration to and retention of MZB cells in the marginal zone (10). Constitutive Notch2 signaling was shown to be sufficient to induce MZB differentiation cells as well as cross-differentiation of FolB to MZB cells (11, 12). Due to their high self-renewal capacity, MZB cells have a long life-span and an innate-like function: Once activated by blood-borne pathogens MZB cells rapidly respond mainly in a TI fashion and generate short-lived plasmablasts, which produce low-affinity IgM antibodies capturing pathogens and apoptotic debris (9).

In contrast to the rapid generation of low affinity antigens by B1 and MZB cells, FolB cells have the unique capability to generate plasma cells secreting antibodies with very high antigen affinity through T cell dependent (TD) immune responses. In germinal centers, cognate B and T cells cooperate to improve the BCR affinity towards antigen in a procedure called “affinity maturation”. This procedure is slow but results in the generation of plasma cells secreting high-affinity antibodies after approximately 14 days (13).

1.1.1.3 The germinal center reaction

Within secondary lymphoid organs CXCR5 expression on FolB cells recruits them into follicles through chemotaxis towards CXCL13. CCR7 expression maintains T cells in the surrounding T cell zones, where stroma cells produce the chemokines CCL19 and 21. FolB cells get activated upon binding to cognate antigen, either in soluble form or presented by follicular dendritic cells (FDCs). This induces the internalization of the BCR-antigen complex, antigen processing and loading onto a major histocompatibility complex class II (MHCII) molecule for cell surface presentation. Simultaneously, the B cell enhances CCR7 expression and thereby migrates to the T cell zone. There the antigen peptide-MHCII complex can be recognized by cognate CD4⁺ helper T (Th) cells, leading to the formation of an immunological synapse (see chapter 1.1.1.5). Co-stimulatory signals lead to full activation of both the B as well as the interacting T cell. At this point, activated B cells



can either rapidly differentiate extra-follicularly to antibody secreting plasmablasts or commit to a germinal center fate through upregulation of the master transcription factor B cell lymphoma 6 (BCL6) (14-18).

Figure 2. The germinal center reaction.

Simplified schematic of affinity maturation in the germinal center, taken from Heesters et al. 2014 (19). At the T cell–B cell border, B cells present antigen to T cells and receive co-stimulation. The selected

cells enter the dark zone of the germinal center and undergo somatic hyper-mutation (SHM). After one cycle or more cycles of proliferation and SHM, the GCB cells migrate to the light zone, where their mutated BCRs are exposed to antigens on follicular dendritic cells (FDCs). GCB cells with very low affinity will not receive survival signals and undergo apoptosis. The remaining GCB cells compete for limited T cell help, which leads to apoptosis of low-affinity clones. Surviving GCB cells can then re-enter the dark zone and undergo further proliferation and SHM or exit the germinal center as plasma cells or memory B cells.

Germinal center B (GCB) cells express high levels of the death receptor Fas and (in mice) downregulate CD38 expression. Additionally, the majority of GCB cells bind to GL-7 antibody, recognizing n-glycolylneuraminic acid, while IgD expression is lost on GCB cells (16, 20). Germinal centers contain three main players, GCB cells, follicular helper T (T_{fh}) cells, which provide co-stimulatory signals to GCB cells, and follicular dendritic cells (FDCs), which serve as antigen presenting cells providing the substrate for affinity-dependent selection (17).

Mature germinal centers are structurally divided into a dark zone (DZ), almost exclusively composed of heavily proliferating GCB cells, named centroblasts (CXCR4^{hi} CXCR5^{low} CD83/CD86^{low}), and a light zone (LZ) consisting of GCB cells named centrocytes (CXCR4^{low} CXCR5^{hi} CD83/CD86^{hi}), as well as T_{fh} cells and FDCs (19). GCB cells get activated and primed through antigen binding to their BCR (21). Upon subsequent antigen-MHCII-complex presentation, GCB cells bind to cognate T_{fh} cells and consequently receive activating stimuli through, amongst others, CD40/CD40L and ICOSL/ICOS interactions (16). Additionally, activation of T_{fh} cells induces them to release interleukin (IL)-4 and IL-21, promoting GCB cell proliferation and maintenance as well as plasmacytic differentiation (22). Sufficient signaling from BCR and T_{fh} co-stimulation allows positive selection of GCB cells (17). Positively selected GCB cells transiently express high levels of c-Myc, initiating their entry to the DZ (23), where they heavily proliferate and actively mutate their BCR sequence in a mechanism called somatic hypermutation (SHM).

SHM is initiated by expression of the mutator enzyme activation-induced cytidine deaminase (AID), which deaminates cytidine residues in the variable regions of immunoglobulin genes, thereby creating U:G mismatches. Subsequent mismatch repair with error-prone DNA polymerases results in C/G-to-T/A transition and other mutations around the AID target sequence. Through AID activity the mutation rate in GCB cells is approximately 10⁶-fold the normal rate of somatic mutation. The more or less random nature of SHM generates an immense sequence diversity, equipping each GCB cell with either improved or decreased antigen affinity or leading to loss of BCR expression (17).

AID is also active in switch regions upstream of the immunoglobulin (Ig) constant loci, where its action ultimately induces double-strand DNA breaks to trigger class-switch recombination (CSR). Thereby, DNA break repair through nonhomologous end joining recombines the switch region upstream of C_μ with target switch regions C_γ3, C_γ1, C_γ2b, C_γ2a, C_ε or C_α, leading to isotype switching of the expressed BCR from IgM to IgG3, IgG2b, IgG2a/c, IgE or IgA, respectively. Which target switch region recombines, depends on additional extrinsic stimuli and the resulting isotype defines the antibody effector function (24).

After completing proliferation and SHM in the DZ, GCB cells migrate back to the LZ to test the antigen affinity of their mutated BCR. Depending on the acquired BCR affinity GCB cells are subsequently either eliminated or positively selected for cyclic re-entry to the germinal center reaction (16, 17, 25). The activation intensity transmitted through T-B entanglement increases in correlation to BCR affinity and thereby determines the number of divisions a GCB cell will undergo upon re-entry to the DZ. Repeated cycling of GCB cells between DZ and LZ ensures effective affinity maturation (17, 25, 26). The germinal center is a highly competitive environment. Due to the limited availability of T cell co-stimulation and pro-survival cytokines the default fate of GCB cells is apoptosis, which is only counteracted in those clones with the highest antigen affinity (27). The affinity selection pressure is further enhanced through limited antigen presentation by FDCs and by the presence of competing antibodies secreted from germinal center-experienced plasma cells (19, 28).

1.1.1.4 Plasma cell differentiation

The final goal of GCB cell maturation is the generation of plasma cells, which can secrete soluble antibodies with very high affinity to efficiently bind and thereby neutralize pathogens and drive their clearance through complement activation or interaction with immune cells (29).

T cell-dependent plasma cell differentiation

Depending on their affinity, B cells can exit the germinal center as memory B cells or differentiate towards antibody-producing plasma cells. It seems that the plasmacytic fate is favored when the affinity for antigen is high (17). To allow exit from the germinal center, expression of the GCB cell master transcription factor BCL6 needs to be terminated. This abrogates BCL6-mediated repression of Blimp1, the master regulator of plasma cell differentiation. The exact triggers initiating plasmacytic differentiation of GCB cells are not yet resolved, but likely involve the strong ligation of CD40 and BCR signaling, with differences depending on the immunoglobulin class (17). The resulting NF- κ B dependent expression of the transcription factor IRF4 represses BCL6, thereby allowing expression of Blimp1. Subsequently, highly proliferative CD138⁺ plasmablasts exit the germinal center from the DZ, migrate first to the T-B border, proliferate in extrafollicular foci, and finally exit the secondary lymphoid organs as circulating plasmablasts. As the cells continue to differentiate into mature plasma cells (PC), they lose their proliferative and migratory capacity. To achieve long term survival, plasma cells depend on the availability of survival factors, which can be provided in survival niches. Due to CXCR4 expression, most germinal center-derived PC are recruited into the BM, rich in the chemoattractant CXCL12. In BM niches they receive survival signals from stromal cells enabling their long-term persistence as terminally differentiated non-dividing long-lived PC (llPC). The majority of llPCs in the BM are germinal center-derived (13, 30-33).

While the generation of plasma cells from germinal centers takes several days, an immediate generation of antibody can be achieved by extrafollicular PC differentiation, which is driven by interactions of B cells with helper T (Th) cells located in extrafollicular areas. CD40-CD40L and ICOS-ICOSL signaling as well as cytokines, such as IL-21, drive the CSR and initiation of differentiation towards Blimp1⁺, CD138⁺, CXCR4⁺ proliferative plasmablasts. Their proliferation is driven by BCR signaling, in correlation to their antigen affinity. Compared to germinal center-derived plasmablasts, the antigen affinity of extrafollicular plasmablasts is lower as they do not undergo affinity maturation. Extrafollicular plasmablasts are short-lived and only rarely differentiate to llPCs (33).

T cell-independent plasma cell differentiation

Two types of antigen can activate B cells in a T cell-independent (TI) manner, meaning that plasma cell differentiation does not require cognate T cell help. TI-1 antigens are microbial structure activating Toll-like receptors (TLR), while TI-2 antigens are polymeric proteins or contain repeated structural motifs to induce extensive BCR crosslinking. CSR can occur independent of T cell interaction, driven by TLR and TACI signaling or cytokines including BAFF, IFN γ and IL-21 (33). The innate-like B1 and MZB cell subsets generally produce short-lived IgM and/or IgA plasma cells through TI responses.

1.1.1.5 B cells as professional antigen-presenting cells

All nucleated cells express major histocompatibility complex I (MHCI), on which they present antigen in case of intracellular infection with for example viruses to activate cytotoxic CD8⁺ T cells and thereby initiate their own elimination. In contrast, MHCII expression is limited to professional antigen-presenting cells, mainly DCs and B cells. In B cells, antigen binding mediates endocytosis of the antigen through BCR internalization. Subsequently, the antigen is being processed, loaded onto MHCII molecules and presented on the B cell surface to stimulate helper T cells (34). Upon T cell recognition of the antigen-MHCII complex, an immunological synapse is formed in which the T and B cells activate each other through a multitude of co-stimulatory receptors:

CD80 and CD86 on B cells bind to CD28 or CTLA-4 on T cells to drive or dampen the immune response, respectively (35). Helper T cells in turn provide co-stimulation to B cells through expression of CD40 ligand (CD40L), activating CD40 (36). The CD40-CD40L interaction is crucial for B cell survival, activation and proliferation (34). In addition, several other co-stimulatory receptors become expressed on T cells after T cell activation, including ICOS, OX40 and 4-1BB. Their respective ligands, ICOSL, OX40L and 4-1BBL, are presented by activated B cells. ICOS signaling in B cells promotes the germinal center-dependent generation of antibody-secreting plasma cells. OX40L engagement promotes B cell activation, proliferation, survival and cytokine production (34). 4-1BB ligation drives T cell survival, cytokine secretion and effector function (37). Furthermore, activated B cells express adhesion molecules including ICAM-1, which enhances the stability of the synapse resulting in an amplification of the activation signals (38). In addition to cell-cell interactions, also cytokines including IL-4, IL-13, IL-21 and TGF β , promote the antigen-presenting cell (APC) function of B cells by upregulating their MHCII expression (34).

1.1.2 Negative selection of autoreactive B cells

The great variation of possible BCR sequences imposes the risk for an autoreactive specificity. However, central tolerance mechanisms counteract the development of autoreactive B cells and their egress to the periphery. During V(D)J rearrangement of the BCR, the immature B cell is still located in the BM and consequently all antigens present in the microenvironment are self-antigens. Ligation of BCR with self-antigens leads to strong intracellular signaling, distinct from the tonic signaling downstream of an unligated BCR. Strong BCR signaling leads to a rapid internalization of the autoreactive BCR to halt B cell maturation and one of two regulatory processes is induced to eliminate the autoreactive cell: (i) continued receptor editing or (ii) clonal deletion (see **Figure 1**).

- (i) BCR engagement by recognition of self-antigen drives the activation of BCR-associated kinases and nuclear translocation of FOXO1, which induces the continued expression of RAG proteins. This allows ongoing light chain rearrangement to change the specificity of the previously autoreactive B cell.
- (ii) If autoreactivity persists, the B cell will eventually be deleted through apoptosis, as the persistent strong BCR signaling entails FOXO1- and E2A-dependent expression of the pro-apoptotic protein BIM (1, 39).

When a functional non-autoreactive heavy-chain:light-chain BCR has been successfully generated, tonic BCR signaling inhibits FOXO1. This terminates V(D)J recombination and decreases BIM expression, thereby promoting cell survival. The positively selected B cell is allowed to mature and migrate to the secondary lymphoid organs (1).

Early transitional T1 B cells remain sensitive to BCR-mediated apoptosis via BIM. B cell survival depends on signaling from the survival cytokine BAFF and signaling from an autoreactive BCR dampens the expression of the BAFF receptor (BAFFR) and of homing receptors including CD62L. Consequently, the capacity to migrate towards secondary lymphoid organs is reduced in B cells with self-reactivity. Accordingly, elevated BAFF levels as well as expression of anti-apoptotic BclxL were shown to enhance the survival of low affinity autoreactive transitional B cells in mice (1, 39, 40).

Central tolerance is imperfect and in humans, 15 % - 20 % of mature B cells in the periphery are still autoreactive (41). Therefore, also peripheral tolerance mechanisms are necessary to inhibit the expansion of escaped autoreactive B cells through (iii) initiation of anergy, (iv) follicular exclusion, (v) reduced plasmacytic differentiation and (vi) repression by T_{reg} cells.

- (iii) In anergic autoreactive B cells, chronic ligand engagement induces BCR internalization and alternative BCR downstream signaling, leading to reduced responsiveness towards BAFF, increased pro-apoptotic activity as well as reduced expression of chemokine and adhesion molecules, thereby limiting T-B interactions. This process produces anergic cells with a short lifespan, due to which they are quickly outcompeted by non-autoreactive B cells, and thereby deleted over time (1, 41-43).

- (iv) Recognition of self-antigen can lead to follicular exclusion of autoreactive B cells, which prohibits their participation in the germinal center reaction. This is, among other mechanisms, due to T cell neglect: autoreactive B cells, which present autoantigen on their MHCII, are unable to initiate T cell help and consequently succumb to apoptosis (as long as T cell tolerance is intact). Under specific circumstances ignorant autoreactive B cells may still be recruited into the germinal center when being triggered by cross-reactive foreign antigen. Additionally, GCB cells can acquire autoreactivity *de novo* through SHM. The mechanisms counter-selecting autoreactive B cells in the germinal center are not fully resolved. Possibly, exposure to very high concentration of ubiquitous self-antigen initiates apoptosis by activation-induced cell death (AICD). Additionally, autoreactive GCB cells have a competitive disadvantage compared to foreign reactive GCB cells. Self-antigens, presented by autoreactive GCB cells, are not sufficient to initiate T_{fh} cell help, which either entails their death by neglect or drives the selection of somatic mutations, which increase the affinity for foreign instead of self-antigen (17, 18, 43-48).
- (v) Chronic BCR engagement by self-antigen induces activation of Erk, which prevents the expression of Blimp1, thereby blocking autoreactive plasma cell differentiation to prohibit autoantibody production (49, 50).
- (vi) As an additional mode of negative selection, naïve autoreactive B cells can be repressed by regulatory T cells (T_{reg}) upon MHCII-restricted self-antigen presentation. Foxp3 deficiency enables autoreactive T and B cell clones to bypass growth-limiting checkpoints in mice and in humans induces a neonatal autoimmune syndrome (43, 51-54).

When autoreactive B cells are not efficiently counter-selected by central and peripheral tolerance mechanisms, there is a risk for the development of autoimmune diseases.

1.1.3 Natural (auto-)antibodies

While the development of a high affinity antibody response is rather slow, an additional, innate-like type of antibodies can be found in individuals prior to antigenic experience, immediately protecting them as a first line of defense upon pathogen encounter. These so-called natural antibodies (NAb) are oligospecific immunoglobulins with low affinity, mainly binding to phylogenetically conserved epitopes, which are expressed from germline encoded heavy- and light-chain variable regions. NAb predominantly originate from B1 and MZB cells and can be of the IgM, IgG and IgA isotypes. It is not known, however, whether they are secreted independent of antigenic BCR activation or require classical B cell activation and maturation steps. Interestingly, a substantial part of NAb can react with autoantigens and are therefore termed natural autoantibodies (NAAb). Damaged or necrotic cells can exhibit autoantigens to adaptive immune cells, which drives the development of autoimmunity. Binding of these self-antigens by NAAbs decreases their exposure and facilitates antigen-mediated removal of dead cells by phagocytosis. Thereby, NAAbs have an anti-inflammatory activity and can mitigate the development of autoimmune diseases (7)

1.1.4 Relevant aspects of T cell biology

The next chapter describes the most relevant T cell developmental steps and mature T cell subsets as well as their function with respect to this thesis.

1.1.4.1 T cell development and TCR tolerance mechanisms

Similar to B cells, T cells express a unique antigen receptor, the T cell receptor (TCR). There are two types of TCR, the less frequent variant, composed of the γ and δ subunits ($\gamma\delta$ T cells), and the most common variant composed of the α and β subunits ($\alpha\beta$ T cells). The $\alpha\beta$ TCR is associated with a CD4 or CD8 co-receptor, needed for binding to the antigen-MHC-complex presented by APCs, and with a complex of CD3 transmembrane proteins, which transduces the signal intracellularly. Early T cell development takes place in the thymus, where CD8⁺/CD4⁺ double positive thymocytes undergo TCR rearrangement and subsequently commit to either the CD4 or CD8 lineage. Depending on their affinity towards autoantigens the T cells are positively or negatively selected. To achieve this, autoantigens are presented by medullary thymic epithelial cells (mTECs), which have the unique ability to express tissue specific antigens through activity of the transcriptional modulator autoimmune regulator (AIRE). Positive T cell selection in the thymus requires MHC recognition but a lack of strong TCR stimulation, allowing the differentiation into conventional mature T cells. In contrast, very strong TCR activation induces negative selection by clonal deletion, while intermediately strong TCR stimulation by autoantigens causes an upregulation of Foxp3 in CD4⁺ T cells, driving the differentiation of regulatory T cells (36, 55, 56).

After thymic development, conventional CD4⁺ and CD8⁺ T cells egress to the periphery as naïve pluripotent cells and home to the secondary lymphoid tissues due to their surface expression of CD62L. There they remain quiescent until encountering their cognate antigen (57).

1.1.4.2 T cell subsets

Conventional $\alpha\beta$ T cells are categorized upon their expression of the glycoproteins CD4 or CD8. CD4 T cells are MHCII restricted and mainly provide help to other immune cells while CD8 T cells are MHCI restricted cytotoxic T cells, which kill their target cells.

Naïve CD8 T cells are activated through recognition of MHCI-antigen-complexes and differentiate stepwise to stem cell memory, central memory, effector memory and finally effector T cells, thereby reducing their memory and proliferative capacity, while increasing effector functions (58).

During activation of naïve CD4 T cells, different microenvironmental signals from pathogens and cytokines induce specific lineage-determining transcription factors, driving the differentiation of different subsets: T helper (Th)1, Th2, Th9, Th17, Th22, follicular

helper T cells (T_{h}), peripheral regulatory T cells (T_{reg}) or follicular regulatory T cells (T_{fr}). These subsets are characterized by different cytokine profiles, rendering them with either pro- or anti-inflammatory functions (57, 58). Once a naïve CD4 T cell recognizes antigen presented on MHCII by APCs, it becomes activated, proliferates and differentiates into an effector cell (CD62L⁻), migrating to the site of infection to eliminate the pathogen. While effector cells are short-lived, a subset of memory T cells (CD44⁺) is formed, with the potential for long-term survival. Memory T cells can be located in the secondary lymphoid organs as central memory (CM) or in recently infected tissues as effector memory (EM) T cells. Antigen re-encounter initiates fast activation and expansion of memory T cells (58).

Non-conventional $\gamma\delta$ T cells have the ability to secrete cytokines for a quick, innate-like response to tissue insult (57).

1.1.4.2.1 Helper T cells

Activation of CD4 helper T cells is initiated by TCR binding to peptide-MHCII complexes and further enhanced through stimulation of the co-stimulatory receptor CD28 by CD80 or CD86 presented on APCs. Subsequent secretion of IL-2 drives proliferation and effector differentiation of the T cell in an autocrine manner. The two main subclasses of effector helper T cells are Th1 and Th2. While Th1 cells produce IFN γ and TNF, which activate macrophages and cytotoxic T cells, and stimulate B cells to secrete IgG2a/c antibodies (59), Th2 cells produce mainly IL-4, IL-5, IL-10 and IL-13, collectively driving B cell antibody production of various isotypes, most prominently IgG1 (60). Through expression of CD40L and other co-stimulatory molecules (see chapter 1.1.2.5), helper T cells provide co-stimulation to B cells (34, 36).

A distinct subset of follicular helper T (T_{fh}) cells expresses BCL6, CXCR5 and programmed cell death protein 1 (PD-1). T_{fh} cells are localized inside the follicle where they conduct B cell selection during the germinal center reaction. In addition to CD40-CD40L stimulation, T_{fh} cells interact with GCB cells via ICOS binding to ICOS ligand (ICOSL) (61).

1.1.4.2.2 Regulatory T cells

Regulatory T cells (T_{reg}) are an anti-inflammatory T cell subset crucial for maintenance of self-tolerance and immune homeostasis. Their precursors are positively selected by thymic self-peptide-MHC recognition and driven to differentiate into antigen-specific suppressive T cells. T_{reg} cells commonly express the master transcription factor Foxp3 and often the activation-induced IL-2 receptor alpha (IL-2R α /CD25) as well as the co-stimulatory repressor CTLA-4. T_{reg} cells consequently lack helper function and instead exert several immunosuppressive functions, which include the following: 1. Due to their high IL-2R expression T_{reg} act as scavengers for soluble IL-2, thereby depriving conventional T cells from IL-2, needed for proliferation and effector differentiation. 2. T_{reg} CTLA-4 competes

for CD80/CD86 binding and potentially depletes CD80/CD86 molecules from the cell surface of APCs, thereby blocking co-stimulatory signaling via CD28 on TCR-stimulated CD4 or CD8 T cells. 3. Additionally, T_{reg} cells produce anti-inflammatory cytokines including IL-10 and TGF β (62).

Foxp3⁺ CXCR5⁺ BCL6⁺ follicular regulatory T cell (T_{fr}), localized in the follicles, suppress the germinal center reaction, thereby dampening affinity maturation and differentiation of plasma cells (63).

1.1.4.2.3 Cytotoxic T cells

Cytotoxic T lymphocytes (CTLs) recognize antigen-MHC-complexes and subsequently produce cytotoxic proteins, which can directly kill virally infected or malignant cells. CD8 T cells were identified as the primary CTL, however subsets of CD4 T cells with cytotoxic capacity have also been described (64). Cytotoxic proteins include the pore-forming protein perforin and a family of serine proteinases known as granzymes, which are stored within lytic granules. Once a CTL becomes activated by binding of cognate antigen-MHC-complexes, exocytosis of the granules is initiated to release the toxins into the synaptic cleft between CTL and target cell. The main function of perforin is the delivery of granzymes into the cytosol of the target cell. This is achieved primarily through perforin polymerization and pore formation either in the synaptic cell membrane or, upon internalization, in endosomes. Upon entering through these pores, cytosolic granzymes induce target cell apoptosis by activating caspase-dependent and caspase-independent pathways (65).

In addition to the granzyme/perforin mechanism, CTLs can induce target cell apoptosis through activation of Fas. Fas ligand (FasL) is stored in distinct lytic granules within the CTL, which, upon TCR activation, fuse with the plasma membrane in the synaptic cleft or exit as extracellular vesicles. The membrane-bound FasL subsequently engages Fas on the target cell to induce apoptosis. FasL externalization requires weaker TCR signals than granzyme/perforin-mediated cytotoxicity but is sufficient for target cell killing (65, 66).

Furthermore, CTLs can produce several cytokines, including TNF and IFN γ , which also exert cytotoxic action when secreted in the vicinity of target cells (67).

Similar modes of cytotoxicity can also be performed by natural killer (NK) cells (68).

CTL-induced cell death is not only important for the elimination of infected but also malignant cells, thus playing a central role in tumor surveillance. The cytotoxic function of CTLs targeting malignant cells is being exploited for CAR T cell therapy. Thereby, autologous T cells, engineered to express a chimeric antigen receptor (CAR), are adoptively transferred into lymphoma patients. The CAR is specific to a target antigen and coupled to co-stimulatory and signal transduction domains. Upon adoptive T cell transfer CAR T cells can recognize tumor targets independent of MHC and kill their target cells through different modes of cytotoxicity, including perforin/granzymes, Fas/FasL and release of cytokines. CAR T cell therapy (e.g. anti-CD19) is highly successful against a variety of hematologic malignancies (69-71).

1.1.4.2.4 T cell exhaustion

T cell exhaustion is a state of cellular dysfunction with reduced effector function, proliferation and differentiation. In the context of antigen persistence (e.g. during chronic infection or cancer), T cells can acquire an exhausted phenotype to minimize the damage caused by continuous T cell-driven inflammation at the expense of an effective immune defense. Exhausted T cells downregulate the expression of cytokines and upregulate inhibitory receptors, including PD-1 and CTLA-4 (57, 72). Sustained CTLA-4 expression prevents co-stimulatory engagement of CD28 (73). Stimulation of PD-1 leads to a diminished immune activity, hampers proliferation and induces apoptosis (73, 74).

In the context of cancer, PD-L1 expression by tumor cells hampers the antitumor activity of exhausted T cells, and PD-1 blockade is efficient to restore effective tumor targeting (72, 74). Also in autoimmune diseases, autoreactive T cells are chronically stimulated. Their induced exhaustion phenotype is, however, associated with a better prognosis (72).

1.2 Signaling in B cells - a matter of life and death

The balance between life and death is one of the major mechanisms regulating the immune system. During infections with pathogenic microorganisms, B cells, which bind pathogen-derived antigens but not self-antigens, must be selected to survive, proliferate and differentiate in order to ensure an effective immune response: 1. Negative and positive selection during B cell development is balanced by pro- and anti-apoptotic cues depending on the BCR signaling strength, where too weak as well as too strong signaling can lead to elimination. 2. The initial activation of B cells upon antigen recognition in the periphery requires sufficient BCR signals or signaling through pattern recognition receptors (PRRs). 3. The recruitment of B cells into the germinal center depends on co-stimulation by cognate T cells. 4. Within the germinal center, the default fate of GCB cells is apoptosis, which can only be countered by proper co-stimulation to drive survival and proliferation. After the infection is cleared, lack of antigen entails the termination of co-stimulation, ensuring proper shutdown of the immune response. 5. Long-term survival of plasma cells depends on the availability of survival factors, which are supplied in BM survival niches. 6. Malignantly transformed B cells can be actively eliminated by cytotoxic cells to prohibit their expansion.

1.2.1 Cell death

Different steps of B cell maturation require targeted elimination to prohibit the expansion of autoreactive cells, ensure effective affinity maturation and avoid uncontrolled expansion of B cells in absence of a foreign threat. Therefore, B cells can enter various transcriptional programs initiating cell death.

1.2.1.1 Programmed cell death: Apoptosis

Apoptosis is a mode of programmed cell death ensuring the organized destruction and clearance of cells while minimizing the damage to surrounding tissues. The main apoptotic pathways are exerted by caspases, a family of cysteine proteases. Once cell damage is detected, “initiator caspases”, such as caspase-8 and -9, are activated from inactive procaspases and continue to activate “effector caspases”, including caspase-3 and -7. This initiates a cascade of events resulting in DNA fragmentation and the destruction of proteins and cytoskeleton. Due to the expression of ligands for phagocytic cells, apoptotic cells are removed through phagocytosis resulting in a containment of the injured tissue and protection of surrounding cells (75).

Apoptosis can be initiated by the cell itself through an intrinsic pathway, which is induced upon growth factor deprivation or sensing of damage, and results in the caspase-9-mediated release of apoptotic factors from the mitochondria. Alternatively, an extrinsic apoptosis pathway can be induced by activation of death receptors, such as Fas or tumor necrosis factor receptor (TNFR), which results in receptor trimerization and the recruitment of Fas receptor-associated protein with death domains (FADD), which in turn binds and activates caspase-8, to activate effector caspases (75).

1.2.1.1.1 Intrinsic apoptosis pathway

The intrinsic pathway, also known as the mitochondrial pathway of apoptosis, is controlled by the Bcl2 protein family. It consists of proteins with partial homology, divided into i.) Bcl2-like pro-survival proteins (Bcl2, BclxL, Bclb, Bclw, Bfl1/a1, Mcl1), ii.) pro-apoptotic initiators (BH3-only proteins: Bad, Bim, Puma, Bid and Noxa) and iii.) pro-apoptotic effectors (Bax, Bak), which are inactivated and bound by pro-survival-proteins under steady-state conditions. Bcl2-family driven apoptosis can be initiated through cytokine and nutrient deprivation or cytotoxic stimuli such as DNA damage and hypoxia. These induce the expression of pro-apoptotic initiators (ii.), which subsequently bind to and thereby sequester the available pro-survival proteins (i.), according to their relative affinity. This enables the release and activation of the effectors Bax and Bak (iii.) which oligomerize to disrupt the mitochondrial outer membrane, leading to cytochrome c release. Subsequently, cytochrome c acts as cofactor for the assembly of the apoptosome, a cytosolic caspase-activating complex, which propagates the caspase activation cascade via the initiator caspase-9 and the executioner caspase-3 (30, 75-77).

1.2.1.1.2 Fas-mediated apoptosis

Apoptotic cell death can also be extrinsically instructed by stimulation of cell death receptors, one of them being Fas (CD95). High surface expression of Fas is typical for GCB cells, which renders them highly susceptible to Fas-induced apoptosis and drives their elimination in case of inefficient simultaneous pro-survival signaling. Thereby, engagement of Fas might mediate the counterselection of GCB cells with low affinity for antigen (78, 79). Its ligand FasL is expressed on the membrane of activated T cells, in the germinal center presumably by T_{fh} cells (80-82). Also cytotoxic T cells employ FasL to kill

target Fas⁺ cells (83, 84). Engagement of FasL drives Fas trimerization and binding to FADD, thereby forming the death-inducing signaling complex (DISC), which subsequently recruits and activates caspase-8. The downstream signaling depends on the amount of active caspase-8 generated at the DISC. In “type I” cells, large amounts of activated caspase-8 directly propagate the death signaling through proteolysis of effector caspases such as caspases-3, -6 and -7. In “type II” cells, including B cells, apoptosis is induced via the mitochondrial pathway. In these cells, low levels of active caspase-8 mediate the cleavage of BH3-interacting domain death agonist (Bid), which promotes the permeabilization of the mitochondrial outer membranes, leading to release of cytochrome c, apoptosome assembly and execution of apoptosis (83, 85, 86).

1.2.1.2 Activation-induced cell death

B cell activation is closely coupled to the upregulation of death receptors, including Fas, which, in the absence of sufficient T cell help or sufficient antigen recognition, initiate apoptosis when engaged by FasL. This activation-induced cell death (AICD) initiation is crucial to ensure the counterselection rather than expansion of autoreactive B cell clones through T cell neglect. AICD is also relevant in the context of B cell responses to foreign antigens: when BCR signals stop upon pathogen clearance, death receptor signals eliminate the no longer needed B cells. Naïve FolB cells generally express low levels of Fas but their Fas expression is increased through CD40 stimulation during TD activation. (87). In MZB cells, TI activation via TLR4 strongly drives TACI expression, which downregulates anti-apoptotic proteins and increases the expression of Fas (88). Both mechanisms predispose the B cells for Fas-mediated cell death, which can be counteracted through BCR activation by foreign antigen with sufficient affinity (89, 90).

In B cell lymphoma cells, strong BCR activation was shown to also induce AICD: artificial IgM crosslinking initiated lymphoma cell apoptosis through altered Ca²⁺ signaling as well as the activation of effector caspases, expression of pro-apoptotic and inhibition of pro-survival genes (91). In primary B cells, BCR signaling drives a metabolic program that induces mitochondrial dysfunction and death, but can be rescued by reception of a second signal through CD40 or TLRs (92).

There are other mechanisms of programmed cell death, amongst them pyroptosis and necroptosis (75).

1.2.1.3 Uncontrolled cell death: Oncosis and necrosis

External insult may damage the cell with an intensity that makes survival impossible. In this case, the cell will die in a signaling independent uncontrolled manner. First, pre-lethal oncosis is initiated, which involves the swelling of the cell and its organelles together with an increase in membrane permeability and energy leakage. Thereby, the mitochondrial membrane transition pore is opened and the released cytochrome c can potentially activate the intrinsic pathway of apoptosis if enough ATP is available. Severe insult to the cell, however, likely induces the loss of ATP, rendering the cell unable to perform apoptosis and instead proceeds to necrotic cell death (75).

Necrosis, induced by external injury including hypoxia or inflammation, involves the upregulation of NF- κ B signaling and expression of pro-inflammatory proteins, resulting in rupture of the cell membrane causing release of the cell contents into surrounding tissues, thereby inducing a cascade of inflammation and tissue damage (75).

1.2.2 Pro-survival signaling by NF- κ B

In the germinal center, those B cells, which receive poor survival signals, succumb to the initiation of cell death, thereby ensuring effective affinity maturation (93). Apoptosis in the germinal center is mainly exerted via the intrinsic mitochondrial apoptosis pathway, induced by lack of nutrients and DNA damage, or via FasL-induced apoptosis. In order to ensure the survival of B cells with a high affinity for their cognate antigen, apoptosis must be counteracted by pro-survival stimuli in correlation to BCR affinity.

A major regulator of B cell intrinsic life or death decisions is the NF- κ B transcription factor family, which drive pro-inflammatory functions and proliferation and inhibit apoptosis. NF- κ B activation can be triggered by stimulation of various cell surface and intracellular receptors. Depending on the type of stimulus, activating signals are intracellularly transduced either via a canonical or an alternative “non-canonical” signaling pathway. Transcription of target genes is ultimately initiated by release of the canonical NF- κ B transcription factors NF- κ B1 (p50), RELA (p65) and c-REL or the non-canonical NF- κ B2 (p52) and RELB. Under steady state conditions, NF- κ B proteins are bound in inactive complexes by members of the inhibitor of κ B (I κ B) family. p50 and p52 are produced as precursor proteins, p105 and p100, which function as I κ B-like NF- κ B inhibitors. Processing of p50 from p105 is constitutive while processing of p52 from p100 is activation dependent (94-96).

Canonical NF- κ B signaling leads to rapid but transient NF- κ B activation. Depending on the activating receptor, different signaling mediators initiate the activation of TGF β -activated kinase 1 (TAK1). TAK1 subsequently phosphorylates and thereby activates the I κ B kinase (IKK) complex, consisting of the catalytic components IKK α and IKK β and the regulatory protein IKK γ /NEMO. Upon activation, IKK β phosphorylates inhibitor of κ B α (I κ B α), thereby initiating its K48-linked ubiquitination and targeting for proteasomal degradation. The subsequent release of the p50/p65 and p50/c-Rel NF- κ B dimers, enables their nuclear translocation and initiation of target gene expression. In B cells, canonical NF- κ B signaling is activated through the BCR, TNFR, TLRs, cytokine receptors (94, 95).

Non-canonical NF- κ B pathway activation is generally induced more slowly but persists longer than canonical signaling. Its activation is based on the processing of p100 to p52 and subsequent nuclear translocation of the p52/RelB NF- κ B dimer. This depends on the activation of IKK α by NF- κ B-inducing kinase (NIK) and the subsequent phosphorylation of p100 by activated IKK α . Under steady state conditions, NIK is captured and ubiquitinated by the cellular inhibitor of apoptosis (cIAP)1/2-TRAF2-TRAF3 E3 ubiquitin ligase complex. Receptor activation results in the recruitment of TRAF3 and subsequent

disruption of the cIAP1/2–TRAF2–TRAF3 complex through cIAP-mediated K48 ubiquitination and proteasomal degradation of TRAF3. This allows the stabilization and subsequent accumulation of NIK, which initiates p100 processing via IKK α . As modes of negative feedback regulation, activated IKK α as well as TANK-binding kinase 1 (TBK1) phosphorylate and thereby destabilize released NIK, to prevent its aberrant accumulation. Non-canonical NF- κ B signaling in B cells is activated through CD40 and BAFF receptor (BAFFR) (96, 97).

1.2.2.1 B cell receptor signaling

The BCR is the basis of adaptive immunity. Each B cell is equipped with a highly distinct antigen specificity and its antigen affinity is further improved in the germinal center reaction. During early B cell development BCR engagement induces negative selection (see chapter 1.1.2). In contrast, in mature B cells in the periphery, encounter of cognate antigen drives B cell activation through multiple signals including canonical NF- κ B signaling. BCR stimulation induces the assembly of the CARD11/Bcl10/MALT1 (CBM) complex. This enables the recruitment and activation of TRAF6, which subsequently activates TAK1 to drive IKK-mediated NF- κ B activation (97). BCR signaling in GCB cells prolongs their survival and facilitates positive selection by priming them to receive T_h cell help (21).

1.2.2.2 CD40 signaling

The main interactor through which B cells receive CD40 stimulation is CD40L expressed on the surface of activated T cells. However, also other cells are capable to express surface CD40L, including activated B cells (98, 99). CD40/CD40L signaling is essential for the development and maintenance of germinal centers where CD40L signals are transferred to GCB by T_h cells in the context of antigen-MHCII recognition. CD40 activation initiates the recruitment of different tumor necrosis factor receptor-associated factors (TRAFs), thereby driving various signaling pathways, including non-canonical NF- κ B signaling, initiated by disruption of the cIAP–TRAF2–TRAF3 complex and subsequent release of NIK (35).

1.2.2.3 Toll like receptor signaling

Toll like receptors (TLR) are pattern recognition receptors that sense microbial patterns in an innate-like fashion. Being expressed among others on macrophages, dendritic cells and B cells, TLR signals drive the capacity of APCs to stimulate T cell help by antigen presentation, co-stimulatory signaling and cytokine secretion (100, 101). TLRs are localized either on the cell surface (TLR1, 2, 4, 5, 6, and 11) to recognize membrane components of pathogens (for example LPS by TLR4) or in intracellular compartments, such as the endoplasmic reticulum (ER), endosomes or lysosomes (TLR3, 7, 8, and 9) to recognize nucleic acids (and in case of TLR9 also CpG-DNA).

TLRs can activate a variety of signaling pathways among them NF- κ B and IFN signaling. Most TLRs transfer signals exclusively via the signaling mediator MyD88, except TLR4, which additionally signals via TRIF, and TLR3, which exclusively signals via TRIF. To induce NF- κ B signal transduction, MyD88 interacts with the intracellular toll-interleukin-1 receptor (TIR) domain of the activated TLR and with members of the IL-1 receptor-associated kinase (IRAK) family of protein kinases. This leads to complex formation and (auto-)phosphorylation of IRAK4, IRAK1 and IRAK2. Activated IRAK1 and 2 dissociate to interact with and thereby activate TRAF6. Subsequent K63-ubiquitination of IRAK1, TRAF6 and NEMO recruits and activates TAK1, which then activates the IKK complex to initiate NF- κ B signal transduction (100, 102, 103).

TLR signaling in B cells increases their antigen presentation, drives differentiation to GCB as well as plasma cells and is vital for T cell-dependent IgM and IgG2b (TLR4) and IgG2c/IgG1 (TLR9) production, which can be enhanced by IL-10. However, TLR signaling is dispensable for T cell-independent IgA and IgG3 production (101, 104).

Dual TLR7/TLR9 and BCR engagement cooperate to strongly drive cytokine and antibody production, and class-switch recombination. TLR7/TLR9 are located in endosomal membrane. Nucleic acids from microbes or endogenous dying cells can be bound by proteins or immunoglobulins to form immune complexes. Those can either be taken up through endocytosis or bound and internalized via BCR or Fc receptors and subsequently presented to TLR7/9 (105). This synergistic effect is particularly relevant in the context of systemic autoimmune diseases: Repeated TLR signaling during B cell development induces tolerance, which can be overcome by simultaneous BCR stimulation (106, 107). Furthermore, autoantibodies directed against nucleic acids can simultaneously engage immunoglobulin-specific autoreactive B cells via the BCR and TLRs (108), and B cell–intrinsic TLR7 signaling is a key requirement for the formation of spontaneous germinal centers (109).

1.2.2.4 BAFF receptors: BAFFR and TACI

The BAFF receptor (BAFFR) is one of the main pro-survival receptors in B cells and its expression is upregulated in pre-B cells in response to tonic BCR signaling. When transitional B cells egress from the BM, they rely on BAFFR signals to rescue them from premature cell death. As the availability of the ligand BAFF is limited, B cells need to compete for this survival factor. BAFFR has two closely related receptors, T cell activator and calcium modulating ligand interactor (TACI) and B cell maturation antigen (BCMA), which, in addition to BAFF, can also bind to a proliferation-inducing ligand (APRIL). BAFFR is expressed on all peripheral B cell subsets except plasma cells. TACI is expressed by activated B cells and plasma cells and its activation triggers CSR. BCMA is constitutively expressed by llPCs, supporting their survival. Shedded soluble TACI and BCMA can act as decoy receptors to capture available BAFF (110, 111). BAFF and APRIL are expressed by a variety of cell types including monocytes, macrophages, DCs, T cells and BM stroma cells and their expression is upregulated under pro-inflammatory conditions (112, 113).

1.2.2.5 Bimodal signal transduction downstream of the TNF receptor

TNF can stimulate two receptors TNFR1 and TNFR2. Stimulation of TNFR2 leads to recruitment of TRAF and subsequent activation of NF- κ B or MAPK signaling. Downstream signaling of TNFR1 is bimodal, as its intracellular death domain can interact with various adaptors, resulting either in cell activation through initiation of NF- κ B activation and MAPK signaling or cell death (via apoptosis, necroptosis or pyroptosis). NF- κ B signaling downstream of TNFR1 is initiated through recruitment of TRADD, TRAF2, RIP1, and cellular inhibitors of apoptosis 1 and 2 (c-IAP1/2). c-IAP1 and 2 are E3 ligases which subsequently polyubiquitinate themselves and RIP1 with K11 and K63 ubiquitin. This allows the recruitment of LUBAC, which mediates linear ubiquitination of target proteins, eventually resulting in NF- κ B dependent gene expression (see **Figure 3**).

Alternatively, TNFR1 stimulation can result in apoptotic signaling. However, the apoptotic signaling cascade is only initiated in response to inhibited or altered NF- κ B signaling which leads to the absence of the NF- κ B target proteins c-IAP1 and 2 and RIP1. Consequently, RIP1 remains unubiquitinated, which leads to its dissociation from the TNFR and alternative association with FADD, which subsequently activates caspase-8, thereby initiating apoptosis (114) (see **Figure 3**).

1.2.3 The balance of life and death in germinal centers

Several mitochondrial apoptosis-inducing stimuli are highly relevant in germinal centers: the immense proliferation makes GCB cells compete for the available cytokines and the active induction of DNA breaks during CSR and SHM can induce danger signals in case of faulty DNA damage repair. In GCB cells Bcl2 expression is repressed by Bcl6 (115), while BclxL expression is increased upon BCR and CD40 signaling (116), thereby protecting against apoptosis and promoting antigen-induced GCB activation and proliferation (117). Whether BclxL can protect GCB cells against Fas-induced apoptosis depends on the available downstream signaling machinery and is not yet unequivocally resolved.

To allow the re-entry of high affinity GCB cells to the germinal center reaction or induce their exit towards plasma cell differentiation, the apoptosis of GCB cells can be directly counteracted through expression of NF- κ B target proteins with anti-apoptotic function. These include among others TRAF2 and cIAP1 and 2, cellular FLICE inhibitory protein (cFLIP), as well as Bcl2 and BclxL. cIAP1 promotes NF- κ B signaling downstream of TNFR1 and cIAP2 inhibits effector caspases. c-FLIP directly inhibits caspase-8, while Bcl2 and BclxL inhibit mitochondrial apoptosis and Fas-induced apoptosis in type II cells (85, 86, 94, 114).

1.3 B cell mediated pathologies

During a human's lifetime, lymphocytes can accumulate thousands of somatic mutations (118, 119). Germinal center B cells are especially prone to the acquisition of deleterious mutations due to their inherent expression of AID. Since AID is targeted to ssDNA at sites where transcription is stalled, erroneous mutational activity can occur also outside the Ig loci. Mutations in oncogenes and tumor suppressor genes or chromosome translocations can initiate lymphoma development (15). Additionally, the random nature of active hypermutation bears the constant threat of escape and activation of autoreactive B cell clones, which can lead to the development of autoimmune diseases.

1.3.1 B cell lymphoma

B cell lymphomas are typically classified either according to their presumed normal immune cell counterpart or based on the pathways responsible for transformation (120). Most non-Hodgkin lymphomas belong to the class of diffuse large B cell lymphomas (DLBCL), which were historically subdivided into the activated B cell (ABC) and the germinal center B cell (GCB) type. Other types of B cell lymphoma include Follicular Lymphoma (FL), Burkitt's lymphoma (BL), chronic lymphocytic leukemia (CLL), splenic marginal zone lymphoma (sMZL) and mucosa-associated lymphoid tissue (MALT) type lymphoma.

1.3.1.1 Aspects of NF- κ B activation during B cell lymphomagenesis

Overall, defective apoptosis through overexpression of anti-apoptotic or loss of pro-apoptotic proteins as well as increased cell cycle activity is a common feature of human B cell lymphoma (77) and an immense involvement of NF- κ B overactivation can be demonstrated in many B cell lymphoma types (121). The underlying genetic alterations include chromosomal translocations leading to an overactivation of BCR signaling, commonly driving sMZL and MALT lymphoma. Furthermore, constitutive CD40 signaling as well as overactivation of TLR downstream signaling by activating mutations in MyD88 or TRAF6 are found in various lymphoma types including HL, CLL, FL, ABC-DLBCL and sMZL. (100, 121-123).

Lymphoma are thought to require the accumulation of several somatic mutations in individual clones to allow their bypass of normal growth control checkpoints (43). In this context, also NF- κ B activation was shown to cooperate with other oncogenic events in lymphomagenesis in mice. Examples are the deletion of Blimp1 in B cells, which in combination with constitutive canonical NF- κ B activation drives the development a disease resembling ABC-DLBCL in mice, as well as the overexpression of Bcl6 in B cells, which cooperates with alternative NF- κ B activation in the development of a GCB-DLBCL-like disease (124, 125).

1.3.1.2 T cell immune surveillance of B cell lymphoma

Immune surveillance constitutes one of the major checkpoints, which inhibit cancer cell expansion. In the context of lymphoma, the cytotoxic activity of T cells is directed against transformed B cells leading to their efficient destruction (126). Consistently, the incidence of cancers, including various types of B cell lymphomas, is strongly elevated in immunosuppressed transplant recipients and AIDS patients (127, 128), an effect that is among other effects due to dysfunctional cancer immune surveillance (127, 128). In immunocompetent human patients, B cell lymphoma cells employ a variety of mechanisms to escape T cell recognition (129-131).

Experimental evidence for T cell control of B cell malignancy comes from mice with engineered oncogenic alterations in their B cells. Overexpression of the EBV protein LMP1, which mimics constitutive CD40 activation, leads to a near absence of B cells. On the other hand, Prdm1/Blimp1 deficiency as well as BCL6 overexpression, which prohibit plasmacytic differentiation of GCB cells, cause only infrequent lymphomagenesis in aged mice. In all of these mouse strains, lymphomagenesis is effectively counteracted through eradication of the transformed B cells by cytotoxic T cells (132, 133). In order to allow full-fledged malignancy, this T cell-mediated immune surveillance needs to be broken down. In the experimental setting this can be achieved by removal of T cells or inhibition of their cytotoxic functions (79, 132-135).

1.3.2 Autoimmune diseases

Up to five percent of the general population develops autoimmune diseases world-wide, and the incidence is rising (136-138).

1.3.2.1 Organ specific and systemic autoimmune diseases

Self-defense against autoimmunity is exerted via elimination or quiescence of autoreactive B and T cell clones through various tolerance mechanisms (see chapters 1.1.2 and 1.1.4.1). The development of autoimmune diseases thus requires the break-down of several control mechanisms to enable or mimic the cooperation of autoreactive B and T cells in promotion of autoreactivity and inflammation. Once initiated, autoreactive B and T cells are being triggered by self-antigens, leading to the secretion of autoantibodies and inflammatory cytokines, which trigger innate immune cells to participate in tissue destruction. In organ-specific immune diseases such as diabetes type 1 or multiple sclerosis, the targeted self-antigen is only expressed at distinct sites of the body. Tissue destruction leads to defects of the organ function and induces disease-specific symptoms. In systemic autoimmune diseases including rheumatoid arthritis (RA), systemic lupus erythematosus (SLE) or primary Sjögren's syndrome (SjS), the autoantigens, for example DNA or collagen, are expressed in almost all cell types and the pathological damage consequently involves many different organs and tissues. The genetic background of autoimmune patients is highly diverse and autoimmunity is thought to result from the simultaneous mutation of multiple

genes involved in immune functions. Inherited and somatic genetic alterations as well as environmental triggers are involved in the initiation of autoreactivity. This makes the development of autoimmune diseases highly stochastic and explains the common latent period before disease onset (43, 139, 140).

Autoimmune diseases have a strong prevalence to occur in females and this correlates with a superior female humoral immunity (141, 142). Sex hormones as well as increased gene dosage of immune-related genes located on the X chromosome (143, 144), including TLR7 (145), could contribute to this phenomenon. Increased B cell survival seems to be a major driver of autoimmunity. Fittingly, excess availability of as well as B cell hyperresponsiveness to the survival factor BAFF is implicated in autoimmunity (43, 113, 146, 147). Furthermore, defective Fas-mediated killing allows the generation of autoreactive B cell clones (148, 149). In humans, Fas mutations frequently result in the development of autoimmune lymphoproliferative syndrome (ALPS), which can be recapitulated by B cell-specific inactivation of *Fas* in mice (48, 150). Also, elevated levels of anti-apoptotic BclxL are implicated in autoimmunity by increasing the likelihood of autoreactive B cells to escape negative selection (151, 152).

Apart from B cells, also T cells are actively involved in the development of autoantibody production by providing co-stimulation to autoreactive B cells during plasmacytic differentiation. Consequently, autoimmunity-driving mutations can also affect T cells. The underlying mechanisms involve amongst others an enhanced T_{h} cell function (153), misfunction of T_{reg} cells (154) and defective central T cell tolerance (155).

1.3.2.2 Systemic lupus erythematosus (SLE)

1.3.2.2.1 SLE pathology

Systemic lupus erythematosus (SLE) is a prototype systemic autoimmune disease, induced by the development of autoantibodies against nuclear components. Antibodies to double stranded (ds) DNA are found in up to 70% of SLE patients at some point during the course of their disease. Additionally, anti-Smith (Sm) antibodies, which target small nuclear ribonucleoprotein (snRNP) particles, are detected in 5–30% of SLE patients (156). Due to their high specificity for SLE, anti-dsDNA and anti-Sm antibodies are used as serological criteria for the diagnosis of SLE (157).

Prerequisite for the production of autoantibodies is the generation of autoreactive plasma cells. A loss of B cells tolerance can happen through failed negative selection of autoreactive cells during the B cell development (see chapter 1.1.2) or autoreactive B cells may be generated *de novo* by somatic hypermutation during the germinal center reaction (158). In addition, autoreactivity can arise from antibody responses to foreign antigens, which cross-react with autoantigens (159). Nuclear autoantigens can become exposed by dying cells and induce the activation of cognate B and T cells. Once autoreactive B cells have been recruited to the germinal center, affinity maturation enhances the binding affinity and further accelerates the pathology. This process is accompanied by a systemic inflammation boosting immune cell activation and proliferation as well as cell death,

enhancing the exposure of autoantigens in a positive feedback loop. In humans, SLE pathology is mainly driven by type I IFN (IFN α and β) signaling at sites of inflammation (160). Other cytokines involved in the pathogenesis of SLE include IL-1, IL-6, IFN γ , TNF, BAFF and IL-10. Interestingly, despite its generally acknowledged function as potent suppressor of inflammatory effector functions, IL-10 can promote B cell proliferation, differentiation and class switching. In SLE, it is thought that IL-10 consequently drives the proliferation and differentiation of autoreactive B cells into plasma cells, thereby contributing to the disease progression (161).

Eventually, plasmacytic cells produce high-affinity autoantibodies. The specificity of SLE antibodies towards dsDNA leads to the generation of chromatin-containing immune complexes, which can vigorously stimulate B cells through combined BCR and TLR crosslinking (162, 163). TLR signaling additionally enhances antigen presentation by B cells, thereby enhancing the recruitment of T cell help. The expression of TLR7 and TLR9 is increased in the peripheral blood mononuclear cells (PBMC) from SLE patients in correlation to their production of IFN- α (164). In summary, once autoreactivity against nuclear components is established, immune complexes amplify and sustain the inflammatory response.

Deposition of immune complexes in the kidney and subsequent inflammation-driven immune cell infiltration induce lupus nephritis. The extent of kidney damage can be evaluated by measurement of the glomerular filtration rate. Renal pathology will eventually develop in up to 50% of SLE patients and represents a major cause of morbidity and mortality (165-167).

Apart from end organ damage, SLE patients have an increased risk to suffer from thromboembolic events due to the development of anti-phospholipid antibodies, which include anti-cardiolipin, anti- β 2-glycoprotein I and anti-phosphatidylserine-prothrombin. Anti-phospholipid antibodies of any type can be found in approximately 50% of SLE patients (168) and induce a secondary anti-phospholipid syndrome, which increases the risk to suffer from thromboembolic events (169, 170). Mechanisms for thrombosis induction involve platelet and complement activation (168, 171-173). The risk for SLE patients to suffer from thromboembolic events is additionally increased in the presence of thrombophilic mutations (174).

To date, treatment of SLE is mainly limited to the use of immunosuppressants such as (hydroxy-)chloroquine and cortisol. In addition, since lymphocytes are key initiators and drivers of the pathology, also antibody treatments targeting B and T cells or inflammatory cytokines are frequently used in SLE therapy (175): The anti-BAFF monoclonal antibody Belimumab (176), the anti-CD38 antibody Daratumumab targeting plasma cells (177), BTK inhibitors like Ibrutinib, blocking early B cell development (178). The whole B cell-targeting anti-CD20 antibody Rituximab failed in clinical trials due to low efficacy. However, a B cell-targeting anti-CD19-CAR-T cell therapy has been proven functional against lupus in mice in 2019 (179) and has efficiently been utilized for the treatment of SLE in a human patient, just recently in 2022 (180).

1.3.2.2 Genetic predisposition of SLE patients

As a prototype multifactorial autoimmune disease, a plethora of genetic and environmental factors is underlying the development of human SLE. Genome wide association studies (GWAS) have identified more than 100 risk loci for SLE susceptibility (181, 182). Many SLE risk mutations affect NF- κ B and TLR signaling, immune complex processing or programmed cell death, ultimately causing reduced tolerance of lymphocytes towards self-constituents. (181, 183-185). As is the case for most systemic autoimmune diseases, also SLE patients are predominantly females at child-bearing age (186). Escape of TLR7, which is localized on the X chromosome, from X inactivation in B cells results in increased TLR7 in females, which is in line with their prevalence for autoimmunity. In line with this fact, copy number variations as well as gain-of-function mutations of TLR7 are associated with SLE development. (100, 145, 183, 187, 188). Elevated BAFF levels have been reported in the serum of SLE patients (147) and excess BAFF was shown to rescue anergized transitional autoreactive cells and promote their maturation (113). BAFFR and TLR signaling also cooperate in mature SLE B cells, as DNA-containing immune complexes activate TLR7, thereby inducing the expression of BAFFR, which supports cell survival (113).

Also, an increased expression of anti-apoptotic proteins has been reported in human SLE patients. These included Bcl-2, Mcl-1 and Bfl-1/A1 (189). Furthermore, elevated BAFF in SLE patients likely drives an enhanced expression of anti-apoptotic proteins in lymphocytes (190). In addition, mutations in either Fas or FasL, disrupting Fas-mediated apoptosis, are associated with SLE susceptibility in humans (184, 191).

1.3.2.3 SLE mouse models

There is a number of spontaneous SLE mouse models used for the investigation of disease mechanisms, evaluation of treatment methods and clinical trials. The spontaneous mouse models New Zealand White and Black intercrossed (NZB/NZWF1) and the NZM mouse strain, generated through continuous breeding of NZB/NZWF1 mice, develop ANA and anti-dsDNA autoantibodies and glomerulonephritis (192, 193). Three susceptibility loci termed sle1,2,3 were identified: sle1, which is expressed in B and T cells, eases the loss of tolerance to chromatin (194, 195), Sle2 induces B cell hyperactivity (196) and Sle 3 confers increased T cell activation (197). Backcrossed to the C57BL/6 strain (B6.Sle1.Sle2.Sle3), only the combination of all three loci is sufficient to induce severe systemic autoimmunity including fatal glomerulonephritis (198).

BSXB male mice carry the susceptibility locus Y autoimmunity accelerator (Yaa) on the Y chromosome (199), which harbors an additional copy of the TLR7 gene. Excess TLR7 enhances the expansion and diversification of B cells in the germinal center (200) and can induce the production of pathogenic autoantibodies through development of spontaneous germinal centers (201). This induces a lupus-like disease evident by anti-cardiolipin and anti-Sm/RNP antibodies (202). TLR7 signaling was shown to be crucial for lupus-like disease development in mice (202).

These spontaneous mouse models of SLE have been complemented by various single-gene knockout models, either systemic or cell-type specific, which also develop lupus-like pathology: Murphy Roths Large (MRL)-lymphoproliferation (lpr) (MRL-lpr) is a lupus-prone mouse strain with a single-gene Fas mutation (Fas^{lpr}) (203). MRL-lpr/lpr mice, carrying two mutant copies of Fas, develop splenomegaly and lymphadenopathy (204). The MRL-lpr pathogenesis is driven by B cells acting as autoantibody producing cells and APCs activating autoreactive T cells (205). A similar phenotype develops in MRL-gld/gld mice, which do not produce functional FasL (206). Also the B cell-specific Fas deficiency induces a lupus-like pathology in mice (150). BAFF transgenic mice develop anti-DNA autoantibodies and autoimmune disease on a mixed genetic background (146). Defective intrinsic apoptosis through loss of pro-apoptotic Bim led to the development of an autoimmune kidney disease and mice with an overexpression of anti-apoptotic Bcl2 in B cells, developed ANAs, immune complex deposition and glomerulonephritis (207, 208).

1.3.3 Connection of autoimmunity and B cell lymphomagenesis

Patients with systemic autoimmune diseases have a strongly increased risk to also develop lymphoma (209). Additionally, autoantibodies can frequently be found at significant levels in patient of various lymphoma types despite the absence of clinical autoimmune symptoms (210). Furthermore, mutations identified in autoreactive B cells are often identical to those frequently found in malignant B cells (211). This overlap strongly suggests a common etiology underlying the development of both B cell driven autoimmune diseases and B cell lymphoma.

In B cell lymphoma, T cells play a central protective role by counteracting the expansion of transformed B cell clones (see chapter 1.3.1.2). On the contrary, in autoimmunity, T cells are mostly driving the pathology by providing co-stimulation to autoreactive B cells or through direct cytotoxicity against self-constituents (43). The factors, which balance the protective versus pathologic functions of T cells in the context of B cell-mediated diseases, remain incompletely understood and will be one major focus of this thesis (see chapter 2: Aim of the thesis).

1.4 Negative regulation of NF- κ B signaling by A20

Under infectious circumstances, the acute induction NF- κ B signaling in immune cells is vital to generate a quick and effective inflammatory response. However, when the infection is cleared the body needs to terminate inflammation and return to its normal state. This requires the tight control and proper termination of NF- κ B signaling through a negative feedback mechanism. The key regulator TNF alpha induced protein 3 (TNFAIP3)/A20 was first reported as a protein, expressed by human umbilical vein endothelial cells (HUVECs) upon TNF stimulation (212, 213). It was subsequently identified as a zinc finger protein, which is induced through the activation of NF- κ B signaling and NF- κ B activation rapidly decays after its induction (213-215). In B cells, A20 was found to be expressed upon activation of CD40 (216).

1.4.1 Structure and function of A20

Due to NF- κ B binding sites in the TNFAIP3 promoter, A20 is itself a target of the NF- κ B transcription factors (214, 217). Upon activation of the canonical NF- κ B signaling pathway, A20 is rapidly induced and subsequently acts as negative feedback regulator to ensure the efficient shutdown of signaling once the activating stimulus was removed. A20 has been reported to change the activation status of its target proteins through different modes of ubiquitin-editing (218):

- (i) Using its deubiquitinase (DUB) function exerted by the OTU domain, A20 removes K63-linked polyubiquitin chains from essential signaling intermediates, such as TRAF6 (219).
- (ii) Through its E3 ligase activity in ZnF4, A20 in concert with other proteins adds K48-linked ubiquitin chains to signal mediators such as RIP1, targeting them for proteasomal degradation (220).
- (iii) M1-linked ubiquitination of NEMO (IKK γ) mediates IKK oligomerization, thereby promoting IKK autophosphorylation and activation (221). Through binding to linear M1-linked ubiquitin chains on NEMO via its ZnF7 domain, A20 can non-enzymatically inhibit the NF- κ B activating function of the IKK complex (218, 222).
- (iv) In addition to NF- κ B regulation, A20 can protect cells from TNF-induced apoptosis through binding to linear ubiquitin chains in the TNFR1 signaling complex I, thereby protecting them from cleavage by DUBs and prohibiting the assembly of the pro-apoptotic complex II (223, 224). Recently, also protective functions against necroptosis and pyroptosis have been described for A20 (225).
- (v) Furthermore, A20 is involved in the inhibition of inflammasome activation (226).

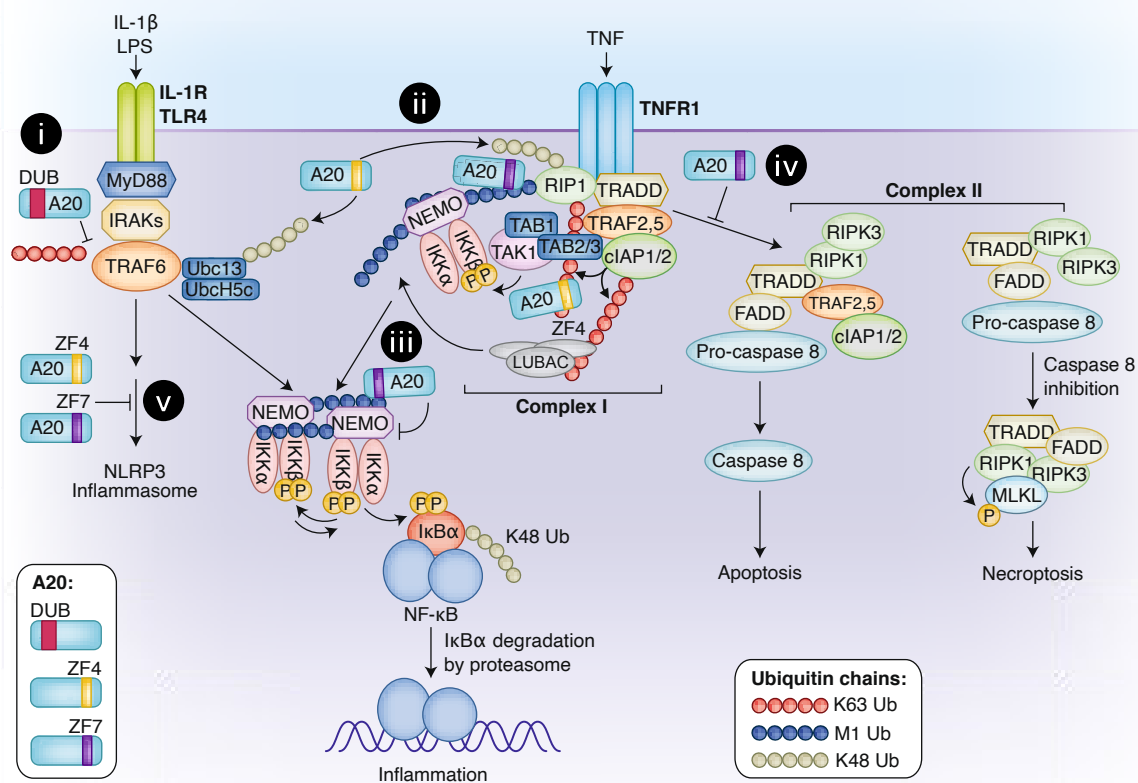


Figure 3. Inhibition of NF- κ B signaling, inflammasome activation and cell death by A20.

Adapted from Sun et al. (2020) (222). Ub = Ubiquitin, ZF = Zinc finger domain, OTU = Ovarian tumor domain.

The expression of A20 is post-transcriptionally regulated. Binding of the TNFAIP3 transcript to different microRNAs hinders translation and binding to the RNA-binding protein (RBP) Roquin1 (Rc3h1) destabilizes the TNFAIP3 mRNA, thereby reducing A20 expression (217).

The function of A20 is post-translationally regulated through phosphorylation at serine 381 by the NF- κ B-activating kinase IKK β . This phosphorylation-mediated activation of A20 is increased under inflammatory conditions to enhance its negative feedback function (227-229). In contrast, MALT1, a subunit of the CBM complex, which connects the BCR to NF- κ B signal transduction can cleave A20 at arginine 439, thereby impairing its inhibitory function (230, 231).

Additionally, the stability of A20 is influenced by cell-extrinsic factors including reactive oxygen species (ROS), which inactivate the A20 DUB-activity by reversible oxidation of the catalytic cysteine residue in its OTU domain, or high glucose levels, which induce the glucosamine-N-acetylation and subsequent K48 ubiquitination of A20, targeting it for proteasomal degradation (232, 233)

1.4.2 A20 knockout and mutation studies

This delicate system of cross-regulation within the NF- κ B signaling pathway is vulnerable to changes. Dysregulation of NF- κ B activation causes an overshooting inflammatory response. A20 knockout (Tnfaip3^{-/-}) mice develop spontaneous systemic inflammation and cachexia and die prematurely (234). This pathology is driven through TLR-induced NF- κ B activation and can be rescued by additional knockout of MyD88, an adaptor molecule involved in signaling from TLRs and the IL-1 receptor (IL-1R) (235, 236).

Mutation studies revealed more and less important functionalities of the different A20 domains: A20^{ZF7/ZF7} mice carrying mutations in the ZnF7 domains were shown to develop spontaneous arthritis and organ inflammation. While ZnF4 is critical for mediating A20 recruitment to ubiquitinated RIP1, ZnF4 mutation (A20^{ZF4/ZF4}) did not cause an inflammatory pathology. A combined loss of ZnF7 and 4 (A20^{ZF4ZF7/ZF4ZF7}) in mice, however, induced death before weaning age from widespread inflammation. A20^{OTU/OTU} mutant mice, lacking DUB activity, did not display an inflammatory pathology. The capacity of A20 to be phosphorylated is delicately linked to its functionality. Several rare mutations in the OTU domain, which decrease A20 phosphorylation, enhance immunity towards viral infection but pose the risk for spontaneous inflammatory disease (227, 237).

Taken together, these studies indicate that the anti-inflammatory action of A20 is mainly exerted via ZnF7, whose function is partially redundant with ZnF4, while the DUB function seems to be largely dispensable for the inhibition of inflammation (222, 226, 229, 238-240). Of note, these mutation studies were performed in body-wide mutant mice. Potentially, particular parts of the A20 protein play key roles in specific cell types or processes, while being negligible in others.

1.4.3 A20-deficiency in humans

Since A20 plays a central role in the regulation of inflammatory processes, its dysfunction is also linked to the development of various human pathologies. Single-nucleotide polymorphisms (SNPs) in or near the *TNFAIP3* gene locus, leading to reduced expression or function of A20, are strongly correlated with the development of various inflammatory and autoimmune diseases (241), including RA (242), SjS (243) and SLE (244-247) (**Figure 4**). In many cases, these autoimmunity-associated SNPs are located in non-coding regions of the *TNFAIP3* gene locus (241, 244, 245, 248), or target loci containing enhancers of *TNFAIP3* gene expression. Polymorphisms in the *TNFAIP3* enhancer region (TT>A) are associated to human SLE and the deletion of this enhancer was sufficient to induce arthritis development in mice carrying a humanized *TNFAIP3* gene locus (248-250).

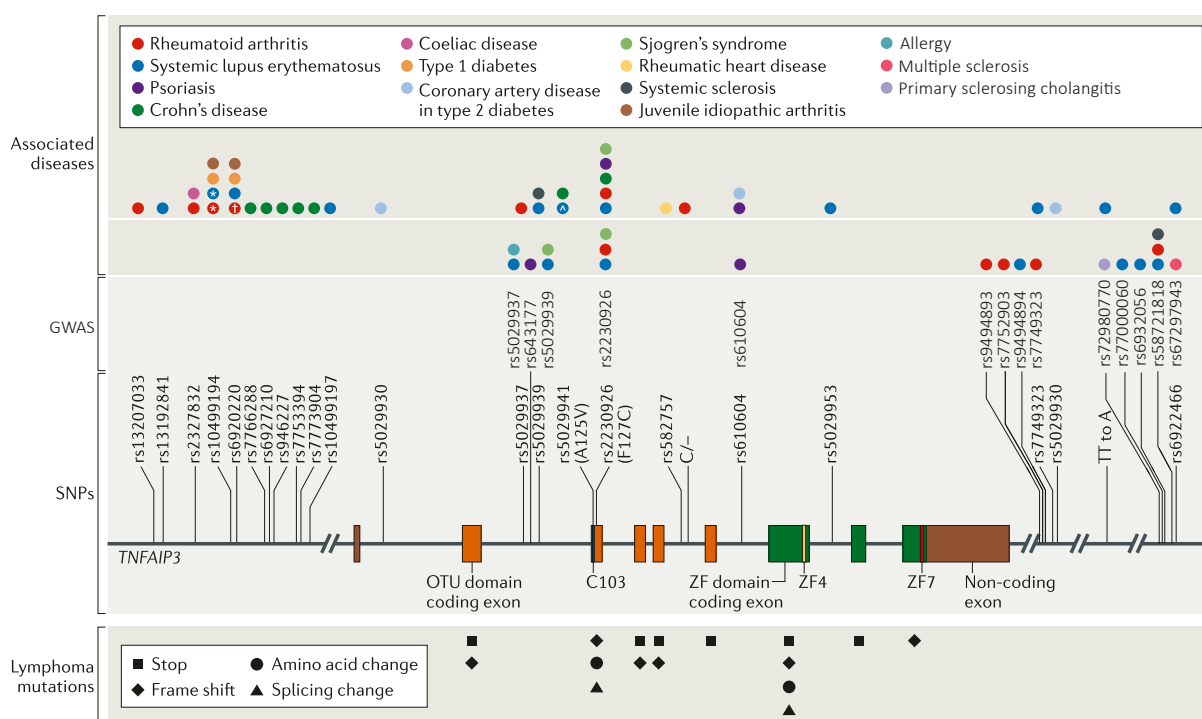


Figure 4. Loss of function mutations of A20 are linked to the development of auto-inflammatory diseases and lymphomagenesis.

Modified from Ma & Malynn, 2009 (241). GWAS added from the GWAS catalog for *TNFAIP3*: <https://www.ebi.ac.uk/gwas/genes/TNFAIP3> (accessed on 16.07.2021 and 23.05.2023, see **Supplementary Table 1**)

Using genome wide association studies (GWAS), several SNPs in the *TNFAIP3* locus have been confirmed as SLE risk loci (181, 244, 245, 247, 250) and novel variants are frequently being identified by whole exome sequencing of SLE patients (251). Overall, GWAS have confirmed several independent correlating mutations and discovered novel mutations linking A20-deficiency to a great number of different autoimmune and autoinflammatory diseases (252, 253). Notably, these disease-associated SNPs generally induce a reduction instead of a complete loss of the expressed A20. Consistently, also in RA patients the amount of *TNFAIP3* mRNA in PBMCs was decreased compared to healthy controls (254).

In 2016, Zhou et al. described a heterozygous germline mutation of *TNFAIP3* causing an early-onset systemic inflammation resembling Behçet's disease and thereby defined a new monogenic autoinflammatory disease termed haploinsufficiency of A20 (HA20) (255). Since then, a large number of HA20 cases have been described, caused by either frameshift mutations or exon deletions. The most common pathological manifestations of HA20 include recurrent fevers, oral ulcers and genital ulcers or polyarthritis and resemble a variety of autoimmune and autoinflammatory diseases including Crohn's disease, Behçet's disease, SLE, and also unclassified autoinflammatory syndromes. Interestingly, the pathology often occurs already in very young patients. The number of described HA20 cases, induced by different SNPs in and near the *TNFAIP3* locus is rising rapidly (256-269).

Also in human lymphoma patients, the *TNFAIP3* gene locus is frequently affected by mutations, chromosomal deletions or promoter methylation (241) (**Figure 4**). In lymphoma samples, both mono- and bi-allelic targeting of *TNFAIP3* have been observed, and in most reported cases, genetic events target both alleles, leading to a complete loss of A20 expression (270-274). Still, heterozygous deficiency was reported in some cases of MZL (270), Hodgkin lymphoma, primary mediastinal B cell lymphoma (271), MALT lymphoma (272) and DLBCL (273) and decreased A20 expression can be observed in non-Hodgkin lymphoma cells (275). This suggests that losing only one copy of A20 is an oncogenic insult, driving lymphomagenesis. However, verification of A20 as heterozygous tumor suppressor in a mouse model is lacking to date.

Importantly, A20-deficiency seems to connect the occurrence of both pathologies, autoimmunity and lymphoma. Most prominently in SjS, genetic variations of *TNFAIP3* were found in 77% of those patients who simultaneously suffered from MALT lymphoma (276). This manifests a parallel role of A20-deficiency in autoimmunity and lymphomagenesis and underlines the common etiology of both pathologies.

1.5 B cell-specific A20-deficiency

While *Tnfrsf25*^{-/-} mice died prematurely from upon tremendous systemic inflammation, subsequent studies sought to evaluate the specific effect of A20-deficiency in different immune cell types by use of conditional A20/*TNFAIP3* alleles. Knockout of A20 specifically in macrophages, neutrophils, mast cells, dendritic cells and T cells consistently induced strong cell hyperactivation and led to a variety of autoinflammatory and autoimmune phenotypes (217, 241, 277).

B cell-specific loss of A20 induces an autoimmune phenotype

The Schmidt-Supprian laboratory and others have previously published mouse models in which (three different) loxP-flanked A20 alleles were combined with CD19Cre to induce B cell-specific ablation of A20 protein expression (278-282). B cell-specific loss of A20 (B-A20^{-/-}) led to increased splenocyte numbers, caused by a combined expansion B, T and myeloid cell types. Even though little to no spontaneous B cell activation could be observed *in vivo* (281, 282), A20^{-/-} B cells were strongly hyperreactive towards various stimuli (anti-IgM, LPS, CD40L and CpG) *in vitro* (280-282). While A20-deficiency had no effect on early B cell development, the maturation to functional MZB cells was impaired, whereas the percentage and number of GCB cells was significantly increased, most prominently in the gut-associated lymphoid tissues (GALT). An increase in splenic plasma cell numbers was accompanied by strongly increased serum concentrations of IgM and IgA antibodies. In addition, B-A20^{-/-} mice developed autoantibodies at the age of approximately 0.5 - 1.5 years. Autoimmune manifestations included the development of IgG autoantibodies directed against nuclear components and cardiolipin as well as IgM immune complex deposition in the kidneys, and was driven by systemically increased IL-6 (280).

These data indicate that A20 expression in B cells protects from the spontaneous production of autoantibodies and that loss of A20 leads to inefficient B cell deletion in the germinal center. Tavares et al. suggested that this is due to increased expression of anti-apoptotic BclxL in A20-deficient GCB cells, which renders them more resistant towards Fas-induced cell death (281).

While all three studies focused on the pathology of B-A20^{-/-} mice, some analyses also included mice with heterozygous A20-deletion in their B cells (B-A20^{-/wt}). B-A20^{-/wt} mice had an equally strong GCB and plasma cell expansion compared to B-A20^{-/-} mice and also seemed to develop similar autoimmune manifestations (280, 281).

Hyperreactivity of B cells with heterozygous loss of A20

Surprisingly, survival analysis of mice with B cell specific loss of A20 revealed a slightly increased mortality of B-A20^{-/wt} mice compared to B-A20^{-/-} mice (unpublished data from the Schmidt-Supprian laboratory). Interestingly, the lifespan of female B-A20^{-/wt} mice was strongly reduced compared to their male counterparts. Both B-A20^{-/wt} and B-A20^{-/-} mice developed signs of autoimmunity, evident by splenomegaly, the development of ANAs and increased serum levels of inflammatory IL-6.

2 Aim of the thesis

The heterozygous loss of A20 is strongly implicated in the development of various inflammatory and autoimmune pathologies in humans and the HA20 disease entity has been defined just seven years ago (255). It is therefore of high relevance to recapitulate the pathology of mono-allelic A20-deficiency in mouse disease models to understand the mechanisms underlying the development and progression of the human pathology, associated with reduced expression and/or heterozygous inactivation of A20. Interestingly, systemic heterozygous A20-deficiency in mice (A20^{-/wt}) was not reported to induce any gross early-onset pathology (234), indicating that reduced levels of A20 are sufficient to maintain homeostasis in most body tissues and can prevent the development of systemic inflammation. However, no analysis has been reported for aged A20^{-/wt} mice and a potential later-onset pathology, driven by A20^{-/wt} hematopoietic cells, has not yet been evaluated (234).

The previously published mouse models with immune cell-specific A20 deletion partially mirrored the development of human autoimmune and autoinflammatory diseases (217, 277, 280-282). However, in all these models, A20-deficiency in immune cells has been investigated mainly by use of cell type-specific bi-allelic A20 knockout. In contrast, in human autoimmune patients TNFAIP3 SNPs mainly induce a reduction rather than a complete loss of the expressed A20 (241). Patients with non-hereditary autoimmunity acquired several disease-predisposing mutations in a single or several cell types during their life (43). Systemic autoimmune diseases can be driven by autoreactive B cells (283), which are particularly pre-disposed for the acquisition of mutations due to the use of highly mutagenic mechanisms involving RAG and AID during V(D)J recombination, SHM and CSR (284, 285). Initial unpublished data from our laboratory indicated that B cell-specific A20-deficiency induces a higher mortality in B-A20^{-/wt} mice compared to B-A20^{-/-} mice (chapter 1.5).

The development of autoimmunity requires the breakdown of several checkpoints, which in human patients requires the acquisition of more than one autoimmunity-predisposing genetic alteration and/or environmentally induced epigenetic remodeling (43). To reproduce the pathology of human B cell-driven autoimmune diseases, I combined two key predispositions – enhanced resistance to apoptosis and hyperactivity of NF-κB signaling – through B cell-restricted BclxL transgene expression combined with haploinsufficiency of A20.

Using this genetic model, I aimed to answer two main questions:

- Which pathology does the heterozygous loss of A20 in B cells induce in mice?
- What are the mechanisms counteracting the development of strong autoimmunity in mice with homozygous loss of A20 in B cells?

3 Materials and methods

3.1 Genetically modified mice

The mice used in this project were intercrossed from published mouse strains (**Table 1**). These strains were either provided by the authors or eligible persons or commercially available from Jackson Laboratory. All mice were housed under specific pathogen-free (SPF) or specific and opportunistic pathogen free (SOPF) conditions. Mice were bred and housed in mouse facilities of the Zentrum für Präklinische Forschung (ZPF), Klinikum rechts der Isar, München (Germany) or at Charles River Calco (Italy). All the mouse strains used in this project were generated on or later backcrossed to a C57BL/6 genetic background. All animal procedures were approved by the Regierung of Oberbayern.

Mouse strain	Official strain name	First published in
A20 ^{F/F}	Tnfaip3 ^{tm1.1Gvl}	Vereecke et al., 2010 (279)
AIDCre	B6.129P2-Aicda ^{tm1(cre)Mnz/J}	Robbiani et al., 2008 (286)
E μ -BclxL ^{tg}	Tg(Emu-BCL2L1)87Nnz	Grillot et al., 1996 (117)
CD19Cre	B6.129P2(C)-Cd19 ^{tm1(cre)Cgn/J}	Rickert et al., 1997 (278)
CD3e ^{$\Delta\Delta$}	CD3e ^{tm1Mal}	Malissen et al., 1995 (287)
Cy1Cre	B6.129P2(Cg)-Ighg1 ^{tm1(cre)Cgn/J}	Casola et al., 2006 (288)
MyD88 ^{F/F}	Myd88 ^{tm1.1Medz}	Schenten et al., 2014 (289)
Nur77 ^{GFP}	B6.FVB(Cg)-Tg(Nr4a1-EGFP) ^{GY139Gsat/WeisMmucd}	Zikherman et al., 2012 (290)
RAG2 ^{$\Delta\Delta$}	B6.129S6-Rag2 ^{tm1Fwa}	Shinkai et al., 1992 (291)

Table 1. Mouse strains used for this project.

Genotyping of genetically modified mice

Genotyping polymerase-chain reactions (PCRs) were run with different protocols. Reaction setups are shown in **Table 2**, **Table 3**, **Table 4** and **Table 5**, PCR programs in **Table 6**, **Table 7**, **Table 8** and **Table 9**. Genotyping primers and expected PCR product sizes in base pairs (bp) are listed in **Table 10**. PCR products were loaded onto 1.5% agarose gels (Thermo Scientific, Cat. No. 16500100) and stained with SYBRsafe (Thermo Scientific, Cat. No. S33102).

Reagent	Volume (μ L)
Mastermix genotyping buffer	25
10x Cresole	3
Primer A (stock 100 pmol/ul)	0.25
Primer B (stock 100 pmol/ul)	0.25
Primer C (stock 100 pmol/ul)	0.25
Homemade polymerase	0.5
DNA	1

Table 2. Genotyping PCR reaction setup for A20, AIDCre, CD19Cre, Cy1Cre and MyD88.

Reagent	Volume (μL)
2x GoTaq Mastermix (Promega, Cat. No. M7423)	15
H ₂ O	13.4
Primer A (stock 100 pmol/ul)	0.25
Primer B (stock 100 pmol/ul)	0.25
DNA	1

Table 3. Genotyping PCR reaction setup for E μ -BclxL.

Reagent	Volume (μL)
10x Reaction buffer complete KCl (Metabion, Cat. No. mi-E8001L)	3
H ₂ O	21
10x Cresole	3
MgCl ₂ (stock 100 mM, Metabion, Cat. No. mi-E8001L)	0.3
dNTP Mix (25 mM, Thermo, Cat. No. R1122)	0.5
Primer A (stock 100 pmol/ul)	0.25
Primer B (stock 100 pmol/ul)	0.25
Primer C (stock 100 pmol/ul)	0.25
mi-Taq polymerase (Metabion, Cat. No. mi-E8001L)	0.5
DNA	1

Table 4. Genotyping PCR reaction setup for CD3e.

Reagent	Volume (μL)
10x Reaction buffer complete KCl (Metabion, Cat. No. mi-E8001L)	3
H ₂ O	21.2
10x Cresole	3
MgCl ₂ (stock 100 mM, Metabion, Cat. No. mi-E8001L)	0.3
dNTP Mix (25 mM, Thermo, Cat. No. R1122)	0.5
Primer A (stock 100 pmol/ul)	0.25
Primer B (stock 100 pmol/ul)	0.25
mi-Taq polymerase (Metabion, Cat. No. mi-E8001L)	0.5
DNA	1

Table 5. Genotyping PCR reaction setup for Nur77^{GFP}.

Cycle No.	Temperature	Duration	Repetition of Cycles
1	94 °C	3 min	
2	94 °C	30 sec	$\Delta T = -0.5 \text{ }^\circ\text{C} / \text{cycle}$, 19 cycles
	65 °C	30 sec	
	72 °C	30 sec	
3	94 °C	30 sec	
4	55 °C	30 sec	
5	4 °C	∞	

Table 6. PCR program for A20, AIDCre, E μ -BclxL, CD19Cre and Cy1Cre.

Cycle No.	Temperature	Duration	Repetition of Cycles
1	95 °C	5 min	
2	95 °C	30 sec	35 cycles
	68 °C	45 sec	
3	72 °C	45 sec	
	72 °C	10 min	
4	4 °C	∞	

Table 7. PCR program for CD3e.

Cycle No.	Temperature	Duration	Repetition of Cycles
1	95 °C	3 min	
2	95 °C	30 sec	$\Delta T = -0.5 \text{ °C / cycle}$, 10 cycles
	70 °C	30 sec	
	72 °C	45 sec	
3	95 °C	30 sec	15 cycles
	65 °C	30 sec	
	72 °C	45 sec	
4	72 °C	7 min	
5	4 °C	∞	

Table 8. PCR program for MyD88.

Cycle No.	Temperature	Duration	Repetition of Cycles
1	94 °C	3 min	
2	94 °C	15 sec	$\Delta T = -1 \text{ °C / cycle}$, 10 cycles
	65 °C	30 sec	
	72 °C	40 sec	
3	94 °C	15 sec	30 cycles
	55 °C	30 sec	
	72 °C	40 sec	
4	72 °C	5 min	
5	16 °C	∞	

Table 9. PCR program for Nur77^{GFP}.

Allele	Primer Name	Primer sequence	PCR product size
A20	A20_28 Fw	CACAGAGCCTCAGTATCATGT	WT: 150 bp Floxed: 230 bp Germline deleted: 370 bp
	A20_31Rv	CCTGTCAACATCTCAGAAAGG	
	A20_30Fw	GCAGCTGGAATCTCTGAAATC	
AIDCre	AicdaCre-1	CACTCGTTGCATCGACCGGTAATG	WT: 484 bp Floxed: 283 bp
	AicdaCre-2	GGACCCAACCCAGGAGGCAGATGT	
	AicdaCre-3	CCTCTAAGGCTTCGCTGTTATTACCAC	
E μ -BclxL	HuMish-fw	GGCGGGCATTTCAGTGACCTG	Transgene: 396 bp
	HuMish-rv	TGAGCCCAGCAGAACCACGCCG	
CD19Cre	Cre8	CCCAGAAATGCCAGATTA	WT: 452 bp Inserted: 500 bp
	CD19c	AACCAGTCAACACCCTTCC	
	CD19d	CCAGACTAGATACAGACCAG	
CD3 ϵ	CD3e fw1	TGGCTACTACGTCTGCTACACACCAGCCTC	WT: 200 bp Mutated: 700 bp
	CD3e rv2	AATGGAATTACCTAGACAACCTCCAGGCCAC	
	CD3e/Neofw1	ATTTCGCAGCGCATCGCCTTCTATCGCCTTC	
Cy1Cre	Cy1Cre A	TGTTGGGACAAAACGAGCAATC	WT: 250 bp Inserted: 470 bp
	Cy1Cre B	GGTGGCTGGACCAATGTAAATA	
	Cy1Cre C	GTCATGGCAATGCCAAGGTCGCTAG	
MyD88	Seq16	CAGTCTCATCTTCCCCTCTGCC	WT: 700 bp Floxed: 600 bp Germline deleted: 400 bp
	Seq19	GGGAATAATGGCAGTCCTCTCCCAG	
	MyD88R	GTCAGAAACAACCACCACCATGC	
Nur77 ^{GFP}	Nr4a1 F1	CCTACCAAGTTTCTTGCTTCCCTT	Inserted: 340 bp
	GFP R2	TAGCGGCTGAAGCACTGCA	

Table 10. Genotyping PCR primers and product sizes

3.2 Buffers and media

Buffer	Ingredients
FACS buffer	500 mL Dulbecco's phosphate buffered saline (DPBS, Gibco, Cat. No. 14190-169) 5 mL heat-inactivated fetal calf serum (FCS, Gibco, Cat. No. 10270-106) 5 g BSA (GE Healthcare, BSA HyClone, Cat. No. SH30574.02) 5 mM EDTA (Invitrogen, Cat. No. 15575020) 10 mM HEPES (Gibco, Cat. No. 15630-056)
Gey's solution	14 mL dH ₂ O + 4 mL Solution A + 1 mL Solution B + 1 ml Solution C Solution A: 654 mM NH ₄ Cl 24.8 mM KCL 4,2 mM Na ₂ HPO ₄ * 12 H ₂ O 8.8 μM KH ₂ PO ₄ 27.7 mM glucose 0.05 g phenol red fill up to 1 L with dH ₂ O Solution B: 20.7 mM MgCl ₂ * 6 H ₂ O 5.68 mM MgSO ₄ * 7 H ₂ O 30.6 mM CaCl ₂ fill up to 100 mL with dH ₂ O Solution C: 268 mM NaHCO ₃ fill up to 100 mL with dH ₂ O
B cell medium	500 mL RPMI-1640 (Gibco, Cat. No. 21875-034) 5 mL heat-inactivated FCS (Gibco, Cat. No. 10270-106) 2 mM L-Glutamine (Gibco, Cat. No. 25030-081) 0.1 mM Non-essential amino acids (NEAA, Invitrogen, Cat. No. L10119) 50 μM 2-Mercaptoethanol (Gibco, Cat. No. 31350-010) 1 mM Sodium pyruvate (Gibco, Cat. No. 11360-039) 10 mM HEPES (Gibco, Cat. No. 15630-056) 5 mL Penicillin-Streptomycin (PenStrep, Cat. No. 15140122)
iGB medium	500 mL RPMI-1640 (Gibco, Cat. No. 21875-034) 5 mL FBS Gold (PAN Biotech, Cat. No. P30-3032) 2 mM L-Glutamine (Gibco, Cat. No. 25030-081) 0.1 mM Non-essential amino acids (NEAA, Invitrogen, Cat. No. L10119) 50 μM 2-Mercaptoethanol (Gibco, Cat. No. 31350-010) 1 mM Sodium pyruvate (Gibco, Cat. No. 11360-039) 10 mM HEPES (Gibco, Cat. No. 15630-056) 5 mL Penicillin-Streptomycin (PenStrep, Cat. No. 15140122) on days 1 to 4 supplemented with 1 ng/mL IL-4 (Peprotech, Cat. No. 214-14) from day 4 supplemented with 10 ng/mL IL-21 (Peprotech, Cat. No. 210-21)

Table 11. Buffers and media.

3.3 Mouse analysis

3.3.1 Preparation of serum

For serum generation blood was aspirated with a syringe from the heart directly after euthanasia or living mice were bled through puncture of the facial vein. The blood was then transferred into a 0.5 or 0.3 ml Microvette (Sarstedt, Cat. No. 20.1308.100 or 20.1343.100) inverted and incubated for 30 - 60 minutes at room temperature. Tubes were centrifuged at 10000 rpm for 10 minutes in a microcentrifuge, serum was carefully aspirated and transferred to a new tube. The serum was stored at -80 °C.

3.3.2 Preparation of citrate plasma

For plasma generation, 60µl of 3.2% sodium citrate in ddH₂O were taken up with a 1 ml syringe. 540µl blood was slowly aspirated from the heart with a 0.9 mm diameter needle attached to the same syringe directly after euthanasia. A small air bubble was taken up and the syringe was gently inverted three times. The mixture was carefully transferred to a tube and centrifuged at 2000g for 10 minutes at room temperature. Afterwards the plasma was aspirated with a pipette aliquoted in tubes and stored at -20 °C.

3.3.3 Organ harvesting and weighing

Hearts were taken from the euthanized animal right after blood withdrawal and laid into a PBS bath. Through repeated application of pressure using forceps, the heart cavity was rinsed and subsequently remaining liquid was pressed out from the heart on a paper cloth. Spleens, mesenteric lymph nodes (mLN), Peyer's patches (PP), livers, kidneys, salivary glands, brain and bones (femurs) were collected, placed in a tube containing FACS buffer (DPBS (Gibco, Cat. No. 14190-169) + 1% FBS (Gibco, Cat. No. 10270-106), 1% BSA (GE Healthcare, Cat. No. SH30574.02), 5 mM EDTA (Invitrogen, Cat. No. 15575020), 10 mM HEPES (Gibco, Cat. No. 15630-056)) or placed on a tissue soaked with FACS buffer and kept on ice until further processing. The weight of the dried organs was measured using a microscale.

3.3.4 Organ fixation for histology and immunofluorescence

Mouse organ tissue samples were fixed in 4% formalin (Carl-Roth, Cat. No. 7398.1) for 24 hours, then dehydrated and embedded in paraffin.

3.3.5 Preparation of single cell suspensions

For generation of single cell suspensions, spleens, mLN, PP, liver and brain were gently dissociated between two microscopic glass slides. The single cell suspension was resuspended in FACS buffer and filtered. Femurs were flushed with medium (RPMI-1640, 10% FBS (Gibco), 10 mM HEPES (Gibco), 2 mM L-glutamine (Gibco), 1 mM sodium

pyruvate (Gibco), 0.1 mM non-essential amino acids (Gibco), 0.05 mM 2-mercaptoethanol (Gibco), Penicillin/Streptomycin (Gibco)) to extract bone marrow cells. To lyse erythrocytes from organ single cell suspensions, after centrifugation and resuspending in 1 mL FACS buffer, 5 mL of Gey's solution, was added and mixed and incubated for 5 minutes on ice. The solution was neutralized through addition of 10 mL FACS buffer. Living cells were counted using a Neubauer counting chamber and Trypan Blue (Gibco).

3.4 Flow cytometry

3.4.1 Staining antibodies

Antigen	Fluorochrome	Clone	Source	Dilution
7-AAD	-	-	eBioscience	1:300
Annexin V	APC	17-8007-74	Invitrogen	1:20
Arginase I	Alexa Fluor 700			1:400
B220	Brilliant Violet 510	RA3-6B2	BioLegend	1:100
B220	Brilliant Violet 650	RA3-6B2	eBioscience	1:200
B220	FITC	RA3-6B2	eBioscience	1:200
B220	PE/Cy7	RA3-6B2	eBioscience	1:200
B220	PerCP/Cy5.5	RA3-6B2	eBioscience	1:200
BAFFR	FITC	eBio7H22-E16	eBioscience	1:100
BCL6	PE	K112-91	BD	1:400
BCL6	PE/Cy7	K112-91	BD	1:400
BclxL	PE	7B2.5	Southern Biotech	1:100
BLIMP1	Brilliant Violet 421	5E7	BD	1:100
BLIMP1	PE	5E7	BioLegend	1:100
CAR	FITC	sc-56892	Santa Cruz	1:50
CD1d	PE	1B1	eBioscience	1:200
CD107a	eFluor450	eBio1D4B	eBioscience	1:100
CD11b	Brilliant Violet 510	M1/70	BioLegend	1:1500
CD11b	eFluor450	M1/70	eBioscience	1:1500
CD11c	PE/Cy7	N418	eBioscience	1:500
CD119	Biotin	2E2	eBioscience	1:100
CD138	APC	281-2	BD	1:50
CD138	Brilliant Violet 421	281-2	BioLegend	1:100
CD16/CD32	none	93	Thermo Fisher	1:200
CD19	Alexa Fluor 700	1D3	eBioscience	1:200
CD19	APC/eF780	eBio1D3	eBioscience	1:300
CD19	Biotin	eBio1D3	eBioscience	1:100
CD19	Brilliant Violet 510	6D5	BioLegend	1:100
CD21/35	FITC	7G6	BD	1:200
CD23	Alexa Fluor 700	B3B4	BioLegend	1:400
CD23	PE/Cy7	B3B4	eBioscience	1:400
CD25	APC	PC61.5	eBioscience	1:500
CD25	PE	PC61.5	eBioscience	1:300
CD38	PE/Cy7	90	Biolegend	1:500
CD4	Brilliant Violet 510	RM4-5	BioLegend	1:400
CD4	Brilliant Violet 605	GK1.5	Biolegend	1:400
CD4	PE/Cy7	GK1.5	eBioscience	1:2000
CD4	PerCP/eFluor710	RM4-5	eBioscience	1:200
CD4	BUV496	GK1.5	BD	1:200

Table 12. Flow cytometry antibodies

Antigen	Fluorochrome	Clone	Source	Dilution
CD5	PE/Cy7	53-7.3	eBioscience	1:2000
CD62L	Brilliant Violet 510	MEL-14	BioLegend	1:200
CD69	APC	H1.2F3	eBioscience	1:400
CD70	PE/Cy7	FR70	BioLegend	1:200
CD80	FITC	16-10A1	eBioscience	1:100
CD83	Brilliant Violet 650	Michel-19	Biolegend	1:50
CD83	PE	Michel-17	eBioscience	
CD86	APC	GL1	eBioscience	1:200
CD86	Brilliant Violet 785	GL1	BioLegend	1:200
CD8α	BUV737	53-6.7	BD	1:200
CD8α	BUV395	53-6.7	BD	
CD8α	FITC	53-6.7	eBioscience	1:100
CD8α	PerCP/eFluor710	53-6.7	eBioscience	1:1000
CD93 (AA4.1)	APC	AA4.1	eBioscience	1:100
CD95 (Fas)	FITC	Jo2	BD	1:100
CD95 (Fas)	PE	Jo2	BD	1:200
CD95 (Fas)	Brilliant Violet 421	Jo2	BD	1:800
CD95 (Fas)	Brilliant Violet 650	Jo2	BD	1:200
CXCR4	Biotin	2B11/CXCR4	BD	1:100
CXCR5	Biotin	L138D7	BioLegend	1:50
Eomes	APC	Dan11mag	Thermo Fisher	1:50
F4/80	Biotin	CI:A3-1	AbD serotec	1:200
Foxp3	eFluor450	FJK-16s	eBioscience	1:800
Foxp3	PE	FJK-16s	eBioscience	1:50
GL-7	eFluor450	GL7	eBioscience	1:200
ICOS	Brilliant Violet 421	C398.A4	BioLegend	1:1000
ICOS	PE	7E.17G9	eBioscience	1:100
ICOSL	Biotin	HK5.3	eBioscience	1:200
IFNγ	eFluor450	XMG1.2	eBioscience	1:200
IFNγ	PE/Cy7	XMG1.2	eBioscience	1:200
IgA	Biotin	C10-1	BD	1:1000
IgA	PE	11-44-2	eBioscience	1:200
IgD	FITC	11-26c/11-26	eBioscience	1:200
IgD	eFluor450	11-26c/11-26	eBioscience	1:200
IgE	Brilliant Violet 510	R35-72	BD	1:200
IgG1	FITC	A85-1	BD	1:1000
IgG2a	Brilliant Violet 605	R19-15	BD	1:200
IgG2b	Biotin	G15-337	BD	1:1000
IgG3	Brilliant Violet 421	R40-82	BD	1:500
IgM	PE/Cy7	II/41	eBioscience	1:800
IgM	PerCP	115-126-075	Jackson ImmunoResearch	1:200
IgM	Superbright 780	II/41	eBioscience	1:50
IL-4	PE/Cy7	BVD6-24G2	eBioscience	1:100
IL-6	PE	MP5-20F3	eBioscience	1:200
IL-10	PE	JES5-7101-81	eBioscience	1:50
IL-10	PE/Cy7	JES5-16E3	BioLegend	1:100
IL-13	PE	eBio13A	eBioscience	1:200
IL-17A	APC	eBio17B7	eBioscience	1:100
IL-17A	Brilliant Violet 605	TC11-18H10	BD	1:50
iNOS	PE	CXNFT	eBioscience	1:500
IRF4	eFluor450	3E4	eBioscience	1:400
IRF4	PE	3E4	eBioscience	1:400
IRF4	PerCP/eFluor710	3E4	eBioscience	1:800
Ki-67	PerCP/eFluor710	SolA15	eBioscience	1:6000
Ly-6C	Brilliant Violet 785	HK1.4	BioLegend	1:800

Table 12 (continued): Flow cytometry antibodies. LD dye = live/dead viability dye.

Antigen	Fluorochrome	Clone	Source	Dilution
Ly-6G (Gr-1)	APC/Cy7	RB6-8C5	eBioscience	1:400
MHCI	eFluor450	AF6-88.5.5.3	eBioscience	1:500
MHCII	PE	M5/114.15.2	eBioscience	1:2000
Near-IR LD dye	Near-IR	-	Invitrogen	1:2500
NK1.1	APC	PK136	eBioscience	1:100
NK1.1	Brilliant Violet 650	PK136	BioLegend	1:50
NK1.1	BUV395	PK136	BD	1:50
NK1.1	BUV737	PK136	BD	1:100
NKG2D	PE	CX5	eBioscience	1:100
OX40	PE	OX-86	eBioscience	1:200
OX40L	Alexa Fluor 647	RM134L	BioLegend	1:400
PAX5	PerCP/Cy5.5	1H9	BioLegend	1:200
PD-1	FITC	J43	eBioscience	1:200
PD-1	PE/Cy7	J43	eBioscience	1:500
PDCA-1	FITC	eBio927	eBioscience	1:100
PromoFluor-840 LD dye	-	-	BioConnect	1:1000
Siglec-F	PE	S17007L	BioLegend	1:200
Streptavidin	Brilliant Violet 510	none	BioLegend	1:200
Streptavidin	Brilliant Violet 605	none	BioLegend	1:50
Streptavidin	Brilliant Violet 650	none	BioLegend	1:200
Streptavidin	BUV395	none	BD	1:200
Streptavidin	BUV737	none	BD	1:100
Streptavidin	eFluor450	none	eBioscience	1:400
Streptavidin	PerCP/Cy5.5	none	eBioscience	1:100
TCRβ	APC	H57-597	BD	1:300
TCRβ	Brilliant Violet 605	H57-597	BD	1:100
TCRβ	Brilliant Violet 510	H57-597	BioLegend	1:50
TCRβ	PerCP/Cy5.5	H57-597	eBioscience	1:100
TNF	APC	MP6-XT22	eBioscience	1:100
Zombie Aqua LD dye	-	-	BioLegend	1:1000

Table 12 (continued): Flow cytometry antibodies. LD dye = live/dead viability dye.

3.4.2 Staining procedure

CFSE labeling

CFSE labeling of 10 million cells was performed in 1 mL warm DPBS (Gibco, Cat. No. 14190-169), supplemented with 1:12000 CFSE (eBioscience, CellTrace CFSE Cell Proliferation Kit, Cat. No. C34570). After 7 minutes incubation with the CFSE dilution at 37 °C in the dark, the cells were washed with FCS (Gibco, Cat. No. 10270-106) to stop the CFSE labeling reaction and subsequently washed with B cell medium. Afterwards, the cells were cultured in B cell medium at 37 °C, 5% CO₂ until analysis.

Antibody staining

For antibody staining, one to eight million cells were transferred into 96-well V-bottom plates (Thermo Scientific, Cat. No. 249944) and kept on ice for all subsequent staining steps. Cells were washed three times with cold 200 μ L PBS (2 minutes, 950 g, 4 °C) to remove protein-containing media or FACS buffer. Afterwards, the cells were resuspended in 30 μ L PBS containing a diluted fixable live-dead dye (**Table 12**) and anti-mouse CD16 / CD32 monoclonal antibodies, used for blocking the unspecific binding of antibodies to Fc receptors, and incubated for 15 to 30 minutes. Cells were then washed with FACS

buffer and stained with fluorochrome-labeled or biotinylated primary antibodies, binding extracellular markers (15 min, 4°C). In the case of biotinylated antibodies, a 2-step staining was performed. The samples were incubated with biotinylated antibodies (15 min, 4°C), washed with FACS buffer and subsequently stained with the extracellular marker antibody mixture containing a streptavidin coupled fluorochrome. After washing with FACS buffer, cells were fixated using the FoxP3 / Transcription Factor Staining Set (eBioscience, Cat. No. 00-5523-00) for 30 minutes or overnight. To maintain GFP or dTomato fluorochrome signals, relevant samples were instead fixated using 2% formaldehyde (Carl Roth, Roti-Histofix 4%, Cat. No. P087.4 diluted 1:1 with PBS) for 45 minutes. For intracellular blocking of Fc receptors, anti-mouse CD16 / CD32 was diluted in 1x Permeabilization buffer of the Foxp3/Transcription Factor Staining Set and incubated with the cells for 30 min. Subsequently, intracellular antibodies were stained for 1 h in 1x Permeabilization buffer. In case of intracellular biotinylated antibodies, staining was carried out in two consecutive steps. In case of Roti-Histofix fixation, the cells were stained intracellularly overnight. Stained cells were finally resuspended in 100-200 µL of FACS buffer and stored for maximum 7 days in the fridge.

Apoptosis detection

For staining of apoptotic cells, the CaspGLOW Fluorescein Active Caspase Staining (BioVision, Cat. No. K180-25) and Annexin V Apoptosis Detection kit (eBioscience, Cat. No. 88-807-72) were used according to manufacturers' instructions. For live/dead staining, unfixated cells were resuspended in FACS buffer containing 1:300 7-AAD (eBioscience, Cat. No. 00-6993-50) 10 minutes before acquisition.

Cell cycle analysis

For cell cycle analysis, DRAQ5 (Abcam, Cat. No. ab108410) was added to the cell suspensions in a dilution of 1:1000 shortly before acquisition.

3.4.3 Sample acquisition and data analysis

Samples were acquired with a BD FACS Canto™, Beckman Coulter CytoFLEX S™ or CytoFLEX LX™ flow cytometers using the FACSDiva or CytExpert software, respectively. Spectral overlap of fluorochromes was compensated using unstained or live-dead stained splenocytes and splenocytes or compensation beads (Thermo Fisher, Cat. No. 01-2222-42) stained with each fluorochrome-labelled antibody individually. Flow cytometry data was analyzed using FlowJo v.10. Cell doublets were excluded by gating on singlets in forward scatter FSC-A vs FSC-H as well as sideward scatter SSC-A vs SSC-W.

3.4.4 LEGENDplex assay for the assessment of the serum cytokine concentration

Cytokine concentrations in the serum were measured using the LEGENDplex™ Mouse B cell Panel Standard kit (BioLegend, Cat. No. 740831) and a custom produced LEGENDplex™ panel (IFN α , IFN β , IL-1 α , IL-1 β , IL-3, IL-7, IL-9, IL-18, IL-21, IL-22, IL-27, IL-33). Serum samples were diluted 1:2 for all analytes and processed according to manufacturer's instructions. Samples were recorded using a Beckman Coulter CytoFLEX LX™ flow cytometer.

3.5 Serum and plasma analyses

3.5.1 Isotype ELISA

Serum isotype ELISAs were performed with Mouse Ig ELISA Quantitation kits (Bethyl Laboratories), according to manufacturer's protocol. The OD405 was measured with an enzyme-linked immunosorbent assay (ELISA)–photometer (Spectramax 340; Molecular Devices, Sunnyvale, CA or Spark, TECAN) and antibody concentrations were determined by comparison with a standard curve.

Product	Manufacturer	Cat. No.
Mouse IgA ELISA Kit	Bethyl Laboratories	E99-103
Mouse IgG ELISA Kit	Bethyl Laboratories	E90-131
Mouse IgG1 ELISA Kit	Bethyl Laboratories	E90-105
Mouse IgG2b ELISA Kit	Bethyl Laboratories	E90-109
Mouse IgG2c ELISA Kit	Bethyl Laboratories	E90-136
Mouse IgG3 ELISA Kit	Bethyl Laboratories	E90-111
Mouse IgM ELISA Kit	Bethyl Laboratories	E99-101

Table 13. Isotype ELISA kits.

3.5.2 Autoantibody ELISA

The detection of anti-nuclear (ANA), anti-cardiolipin, anti-serin-prothrombin, anti-Smith and anti-ssDNA autoantibodies was performed by using commercially available ELISA Kits (Varelisa or IBL/Tecan). For detection of mouse antibodies, a secondary goat anti-mouse IgG-HRP (Southern Biotech, Cat. No. 1030-05) was diluted 1:4000 in Sample Diluent. For ANA IgM detection, a secondary biotinylated IgM (BD, Cat. No. 553406) antibody was diluted 1:500 and incubated for 30 minutes, followed by a 30 minutes incubation with Streptavidin-HRP (Biolegend, Cat. No. 405210) diluted 1:10000 in Sample Diluent. The incubation of kit standards with secondary antibody and all other steps were performed according to manufacturer's instructions. Absorbance was measured at 450 nm with a plate reader (Spark, TECAN). For ANA and anti-ssDNA, absorbance values of samples were normalized by division through the absorbance value of the kit positive

control. For all other autoantibodies, antibody concentrations were determined by comparison with a standard curve.

Product	Manufacturer	Cat. No.
ANA Screen 8 ELISA	IBL International	RE75421
ReCombi ANA Screen	Varelisa	125 96
Sm-Ab ELISA	IBL International	RE75221
Cardiolipin IgG ELISA	IBL International	RE70511
Cardiolipin Screen ELISA	IBL International	RE70501
Serin-prothrombin ELISA	IBL International	RE70611
ssDNA Screen ELISA	IBL International	RE70231

Table 14. Autoantibody ELISA kits.

For detection of antibodies against dsDNA, MaxiSorp ELISA plates (Nunc) were coated with poly-L-Lysine (Trevigen, Cat. No. 3438-100-01) and PBS (ratio 1:1) for 1 hour. Plates were washed with Tris-NaCl (50 mM Tris and 0.14 M NaCl, pH 7.5), and dsDNA from mouse embryonic stem cells was coated in saline-sodium citrate (pH 7.0) buffer overnight. After blocking with Tris-NaCl, 1% BSA for 30 minutes, diluted samples were added to the plate and incubated for 60 minutes. Sera from 24 weeks old C57BL/6^{lpr/lpr} and 24 weeks old MRL^{lpr/lpr} mice, as well as IgG-poor serum, were used as controls. HRP-conjugated antibody against mouse IgG (Bethyl Laboratories, Cat. No. A90-131P) was used as secondary antibody. Absorbance was measured at 450 nm with a Sunrise plate reader (TECAN).

3.5.3 D-Dimer ELISA

The D-Dimer concentration was analyzed in serum samples using the Mouse D-Dimer ELISA Kit (Abbeva, Cat. No. abx258705) according to the manufacturer's instructions.

3.6 Urine analyses

3.6.1 Total protein content in urine

Urine was collected into a microtube and urine protein concentration was measured using a Pierce™ BCA Protein Assay Kit (Thermo Scientific, Cat. No. 23227).

3.6.2 Albuminuria

The kidney function of mice from every group was determined by measuring serum creatinine levels using the Jaffe method following the manufacturer's instructions (DiaSys Diagnostic Systems, Cat. No. 117119910021). Albuminuria was determined with the Mouse Albumin Quantitation Set (Bethyl Laboratories, Cat. No. E99-134) as described

below and the albumin creatinine ratio was calculated. Urinary albumin excretion was evaluated by a double-sandwich ELISA. First, 96-well plates were coated with purified goat anti-mouse albumin antibody (Bethyl Laboratories, Cat. No. A90-134A), and plates were incubated overnight at 4 °C. After blocking at room temperature in 0.5% BSA in PBS with 0.05% Tween20, urine samples and mouse albumin standard (Sigma-Aldrich, Cat. No. A3139) were added on the plate in triplicates and incubated for 2 hours. Mouse urine samples were diluted in serial dilutions ranging from 1:10² to 1:10⁷. As a secondary antibody, HRP-conjugated anti-mouse albumin antibody (Bethyl Laboratories, Cat. No. A90-134P) was used.

3.6.3 Blood urea nitrogen (BUN)

Blood urea nitrogen was measured by standard method for quantitative *in vitro* determination of urea on photometric systems following the manufacturer's instructions (DiaSys Diagnostic Systems, Urea FS kit, Cat. No. 131019990314).

3.7 Histopathological organ analyses

3.7.1 Periodic Acid Schiff staining (PAS)

For histopathological analysis, paraffin-embedded kidneys were cut into 2 µm thick sections and stained with periodic acid-Schiff (PAS) according to a standard protocol. In brief, re-hydrated sections were incubated for 5 min in 1% (w/v) periodic acid (Merck) followed by washing in distilled water and incubation with Schiff's reagent (Sigma Aldrich) for 5 min. After washing, sections were incubated for 2 min with Mayer's hemalaun (Merck) followed by washing in tap water and dehydration for final covering with Entellan (Merck) and a coverslip. Renal histology changes were examined by light microscopy and assessed at a magnification of 200-400x. A sum score of pathologic changes assessed the presence of each of 7 characteristic glomerular changes in lupus nephritis. One point was given if 1. glomerular basement membrane was thickened, 2. mesangial matrix was enlarged, 3. hypercellularity occurred, 4. intracapillary thrombi were seen, 5. apoptotic cells, 6. extracellular proliferation, or 7. segmental sclerosis occurred, and points were summed up into a glomerular pathology score. Representative photomicrographs were taken using an upright BX60 light microscope with an XC30 camera (Olympus) at 300-fold magnification.

3.7.2 Sirius Red staining

Tissue sections were deparaffinized and re-hydrated. 0.1 % picro-sirius red solution (Direct Red 80 (Sigma-Aldrich, Cat. No. 365548) in Picric acid (Sigma-Aldrich, Cat. No. P6744-1GA)) was applied for 60 minutes and washed twice with acidified water. After

dehydration with ethanol, tissue was cleared using xylene and covered with mounting medium.

3.7.3 IgG immunostainings on kidney sections

Immunostaining was performed on 2 μ m sections of paraffin-embedded kidneys, using biotinylated anti-mouse IgG (Vector Laboratories, Cat. No. BA-9200, 1:100). The degree of IgG deposition was scored semiquantitatively (grade 0 = no trace; grade 1 = mild; grade 2 = moderate; grade 3 = severe) in the mesangium and along the glomerular capillary loops.

3.7.4 Kidney immune cell infiltration

For immunohistochemistry the following antibodies were used: anti-mouse/human Mac2 (BioLegend, Cat. No. 125402, 1:3000), anti-mouse CD45 (BD, Cat. No. 553076, 1:100) and anti-mouse CD138 (BD Biosciences, Cat. No. 553712, 1:100). For quantitative analysis, glomerular cells were counted in 15 - 20 cortical glomeruli per section (from “n” mice in the group, as indicated in the figure legend) or were quantified using Photoshop CS6 Extended (Adobe) as % of stained high power field (%HPF).

3.7.5 B cell infiltrations in the salivary glands

Mouse organ tissue samples were fixed in 4% formalin (Carl-Roth, Cat. No. 7398.1) for 24 hours and embedded in paraffin. 2 μ m sections were deparaffinized, dehydrated, and stained with hematoxylin-eosin (H&E, Dako, Cat. No. CS70030-2 and CS70130-2). For immunohistochemistry, antigen retrieval was conducted in preheated 10 mM citrate buffer (pH 6.0) or EDTA buffer (pH 9.0) in a microwave for 20 minutes. Afterwards the slides were incubated with a target-specific antibody. The following antibodies were used: anti-mouse B220 (BD, Cat. No. 550286). Signal detection was performed by using the Dako REAL detection system.

3.7.6 Histology in lymphoma samples

Within the T cell-deficient mouse cohort obviously sick mice were analyzed for lymphoma in spleen, LN and liver. Tissues were dehydrated (ASP300S, Leica) and embedded in paraffin after fixation in neutral-buffered formaldehyde for 48 hours. Serial 2 μ m thin cuts were prepared using a rotary microtome (HM355S, ThermoFisher Scientific). Slides were stained with H&E after deparaffinization according to standard protocols and cover slipped. Slides were digitized using a slide scanner (AT2, Leica) and the resulting svx files were reviewed using ImageScope (v2.4.3.4008). All slides were evaluated by an experienced comparative pathologist (Prof. Dr. Katja Steiger) with an Olympus BX53 stereomicroscope and classified according to the consensus classification of lymphoid neoplasms in mice (292). The most recent immunohistochemical phenotyping description of rodent lymphoid tissue (293) and the classification of non-nonproliferative and

proliferative lesions of the rat and mouse hemolymphoid system by INHAND (International Harmonization of Nomenclature and Diagnostic Criteria for Lesions in Rat and Mice) (294) were taken into account.

3.8 Sequencing analyses

3.8.1 Bulk RNA sequencing

Cell sorting

For bulk RNA sequencing of B-BclxLtg cells and controls, splenocytes were stained with LIVE/DEAD fixable Near-IR dye (Invitrogen) and anti-mouse CD16/CD32 monoclonal antibody (eBioscience, Cat. No. L10119) on ice for 30 minutes. Cells were then washed with FACS buffer, stained with the fluorochrome-labeled antibody mix, and washed again in FACS buffer. The stained single cell suspension was then filtered through a 35 µm nylon mesh (Fisher Scientific, Cat. No. 08.771.23) and sorted for single, living follicular B cells (CD138⁻ TCRβ⁻ B220⁺ CD19⁺ CD38⁺ CD95^{low}), germinal center B cells (CD138⁻ TCRβ⁻ B220⁺ CD19⁺ CD38^{low} Fas^{high}) and plasmacytic cells (CD138⁺ B220⁻) in the BD FACSAria™ II. Per sample 1000 cells were sorted into each well of a 96-well PCR plate pre-filled with 5µl RLT lysis buffer (Qiagen, Cat. No. 79216). Whenever possible, two wells (technical replicates) were sorted for each population. Plates were then sealed, centrifuged and stored at -80°C.

Sequencing

For bulk 3'-sequencing of poly(A)-RNA library preparation was done as described previously (295). Briefly, frozen cell lysates from sorted cell populations (follicular B cells, germinal center B cells or plasma cells) were thawed and RNA was isolated using Agencourt AMPure XP magnetic beads. Barcoded cDNA of each sample was generated with Maxima RT polymerase (Thermo Fisher, Cat. No. EP0742) using oligo-dT primer containing barcodes, unique molecular identifiers (UMIs) and an adaptor. 5' ends of the cDNAs were extended by a template switch oligo (TSO) and full-length cDNA was amplified with primers binding to the TSO-site and the adaptor. NEBNext® Ultra II FS kit (New England Biolabs, Cat. No. E7805L) was used to fragment cDNA. After end repair and A-tailing a TruSeq adapter was ligated and 3'-end-fragments were finally amplified using primers with Illumina P5 and P7 overhangs. In comparison to Parekh et al. (2016), the P5 and P7 sites were exchanged to allow sequencing of the cDNA in read1 and barcodes and UMIs in read2 to achieve a better cluster recognition. The library was sequenced on a NextSeq 500 (Illumina) with 59 cycles for the cDNA in read1 and 16 cycles for the barcodes and UMIs in read2. Data was processed using the published Drop-seq pipeline (v1.0) to generate sample- and gene-wise UMI tables (296). Reference genome (GRCm38) was used for alignment. Transcript and gene definitions were used according to the GENCODE version M25.

Bioinformatic analyses

Gencode gene annotations M18 and the mouse reference genome GRCm38 were derived from the Gencode homepage (EMBL-EBI). Dropseq tools v1.12 (296) was used for mapping raw sequencing data to the reference genome. The resulting UMI filtered count matrix was imported into R (v 3.4.4). The UMI filtered count matrix was imported into R (v 4.1.3) and differential expression was analyzed with DESeq2 v1.34.0 (297) for all genes with row count of 10 or higher. Dispersion of the data was estimated with the genotype as explanatory variable for the model fit. Subsequently the LRT test was applied using an intercept-only model, and a gene was considered to be differentially regulated between the genotypes if the adjusted p value was below 0.05 or if the normal p value was below 0.05. Significant genes were clustered and the resulting dendrogram was computationally split into 2 or 5 subclusters. All heatmaps display z-scaled data after quantile normalization.

For the visualization of the relative expression of activation markers, differential expression was plotted for all genes with a row count of 1 or higher, independent of their significant regulation, and samples were ordered by genotype. RNA sequencing graphs were generated with R (v 4.2.1 or 3.4.4) and R Studio (version 1.3.959)

Log2 fold changes were used as input for gene set enrichment analysis (GSEA) with compiled marker gene sets or database gene sets using the GSEA software (298) v4.1.0 ([build 27], Broad Institute, MIT, University of California) in the preranked mode with default parameters.

For principal component analysis (PCA) the 10 percent most variant (based on standard deviation) genes were selected after quantile normalization and the first two principal components are shown.

3.8.2 Assessment of somatic hypermutation

For somatic hypermutation analysis, mice were immunized with 100 µg 4-hydroxy-3-nitrophenyl-acetyl chicken γ-globulin (NP-CG; Biosearch Technologies, Cat. No. N-5055C) in alum (Thermo Fisher Scientific, Cat. No. 77161). 14 days after immunization, 40,000 splenic GCB cells (CD19⁺ IgD⁻ CD43⁻ PNA^{high} Fas^{high} CD38^{low}) and non-GCB cells (CD19⁺ IgD⁺ IgM⁺ Fas⁻ CD38^{high}) were purified using a BD FACS Aria. PCR fragments from isolated DNA of these cell populations were amplified using primer J558Fr3 5'-CAGCCTGACATCTGAGGACTCTGC-3', which anneals in the framework region of most VHJ558 genes, and primer JHCHint 5'-CTCCACCAGACCTCTCTAGACAGC-3', which hybridizes in the intron 3 of exon JH4. The PCR fragments were subcloned into the pJet1.2 cloning vector (Promega), and the resulting plasmids were sequenced with the primer JHCHint using the BigDye™ Terminator v3.1 chemistry (Applied Biosystems). A stretch of 550 bp intron sequence immediately downstream of the JH4 gene segment was analyzed for somatic mutations. Analysis of somatic mutations was conducted as published (299), with the use of Lasergene (DNASTAR) software and SHMTool (300). A similar analysis was performed for the determination of the frequency of the high-affinity W33L mutation in the V186.2 gene using primer pairs that are specific for the V186.2 and JH2 genes.

3.8.3 Immunoglobulin heavy- and light-chain amplification for clonality assessment

To analyze IGH and IGK rearrangements, two different PCRs were performed on genomic DNA isolated either from dissociated cells or RNA stabilized tissue.

For analysis of IGV_κ-IGJ_κ rearrangements, the thermal cycling conditions used were 94°C for 60 sec, 30 cycles: 94°C for 30 sec, 60°C for 90 sec, 72°C for 90 sec and 72°C for 42 sec (Vkdeg forward primer 5'-GGCTGCAGSTTCAGTGGCAGTGGRTCWGGGRAC-3', Jk2AR reverse primer 5'-TTAGACTTAGTGAACAAGAGTTGAGAA-3', Jk5BR reverse primer 5'-CGTCAACTG ATAATGAGCCCTCTC-3').

Amplification of the IgH rearrangements for the different IGHJ gene segments (JH1-JH4) were performed using the following thermal cycler conditions: 98 °C for 10 min, 35 cycles of 98 °C for 10 sec, 67 °C for 30 sec, 72°C for 30 sec and 72°C for 10 min (MsVhe AH forward primer 5'-TCGAGTTTTTCAGCAAGATGAGGTGCAGCTGCAGGAGTCTGG-3', Jh4 reverse primer 5'-CTGAGGAGACGGTGACTGAGG-3').

Based on the results of the described PCRs, clonality of the B cells of tumors was classified into 3 different categories: - no evidence for clonality, PCR results similar to wildtype; + polyclonal, clear deviation from wildtype but still multiple amplicons detected and no clear dominating amplicon present in more than 1 PCR; ++ clonal, one clear dominating amplicon present in at least 2 of the 3 PCRs.

3.9 *In vivo* analyses

3.9.1 *In vivo* T cell depletion

For the depletion of T cells, mice were intraperitoneally injected with either 300µg anti-CD8 (InVivoMab, Cat. No. BE0119) or with a mixture of 300µg anti-CD8 (InVivoMab, Cat. No. BE0119), anti-CD4 (InVivoMab, Cat. No. BE0061) and anti-Thy1 (Absolute Antibody, Cat. No. Ab00212-2.0) antibody, each. Control mice received an equal volume of PBS. Mice were first injected twice within 24 hours and subsequently twice a week for 15 days.

3.9.2 *In vivo* TNF depletion

For depletion of systemically available TNF, mice were intraperitoneally injected with 250 µg anti-TNF antibody (Ultra-LEAF™ Purified anti-mouse TNF-α Antibody, BioLegend, Cat. No. 506332). Control mice received an equal volume of PBS. Mice were injected four times on days 1, 4, 7 and 10 and were analyzed on day 14.

3.9.3 Competitive bone marrow chimeras

Bone marrow cells from both femurs and tibiae of B-BclxL^{tg}, B-BclxL^{tg}-A20^{-wt} and B-BclxL^{tg}-A20^{-/-} donor mice were depleted from B and T cells by magnetic activated cell sorting (MACS). Therefore, BM cells were resuspended in the following antibody mix, diluted in MACS Separation Buffer (Miltenyi, Cat. No. 130-091-221), and incubated for 20 minutes on ice:

Antibody	Clone	Vendor	Dilution
anti-B220-PE	RA3-6B2	eBioscience	200
anti-TCR β -PE	H57-597	eBioscience	300
anti-CD138-PE	281-2	BioLegend	500
anti-CD19-PE	eBio1D3	eBioscience	200

Table 15. Antibody mixture used for the MACS-based depletion of B and T cells.

After washing by centrifugation, the BM cells were incubated with Anti-PE MicroBeads (Miltenyi, Cat. No. 130-048-801), diluted 1:4 in MACS Separation Buffer (Miltenyi, Cat. No. 130-091-221), for 20 minutes at 4 °C. Subsequently, MACS separation was performed using an autoMACS[®] Separator (Miltenyi) with the DepleteS sensitive mode. The purified BM cell were then counted and equal numbers of cells from two donor mice were mixed. Of these mixtures, 40,000 cells were transplanted into 6 to 8 weeks old sublethally irradiated (4.5 Gy) female Rag2^{ΔΔ} mice by injection into the tail vein. The recipient mice were treated with antibiotics for two weeks (Borgal[®] 24%, Virbak) diluted 1:250 in drinking water. The chimeras were analyzed 6 to 7 weeks after BM transfer.

In each pairwise cell mixture, the cells from one donor mouse conditionally expressed a CAR reporter (301) to enable their identification by flow cytometry. Each pairwise mixture was analyzed by flow cytometry to assess the fraction of cells from both donors within each mixture at the time of transplant.

3.9.4 FeCl₃-induced thrombus formation in the Carotis artery

In anesthetized mice (fentanyl 0.05 mg/kg, midazolam 5.0 mg/kg and medetomidine 0.5 mg/kg i.p.) the right common carotid artery was surgically prepared and vessel injury was induced by application of FeCl₃ (1 μ L of 10% FeCl₃, soaked in 1 mm² Whatman paper) for 2 minutes. For intravital microscopy, platelets were labeled by injection of a fluorescently labeled non-blocking platelet antibody (anti-mouse GPIIb β -X488, Emfret, Cat. No. X488; 0.5 μ L/g body weight) before application of FeCl₃. Vessel injury-induced thrombus formation was monitored and imaged for 30 minutes by *in vivo* video fluorescence microscopy with a frequency of 1 picture per second (Zeiss Axio Zoom.V16 microscope equipped with a Zeiss AxioCam). Thrombus size was calculated from single images using ImageJ software.

3.10 *In vitro* analyses

3.10.1 *In vitro*-derived germinal center B cells (iGB) culture

The *in vitro* derived germinal center B cell (iGB) culture system was previously described (302). Briefly, one day prior to the start of the iGB culture (day 0), 40LB feeder cells were irradiated (120 Gy, γ -rays) and seeded into petri dishes to form a confluent layer. On day 1, naïve B cells were purified from splenocytes by depletion of other immune cell types through magnetic activated cell sorting (MACS). Therefore, splenocytes were resuspended in the following antibody mix, diluted in MACS Separation Buffer (Miltenyi, Cat. No. 130-091-221), and incubated for 15 minutes on ice:

Antibody	Clone	Vendor	Dilution
anti-CD4-Biotin	RM4-5	eBioscience	1:200
anti-CD8 α -Biotin	53-6.7	eBioscience	1:200
anti-CD11b-Biotin	M1/70	eBioscience	1:200
anti-CD11c-Biotin	N418	eBioscience	1:1000
anti-CD43-Biotin	S7	BD	1:200
anti-CD93-Biotin	AA4.1	eBioscience	1:100
anti-CD95-Biotin	Jo2	BD	1:200
anti-TCR β -Biotin	H57-597	eBioscience	1:100
anti-Ter119-Biotin	Ter119	eBioscience	1:200

Table 16. Antibody mixture used for the MACS-based purification of B cells.

After washing by centrifugation, the splenocytes were incubated with Anti-Biotin MicroBeads (Miltenyi, Cat. No. 130-090-485), diluted 1:4 in MACS Separation Buffer (Miltenyi, Cat. No. 130-091-221), for 15 minutes at 4 °C. Subsequently, MACS separation was performed using an autoMACS[®] Separator (Miltenyi) with the DepleteS sensitive mode. The purified B cells were seeded at a density of 20,000 cells/mL onto the 40LB feeder layer in iGB medium (RPMI-1640, 10% FBS Gold, 10 mM HEPES, 2 mM L-Glutamine, 1 mM Sodium Pyruvate, 0.1 mM non-essential amino acids, 50 μ M 2-Mercaptoethanol, 1% Penicillin/Streptomycin), supplemented with 1 ng/ml IL-4 (Peprotech, Cat. No. 214-14), and incubated at 37°C, 5% CO₂. After 72 hours (day 4) cells were dissociated from the plate through 5 minutes incubation with 37 °C warm 2 mM EDTA (Invitrogen, Cat. No. 15575020) in DPBS (Gibco, Cat. No. 14190-169), centrifuged at 1200 rpm for 10 minutes and resuspended in iGB medium. B cell numbers were counted and re-seeded at a density of 20,000 cells/mL onto a new plate with adherent irradiated 40LB feeder cells in iGB medium, supplemented with 10 ng/mL IL-21 (Peprotech, Cat. No. 2010-21). The remaining harvested cells were processed for FACS analysis. Subsequently, the iGB cells were dissociated, diluted and re-seeded in IL-21-containing medium every second day until day 10.

For the survival assay of PC-like cells, some iGB cells were alternatively seeded onto a confluent adherent layer of non-irradiated EL08 cells (303) on days 10 and 12. Additionally, in some iGB cultures, the medium was supplemented with different combinations of 10 ng/mL IL-21 (Peprotech, Cat. No. 2010-21), 100 ng/mL APRIL

(Peprotech, Cat. No. 315-13) and 10 ng/mL IL-6 (Novus Biologicals, Cat. No. 406-ML) on days 10 and 12.

Calculation of theoretical iGB cell numbers

Theoretical cell numbers per measurement timepoint were calculated, to account for the assumption that no dilution of iGB cells has been performed. For calculation of theoretical cell numbers, the number of cell divisions (n) of iGB cells between two measurement timepoints (t_1, t_0) was calculated from the cell number increase between two measurement timepoints (N_1, N_0): $n = (\log(N_t) - \log(N_0)) / \log(2)$. The theoretical cell number was then calculated as $N_{1-theor} = N_{0-theor} * 2^n$.

iGB FasL killing assay

To assess the sensitivity of iGB cells towards Fas-induced cell death, FasL-expressing 40LB feeder cells (304) (40LB-FasL) were irradiated (120 Gy, γ -rays) and seeded into petri dishes to form a confluent layer. iGB cells, which were previously kept in IL-4 containing iGB medium for 4 or 6 days, were seeded onto 40LB-FasL cells. The fraction of dead 7-AAD stained iGB cells was assessed by flow cytometry 4, 6, 8 and 20 hours after seeding them onto 40LB-FasL cells.

3.10.2 *Ex vivo* cytokine stimulation

For the analysis of cytokine production potential, 40 million splenocytes were used. For each sample, 2/3 of cells were stimulated *ex vivo* and 1/3 were used as unstimulated control. Splenocytes were resuspended in B cell medium at a concentration of 10×10^6 cells/mL. The stimulated samples were supplemented with 100 ng/ml Phorbol-12-myristat-13-acetat (PMA, InvivoGen, Cat. No. tlrl-pma), 1 μ M ionomycin (Merck Millipore, Cat. No. 407951) and 2 μ M monensin (eBioscience, Cat. No. 00-4505-51), while the unstimulated controls were only treated with 2 μ M monensin. The samples were incubated for 4 hours at 37 °C. Subsequently, the cells were washed with PBS (Gibco, Cat. No. 14190-169) and stained for flow cytometric analysis. For staining of intracellular cytokines, the cells were fixed with 2% formaldehyde (Carl Roth, Roti-Histofix 4%, Cat. No. P087.4, diluted 1:1 with PBS) for 30 minutes at 4 °C and the intracellular staining antibodies were incubated overnight.

3.10.3 TNF stimulation *in vitro*

Per mouse three replicates of three million splenocytes per well were seeded into two 96-well plates, each. After centrifugation, the cells of the three replicates were resuspended in B cell medium, supplemented with either 10 ng/mL or 100 ng/mL TNF (Peprotech, Cat. No. 315-01A) or without TNF. Subsequently, the two plates were incubated at 37 °C for 3 hours or 24 hours, respectively. At the time of seeding, four million splenocytes were additionally prepared for flow cytometric analysis (timepoint 0 hours). After incubation,

the cells were harvested and also prepared for flow cytometric analysis of apoptosis. Therefore, the cells were stained with the CaspGLOW Fluorescein Active Caspase Staining kit (BioVision, Cat. No. K180-25) and Annexin V Apoptosis Detection kit (eBioscience, Cat. No. 88-807-72) according to the manufacturers' instructions.

3.11 Statistical analysis

Graphs

Boxplots extend from the 25th to 75th percentile, individual values are shown as circles and the median is highlighted with a thick line. If only mean values are shown, error bars represent the standard deviation (SD). If not stated otherwise, male and female mice were combined for the analyses. Graphs and heatmaps were generated with GraphPad Prism (version 7.0 to 9.4.1) or with R version 4.1.3 (GUI 1.77 High Sierra build (8051)).

Normality and significance

Normal distribution of the data was assessed by the Shapiro-Wilk test. If all groups followed a normal distribution, an Unpaired t test with Welch's correction was performed to compare two specific groups or an Uncorrected Fisher's LSD test for multiple population comparisons was performed to compare all groups within the experiment. In case one or more groups did not follow a normal distribution according to the Shapiro-Wilk test, the Kolmogorov-Smirnov test or the Uncorrected Dunn's test were performed, respectively. Statistical analysis was performed with GraphPad Prism (version 7.0 to 9.4.1) unless stated otherwise in the figure legend.

Calculation of the relative surface marker expression

The geometric mean fluorescence intensity (gMFI) of specific markers or GFP, as assessed by flow cytometry, was calculated with FlowJo v10. The relative expression was calculated by dividing the gMFI of the experimental cell populations by the mean gMFI of CD19Cre control cell populations, acquired in the same experiment. The relative expression values were transformed to log₂ (log₂-fold change). The mean log₂-fold change value from all analyzed samples was depicted in a heatmap or all individual values were depicted in a boxplot.

4 RESULTS

Mice with B cell-specific homo- and heterozygous loss of A20 develop autoantibodies (280-282). However, the pathology only occurs at high age and is most prevalent in female mice with heterozygous A20-deficiency. Also, the increased expression of anti-apoptotic BclxL is implicated in autoimmunity in mice, as it raises the likelihood of autoreactive B cells to escape negative selection (151, 152). Both haploinsufficiency of A20 as well as defective apoptosis are known to be involved in the human SLE pathology (189, 207, 208, 241, 305). In these systemic autoimmune patients, disease development is thought to require the combination of more than one autoimmunity-predisposing genetic alteration (43). To experimentally reproduce this multimodal disease initiation, I combined A20-deficiency (280) with B cell restricted E μ -BclxL transgene (117) expression, thereby rendering B cells hyperreactive towards NF- κ B signaling and enhancing their resistance towards apoptosis (**Figure 5A**).

4.1 Analysis of B-BclxL^{tg} A20-deficient mice

4.1.1 Enhanced BclxL^{tg} expression does not protect GCB-like cells from Fas-induced cell death

One suggested mechanism by which A20-deficient B cells break tolerance is their increased expression of the anti-apoptotic protein BclxL upon CD40 stimulation. This was suggested to protect B cells against Fas-induced cell death, thereby allowing autoreactive B cells to escape counterselection in the germinal center (281).

Using intracellular flow cytometry, I confirmed that *ex vivo* isolated splenic B as well as GCB cells from A20 knockout (B-A20^{-/-}) mice contained higher levels of BclxL compared to cells from A20 heterozygous (B-A20^{-/wt}) and control (Ctl) mice. Additional B cell-specific expression of an E μ -BclxL transgene (B-BclxL^{tg}) (117) further increased intracellular BclxL levels independent of the A20 zygosity (Figure 5A, B). Overall, the expression of BclxL appeared to be higher in GCB cells compared to naïve B cells in all genotypes.

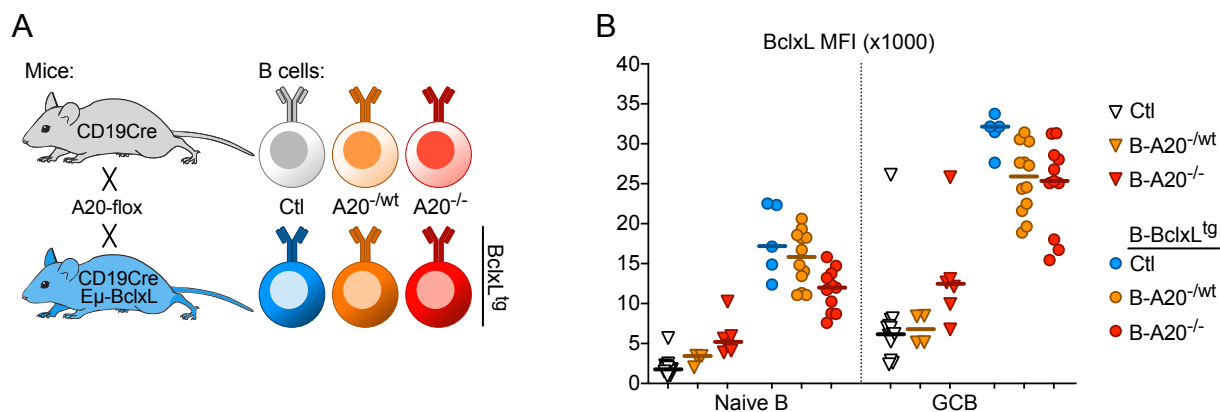


Figure 5. BclxL expression in A20-deficient B cells.

(A) Scheme depicting the genetics of mice and their respective B cells. **(B)** Mean fluorescence intensity of intracellular BclxL-PE in naïve B (CD19⁺ B220⁺) and germinal center B (GCB, CD19⁺ B220⁺ Fas⁺ CD38^{low}) measured by flow cytometry. Data points represent individual samples and lines depict the mean per group. No statistical testing was performed.

Through co-culture with fibroblasts expressing CD40L and BAFF (40LB feeder cells) and addition of IL-4, I generated *in vitro*-derived germinal center B (iGB) cells (302), which resemble GCB phenotypically (**Figure 6A**). Being an NF-κB target gene, BclxL expression was increased upon stimulation in the iGB culture, and its induction was especially strong in A20^{-/-} iGB cells. (**Figure 6B**). Consequently, I was able to confirm the previously published observation that BclxL expression is induced in B cells upon CD40 stimulation and that its induction is particularly strong in the absence of A20 expression (281).

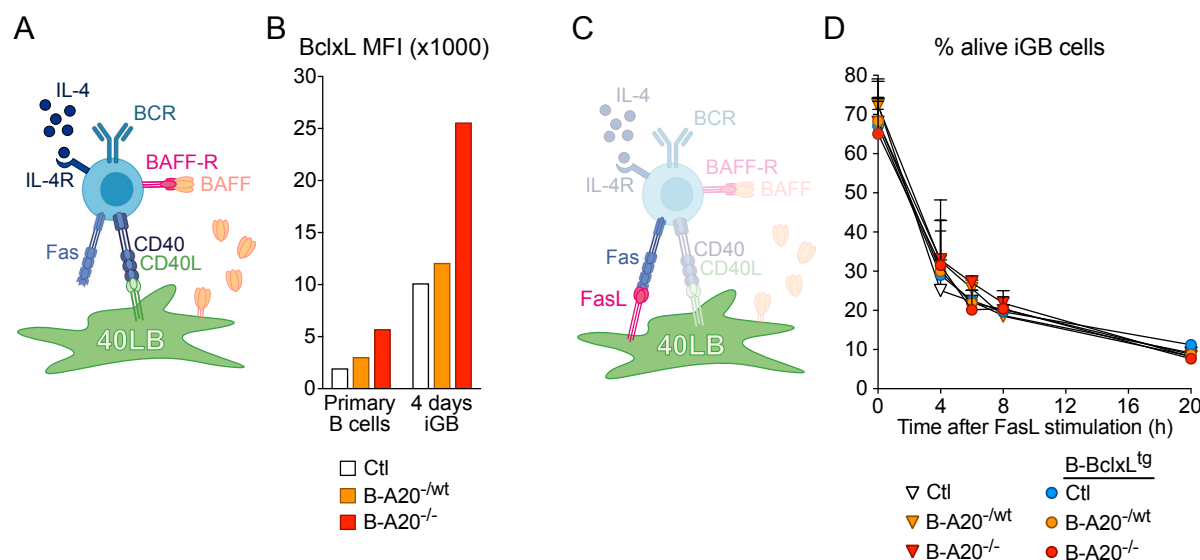


Figure 6. BclxL expression does not protect iGB cells against Fas-induced cell death.

(A) Scheme depicting the stimulation of B cells in the iGB culture system (302). **(B)** Mean fluorescence intensity (MFI) of intracellular BclxL-PE measured in B cells by flow cytometry in ex-vivo isolated primary B cells and in iGB cells after 4 days of culture. Each bar represents one biological replicate. **(C)** FasL expression on 40LB feeder cells in the iGB culture system. **(D)** Fraction of living iGB cells over time after co-culture with FasL-expressing 40LB feeder cells. Mean values and SD from 1 to 3 replicates, measured in 2 independent experiments, are shown.

In the germinal center, the intrinsic apoptosis pathway - induced mainly by nutrient scarcity and DNA damage - is crucial for the negative selection of low-affinity GCB cell clones. It is therefore likely that enhanced expression of anti-apoptotic BclxL through the B-BclxL^{tg} can increase the survival of GCB cells. However, whether the FasL-dependent apoptosis pathway in GCB cells employs the mitochondria-independent (type I) or the mitochondria-dependent (type II) pathway has - to my knowledge - not yet been investigated experimentally. Co-cultures with 40LB feeder cells, which additionally express FasL (**Figure 6C**) (304), allow the Fas-mediated selection of iGB cells. With these co-cultures, I observed that neither A20-deficiency, nor E μ -BclxL transgene expression, nor both combined protected the B cells from Fas-induced apoptosis (**Figure 6D**). This data shows that iGB cells stimulated with membrane-bound FasL exert Fas-induced apoptosis via the type I pathway, which cannot be inhibited by BclxL or other Bcl2 family members (306).

Collectively, I confirmed that BclxL expression is increased in B cells lacking A20 and can be further enhanced by combined CD40, BAFF and IL-4 stimulation. Importantly, I demonstrated that A20-deficiency and increased BclxL expression did not protect GCB-like iGB cells from Fas-induced apoptosis.

4.1.2 B cell subsets in B-BclxL^{tg} A20-deficient mice

Previously published data of A20-deficiency specifically in B cells (using CD19Cre mice) (280-282) suggested a possible enhancement of autoimmunity upon combined B cell-specific BclxL^{tg} expression and A20-deficiency. To verify this, I generated a mouse line with combined B cell-specific BclxL^{tg} expression and A20 deficiency. B-A20^{-/-}, B-A20^{-/wt} and control mice with and without B-BclxL^{tg} expression were born at mendelian ratios, excluding any detrimental effects during fetal development (**Supplementary Figure 1**). Both genetic modifications target all mature B cell subsets, boosting their NF- κ B dependent activation as well as protection against intrinsic apoptosis. For this reason, I expected an effect on the composition of immune cells, most prominently an expansion of the B lineage cell numbers. I therefore first investigated cellular changes in the immune cell composition within the secondary and primary lymphoid organs. For this project, I mainly analyzed young mice aged 3 to 5 months (whenever graphs contain data from mice younger or older than 3 to 5 months, this is indicated in the figure legend and main text).

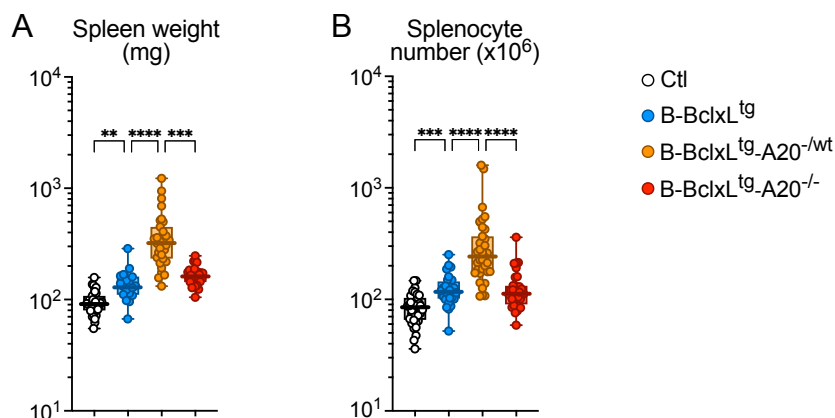


Figure 7. Spleen weight and cellularity in B-BclxL^{tg}-A20 mice.

(A) Spleen weight and (B) absolute numbers of splenocytes in mice with the indicated genotypes. Data is displayed as box-whisker-plot. Dots represent individual samples, and thick lines highlight the median value. Assessment of normality and statistical testing were performed as described in the Methods section (chapter 3.11). Only relevant comparisons are depicted on the graphs.

Compared to CD19Cre control (Ctl) mice, B-BclxL^{tg} expression induced a slight increase of the average spleen weight. The simultaneous loss of one copy of A20 (B-BclxL^{tg}-A20^{-/wt}) led to an additional more than 2-fold increase of the average spleen weight. In contrast, mice with a loss of both copies of A20 (B-BclxL^{tg}-A20^{-/-}) had spleen weights comparable to B-BclxL^{tg} mice (**Figure 7A**). Corresponding to the extent of splenomegaly, also the absolute number of splenocytes was strongly elevated in B-BclxL^{tg} A20^{-/wt} but not in B-BclxL^{tg}-A20^{-/-} mice (**Figure 7B**).

I next analyzed the effect of combined BclxL^{tg} expression and loss of A20 on terminal B cell differentiation in the spleen. As expected upon enhanced B cell survival (152), the total number of immature peripheral B cells in the spleen was increased in all mice with B-BclxL^{tg} expression (**Figure 8A**). Analysis of the splenic cell composition within the mature B cell subset revealed that the major fraction was shifted towards the B2 lineage in B-BclxL^{tg} and B-BclxL^{tg}-A20^{-/wt}, and towards the B1 lineage in B-BclxL^{tg}-A20^{-/-} mice (**Figure 8B, C**). Within the B1 compartment, the distribution was skewed towards the B1b subclass in B-BclxL^{tg} and B-BclxL^{tg}-A20^{-/wt} but not in B-BclxL^{tg}-A20^{-/-} mice (**Figure 8D**).

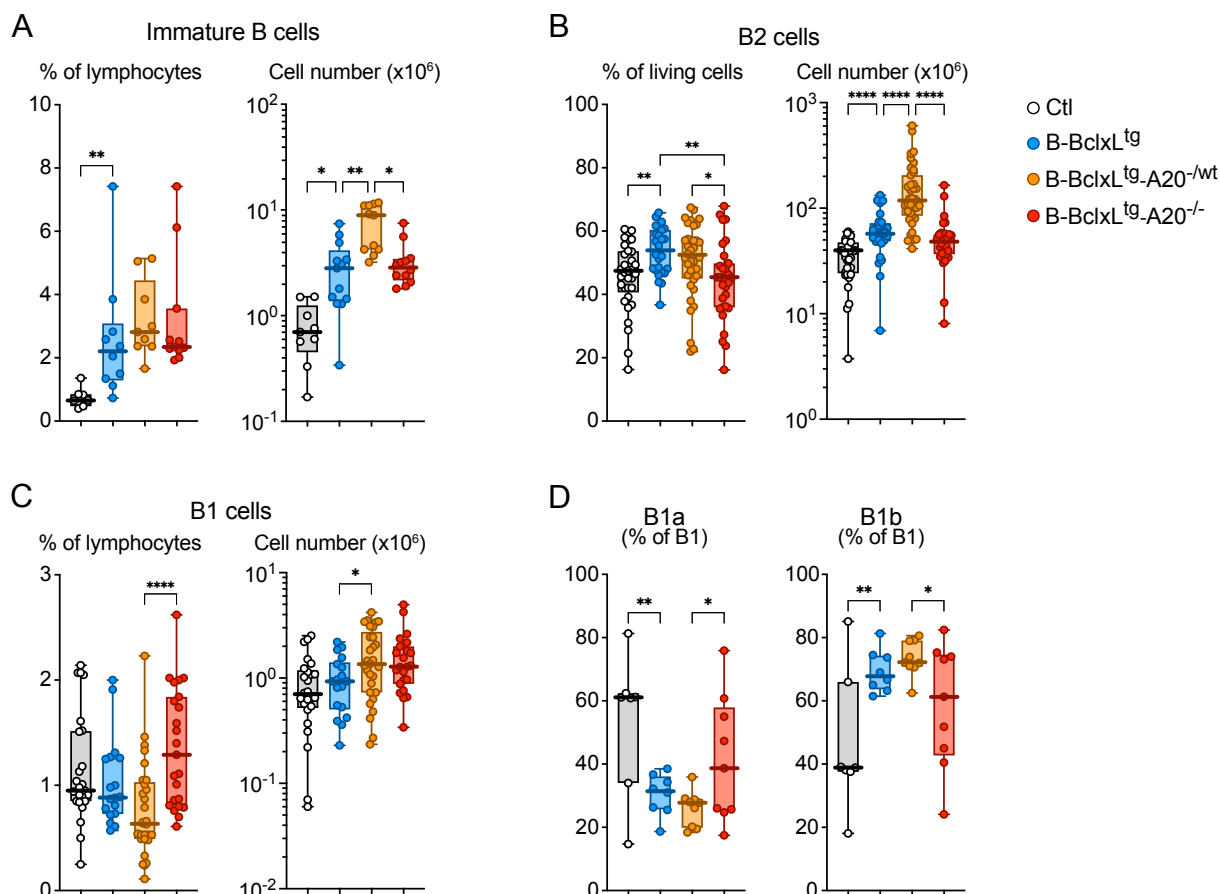


Figure 8. Splenic B cell subsets in B-BclxL^{tg}-A20 mice.

(A-C) Fraction and absolute numbers of **(A)** immature B cells (AA4.1⁺ B220⁺), **(B)** B2 cells (CD19⁺, B220⁺) and **(C)** B1 cells (CD19⁺, B220^{low}). **(D)** Fraction of B1a (CD5⁺) and B1b (CD5⁻) within B1 cells. Data is displayed as box-whisker-plot. Dots represent individual samples, and thick lines highlight the median value. Assessment of normality and statistical testing were performed as described in the Methods section (chapter 3.11). Only relevant comparisons are depicted on the graphs.

In correlation with the total splenocyte number (see **Figure 7B**), the absolute number of immature, as well as mature B1 and B2 cells was highest in the spleens from B-BclxL^{tg}-A20^{-wt} mice (**Figure 8A-C**, right panels). However, despite the apparent splenomegaly, their percentage of B2 cells among all living splenocytes was barely altered compared to B-BclxL^{tg} controls (**Figure 8B**, left panel). This shows that in concert with B cells also other splenic immune cell types must be expanded (see chapters 2.1.5 & 2.1.6). Surprisingly, in B-BclxL^{tg}-A20^{-/-} mice, the fraction and absolute number of B2 cells were lower compared to B-BclxL^{tg} control mice, while their spleen size was largely similar (**Figure 8B** and see **Figure 7A, B**). This indicated a detrimental effect of complete A20-deficiency on B2 cell expansion.

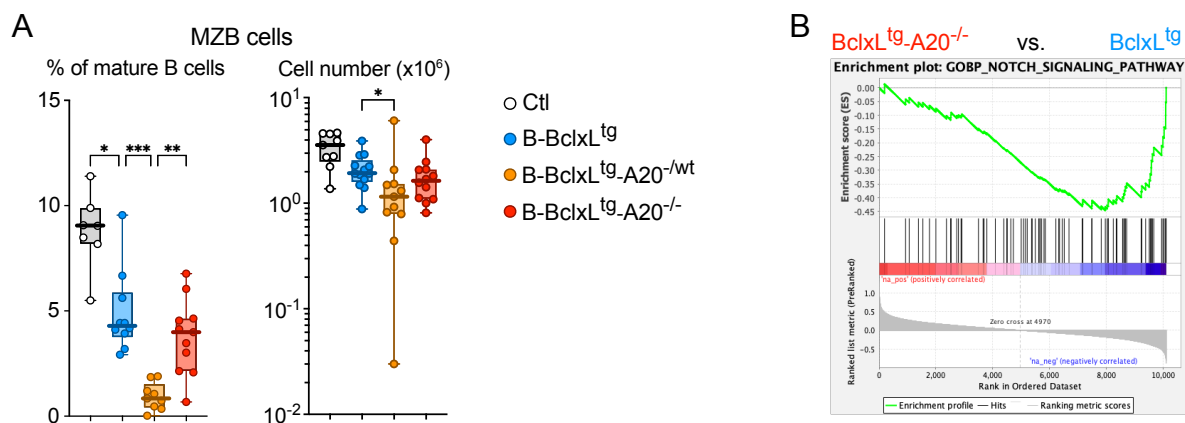


Figure 9. Marginal zone B cells in B-BclxL^{tg}-A20 mice.

(A) Fraction and absolute numbers of marginal zone B (MZB) cells (AA4.1⁻ B220⁺ CD1d⁺ CD21⁺). Data is displayed as box-whisker-plot. Dots represent individual samples, and thick lines highlight the median value. Assessment of normality and statistical testing were performed as described in the Methods section (chapter 3.11). Only relevant comparisons are depicted on the graphs. **(B)** Gene set enrichment analysis (GSEA) for genes involved in Notch signaling, taken from the GOBP database. Bulk RNA sequencing data from 1000 sorted B220⁺ CD19⁺ CD95⁻ CD38⁺ cells from 4 to 5 B-BclxL^{tg}-A20^{-/-} and B-BclxL^{tg} mice were analyzed.

Our laboratory and others had previously shown that B cell specific complete loss of A20 in B cells (B-A20^{-/-}) influences the terminal B cell differentiation by enhancing follicular B (FolB) and germinal center B (GCB) cell expansion at the expense of marginal zone B (MZB) cell differentiation (280-282). I found that also in the context of BclxL^{tg} expression, MZB cells were significantly reduced in B-BclxL^{tg}-A20^{-/-} mice. Unexpectedly, this effect was even stronger in B-BclxL^{tg}-A20^{-/wt} mice (**Figure 9A**). The reduced amount of MZB cells indicated that A20-deficiency skews B2 cell differentiation towards a FolB-fate, likely through potentiated NF- κ B and simultaneously reduced Notch2 signaling (11, 307). To investigate the gene expression patterns underlying the differentiation fates of B cells with different A20 gene dose, I performed bulk RNA sequencing on sorted cells. In line with the assumption that A20-deficiency reduces the drive towards MZB differentiation, BclxL^{tg} A20^{-/-} non-GCB cells had a reduced expression of Notch signaling genes compared to BclxL^{tg} control cells (**Figure 9B**).

4.1.2.1 Heterozygous loss of A20 cooperates with BclxL^{tg} expression to drive a strong expansion of GCB cells

While MZB cell numbers were reduced, GCB cells were strongly expanded upon BclxL^{tg} expression and even more expanded upon heterozygous but not homozygous A20 deletion (**Figure 10A**). In CD19Cre control mice, GCB cells made up less than 2% of B cells, which is similar to the amount reported for unimmunized wildtype mice housed under SPF conditions (308) (**Figure 10A**, left panel).

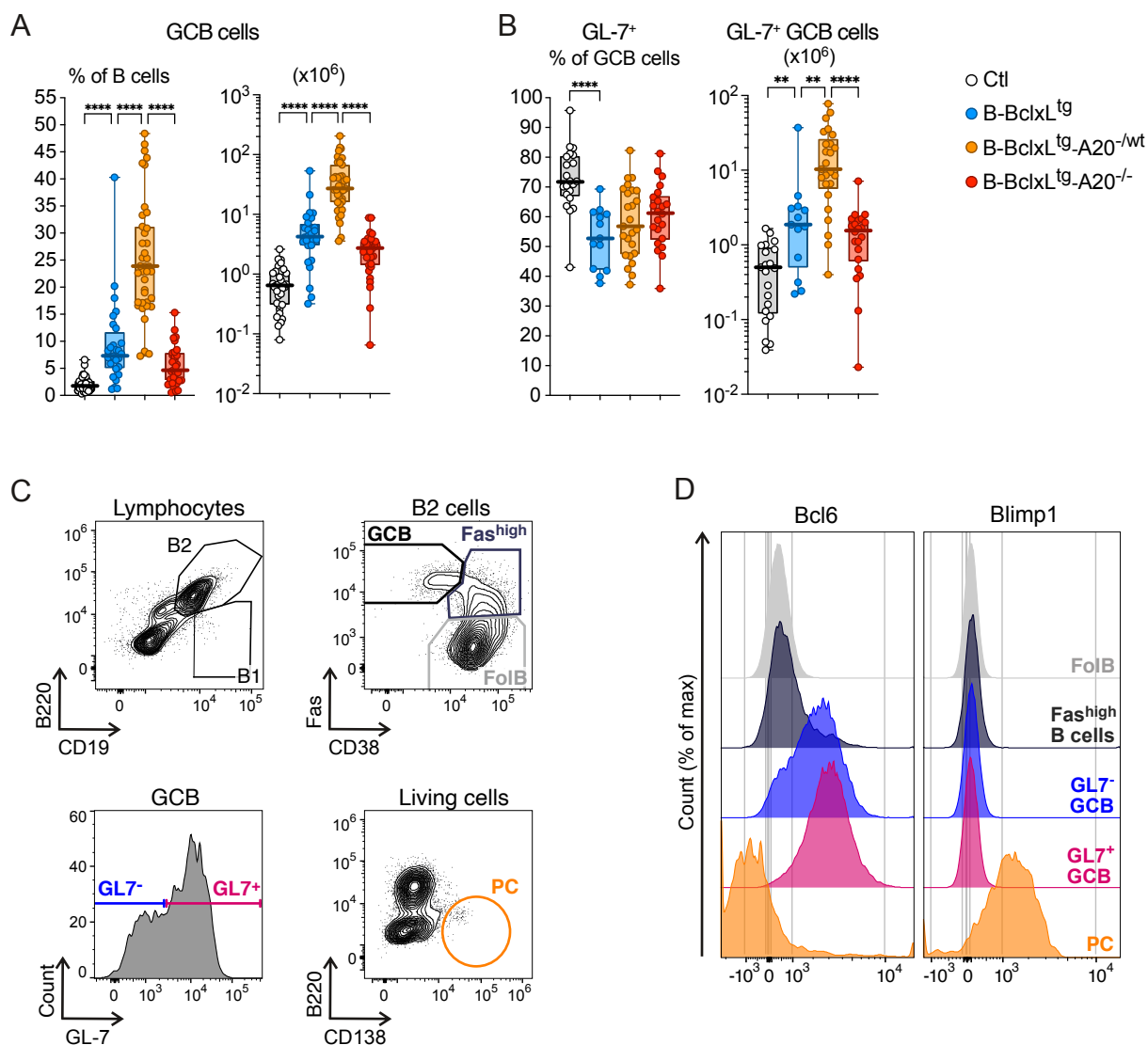


Figure 10. Splenic GCB cells in B-BclxL^{tg}-A20 mice.

(A) Percentage and absolute number of GCB cells in spleen. **(B)** Percentage of GL7-positive (GL7⁺) GCB cells and absolute number of splenic GL7⁺ GCB cells. **(C)** Representative flow cytometry plots and histogram for splenic GCB cells of a B-BclxL^{tg} mouse, indicating the gating strategy used to define the populations reported in (D). **(D)** Histograms for the intracellular expression of BCL6 and Blimp1 in follicular B cells (FolB, B220⁺ CD19⁺ CD38⁺ Fas⁻), Fas^{high} B cells, GL7⁺ and GL7⁻ GCB (B220⁺ CD19⁺ CD38⁺ Fas^{high}) and plasma cells (PC, B220^{low} CD138⁺) of a representative B-BclxL^{tg} mouse. The color code corresponds to the flow cytometry plots (C). (A-B) Data is displayed as box-whisker-plot. Dots represent individual samples, and thick lines highlight the median value. Assessment of normality and statistical testing were performed as described in the Methods section (chapter 3.11). Only relevant comparisons are depicted on the graphs.

In B-BclxL^{tg} mice, the fraction of GCB cells expanded 4-fold and in B-BclxL^{tg}-A20^{-/-wt} mice more than 20-fold compared to controls (**Figure 10A**, left panel). In the latter, approximately 25 % of all splenocytes were GCB cells, corresponding to a total of 27x10⁶ GCB cells per spleen on average (**Figure 10A**, right panel). Surprisingly, B-BclxL^{tg}-A20^{-/-} mice had slightly lower fractions and numbers of GCB cells compared to B-BclxL^{tg} control mice (**Figure 10A**). However, the ability of B cells from B-BclxL^{tg}-A20^{-/-} mice to undergo the germinal center reaction was not impaired, which is further proven by the existence of follicular helper T (T_{fh}) cells and class switched plasma cells in these mice (see **Figure 13** and **Figure 20**).

The expansion of GCB cells depends on the stimulation of the BCR by cognate antigen and on their co-stimulation by activated T_{fh} cells. Physiologically, this condition is induced by pathogens entering the body and exhibiting foreign antigen. All analyzed mice were housed under controlled SPF conditions and mice with the three different A20 zygositys were born as litter mates and housed together. Therefore, the observed GCB cell expansion occurred under non-infectious conditions, and must have been triggered either by commensal bacteria or autoantigens present in the body. This issue will be further elucidated in chapter 4.2.

GCB cells in mice can be identified by their high surface expression of CD95/Fas and a downregulation of CD38 expression (**Figure 10C**). Additionally, the anti-glycan antibody GL7, which recognizes alpha2,6 Sia Neu5AC on activated B cells, is frequently used to define GCB cells (20, 309). Interestingly, BclxL^{tg} expression induced a large population of the GL7-negative GCB cells (GL7⁻, 50 %). The fraction of GL7⁻ GCB cells remained elevated also upon additional heterozygous and homozygous A20 deletion (45 - 40 %) (**Figure 10B**, C). Nevertheless, also the absolute number of splenic GL7⁺ Fas^{high} CD38⁻ GCB cells was significantly higher in B-BclxL^{tg}-A20^{-/-wt} mice compared to B-BclxL^{tg} and B-BclxL^{tg}-A20^{-/-} mice (**Figure 10B**). Both, GL7⁺ and GL7⁻ Fas^{high} CD38⁻ cells, were positive for the GCB cell key transcriptional regulator Bcl6 and negative for the plasmacytic marker Blimp1, while Fas^{high} CD38⁺ activated B cells were negative for Bcl6 and CD138⁺ B220^{low} plasma cells expressed Blimp1 (**Figure 10D**). Therefore both, GL7⁺ and GL7⁻ Fas^{high} CD38⁻ cells, were included in the GCB cell gate for all subsequent analyses.

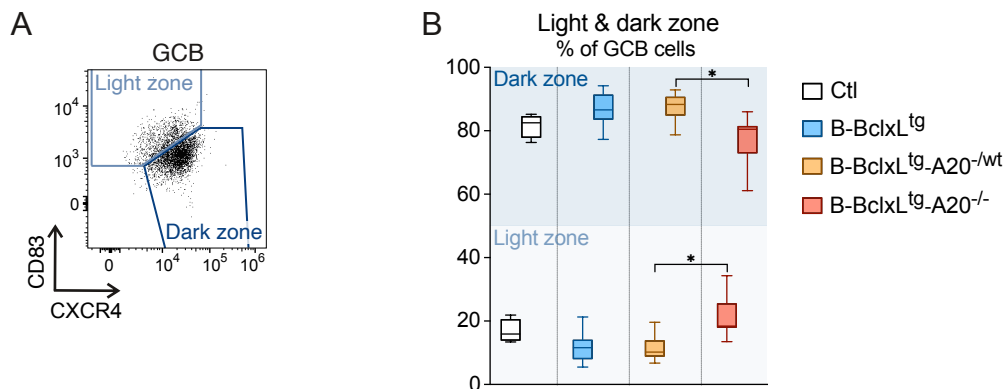


Figure 11. Light zone / dark zone distribution.

(A) Representative FACS plot depicting the gating strategy for light zone and dark zone cells within CD19⁺ B220⁺ CD95^{high} CD38^{low} GCB cells in a CD19Cre control mouse. (B) Percentage of GCB cells with a light zone (CD83^{high} CXCR4^{low}) or dark zone (CD83^{low} CXCR4^{high}) phenotype. Data is depicted as box plots. Assessment of normality and statistical testing were performed as described in the Methods section (chapter 3.11). Only relevant comparisons are depicted on the graphs.

Phenotyping revealed that BclxL^{tg} as well as BclxL^{tg} A20^{-wt} GCB cells had an increased fraction of CXCR4^{high} CD83^{low} centroblasts, which reside in the dark zone (DZ) of the germinal center (**Figure 11A, B**). Since the DZ is the location of high proliferation, this matches with the high number of GCB cells observed in these mice. In the light zone (LZ), CXCR4^{low} CD83^{high} centrocytes (**Figure 2.1.7A, B**) compete for T_{fh} cell help to avoid apoptosis and allow either re-entry to the DZ or exit from the germinal center for plasma cell or memory B cell differentiation. BclxL^{tg} A20^{-/-} GCB cells had a higher fraction of LZ centrocytes compared to BclxL^{tg} A20^{-wt} GCB but similar to Ctl GCB cells, indicating an overall diminished proliferation and a higher selective pressure (**Figure 11A, B**).

The generally lower number of GCB cells in B-BclxL^{tg}-A20^{-/-} mice (see **Figure 10A**) might additionally be caused by a premature exit from the germinal center due to enhanced plasmacytic differentiation. A reduced time spent in the germinal center and consequently fewer rounds of cycling and somatic hypermutation (SHM) would entail a reduced accumulation of mutations in the BCR gene locus.

The BCR mutation frequency was analyzed by Dr. Yuanyuan Chu in A20-deficient mice without BclxL^{tg} expression 14 days after immunization with NP-CG (unpublished data from our group). Indeed, A20^{-/-} GCB cells had a decreased mutation frequency in the BCR (**Figure 12A**) and less high affinity W33L hotspot mutations (**Figure 12B**), indicating reduced affinity maturation. This supports the notion that A20^{-/-} GCB cells cycle a reduced number of iterations within the germinal center. This could have several reasons, including an increased sensitivity of A20^{-/-} GCB cells towards intrinsic or Fas-induced apoptosis, less help from cognate T cells or an enhanced plasmacytic differentiation.

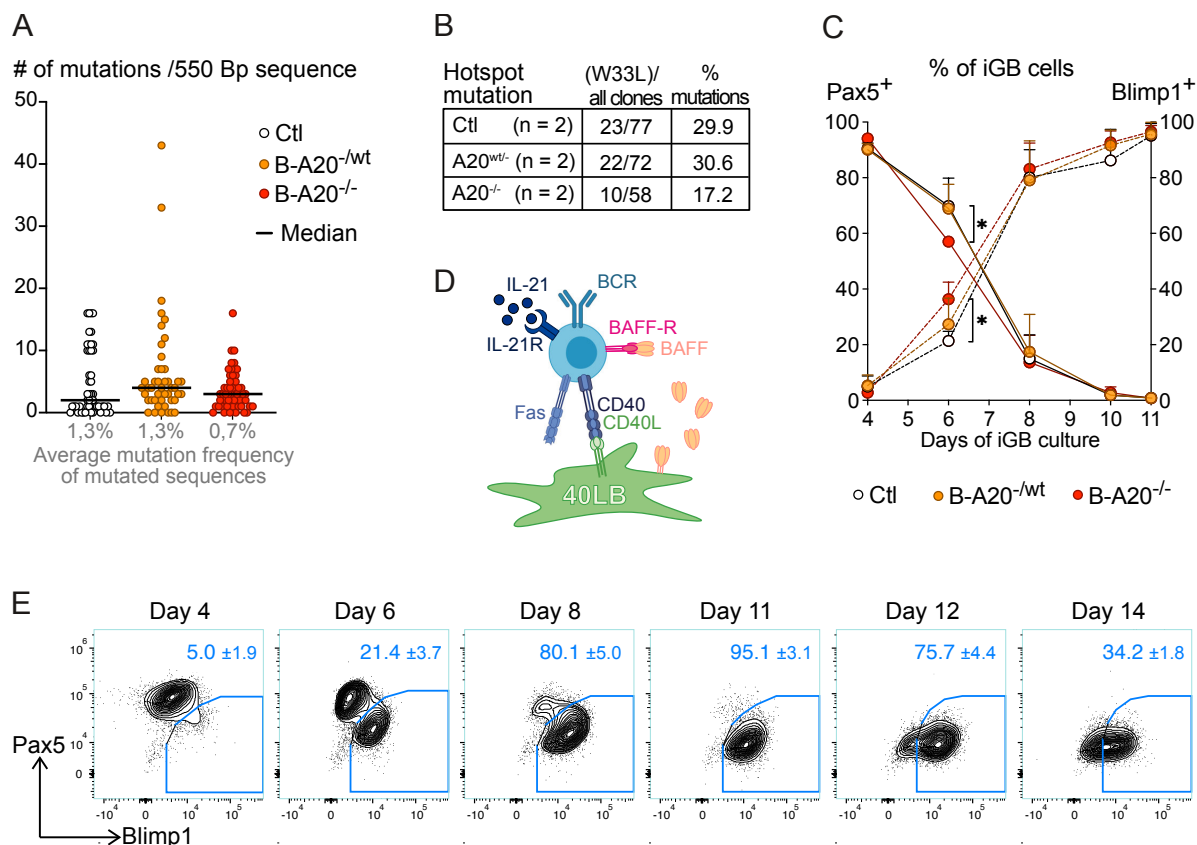


Figure 12. Premature exit of A20 homozygous B cells from the germinal center.

(A) Assessment of somatic hypermutation in FACS-purified splenic GCB cells 14 days after immunization with NP-CG. Mutations in individual unique sequences within a 550 Bp region in the intron downstream of the rearranged VH-DH-JH4 joints are shown. Below each scatter plot the mean mutation frequency of the mutated sequences is shown. (B) Frequency of the high-affinity tryptophan to leucine (W33L) mutation in codon 33. Unique sequences were amplified from the V186.2 gene by PCR using primer pairs, which anneal in the V186.2 and JH2 genes. DNA was purified from splenic GCB cells at day 14 after immunization with NP-CG. (C) Fraction of Pax5⁺ and Blimp1⁺ iGB cells on days 4 to 11 of the iGB cell culture (302): on day 0, B cells were seeded on a feeder layer expressing CD40L and BAFF and incubated in the presence of IL-4. After four days IL-4 was replaced with IL-21 and Pax5 and Blimp1 expression was analyzed until day 11. Mean values and SD from 3-4 biological replicates analyzed in 2-3 independent experiments are depicted for the Pax5⁻ and Blimp1⁺ iGB populations. Assessment of normality and statistical testing were performed as described in the Methods section (chapter 3.11). Only relevant comparisons are depicted on the graphs. (D) Scheme depicting the survival signals, which B cells receive from 40LB feeder cells in the iGB culture (302). (E) Representative FACS plots showing the development of intracellular Pax5 and Blimp1 expression in iGB cells on days 4, 6, 8, 10, 12 and 14 of culture for CD19Cre control iGB cells with serial dilution and re-seeding on a fresh layer of 40LB feeder cells on every second day. (A-B) BCR mutation analyses were performed by Yuanyuan Chu. Data used with permission.

After several rounds of positive selection and proliferation, GCB cells upregulate the transcriptional repressor Blimp1, repressing the expression of Bcl6 as well as the B cell lineage gene Pax5, and thereby initiate plasmacytic differentiation. To investigate the cell intrinsic drive of A20^{-/-} B cells towards plasmacytic differentiation, I monitored the changes in Pax5 and Blimp1 expression in induced GCB (iGB) cells, stimulated with IL-21 *in vitro*.

With the iGB culture system, originally published by Nojima et al. (302), GCB cell-like iGB cells can be generated from non-GCB cells within 4 days through stimulation with CD40L and BAFF (expressed by 40LB fibroblast feeder cells) and the addition of soluble IL-4 (see **Figure 6A**). Simultaneously, class switching to IgG1 and IgE is initiated. Subsequent stimulation with IL-21 induces the differentiation to IgG1⁺ and IgE⁺ short-lived plasmablasts (**Figure 12D**). Due to the rapid proliferation of iGB cells, an extreme cell density after 8 days of culture prohibits further expansion. Through serial dilution and re-seeding on a fresh layer of feeder cells, I was able to prolong the survival of iGB cells and until day 14 (**Figure 12E**). I quantified the fraction of Pax5⁺ GCB-like and Blimp1⁺ plasmablast-like iGB over time to get an estimate of differentiation speed. Indeed, A20^{-/-} iGB cells differentiated more rapidly from Pax5⁺ GCB-like to Blimp1⁺ plasmablast-like iGB cells (**Figure 12C**), supporting the assumption that A20-knockout in B cells favors a plasmacytic differentiation program and thereby causes premature exit from the germinal center.

The iGB cell proliferation rate rapidly decreased after day 10, simultaneous to the generation of plasmablasts with a limited capacity of self-renewal (Supplementary Figure 2A and B). I was not able to keep the plasmablasts alive in culture for longer than day 14, even upon addition of the plasma cell survival factor APRIL or co-culture with EL08 feeder cells, a cell line providing support for a range of different hematopoietic cells (303). After day 12, iGB cells lost any definite identity, corresponding to very low cell viability (**Figure 12E**) and the longevity of plasmablast-like iGB cells was independent of the A20 gene dose (**Supplementary Figure 2C**).

4.1.2.2 A20-deficiency strongly affects plasmacytic cells in the spleen

GCB cells give rise to mutated, class-switched plasmablasts, which have a short survival time and can further differentiate to long-lived plasma cells (llPC), homing to the bone marrow. Due to the lack of analyzed markers to specifically differentiate between short-lived plasmablasts and llPC, plasmacytic cells in the secondary lymphoid tissues were defined by simultaneous expression of IRF4 and CD138. These IRF4⁺ CD138⁺ cells were Blimp1⁺ (see **Figure 10D**) and included B220⁺ dividing plasmablasts (PB) as well as B220^{low} plasma cells (PC) (**Figure 13A**) (310). Therefore, IRF4⁺ CD138⁺ cells will subsequently be termed plasma cells/plasmablasts (PC/PB) or plasmacytic cells. The fraction and absolute number of splenic PC/PB was slightly increased in B-BclxL^{tg} mice and further strongly increased upon simultaneous heterozygous A20-ablation (**Figure 13B**). Despite the relatively low splenic B and GCB cell numbers in B-BclxL^{tg}-A20^{-/-} mice (see **Figure 8** and **Figure 10**), their amount of PC/PB was significantly higher than in B-BclxL^{tg} control mice (**Figure 13B**). This result further supports the notion of increased plasmacytic differentiation of BclxL^{tg} A20^{-/-} B cells, which likely happens through both germinal center-dependent as well as extrafollicular pathways.

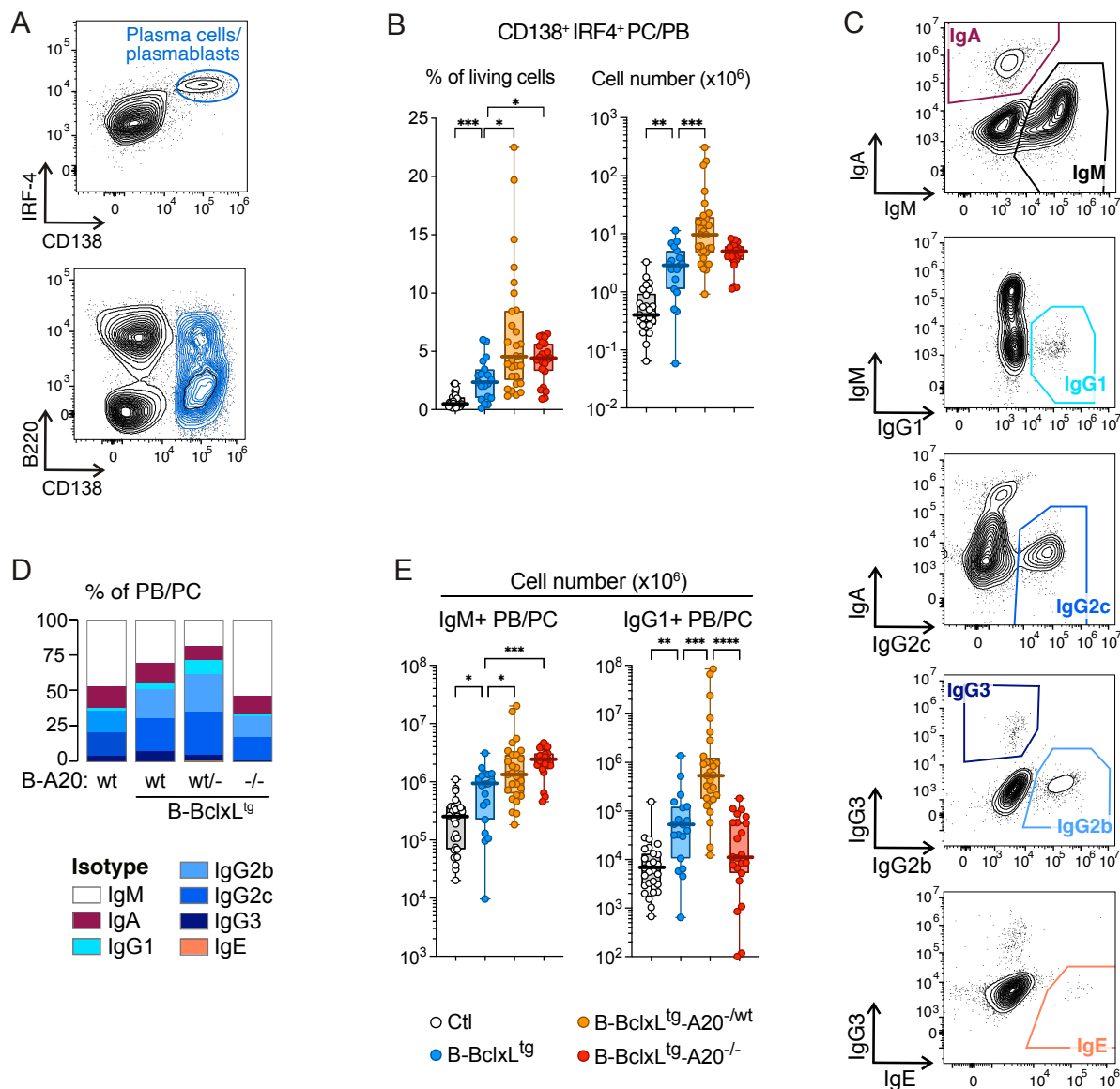


Figure 13. Class switching in the spleen of B-BclxL^{tg}-A20 mice.

(A) Representative flow cytometry plots for IRF4⁺ CD138⁺ plasmacytic cells in the spleen of a B-BclxL^{tg}-A20^{-wt} mouse, pre-gated on living single cells. (B) Percentage and total number of IRF4⁺ CD138⁺ plasmacytic cells in the spleen. (C) Representative flow cytometry plots depicting plasmacytic cell isotypes in a CD19Cre control mouse. (D) Percentage of isotypes within splenic plasmacytic cells. (E) Absolute number of IgG1⁺ and IgM⁺ plasmacytic cells in the spleen. (B, E) Data is displayed as box-whisker-plot. Dots represent individual samples, and thick lines highlight the median value. Assessment of normality and statistical testing were performed as described in the Methods section (chapter 3.11). Only relevant comparisons are depicted on the graphs.

The composition of plasma cells was defined by measuring the fraction of intracellular immunoglobulin expression within the PC/PB population (Figure 13C, D). The isotype composition varied greatly between the different genotypes: BclxL^{tg} expression induced only a slight expansion of class-switched (non-IgM) PC/PB. In mice with simultaneous heterozygous A20 deletion a large fraction of plasmacytic cells was switched to one of the IgG classes, while fewer cells were IgA⁺ and less than 20% of PC/PB remained unswitched IgM⁺ (Figure 13D). This suggested that splenic BclxL^{tg} A20^{-wt} plasmacytic cells were mainly derived from the germinal center, in line with their enormously increased number

of GCB cells (see **Figure 10A**). In contrast, the largest fraction of BclxL^{tg} A20^{-/-} plasmacytic cells was IgM⁺ and thereby either differentiated extrafollicularly and/or from unswitched GCB cells. Since the absolute number of BclxL^{tg} A20^{-/-} and BclxL^{tg} GCB cells was similar, there indeed appears to be a reduced output of switched plasmablasts from GCB cells in B-BclxL^{tg}-A20^{-/-} mice (see **Figure 10A** and **Figure 13B, D**). Correspondingly, B-BclxL^{tg}-A20^{-/-} mice had very high absolute numbers of IgM⁺ plasmacytic cells, while IgG-type (especially IgG1⁺) PC/PB were most enriched in the spleen of B-BclxL^{tg}-A20^{-/wt} mice (**Figure 13E**).

4.1.2.3 Class switching of A20-deficient B cells *in vitro*

In vivo, I observed a high number of IgG1⁺ plasmacytic cells in B-BclxL^{tg}-A20^{-/wt} and a high number of IgM⁺ plasmacytic cells in B-BclxL^{tg}-A20^{-/-} mice. To investigate if the respective B cells have an intrinsically different potential for class switching, I analyzed the isotype development (IgM, IgG1 and IgE) in A20-deficient iGB cells (without BclxL^{tg} expression) over time.

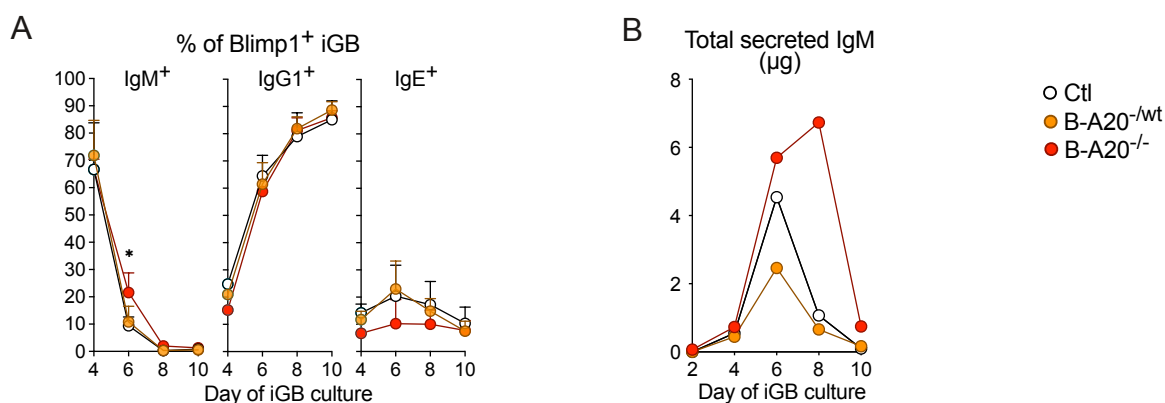


Figure 14. Class switching in the iGB culture.

(A) Fraction of IgM⁺, IgG1⁺ and IgE⁺ cells within Blimp1⁺ iGB quantified of days 4, 6, 8 and 10. Mean values and SD from 3-4 biological replicates analyzed in 2-3 independent experiments are depicted. Assessment of normality and statistical testing were performed as described in the Methods section (chapter 3.11). Only relevant comparisons are depicted on the graphs. **(B)** Concentration of IgM in the supernatant of iGB cultures measured by ELISA. Data from 1 experiment, 1 biological replicate per genotype. (A-B) iGB cells did not express the E μ -BclxL transgene. (B) iGB culture and ELISA were performed by my supervised student Sophie Levantovsky.

By day 8, almost all PC-like iGB cells had switched to either IgG1 or IgE. Interestingly, there was a slight delay of class switching in A20^{-/-} Blimp1⁺ iGB cells, showing that a larger fraction of unswitched A20^{-/-} GCB-like iGB cells differentiated to plasmablast-like iGB cells. Correspondingly, A20^{-/-} iGB cells showed a trend towards the lowest fraction of both, IgG1⁺ and IgE⁺ (**Figure 14A**). Consistent with the delayed isotype switching, A20^{-/-} plasmablast-like iGB cells secreted soluble IgM (detected in the supernatant) until day 8, while IgM secretion seized in Ctl and A20^{-/wt} iGB cells already after day 6 (**Figure 14B**).

4.1.2.4 B cell differentiation in the gut associated lymphoid tissues

Mesenteric lymph nodes (mLN) and Peyer's patches (PP) are part of the gut associated lymphoid tissues (GALT). Unlike the spleen, lymphocytes in the GALT are constantly triggered by resident commensal bacteria, and plasmacytic cells produce high levels of secreted IgA upon T cell-dependent IgA switching of B cells in the germinal center or independent of T cell help (311, 312).

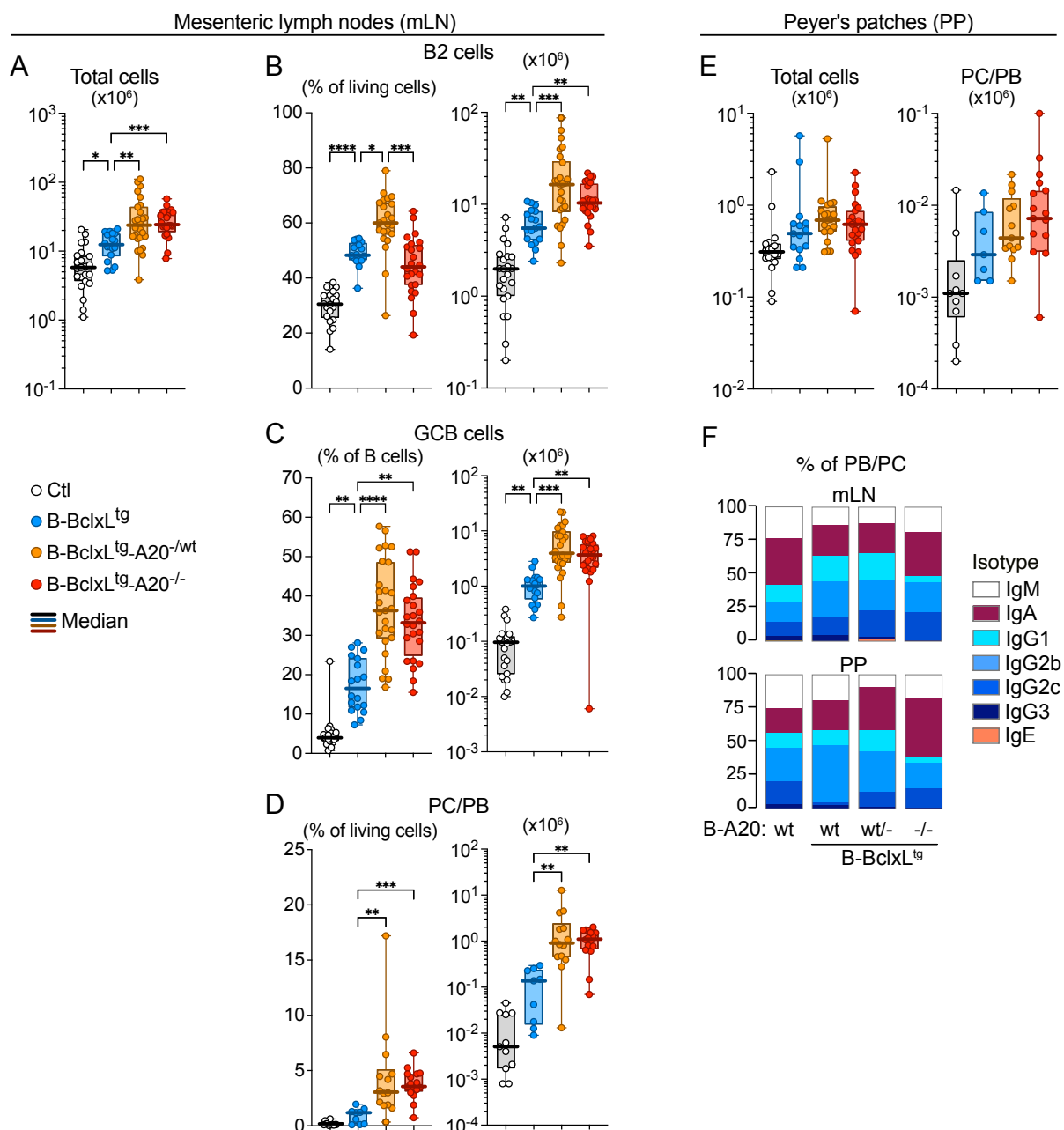


Figure 15. B cell differentiation in GALT of B-BclxL^{tg}-A20 mice.

(A) Absolute number of living cells in mesenteric lymph nodes (mLN). (B-D) Fraction and absolute number of (B) B2 cells (CD19⁺ B200⁺), (C) germinal center B (GCB, CD19⁺ B200⁺ CD95⁺ CD38⁻) cells and (D) plasma cells/plasmablasts (PB/PC, CD138⁺ B200^{low}) in mLN. (E) Absolute number of living cells (left) and plasma cells/plasmablasts (PB/PC, CD138⁺ B200^{low}, right) in Peyer's patches

(PP). **(F)** Percentage of isotypes within plasmacytic cells in mLN (upper panel) and PP (lower panel). (A-E) Data is displayed as box-whisker-plots. Dots represent individual samples, and thick lines highlight the median values. Assessment of normality and statistical testing were performed as described in the Methods section (chapter 3.11). Only relevant comparisons are depicted on the graphs.

The absolute numbers of living cells as well as B2 cells in mLN and PP were slightly increased in B-BclxL^{tg} and strongly increased in both B-BclxL^{tg}-A20^{-/wt} and B-BclxL^{tg}-A20^{-/-} mice (**Figure 15A, B, E**). The amount of GCB cells was largely equal in mLN from B-BclxL^{tg}-A20^{-/wt} and B-BclxL^{tg}-A20^{-/-} mice, both significantly higher than in B-BclxL^{tg} controls (**Figure 15C**). In contrast to spleens, the absolute number of plasmacytic cells in mLN as well as PP from B-BclxL^{tg}-A20^{-/-} exceeded the number of plasmacytic cells in B-BclxL^{tg}-A20^{-/wt} mice (**Figure 15D, E**).

The largest fraction of plasmacytic cells in GALT is typically class switched, mainly to IgA (312). BclxL^{tg} expression and heterozygous loss of A20 shifted the isotype distribution slightly towards the IgG1 and IgG2b classes. In contrast, in B-BclxL^{tg}-A20^{-/-} mice, the fraction of IgA⁺ PC/PB was expanded at the expense of all IgG classes in PP but not mLN (**Figure 15F**). The increased generation of mainly IgA⁺ PC/PB and the simultaneous expansion of GCB cells in the GALT of B-BclxL^{tg}-A20^{-/-} mice indicates an advantage of A20-knockout for T cell-dependent and -independent plasmacytic B cell differentiation in the context of strong innate triggering. Different triggers exist in the splenic microenvironment, where overall BclxL^{tg}-A20^{-/wt} were more prominently expanded than BclxL^{tg}-A20^{-/-} B and plasmacytic cells.

4.1.2.5 Long lived plasma cells in the bone marrow

Plasmacytic cells derived from the germinal center home from the secondary lymphoid organs to the bone marrow (BM) where they can reside in survival niches as long-lived plasma cells (llPC) and continue to produce antibodies. A large fraction of BM llPCs consist of GALT-derived IgA⁺ cells (312).

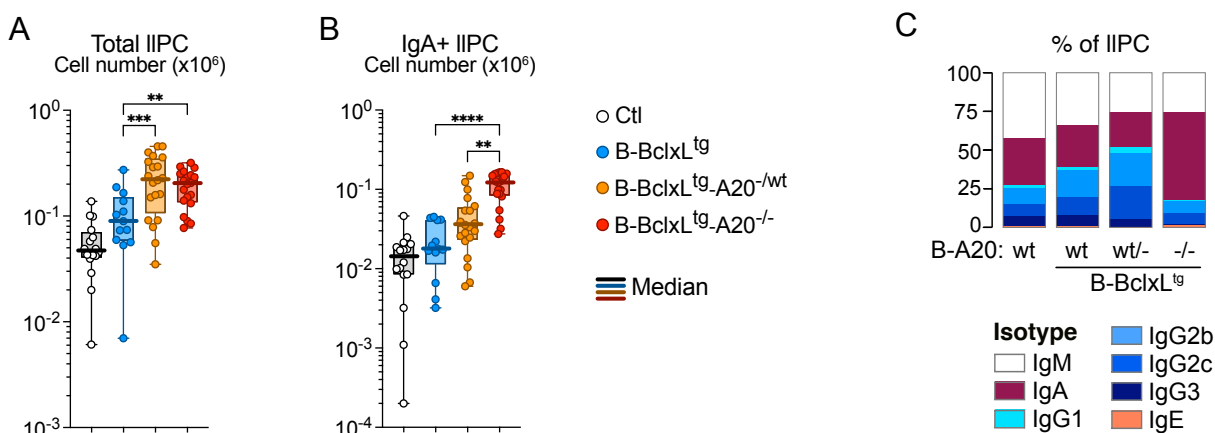


Figure 16. Long-lived plasma cells in the bone marrow.

(A-B) Absolute number of **(A)** long-lived plasma cells (llPC) and **(B)** IgA⁺ llPC in the BM. **(C)** Percentage of isotypes within BM llPCs. (A, B) Data is displayed as box-whisker-plots. Dots represent individual samples, and thick lines highlight the median values. Assessment of normality and statistical testing were performed as described in the Methods section (chapter 3.11). Only relevant comparisons are depicted on the graphs.

Both, B-BclxL^{tg}-A20^{-/wt} and B-BclxL^{tg}-A20^{-/-} mice had significantly more llPC in the BM than B-BclxL^{tg} and control mice (**Figure 16A**). In B-BclxL^{tg} and B-BclxL^{tg}-A20^{-/wt} mice, the composition of isotypes within the BM llPCs (**Figure 16C**) largely reflected the composition of isotypes in splenic PC/PB (see **Figure 13D**), showing that their high prevalence for the IgG classes was preserved in the BM llPC pool. In B-BclxL^{tg}-A20^{-/-} mice, however, the largest fraction (57 %) of llPCs expressed IgA. Strikingly, the absolute number of BclxL^{tg} A20^{-/-} IgA⁺ llPCs in the BM was almost 10-times higher than in control mice (**Figure 16B**). These IgA⁺ llPCs likely immigrated mainly from the GALT and apparently had a much higher capacity for BM homing than their IgG-switched counterparts.

4.1.3 Antibody production varies greatly between mice with heterozygous and homozygous loss of A20 in B cells

Immunoglobulins can be secreted into the blood stream by all plasmacytic cells. The antibody serum concentration in mice from all genotypes largely corresponded to the relative distribution of PC/PB isotypes in their secondary lymphoid tissues and BM (**Figure 17**). Compared to B-BclxL^{tg} mice, B-BclxL^{tg}-A20^{-/wt} mice had strongly increased serum IgG1 and slightly elevated levels of the other IgG classes, while B-BclxL^{tg}-A20^{-/-} mice had a significantly elevated serum IgM concentration. This IgM bias supports an enhanced extrafollicular differentiation of unswitched BclxL^{tg} A20^{-/-} short-lived plasmablasts. The concentration of IgA antibody was increased in the serum of both B-BclxL^{tg}-A20^{-/wt} and B-BclxL^{tg}-A20^{-/-} compared to B-BclxL^{tg} control mice but did not correspond to the dramatically expanded number of IgA⁺ II PCs in the BM of B-BclxL^{tg}-A20^{-/-} mice (**Figure 17** and see **Figure 16B**).

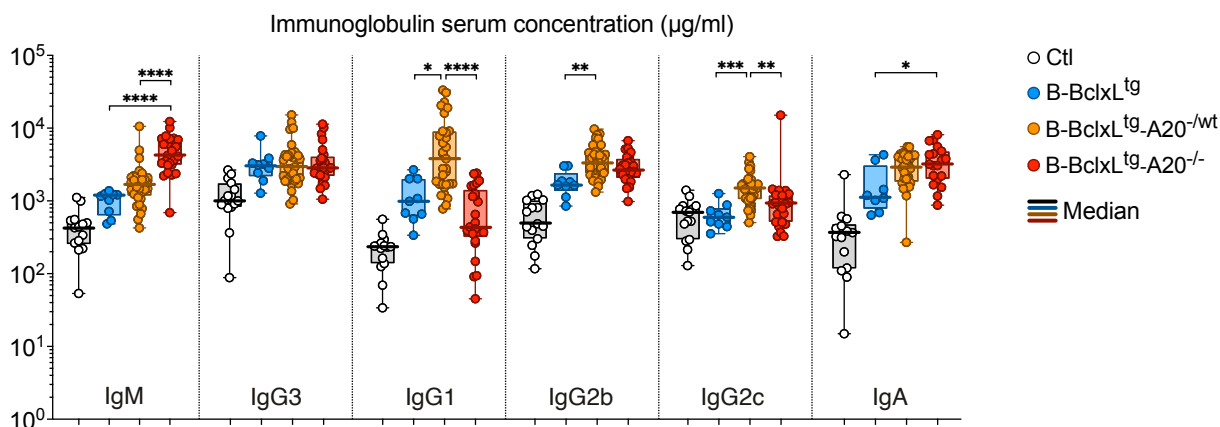


Figure 17. Serum immunoglobulin in B-BclxL^{tg}-A20 mice.

Serum concentration ($\mu\text{g/ml}$) of the indicated immunoglobulins, measured by ELISA. Data is displayed as box-whisker-plot. Dots represent individual samples, and thick lines highlight the median value. Assessment of normality and statistical testing were performed as described in the Methods section (chapter 3.11). Only relevant comparisons are depicted on the graphs.

Collectively, the analysis of B cell subsets in B-BclxL^{tg}-A20 mice demonstrated that heterozygous A20 ablation in combination with overexpression of anti-apoptotic BclxL induces an expansion of GCB cells, which is followed by the generation of a high number of class-switched plasmacytic cells. The complete loss of A20 in B cells, however, mainly increased (extrafollicular) plasmacytic differentiation to short-lived IgM⁺ plasmacytic cells in the spleen and to IgA⁺ plasmacytic cells in the GALT.

4.1.4 B cell activation

A20-deficiency increases the NF- κ B signaling strength and duration in B cells upon activation and consequently enhances the expression of cell surface activation markers. Previously published data shows that the activation of *ex vivo* isolated B cells, as measured by the surface expression of CD69, CD80 and Fas, was increased in B-A20^{-/-} mice (281). The responsiveness of B cells towards LPS or anti-CD40 stimulation *in vitro*, measured by their expression of CD86, CD25 and Fas, inversely correlated with the A20 gene dose (280).

To investigate the *in vivo* activation status of B cells with hetero- and homozygous A20 deletion on the background of BclxL^{tg} overexpression, I analyzed their surface expression of the activation markers CD25, CD44, CD62L, CD69, CD80, CD86, CD119 (IFNGR1), BAFF receptor (BAFFR), ICOS ligand (ICOSL) and MHCII by flow cytometry. Overall, BclxL^{tg} A20^{-/wt} B cells showed a strong activation signature and BclxL^{tg} A20^{-/-} B cells an intermediate activation signature compared to BclxL^{tg} control B cells (**Figure 18**).

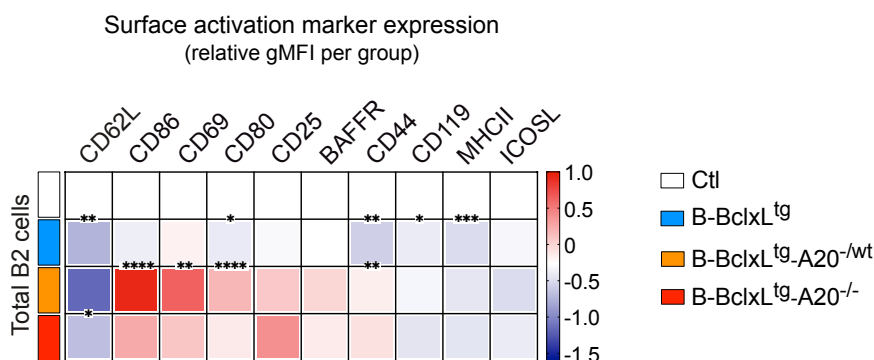


Figure 18. Surface activation markers on B cells.

Surface activation marker expression of B2 cells (B220⁺ CD19⁺). The geometric mean fluorescent intensity (gMFI) of the indicated surface markers was extracted from flow cytometry data of B220⁺ CD19⁺ B2 cells. gMFI values were normalized to the gMFI values of CD19Cre control B2 cells within each experiment. The heatmap depicts the mean log₂ values of each group. Asterisks indicate significant differences between the reported comparisons. Each value is the mean of at least 4 replicates from minimum 3 independent experiments.

B cells from all groups with BclxL^{tg} expression had reduced surface L-selectin (CD62L) (**Figure 18**). Since CD62L is being shed from B cells upon signaling through TLRs (313), the low surface CD62L on BclxL^{tg} A20^{-/wt} B cells indicates strong and persistent TLR activation.

CD44 is expressed on antigen-primed B cells (314). Interestingly, the mean expression of CD44 on BclxL^{tg} B cells was lower than in CD19Cre control cells, but higher upon simultaneous heterozygous and homozygous A20 deletion. This indicates that a higher fraction of BclxL^{tg} A20^{-/wt} and BclxL^{tg} A20^{-/-} B cells adopted an antigen-experienced phenotype *in vivo*.

I observed the strongest increase of surface expression for CD69, CD86 and CD80 on BclxL^{tg} A20^{-/wt} B cells (**Figure 18**). These three markers are all upregulated by B cells upon BCR binding to cognate antigen (34, 315). CD80 and CD86 can additionally be induced by TLR stimulation (34). Of note, B cell subpopulations *per se* express different levels of several of the analyzed markers and a high expression of CD69, CD80 and CD86 is intrinsic to GCB cells. CD69, an early activation marker on lymphocytes is induced by various activating stimuli, including BCR crosslinking. CD80 and CD86 are posing an important co-stimulatory function to T cells by binding to CD28. In B cells, CD80/CD86 signaling enhances IgG secretion (316) and CD86 is highly expressed on light zone GC B cells (317). Since GCB cells were over-represented in B-BclxL^{tg}-A20^{-/wt} mice, the MFI of CD86 was consequently higher in the total B cell population of these mice.

Surface CD25, which is generally only weakly expressed on B cells had the highest MFI on BclxL^{tg} A20^{-/-} B cells (**Figure 18**). Surface MHCII was lower on all BclxL^{tg} groups, indicating a slightly reduced APC function of these B cells. BclxL^{tg} expression also had a negative impact on the B cell surface levels of CD80 and CD119 (IFN γ receptor). The slightly increased BAFFR surface expression suggested a higher capacity of BclxL^{tg} A20^{-/wt} and BclxL^{tg} A20^{-/-} B cells to consume the available BAFF. Interestingly, the MFI of ICOSL was reduced on the B cells from B-BclxL^{tg}-A20^{-/wt} but not B-BclxL^{tg}-A20^{-/-} mice. ICOSL is shed from the B cell surface upon contact with ICOS, presented by T cells (318). Since the ICOSL mRNA expression in BclxL^{tg} A20^{-/wt} FolB cells was on average rather high (data not shown), their lower cell surface level of ICOSL was likely a consequence of enhanced interaction with T cells.

The Schmidt-Supprian laboratory and others have previously shown that *in vitro* A20^{-/-} B cells are more reactive towards activating stimuli (CpG, anti-IgM, anti-CD40) than A20^{-/wt} B cells (280, 281). However, the activation status of *ex vivo* isolated A20-deficient B cells did not reflect their intrinsic potential to upregulate surface activation markers upon stimulation *in vitro*. This indicated that *in vivo* activating stimuli might be more abundant in B-BclxL^{tg}-A20^{-/wt} compared to in B-BclxL^{tg}-A20^{-/-} mice, which will be further elucidated in chapter 4.2.

4.1.5 T cell subsets in B-BclxL transgenic A20-deficient mice

B cell and especially GCB cell expansion depends on co-stimulation by cognate helper T cells. CD4 T cells can either be T helpers - which activate other immune cell types, thereby driving the immune response - or Foxp3⁺ regulatory T cells - which dampen the immune response. CD8 T cells have a mainly cytotoxic function to eliminate virally infected or malignant cells.

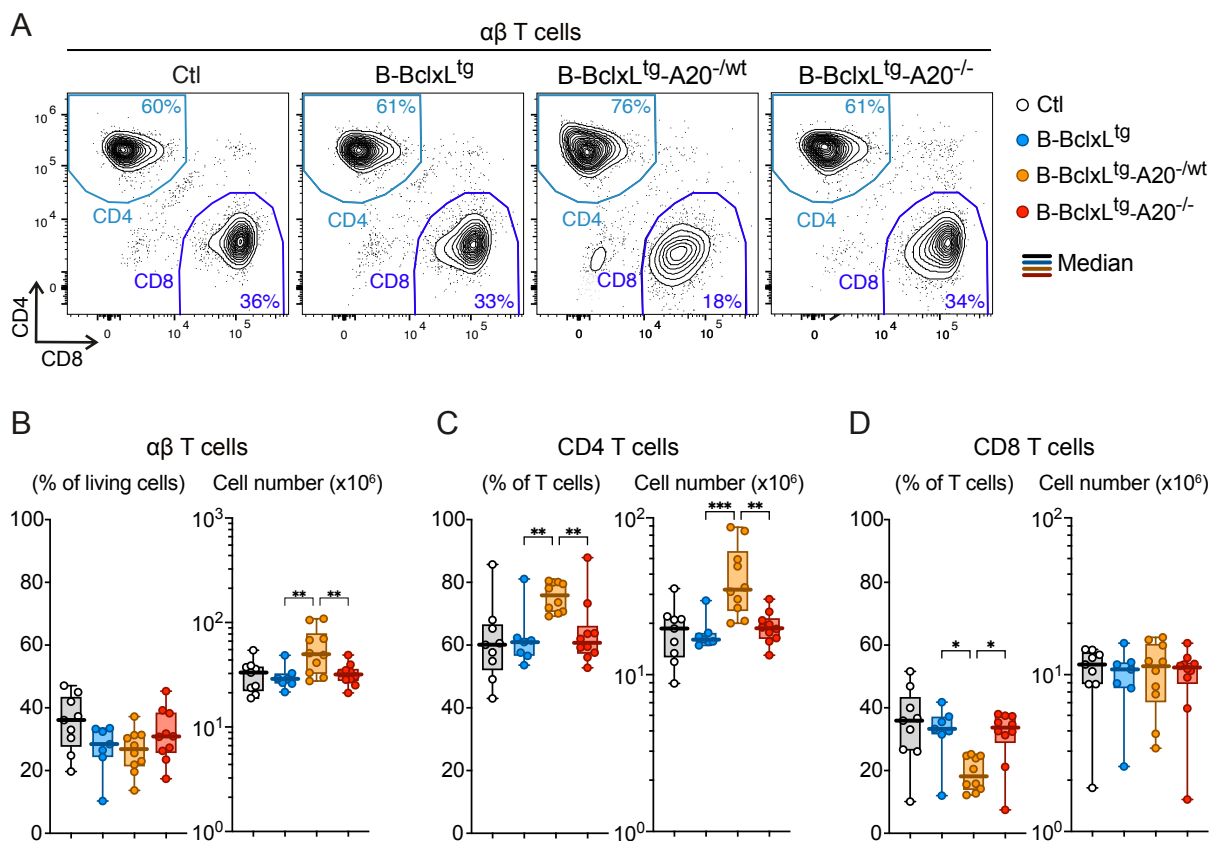


Figure 19. CD4 and CD8 T cells in the spleen of B-BclxLtg-A20 mice.

(A) Representative FACS plots depicting the fraction of CD4⁺ and CD8⁺ cells within TCR β ⁺ T cells for the indicated genotypes. **(B-D)** Fraction and absolute number of splenic **(B)** $\alpha\beta$ T cells (B220⁺ TCR β ⁺), **(C)** CD4 T cells (B220⁺ TCR β ⁺ CD4⁺) and **(D)** CD8 T cells (B220⁺ TCR β ⁺ CD8⁺). **(B-D)** Data is displayed as box-whisker-plot. Dots represent individual samples, and thick lines highlight the median value. Assessment of normality and statistical testing were performed as described in the Methods section (chapter 3.11). Only relevant comparisons are depicted on the graphs.

Within spleens, the percentage of B2 cells was increased in B-BclxL^{tg} and B-BclxL^{tg}-A20^{-wt} mice (see **Figure 8**). Correspondingly, the percentage of splenic $\alpha\beta$ T cells within all splenocytes was slightly reduced (**Figure 19B**). However, due to their strong splenomegaly, the absolute number of splenic $\alpha\beta$ T cells in B-BclxL^{tg}-A20^{-wt} mice was increased compared to the other groups (**Figure 19B**). I did not analyze the $\gamma\delta$ subclass of T cells and in all subsequent analyses, “T cells” refers to $\alpha\beta$ T cells. The composition of T cells in B-BclxL^{tg}-A20^{-wt} spleens was shifted towards more CD4 and less CD8 expressing cells. This resulted in an enrichment of the absolute CD4 but not CD8 T cell numbers in these mice. In all other groups, the composition as well as absolute number of CD4 and CD8 T cells was unaltered (**Figure 19A, C, D**).

4.1.5.1 **BclxL^{tg} A20^{-wt} B cells induce an expansion of most CD4 T cell subsets**

CD4⁺ follicular helper T cells (T_{fh}) are involved in B cell expansion and differentiation by providing CD40 stimulation to cognate B cells in the germinal center. Oppositely, regulatory T cells (T_{reg}) have an anti-inflammatory function, dampening immune responses through cytokine secretion and direct cell-cell interaction. A small subset of follicular T cells has a Foxp3⁺ regulatory phenotype. These follicular regulatory T cells (T_{fr}) originate from thymic-derived Foxp3⁺ precursors, which undergo the Bcl6-dependent T_{fh} differentiation pathway. They are specialized suppressor cells, controlling the germinal center response by limiting T_{fh} cell and GCB cell numbers (319).

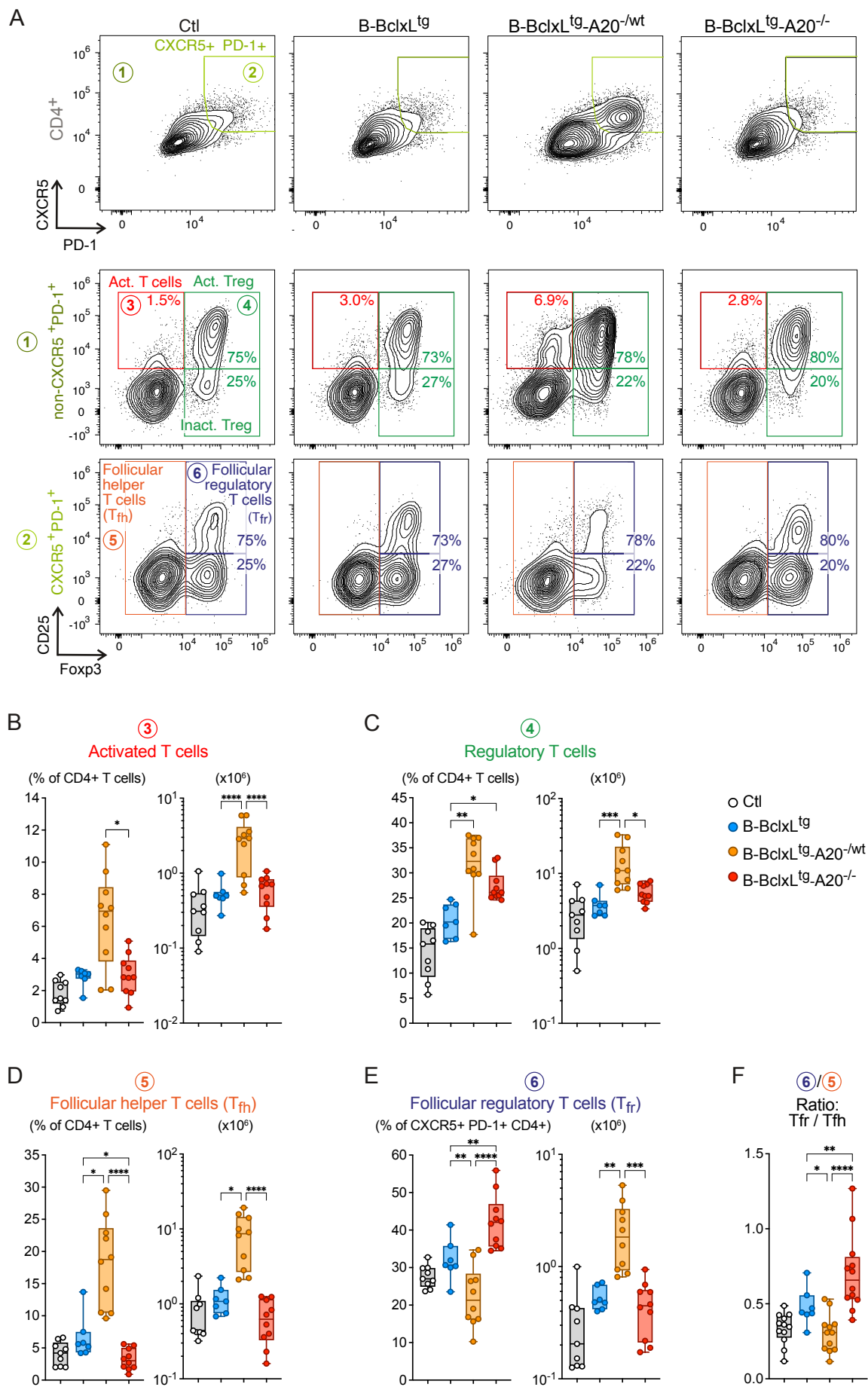


Figure 20. CD4 T cell subsets in B-Bclxl^{tg}-A20 mice.

Figure 20. CD4 T cell subsets in B-BclxL^{tg}-A20 mice (Legend)

(A) Representative FACS plots displaying the gating strategy for activated T cells (3): CXCR5⁻ PD-1⁻ CD25⁺ Foxp3⁻; T_{reg} (4): CXCR5⁻ PD-1⁻ CD25⁺ Foxp3⁺; T_{fh} (5): CXCR5⁺ PD-1⁺ Foxp3⁻ and T_{fr} (6): CXCR5⁺ PD-1⁺ Foxp3⁺. The median percentage of CD25⁺ and CD25⁻ cells within the T_{reg} and T_{fr} populations are shown on the respective plots. (B-E) Fraction and absolute numbers of splenic (B) activated T cells (C) T_{reg}, (D) T_{fh} and (E) T_{fr} cells. (F) Ratio of T_{fr} and T_{fh} cell number per spleen. Data is displayed as box-whisker-plot, dots represent individual samples. (B-F) Data is displayed as box-whisker-plots, dots represent individual samples. Assessment of normality and statistical testing were performed as described in the Methods section (chapter 3.11). Only relevant comparisons are depicted on the graphs.

In B-BclxL^{tg}-A20^{-wt} mice, a larger fraction of CD4 T cells expressed CD25 (IL2R α), the high affinity receptor for IL-2 (Figure 20A, B). Accordingly, the fraction and number of Foxp3⁺ regulatory T_{reg} cells was elevated in B-BclxL^{tg}-A20^{-wt} as well as B-BclxL^{tg}-A20^{-/-} spleens indicating the initiation of anti-inflammatory mechanisms (Figure 20A, C). Most strikingly, T_{fh} cells were strongly enriched specifically in B-BclxL^{tg}-A20^{-wt} mice, demonstrating the establishment of functional germinal centers in which the expanded GCB cells can receive adequate T cell help (Figure 20A, D and see Figure 10A). In contrast, T_{fh} cell numbers were not elevated in B-BclxL^{tg}-A20^{-/-} spleens and moreover these contained an increased fraction of Foxp3⁺ T_{fr} cells (Figure 20A, E). This T_{fr} bias in B-BclxL^{tg}-A20^{-/-} spleens is in line with their apparently diminished germinal centers, evident by the reduced number of GCB and T_{fh} cells. The ratio of CD25⁺ early/immature and CD25⁻ terminally-differentiated T_{fr} (320, 321) was equal in all groups (Figure 20A). However, the ratio of germinal center-promoting (T_{fh}) and immunosuppressive (T_{fr}) germinal center-resident T cells was strongly skewed towards the anti-inflammatory branch in B-BclxL^{tg}-A20^{-/-} spleens (Figure 20F), indicating an ongoing active immunosuppression.

4.1.5.2 T cell activation

Effective activation of T cells requires TCR binding to cognate MHC-bound antigen and simultaneous CD28 stimulation via CD80 or CD86. This entails the surface expression of CD69, CD44 as well as CD25 (IL2R α), which renders the T cells more responsive to IL-2 signals. Also, the inducible co-stimulator (ICOS) is expressed on CD4 T cells upon stimulation and highly expressed on T_{fh} cells. ICOS:ICOSL interaction plays a key role in the T cell-B cell cross-stimulation.

CD4 and to a lesser extent CD8 T cells in B-BclxL^{tg}-A20^{-wt} mice showed a hyperactivated phenotype with regards to their surface expression of ICOS (Figure 21A, B) and other activation markers (Figure 21B). ICOS was uniformly elevated on CD4 T cells in B-BclxL^{tg}-A20^{-wt} mice (Figure 21A), which could not singularly be accounted to their elevated proportion of T_{fh} cells. While T cells in B-BclxL^{tg}-A20^{-/-} mice appeared slightly more activated compared to B-BclxL^{tg} mice, they were significantly less activated than in B-BclxL^{tg}-A20^{-wt} mice with regards to CD62L, CD44 and CD25 expression (Figure 21B).

CD62L shedding is initiated in antigen-activated T cells and induces the lytic activity of CD8 T cells (322). The low CD62L surface expression on CD4 and CD8 T cells (**Figure 21B**) indicates that a large fraction has acquired effector function (see chapter 4.1.5.3). Once T cells have acquired effector T cell function, they become independent from further co-stimulation and have a high capacity to activate B cells.

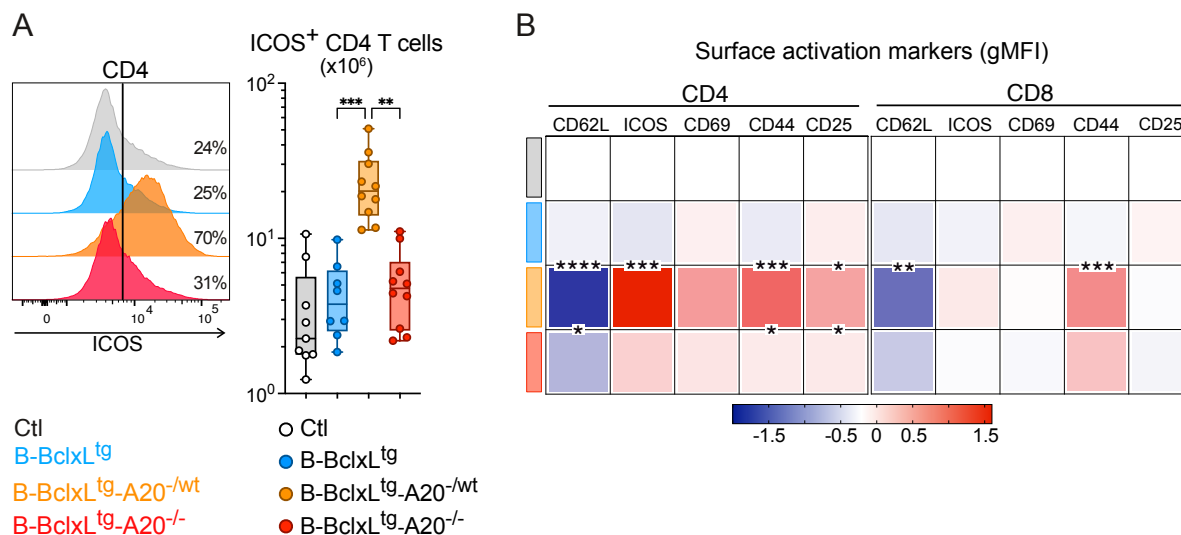


Figure 21. T cell activation in B-BclxL^{tg}-A20 mice.

(A) Representative histograms depicting the signal intensity of surface ICOS on splenic CD4⁺ TCRβ⁺ T cells (left). Absolute number of splenic ICOS⁺ CD4⁺ TCRβ⁺ T cells (right). Data is displayed as box-whisker-plot, dots represent individual samples. Assessment of normality and statistical testing were performed as described in the Methods section (chapter 3.11). Only relevant comparisons are depicted on the graphs. **(B)** Geometric mean fluorescent intensity (gMFI) on CD4⁺ and CD8⁺ TCRβ⁺ T cells was extracted from flow cytometry data for the surface markers CD62L, ICOS, CD69, CD44 and CD25. gMFI values were normalized to the gMFI values of the same cell type in CD19Cre control mice within each experiment. The heatmap depicts the mean log₂ values of each group. Asterisks indicate significant differences between the groups. Each value is the mean of at least 4 replicates from minimum 3 independent experiments.

Overall, CD4 T cells in B-BclxL^{tg}-A20^{-/wt} mice showed a hyperactivated phenotype, which renders them more potent to stimulate cognate B cells. Since the genetic modifications were restricted to the B cell lineage, the initial activation of CD4 T cells was very likely induced by hyperreactive B cells. Upon establishment of an immunological synapse, in the context of available antigen, the cross-stimulation of B and T cells presumably sustained their activation. In addition to cross-activation through direct cell-cell contact, T cell activation was likely also driven by systemically available inflammatory cytokines, which will be further evaluated in chapter 4.2.2.

4.1.5.3 Effector memory T cell expansion

Once they are activated by cognate antigen, T cells acquire a memory phenotype. These central memory-like (CML) T cells express CD44. When these T cells acquire an effector function, they lose the surface expression of CD62L and migrate to the site of infection. I will refer to T cells with high surface CD44 and low surface CD62L as effector memory-like (EML) here.

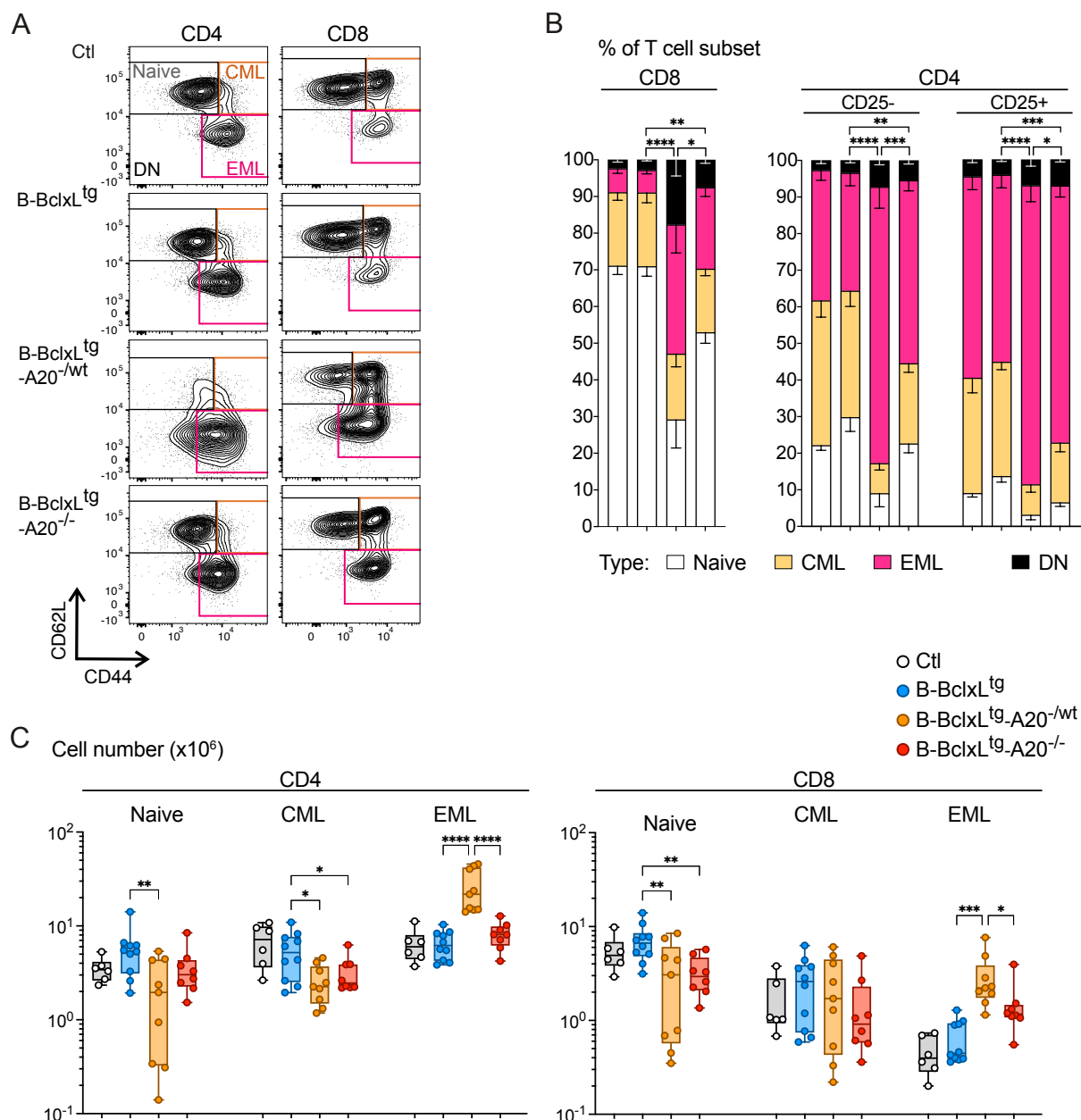


Figure 22. Effector and memory T cell differentiation in B-BclxL^{tg}-A20 mice.

(A) Representative FACS plots displaying the gating strategy for naive, central-memory-like (CML) and effector-memory-like (EML) CD4 and CD8 T cells. Cells which do not fall in any of these gates are termed CD44/CD62L double negative (DN). **(B)** Fraction of naive, CML, EML and DN T cells within CD8 as well as CD25⁺ and CD25⁻ CD4 T cells. **(C)** Absolute number of naive, CML and EML CD4 and CD8 T cells. Data is displayed as box-whisker-plot, dots represent individual samples. Assessment of normality and statistical testing were performed as described in the Methods section (chapter 3.11). Only relevant comparisons are depicted on the graphs.

B-BclxL^{tg}-A20^{-/wt} mice, displayed a significantly increased fraction of EML cells (CD44⁺ CD62L⁻), especially in the CD4 T cell compartment (**Figure 22A, B**). EML CD4 T cells provide help to B cells, thereby supporting their expansion, and may additionally play a detrimental role by driving inflammation (323, 324). Strikingly, naïve CD4 T cells were essentially absent in several B-BclxL^{tg}-A20^{-/wt} mice (**Figure 22C**). Compared to B-BclxL^{tg} and control mice, also B-BclxL^{tg}-A20^{-/-} mice had an increased fraction of EML CD4 as well as CD8 T cells (**Figure 22A, B**) and a significantly reduced number of naïve CD8 T cells, indicating their enhanced activation (**Figure 22C**).

4.1.5.4 T cell exhaustion phenotype

In the context of antigen persistence, T cells acquire an exhausted phenotype, which is characterized by a strong upregulation of surface PD-1. Exhausted T cells are commonly found during chronic infection, cancer or autoimmunity (72). PD-1 expression is transiently upregulated in all T cells after TCR activation and CXCR5⁺ T_{fh} cells are intrinsically PD-1⁺ (73) (**Figure 23A**). The relative and absolute number of T_{fh} cells was strongly increased in B-BclxL^{tg}-A20^{-/wt} mice (see **Figure 20D**). Therefore, to investigate the exhaustion phenotype on non-T_{fh} cells, CD4 as well as CD8 T cells were pre-gated on CXCR5⁻ cells. In B-BclxL^{tg}-A20^{-/wt} mice the mean expression of PD-1 on both CD4 and CD8 T cells was significantly higher than in all other groups, which indicated chronic antigen exposure of the T cells in these mice (**Figure 23B, C**).

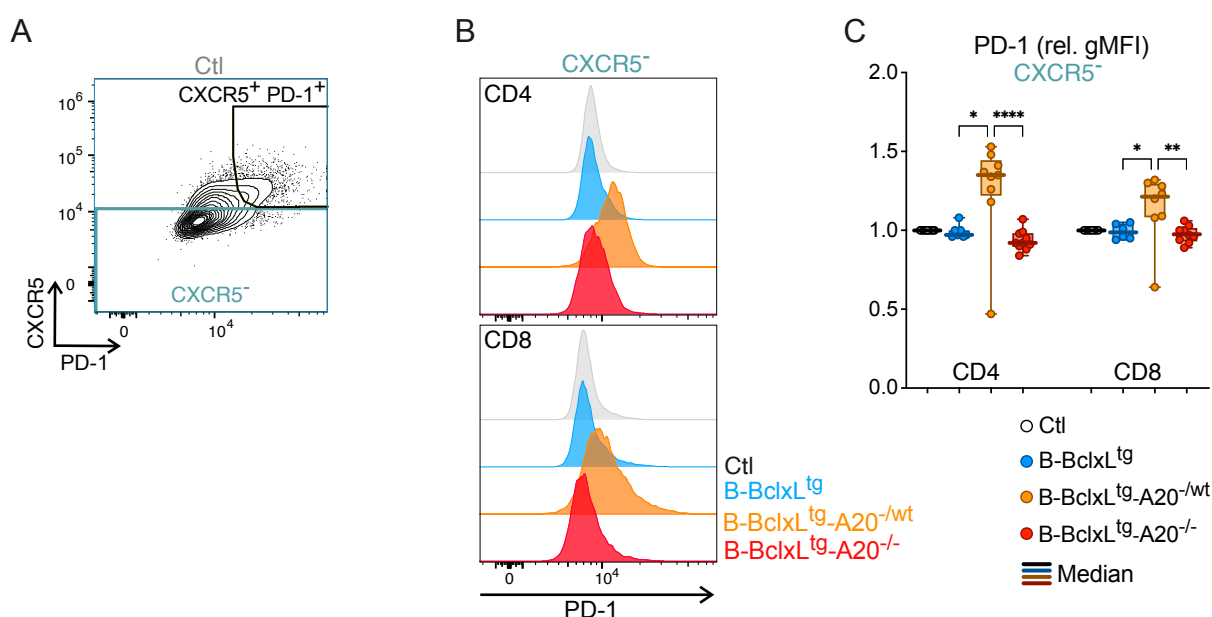


Figure 23. T cell exhaustion in B-BclxL^{tg}-A20 mice.

(A) Representative FACS plots displaying the gating strategy for CXCR5⁺ PD-1⁺ follicular helper T cells and CXCR5⁻ T cells in a CD19Cre control mouse. **(B)** Representative histograms displaying the PD-1 signal intensity in CXCR5⁻ CD4 and CD8 T cells. **(C)** Geometric mean fluorescent intensity (gMFI) was extracted for surface PD-1 on CD4 and CD8 T cells. gMFI values were normalized to the gMFI values of the same cell type in CD19Cre control mice and the relative gMFI (rel. gMFI) was displayed as box-whisker-plot. Dots represent individual samples, and thick lines highlight the median values. Normal distribution of the data was assessed using the Shapiro-Wilk test. The significance was tested with an Uncorrected Dunn's test. Only relevant comparisons are depicted on the graphs. The same data was used in the heatmap shown in Figure 21B.

4.1.6 Myeloid cells in the spleen

The myeloid lineage of cells comprises monocytes, which can give rise to dendritic cells (DCs) and macrophages, as well as granulocytes (325). Most myeloid cells exert innate immune functions, through phagocytosis and secretion of inflammatory cytokines (326). While being part of the myeloid branch, DCs act as antigen-presenting cells, which capture, process and present antigens to lymphocytes and thereby serve as the main inducers of adaptive immune cell responses (327, 328).

In correlation with the increased splenocyte number in B-BclxL^{tg}-A20^{-wt} mice, also several members of the myeloid lineage were expanded in their spleens. Most strikingly, the number of conventional dendritic cells (cDC) was strongly increased in B-BclxL^{tg}-A20^{-wt} spleens (**Figure 24A**). In B-BclxL^{tg}-A20^{-/-} spleens, however, I observed a significantly higher number of plasmacytoid dendritic cells (pDC) (**Figure 24B**). This cell type is suggested to play a major role in the pathology of human SLE by secreting large amounts of type I interferons (IFN) upon stimulation by DNA-containing immune complexes (329, 330). In lupus-prone mouse models pDCs numbers and their IFN secretion were elevated in pre-disease mice but decreased with disease progression (331, 332).

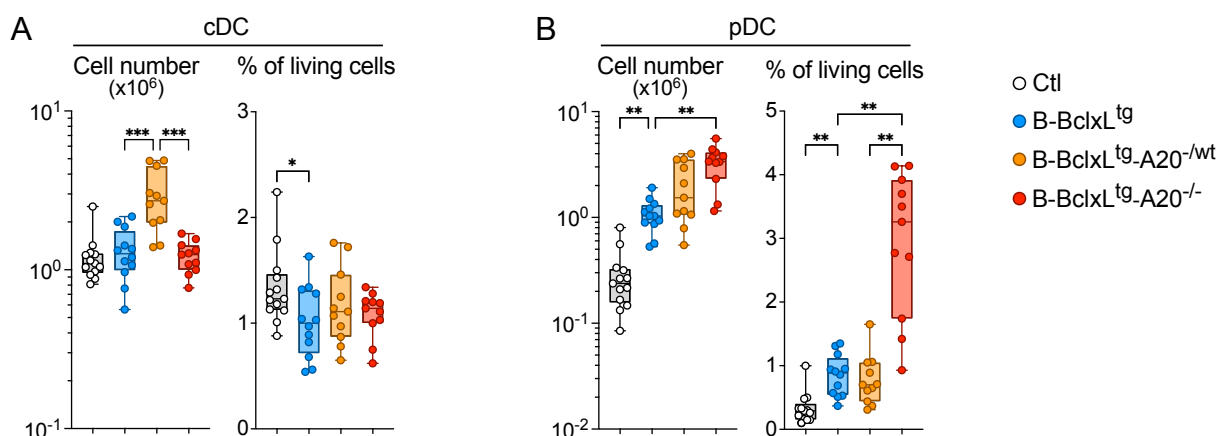


Figure 24. Dendritic cells in the spleen.

(A-B) Fraction and absolute number of **(A)** CD11c^{high} conventional dendritic cells (cDC) and **(B)** B220⁺ CD11c^{int} plasmacytoid dendritic cells (pDC). Data is displayed as box-whisker-plot, dots represent individual samples. Assessment of normality and statistical testing were performed as described in the Methods section (chapter 3.11). Only relevant comparisons are depicted on the graphs.

Granulocytes, which comprise neutrophils, basophils and eosinophils, are circulating, non-proliferative cells, rapidly recruited into tissues sites upon pathogen invasion (326). The number of splenic neutrophils was similar in mice from all groups (**Figure 25A**). The number of eosinophils, however, was strongly increased specifically in B-BclxL^{tg}-A20^{-/-} spleens compared to all other groups (**Figure 25A**). These high eosinophil numbers are likely due to their increased recruitment into the spleen and could indicate an ongoing Th2 response in B-BclxL^{tg}-A20^{-/-} mice (see chapter 4.2.2) (333).

Natural killer (NK) cells, next to CD8 T cells, have a cytotoxic function to eliminate malignant or infected target cells. Stimulation of germline-encoded NK cell activation receptors and myeloid cell-derived inflammatory cytokines drive their activity (334). B-BclxL^{tg}-A20^{-/wt} spleens had a decreased, while B-BclxL^{tg}-A20^{-/-} spleens had an increased percentage of NK cells. However, due to the strongly different splenocyte numbers, the absolute number of splenic NK cells was equal in all groups (**Figure 25B**). Also the number of B220⁺ CD11c⁺ NK1.1⁺ cells, an IFN γ -producing subset of NK cells, was largely similar in all groups (**Figure 25B**).

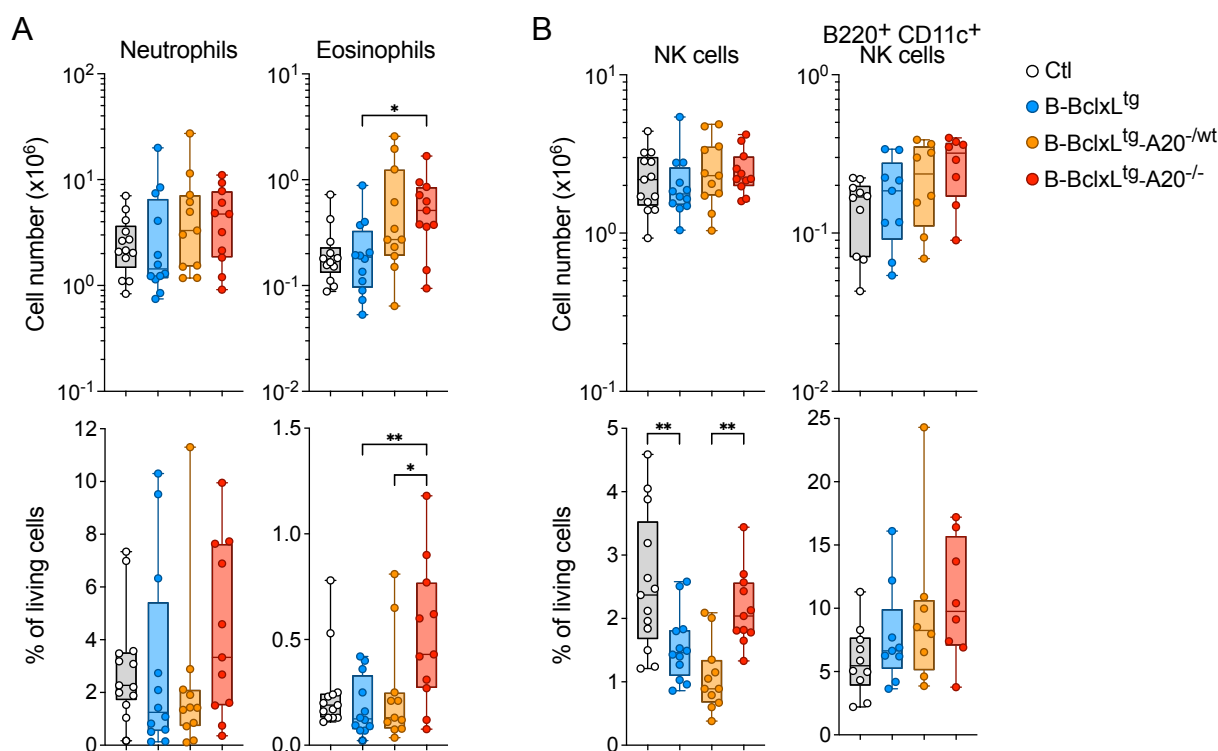


Figure 25. Granulocytes and NK cells in the spleen.

(A-B) Fraction and absolute number of (A) Gr-1(Ly-6G)^{high} Ly-6C^{int} neutrophils (left) and Siglec-F⁺ SCC^{high} eosinophils (right) and (B) NK1.1⁺ TCR β ⁻ NK cells (left) and B220⁺ CD11c⁺ NK cells (right). Data is displayed as box-whisker-plot, dots represent individual samples. Assessment of normality and statistical testing were performed as described in the Methods section (chapter 3.11). Only relevant comparisons are depicted on the graphs.

Monocytes can acquire an inflammatory (Ly-6C^{high} Gr-1⁺) phenotype and migrate to injured or infected site, and inflammatory monocytes can be involved in the propagation of chronic diseases (335). Macrophages mainly ingest pathogens by phagocytosis or scavenge dead cells and cellular debris. Depending on the microenvironmental setting, macrophages can be polarized to gain either a pro-inflammatory function (M1-like), induced by IFN γ , or a suppressive function (M2-like), induced by IL-4 and IL-13 (327).

In B-BclxL^{tg}-A20^{-/wt} spleens, there was a slight expansion of F4/80^{high} CD11b⁻ red pulp macrophages, F4/80^{int} CD11b^{int} macrophages as well as CD11b⁺ Ly-6C⁺ inflammatory monocytes in correspondence to the general expansion of splenocytes (**Figure 26A**). Interestingly, both M1 and M2 polarization were reduced in macrophages from B-BclxL^{tg}-A20^{-/wt} spleens. In contrast, B-BclxL^{tg}-A20^{-/-} spleens had an expanded fraction of M1-type pro-inflammatory macrophages, indicating local inflammation (**Figure 26B**).

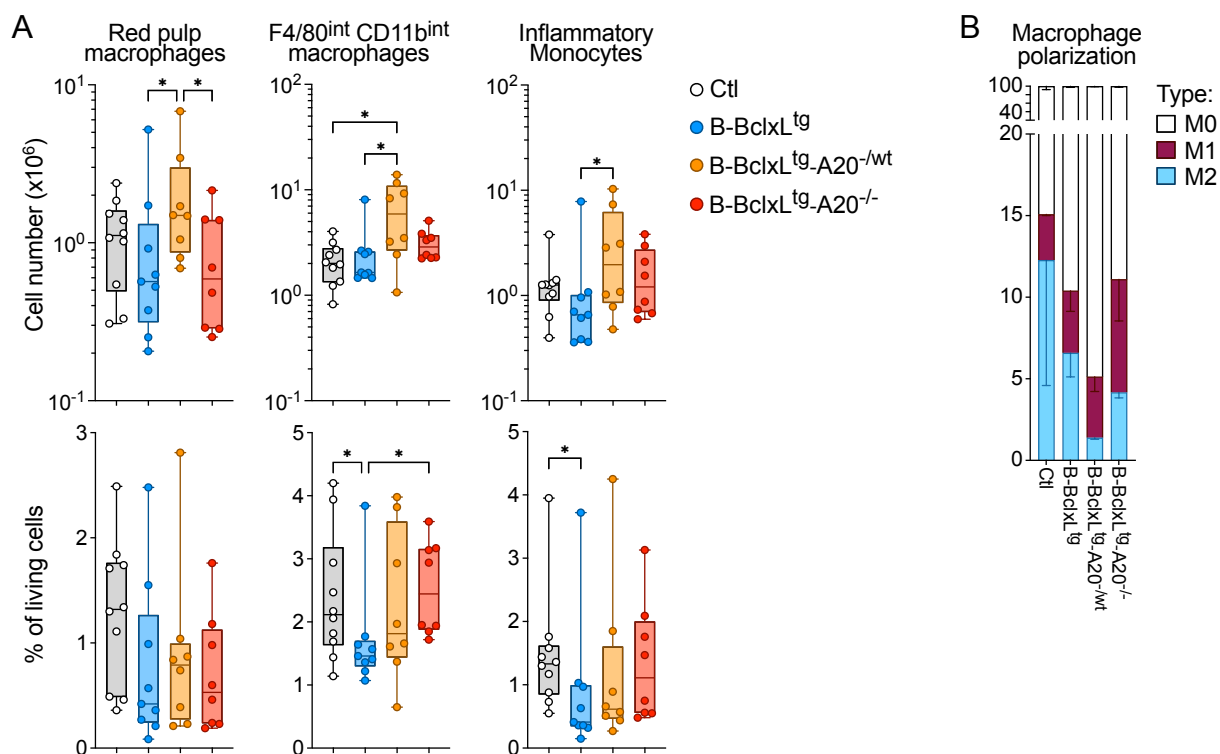


Figure 26: Macrophages and monocytes in the spleen.

(A) Fraction and absolute number of F4/80^{high} CD11b^{low} red pulp macrophages (left), F4/80^{int} CD11b^{int} macrophages (middle) and CD11b⁺ Ly-6C^{high} inflammatory monocytes (right). Data is displayed as box-whisker-plot, dots represent individual samples. Assessment of normality and statistical testing were performed as described in the Methods section (chapter 3.11). Only relevant comparisons are depicted on the graphs. **(B)** Macrophage polarization determined by the surface expression of iNOS: M1 (pro-inflammatory), Arginase I: M2 (suppressive) or neither of the two markers: M0 (non-polarized). The macrophage population included red pulp macrophages and F4/80^{int} CD11b^{int} macrophages. Each bar represents the mean value and SD from two biological replicates measured in two individual experiments.

Collectively, the analysis of myeloid lineage cells by showed that apart from a massive increase in dendritic cells and subtle changes in the macrophage/monocyte subsets, the innate branch of the immune system remained largely unaffected by the B cell hyperactivation in B-BclxL^{tg}-A20^{-/wt} mice.

Altogether, characterization of the immune cell composition in the secondary lymphoid organs and BM demonstrated that B-BclxL^{tg}-A20^{-/wt} mice suffer from splenomegaly. This is mainly caused by an expansion of lymphocytes and cDCs but barely involves other myeloid subsets. Since only B cells are targeted by the conditional loss of A20 and BclxL^{tg} expression, the expansion of other immune cell types must be induced by the genetically altered B cells either through direct cell-cell contact or through indirect mechanisms, such as cytokine signaling, which will be discussed in chapter 4.2.2.

4.2 Pathology of B-BclxL^{tg}-A20^{-/wt} mice

4.2.1 B-BclxL^{tg}-A20^{-/wt} mice develop a lethal autoimmune pathology

A20-deficiency in B cells was previously reported by the Schmidt-Supprian laboratory and others to cause the development of autoantibodies and mild autoimmune manifestations (280-282). In the previous chapters I showed that the combination of B-BclxL^{tg} expression with heterozygous but not homozygous B cell-specific loss of A20 in mice resulted in dramatically increased B cell activation *in vivo*. Notably, this activation led to the production of substantial quantities of GCB cells and class-switched plasmacytic cells. I subsequently investigated the development of autoimmunity in B-BclxL^{tg}-A20 mice.

In line with the strong B cell expansion and activation, B-BclxL^{tg}-A20^{-/wt} mice also developed a severe pathology. B-BclxL^{tg}-A20^{-/wt} mice died at young age with a median survival of only 8 months. In contrast, B-BclxL^{tg} as well as B-BclxL^{tg}-A20^{-/-} mice had life spans comparable to control mice (**Figure 27A**). When splitting the mice by sex, there was no prevalence for female lethality within any of the groups (data not shown). Interestingly, more than 1/3 of all observed B-BclxL^{tg}-A20^{-/wt} mice survived to old age, demonstrating that fatal disease is not a definite fate of B-BclxL^{tg}-A20^{-/wt} mice but the genetic predisposition rather poses a strong risk for disease development. Previous mouse models of A20-deficiency in B cells developed mild autoimmune manifestations in aged B-A20^{-/-} animals (280, 281). Data on the corresponding mice with heterozygous B cell-specific A20 deletion remained scarce but suggested autoreactivity as well as renal involvement in B-A20^{-/wt} mice (281). To determine whether the strong lethality of B-BclxL^{tg}-A20^{-/wt} mice was also caused by autoimmunity, I performed several systemic and organ-specific analyses.

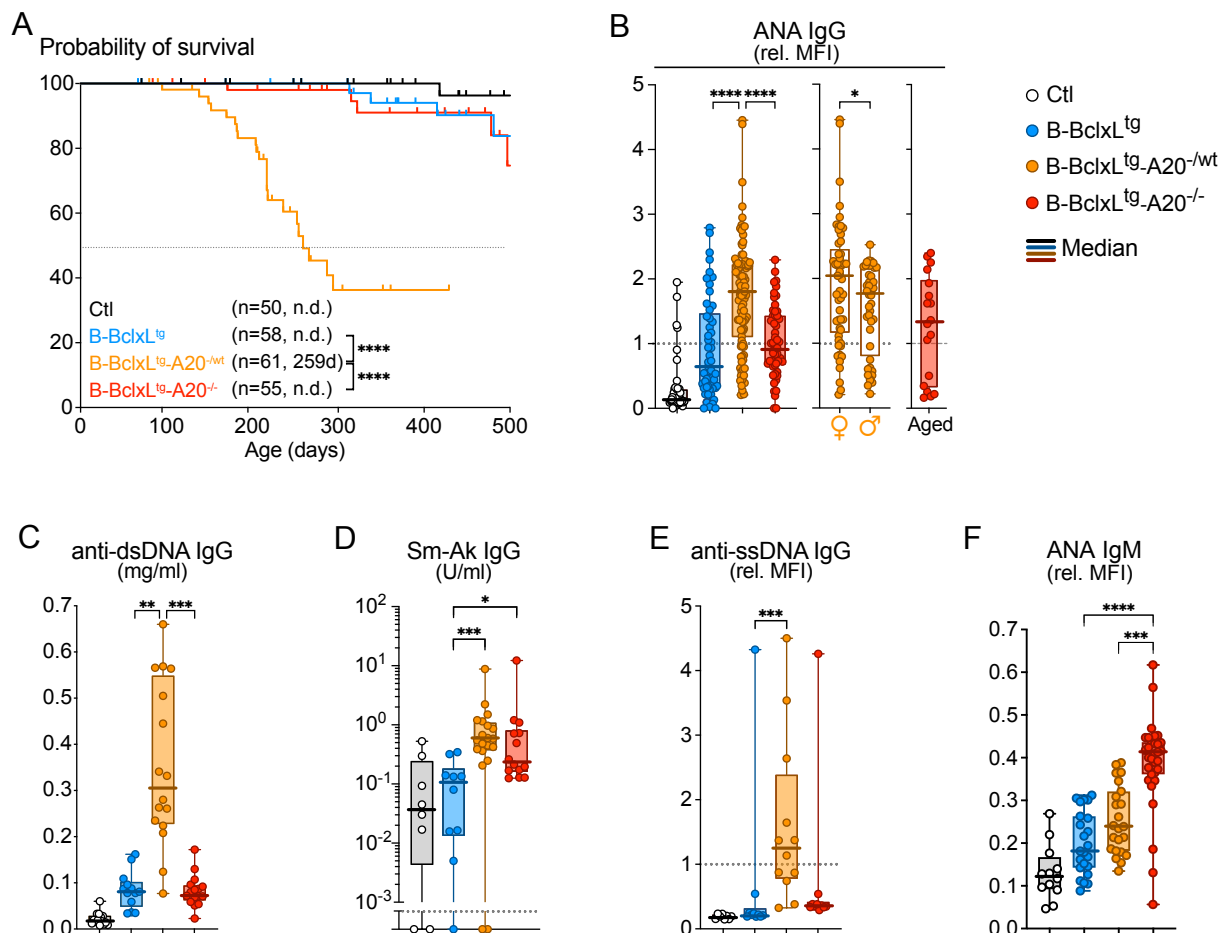


Figure 27. Systemic autoantibodies and survival.

(A) Kaplan Meier survival curves of B cell-specific A20-deficient BclxLtg mice. Cohort sizes and median survival times are shown. (B-F) (B) Serum levels of anti-nuclear IgG antibodies (ANA, normalized to positive control) in young mice, 2-7 months (left), ANA in young B-BclxL^{tg}-A20^{wt/-} mice separated by sex (middle) and ANA in aged B-BclxL^{tg}-A20^{-/-} mice, >9 months (right). (C) Serum concentration of anti-double stranded DNA (dsDNA) IgG (mg/ml). (D) Serum levels of anti-single stranded DNA (ssDNA) IgG antibodies (normalized to positive control). (E) Serum concentration of anti-Smith (Sm) IgG (U/ml). (F) Serum levels of ANA IgM (normalized to positive control). (C-F) Measured in young mice (3 – 5 months age). (B-F) Data is displayed as box-whisker-plot. Dots represent individual samples, and thick lines highlight the median value. Assessment of normality and statistical testing were performed as described in the Methods section (chapter 3.11). Only relevant comparisons are depicted on the graphs. (A) *The survival graph was generated by Dr. Yuanyuan Chu.* (C) *The dsDNA ELISA was performed by Prof. Dr. Maciej Lech (LMU, München).*

Serum analysis revealed that mice of all BclxL transgenic groups (B-BclxL^{tg}, B-BclxL^{tg}-A20^{-/wt} and B-BclxL^{tg}-A20^{-/-}) carried detectable amounts of serum anti-nuclear IgG autoantibodies (ANA) (Figure 27B, left). This is in line with reports that Eμ-BclxL transgene expression causes an autoimmune predisposition in mice (117, 152, 336). In B-BclxL^{tg}-A20^{-/wt} and B-BclxL^{tg}-A20^{-/-} mice, these autoantibodies were already detectable in young adolescent mice at the age of 2 months (data included in Figure 27B, left and middle panel). Overall, in young adult mice, within the age range of 2 – 7 months, the concentration of ANA IgG was significantly higher in B-BclxL^{tg}-A20^{-/wt} mice compared to all other groups (Figure 27B, left).

Interestingly, the ANA load was slightly higher in females (**Figure 27B**, middle), despite the similar survival of male and female mice. It is worth noting that, ANA levels did not further increase in B-BclxL^{tg}-A20^{-/-} with age (**Figure 27B**, right), showing that no strong autoimmunity developed in these mice throughout their life.

The utilized ANA Screen kit detected autoantibodies against 8 nuclear constituents, among them dsDNA. Since dsDNA is the major target of autoantibodies in human SLE, I specifically measured the serum concentration of anti-dsDNA autoantibodies. The total amount of anti-dsDNA IgG was significantly higher in B-BclxL^{tg}-A20^{-wt} mice compared to all other groups (**Figure 27C**). Since anti-dsDNA antibodies are highly indicative of a SLE-like pathology, I additionally analyzed the serum concentration of anti-Sm (Smith) antibodies, which are a definite criterion for the diagnosis of SLE in human patients (337, 338), as well as anti-ssDNA antibodies. Both, anti-Sm IgG and anti-ssDNA IgG levels were significantly elevated in the sera of B-BclxL^{tg}-A20^{-wt} mice (**Figure 27D**, E).

I showed that B-BclxL^{tg}-A20^{-/-} mice harbored extremely high total IgM serum levels (see **Figure 17**). To evaluate whether these contained also autoreactive antibodies, I performed a semi-quantitative analysis of ANA IgM. Interestingly, autoreactive ANA IgM levels were significantly elevated in B-BclxL^{tg}-A20^{-/-} mice. Since this assay allowed no conclusion about the antibody affinity, these ANA IgM might, at least partially, be natural autoantibodies (NAAb). Since NAAb generally protect against autoimmune pathology, their existence might contribute to the protection of B-BclxL^{tg}-A20^{-/-} mice against premature death.

The occurrence of anti-nuclear and more specifically anti-dsDNA as well as anti-Sm autoantibodies indicated the development of a systemic autoimmune phenotype resembling human SLE. This disease is associated with a specific cytokine pattern, which includes high concentrations of type I IFNs, BAFF and IL-10 (161, 339, 340). Therefore, I next investigated the cytokines produced in this A20-deficient autoimmune mouse model.

4.2.2 B cell autoreactivity in B-BclxL^{tg}-A20^{-wt} mice induces a systemic inflammation

Systemic autoimmune pathologies pose a state of high inflammation in the body due to the constant activation of an immune response. Even though A20-deficiency in my mouse model is limited to the B cell lineage, there was a strong activating effect also on other immune cell types, including T cells, dendritic cells and some myeloid cells. Apart from the activation of these cells through direct contact with B cells, they were likely activated by systemically altered cytokine levels. To investigate if the pathology of B-BclxL^{tg}-A20^{-wt} mice posed a systemic hyperinflammatory state *in vivo* and if the cytokine patterns of B-BclxL^{tg}-A20^{-/-} mice were largely different, potentially exerting a protective effect, I analyzed the serum concentration of 26 analytes by multiplexed FACS analysis.

4.2.2.1 Serum cytokine concentration

Through the evaluation of serum cytokines, I could identify several inflammatory cytokines, which were elevated in the serum of B-BclxL^{tg}-A20^{-wt} mice compared to the other genotypes (**Figure 28A**, group 1). Since these cytokines can act systemically as mediators of inflammation, they are likely involved in the activation and proliferation of the various immune cell types, observed in these mice.

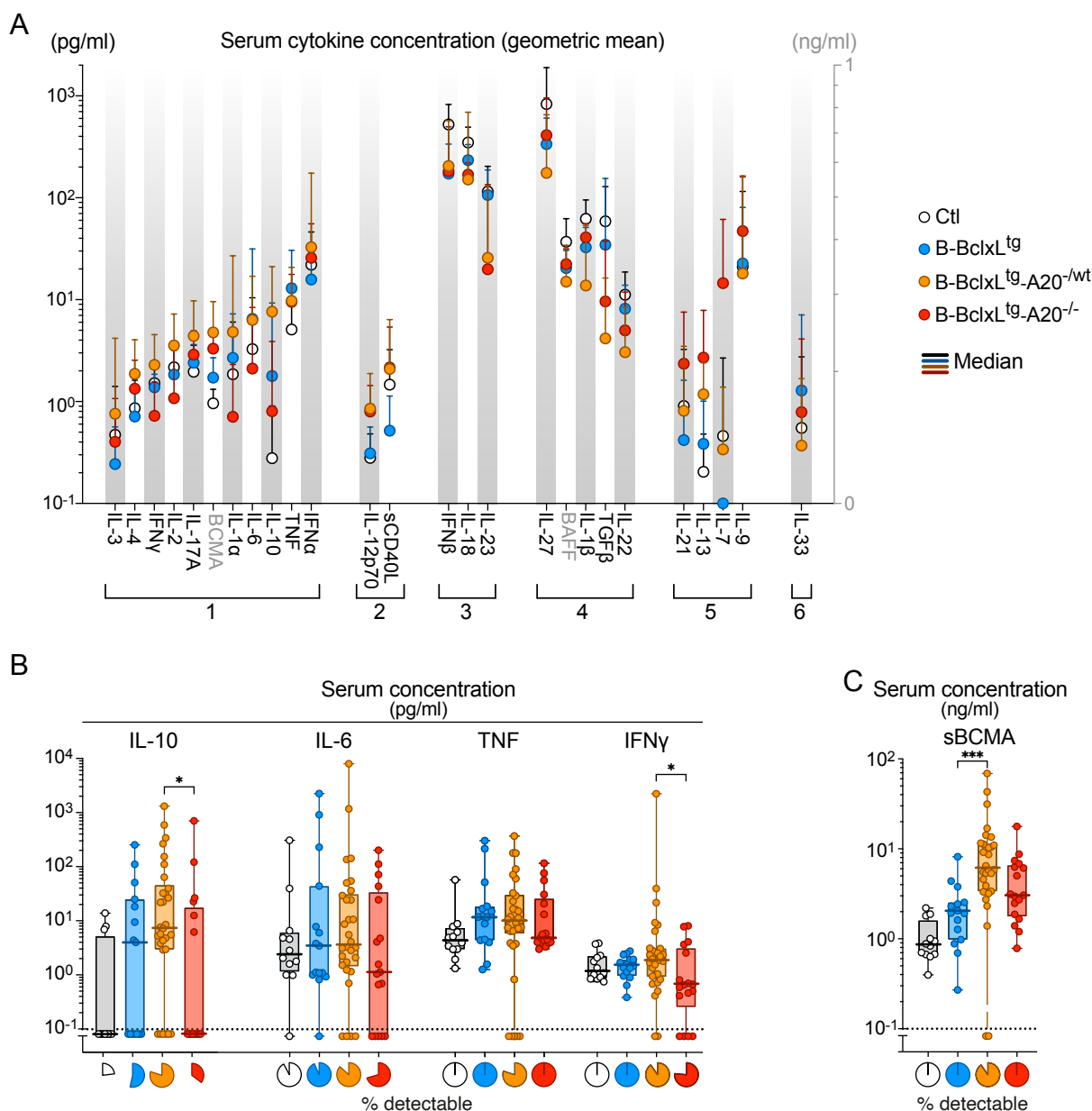


Figure 28. Serum cytokine concentration quantified with multiplexed FACS analysis.

(A) Serum concentration (pg/ml: black or ng/ml: grey) of 26 analytes as indicated on the plot. Geometric mean value and 95% CI are shown for 11-12 samples per genotype. Groups were assigned according to the relative analyte expression between genotypes: 1) highest concentration in B-BclxL^{tg}-A20^{-wt} mice, 2) highest concentration in B-BclxL^{tg}-A20^{-wt} and B-BclxL^{tg}-A20^{-/-} mice, 3) lowest concentration in B-BclxL^{tg}-A20^{-wt} and B-BclxL^{tg}-A20^{-/-} mice, 4) lowest concentration in B-BclxL^{tg}-A20^{-wt} mice 5) highest concentration in B-BclxL^{tg}-A20^{-/-} mice 6) other. (B) Serum concentration of IL-10, IL-6, TNF and IFN γ (pg/ml). (C) Serum concentration of sBCMA (ng/ml). (B-C) Data is displayed as box-whisker-plots. Dots represent individual samples, and thick lines

highlight the median values. Assessment of normality and statistical testing were performed as described in the Methods section (chapter 3.11). Only relevant comparisons are depicted on the graphs. Pie charts depict the percentage of samples with concentration above the detection limit. (A-C) *The Legendplex assay was performed by Julia Knogler.*

Group 1

Among the cytokines elevated in B-BclxL^{tg}-A20^{-wt} mice was IL-6 (**Figure 28A**, group1 and **Figure 28B**), which was previously reported to be involved in the autoimmune pathology in mice with B cell specific A20-deficiency (280, 281). In human SLE patients, IL-6 levels correlate with disease activity (341) and in lupus-prone mice, IL-6 exacerbates inflammation and renal pathology (342). IL-6 can be produced by B cells to enhance spontaneous germinal center formation in SLE model mice (343).

One main driver of the human SLE pathology is type I interferon (IFN) signaling (339, 344, 345). Type I IFN signaling in B cells through IFN α and IFN β was recently shown to drive splenomegaly, B cell activation and GCB accumulation as well as auto-antibody production in a spontaneous lupus mouse model (346). IFN α had the highest mean serum concentration in B-BclxL^{tg}-A20^{-wt} mice, however the difference to all other groups was not significant. IFN β levels were reduced in all BclxL-overexpressing lines (**Figure 28A**, group 1 and 3). This indicated that type I IFN signaling is not the main driver of pathology in B-BclxL^{tg}-A20^{-wt} mice.

Especially, the concentration of the type II interferon IFN γ was strongly elevated in the serum of B-BclxL^{tg}-A20^{-wt} mice (**Figure 28A**, group1, and **Figure 28B**). In humans, IFN γ can be used as SLE biomarker and enhancement of the IFN γ signaling, which induces autoantibody generation, even precedes SLE manifestations (347, 348). In B cells, IFN γ drives class-switching to IgG2a/2c (349), which correlates with the increased percentage of IgG2c switched plasma cells in B-BclxL^{tg}-A20^{-wt} mice (see **Figure 13D**).

Also, serum IL-4 was especially high in B-BclxL^{tg}-A20^{-wt} sera (**Figure 28A**, group 1), consistent with their strong tendency for IgG1 class switching (see **Figure 13D**). In contrast, many B-BclxL^{tg}-A20^{-/-} mice showed a very low serum concentrations of IL-4 as well as IFN γ , in line with their reduced IgG1 and IgG2c class switching (see **Figure 13D**).

Also, the inflammatory cytokines IL-1 α and TNF were increased in the sera of B-BclxL^{tg}-A20^{-wt} mice (**Figure 28A**, group 1). High concentrations of TNF in combination with IL-4 and IFN γ likely contributed to sustaining germinal center reactions and IgG class switching in B-BclxL^{tg}-A20^{-wt} mice (349, 350). Interestingly, IL-6, IL-1 α , TNF as well as IFN α were not elevated in B-BclxL^{tg}-A20^{-/-} mice compared to the control groups, indicating the absence of systemic inflammation (**Figure 28A**).

The serum concentration of soluble BCMA (sBCMA) correlated with the total number of plasmacytic cells in all genotypes and was therefore highest in B-BclxL^{tg}-A20^{-wt} mice (**Figure 28A**, group1, and **Figure 28C**). BCMA can be directly shed from the cell surface by γ -secretase and in human SLE patients, serum sBCMA strongly correlates with disease activity (111, 340, 351).

Remarkably, half of the B-BclxL^{tg}-A20^{-wt} mice had a strongly elevated serum concentration of IL-10 (**Figure 28A**, group 1, and **Figure 28B**), which is a common feature in human SLE patients and positively correlates with disease activity and severity as well as anti-dsDNA antibody titers (348, 352). In SLE patients, IL-10 drives autoantibody production, by inducing IgG switch recombination in CD40-activated B cells (353, 354) and triggers activated B cells to produce large amounts of antibodies (355). While IL-10 was shown to inhibit IgM and IgG secretion upon stimulation with TI antigens when other T cell-derived cytokines are missing (356), in cooperation with IL-4, IL-10 strongly increases the viability and plasmacytic differentiation of B cells (161, 355, 357).

The relatively high concentration of IL-2 (**Figure 28A**, group 1) in B-BclxL^{tg}-A20^{-wt} mice might contribute to their enhanced T cell effector function.

Group 2

Two cytokines, sCD40L and IL-12p70 were equally increased in B-BclxL^{tg}-A20^{-wt} and B-BclxL^{tg}-A20^{-/-} mice compared to the other groups (**Figure 28A**, group 2).

In B cells, the activation of surface CD40 by its ligand CD40L is required for T cell-dependent differentiation and the germinal center reaction (358, 359). Misfunction of CD40/CD40L interactions causes the X-linked immunodeficiency hyper IgM-syndrome (360). Despite its original description as being expressed on the surface of activated CD4 T cells (361, 362), CD40L can be expressed by a variety of hematopoietic and non-hematopoietic cells, including activated B cells (363-365). The soluble form of CD40L (sCD40L) is released from the cell surface through proteolytic cleavage upon activation (366) and has the capacity to activate B cells, drive class switching as well as antibody production and enhance their APC-function (367). Ligation of CD40 on B cells stimulates the synthesis of IL-2, IL-6, IL-10, TNF, lymphotoxin- α and TGF β (363). Therefore, in B-BclxL^{tg}-A20^{-wt} and B-BclxL^{tg}-A20^{-/-} mice, systemically available sCD40L could likely stimulate a positive feedback loop of inflammatory cytokine production by aberrant B cells. In human SLE patients, serum sCD40L is increased during active disease and correlates with the level of autoantibodies (368, 369). Interestingly, also the amount of B cells that spontaneously express high levels of CD40L is strongly elevated in active SLE patients (370). Correspondingly, ectopic expression of CD40L on B cells is sufficient to induce lupus-like disease in mice (349) and anti-CD40L targeting is discussed as potential SLE therapy. However, I was not able to demonstrate autocrine CD40L expression by BclxL^{tg} A20^{-wt} and BclxL^{tg} A20^{-/-} B cells (using flow cytometry and RNA sequencing), which would render the systemic inflammation independent of T cell help. Interestingly, compared to SLE patients, serum sCD40L is even more strongly elevated in patients with Behçets disease, an autoinflammatory pathology with a high similarity to HA20 (371).

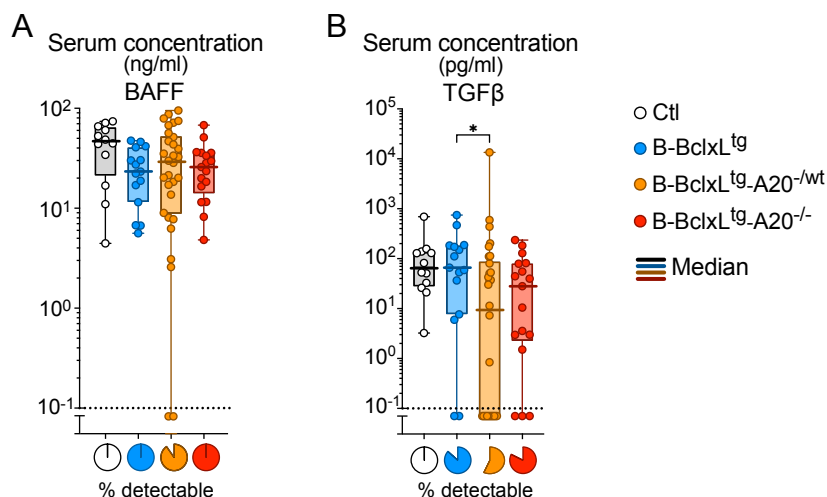


Figure 29. Serum concentration of BAFF and TGF β .

(A) Serum concentration (ng/ml) of BAFF. (B) Serum concentration (pg/ml) of TGF β . (A-B) Data is displayed as box-whisker-plots. Dots represent individual samples, and thick lines highlight the median values. Assessment of normality and statistical testing were performed as described in the Methods section (chapter 3.11). Only relevant comparisons are depicted on the graphs. Pie charts depict the percentage of samples with concentration above the detection limit. (A-B) *The Legendplex assay was performed by Julia Knogler.*

Group 3

Only few cytokines had a trend towards lower serum concentration in B-BclxL^{tg}-A20^{-/-} mice compared to the other genotypes (Figure 28A, group 3). Among these cytokines were IFN β , a mediator of type I IFN signaling, which is one of the key drivers of human SLE pathology, as well as IL-23, which seems to be positively correlated to lupus disease severity and renal involvement (372).

Group 4

Additionally, I identified several cytokines, which had the lowest mean serum concentration in B-BclxL^{tg}-A20^{-/wt} mice (Figure 28, group 4), among them BAFF, IL-1 β , TGF β and IL-22.

An increased serum concentration of BAFF is characteristic of the SLE pathology (340) and excessive BAFF production in mice through a BAFF transgene is sufficient to induce an autoimmune pathology (146). In some B-BclxL^{tg}-A20^{-/wt} mice the serum BAFF concentration was elevated compared to B-BclxL^{tg}-A20^{-/-} sera (Figure 29A). On average, however, the mean serum BAFF concentration was reduced in all BclxL transgenic groups compared to control mice (Figure 28, group 4 and Figure 29A). This is most likely due to the strongly elevated number of B cells, coinciding with an increased consumption of the available soluble BAFF *in vivo*.

Serum IL-1 β was significantly reduced upon BclxL^{tg} expression, which is in line with previously published data demonstrating the suppression of IL-1 β production upon BclxL overexpression through inflammasome inhibition via NALP1 (373), indicating that a substantial part of systemically available IL-1 β could be produced by B cells. Even though IL-1 β is required for the induction of experimental SLE in mice (374), systemic IL-1 β levels are negatively correlated to the severity of SLE pathology in humans (375, 376).

B-BclxL^{tg}-A20^{-wt} mice also had the lowest serum concentration of TGF β (**Figure 29B**), which is typical for high disease activity in SLE patients (376). TGF β induces class switching to IgG2b (in cooperation with LPS) or IgA (in cooperation with CD40L), and low TGF β might contribute to the reduced IgA switching in B-BclxL^{tg}-A20^{-wt} mice (see **Figure 13**).

Serum IL-22 levels were reported to be decreased in SLE patients, especially those with lupus nephritis (377-379). This observation suggests a protective role for IL-22 in SLE as well as its therapeutic potential based on its anti-inflammatory function (380).

Group 5

Within the panel of 26 analytes, only four, IL-7, IL-9, IL-13 and IL-21, had the highest mean concentration in the serum of B-BclxL^{tg}-A20^{-/-} mice (**Figure 28A**, group 5).

B-BclxL^{tg}-A20^{-/-} mice had significantly elevated IL-7 serum levels. A counteracting effect of IL-7 on switch transcription was recently demonstrated by Dauba et al. (381) in the absence of strong switch-inducing factors such as LPS. Thereby, high IL-7 might contribute to the reduced amount of class switched splenic plasmablasts in B-BclxL^{tg}-A20^{-/-} mice (see **Figure 13**). Additionally, since local IL-7 expression recruits B cells to the germinal center, the 3-fold higher systemic IL-7 concentration in B-BclxL^{tg}-A20^{-/-} mice might interfere with this gradient-driven recruitment (382).

The serum IL-13 concentration was slightly higher in B-BclxL^{tg}-A20^{-/-} mice than in mice with the other genotypes. IL-13 can be produced by B cells upon CD40 and IL-4 signaling and drives MHCII expression as well as proliferation of activated B cells (383, 384). Furthermore, IL-13 inhibits inflammatory cytokine production induced by LPS in human peripheral blood monocytes (385). Consequently, IL-13 might counteract a systemic inflammation in B-BclxL^{tg}-A20^{-/-} mice.

IL-21, the cytokine driving plasma cell differentiation (386), was even more elevated in B-BclxL^{tg}-A20^{-/-} than in B-BclxL^{tg}-A20^{-wt} mice. This is in line with the fact that both groups had a largely equal fraction of plasmacytic cells (see **Figure 13B** and **Figure 15D, E**).

4.2.2.2 Cytokine producing cells

In order to investigate which cells produced the systemically available cytokines, I analyzed the intracellular cytokine content of lymphocytes by flow cytometry (**Figure 30**).

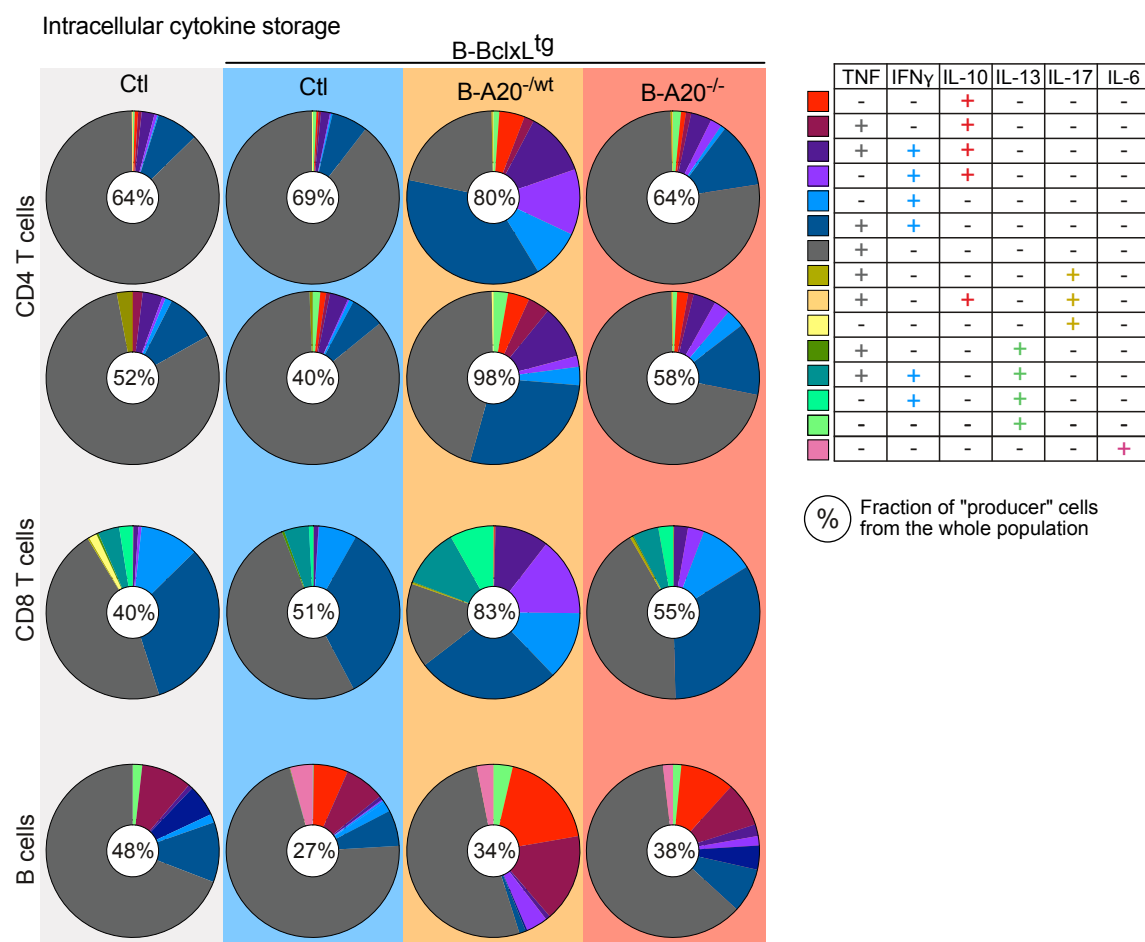


Figure 30. Cytokine producers.

Pie charts depict the fraction of CD4 T, CD8 T and B cells, which express individual or combinations of several cytokines from the pool of "producer" cells (= cells producing at least one of the 6 investigated cytokines). 1 spleen is shown for CD8 T cells and B cells each; two individual spleens analyzed in independent experiments are shown for CD4 T cells. The fraction of "producer" cells is depicted in the middle of each pie chart.

The fraction of CD4 and CD8 T cells producing at least one of the 6 investigated cytokines (= "producer") was approximately 40 – 60 % in control spleens. In B-BclxL^{tg} and B-BclxL^{tg}-A20^{-/-} mice this fraction was only slightly increased, but it was tremendously higher (80 – 98 %) in B-BclxL^{tg}-A20^{-wt} spleens. In all analyzed mice, independent of the genotype, approximately 70 – 80 % of "producer" CD4 T cells expressed TNF. B-BclxL^{tg}-A20^{-wt} mice additionally had a large fraction (50 – 75 %) of IFN γ ⁺ CD4 T cells, mainly expressing TNF simultaneously. In mice of all other genotypes, IFN γ ⁺ CD4 T cells were rare (10 – 20 %).

Interestingly, around 25% of “producer” CD4 and CD8 T cells in B-BclxL^{tg}-A20^{-/wt} mice expressed IL-10, most of them as double producers of IFN γ and IL-10 or triple producers of TNF, IFN γ and IL-10. IFN γ /IL-10 co-producing T cells were reported to occur in humans during infection and develop through upregulation of IL-10 expression in conventional IFN γ producing Th1 cells, to induce a self-regulatory function (387, 388). Classically, T_{reg} cells are the main producers of IL-10, which exerts an inflammatory function. In autoimmune patients with rheumatoid arthritis, however, T_{reg} cells insufficiently suppress TNF and IFN γ expression in effector T cells (389). Additionally, T_{reg} cells can become producers of IFN γ themselves. Recent data suggests that IFN γ production by T_{reg} cells induces an effector-like T_{reg} state, decreasing their immunosuppressive function, which is necessary to enable an effective anti-tumor response during anti-PD1 therapy (390). The absolute number of Foxp3⁺ CD25⁺ T_{reg} cells was strongly enriched in B-BclxL^{tg}-A20^{-/wt} mice (see **Figure 20D**) and likely pose the major fraction of IL-10 producing CD4 T cells (**Figure 30**) As a large fraction of IL-10 producing CD4 T cells was simultaneously producing IFN γ and TNF, the suppressive function of these T_{reg} cells might be compromised. In summary, the high IFN γ expression in T cells of B-BclxL^{tg}-A20^{-/wt} mice corresponds to their strongly increased serum IFN γ concentration and the co-expression of IL-10 with IFN γ suggest a reduced immunosuppressive function of T_{reg} cells in these mice. Apart from one control mouse, there were barely any IL-17-producing CD4 Th17 cells detected. In B-BclxL^{tg}-A20^{-/wt} mice, also more than 80 % of “producer” CD8 T cells expressed IFN γ and partially co-produced either IL-10 (25 %), TNF (25 %) and/or IL-13 (20 %) (**Figure 30**). Surprisingly, while B-BclxL^{tg}-A20^{-/-} mice had the highest serum concentration of IL-13 (see **Figure 28A**), they had less IL-13 producing T cells. IL-13 producing CD8 T cells are involved in the pathogenesis of fibrotic diseases (391).

In the B-BclxL^{tg}-A20 mouse model, A20-deficient B cells are hyperreactive to NF- κ B stimulation and systemically available cytokines potentially trigger the B cells to release inflammatory cytokines themselves. Indeed, cytokine production by B cells has been reported to drive the autoimmune pathology (392, 393). The fraction of cytokine-“producer” B cells was equally low in all the groups. However, the types of cytokines varied between the genotypes. A lower percentage of BclxL^{tg} A20^{-/wt} “producer” B cells was producing TNF, while a strongly increased fraction was expressing IL-10 (> 30 %). Among BclxL^{tg} and BclxL^{tg} A20^{-/wt} “producer” B cells there was a small but detectable fraction of IL-6 producing cells. Next to lymphocytes, also myeloid cell types, including DCs and macrophages have the ability to secrete IL-10 and other cytokines (327, 394). However, I did not evaluate the cytokine-producing capacity of these cell types in B-BclxL^{tg}-A20 mice.

Overall, the similarity between the cytokine expression patterns in B and T cells and the respective serum cytokine concentrations indicated that lymphocytes contribute significantly to the systemically available cytokines. Still, also myeloid cells might be triggered to secrete cytokines but I have not performed the corresponding analyses. The total cytokine content varied greatly between the individual mice and likely depended on the overall inflammatory state and thereby on the severity of the autoimmune pathology.

One serum sample from a very inflamed B-BclxL^{tg}-A20^{-/wt} mouse was highly positive for a large number of pro-inflammatory cytokines (**Supplementary Figure 3**). This indicates that sustained over-activation induces a positive feedback loop of inflammatory signaling and cytokine production, which can ultimately induce a potentially lethal cytokine storm.

4.2.3 Kidney pathology

4.2.3.1 Immune complex deposition

In humans, SLE pathology is driven by the development of immune complexes (IC). The deposition of IC in the kidney and subsequent development of lupus nephritis is one of the major complications and a frequent cause of SLE mortality (395).

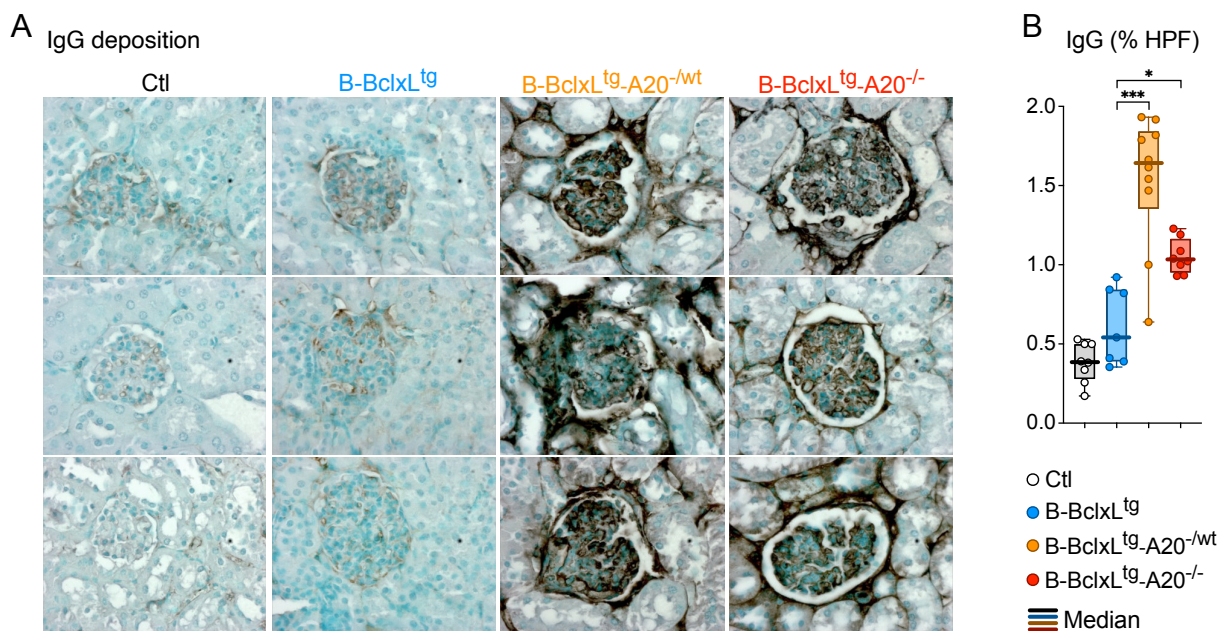


Figure 31. Renal immune complex deposition.

(**A**) Representative pictures and (**B**) quantified IgG immune complex deposition (% of high-power field, HPF) in kidney glomeruli. Per genotype 18 - 120 glomeruli have been evaluated in a total of 7 to 10 kidneys. Data is displayed as box-whisker-plots. Each dot represents the mean %HPF value for one kidney, thick lines highlight the median values per genotype. Assessment of normality and statistical testing were performed as described in the Methods section (chapter 3.11). Only relevant comparisons are depicted on the graphs. (*A-B*) Staining, confocal microscopy and quantification were performed by Prof. Dr. Maciej Lech (LMU, München).

In collaboration with the LMU department of medicine (Munich), I analyzed the deposition of immune complex as well as immune cell infiltration in the kidneys of B-BclxL^{tg}-A20 mice by immunohistochemistry. We could detect strong glomerular IgG immune complex deposition in the kidneys of B-BclxL^{tg}-A20^{-/wt} mice and less pronounced but clearly apparent IgG immune complex deposition B-BclxL^{tg}-A20^{-/-} mice (**Figure 31A, B**).

4.2.3.2 Immune cell infiltration

To investigate whether immune complex deposition entailed kidney inflammation, we analyzed them for infiltration by different immune cells. Staining of kidney tissue for CD45 and Mac-2 revealed glomerular infiltration by CD45⁺ leukocytes (**Figure 32A**), specifically Mac-2⁺ inflammatory macrophages, in B-BclxL^{tg}-A20^{-/wt} mice (**Figure 32B**) (396). In humans, macrophage infiltrates indicate renal inflammation and actively contributes to the pathogenesis of lupus nephritis (397).

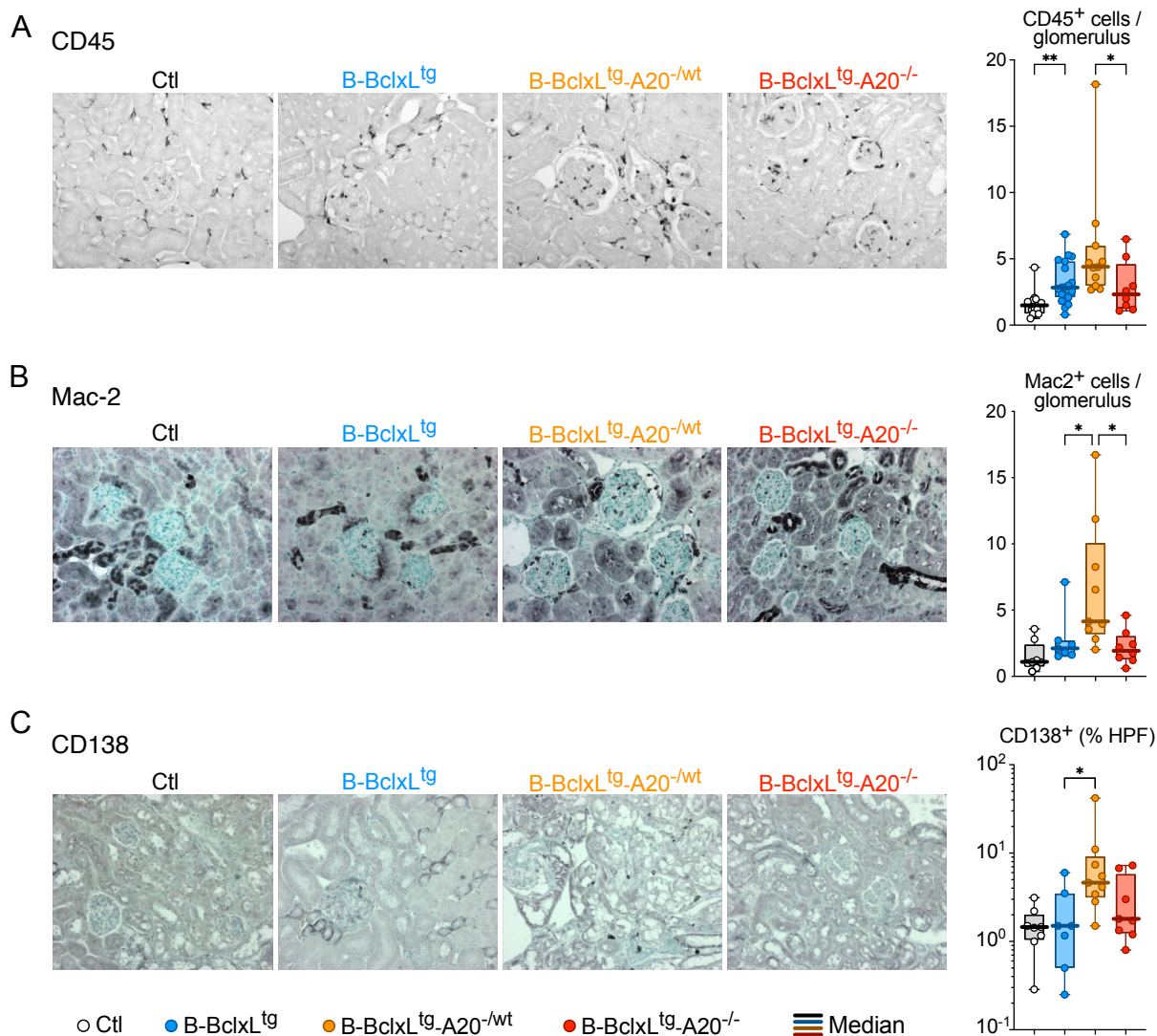


Figure 32. Kidney immune cell infiltration.

(A-C) Representative pictures for confocal microscopy of immunohistochemical stained kidney slides (left) and quantified cell count (right) of **(A)** CD45⁺ leukocytes per glomerulus, **(B)** Mac-2⁺ inflammatory macrophages per glomerulus and **(C)** CD138⁺ plasmacytic cells, quantified as percent of high-power field (% HPF). Per genotype 6 - 8 glomeruli were evaluated in a total of 7 to 10 kidneys. Data is displayed as box-whisker-plots. Each dot represents the mean value for one kidney, thick lines highlight the median values per genotype. Assessment of normality and statistical testing were performed as described in the Methods section (chapter 3.11). Only relevant comparisons are depicted on the graphs. (A-B) Staining, confocal microscopy and quantification were performed by Dr. Mohsen Honarpisheh and Prof. Dr. Maciej Lech (LMU, München).

Additionally, we could detect CD138⁺ plasmacytic cells infiltrating the kidneys of B-BclxL^{tg}-A20^{-/wt} (**Figure 32C**). Renal autoreactive plasma cells were previously reported to appear in NZB/W mice with nephritis (398) and may therefore be an additional measure for kidney inflammation and damage. Renal macrophage and plasma cell infiltration was significantly less pronounced in B-BclxL^{tg}-A20^{-/-} mice.

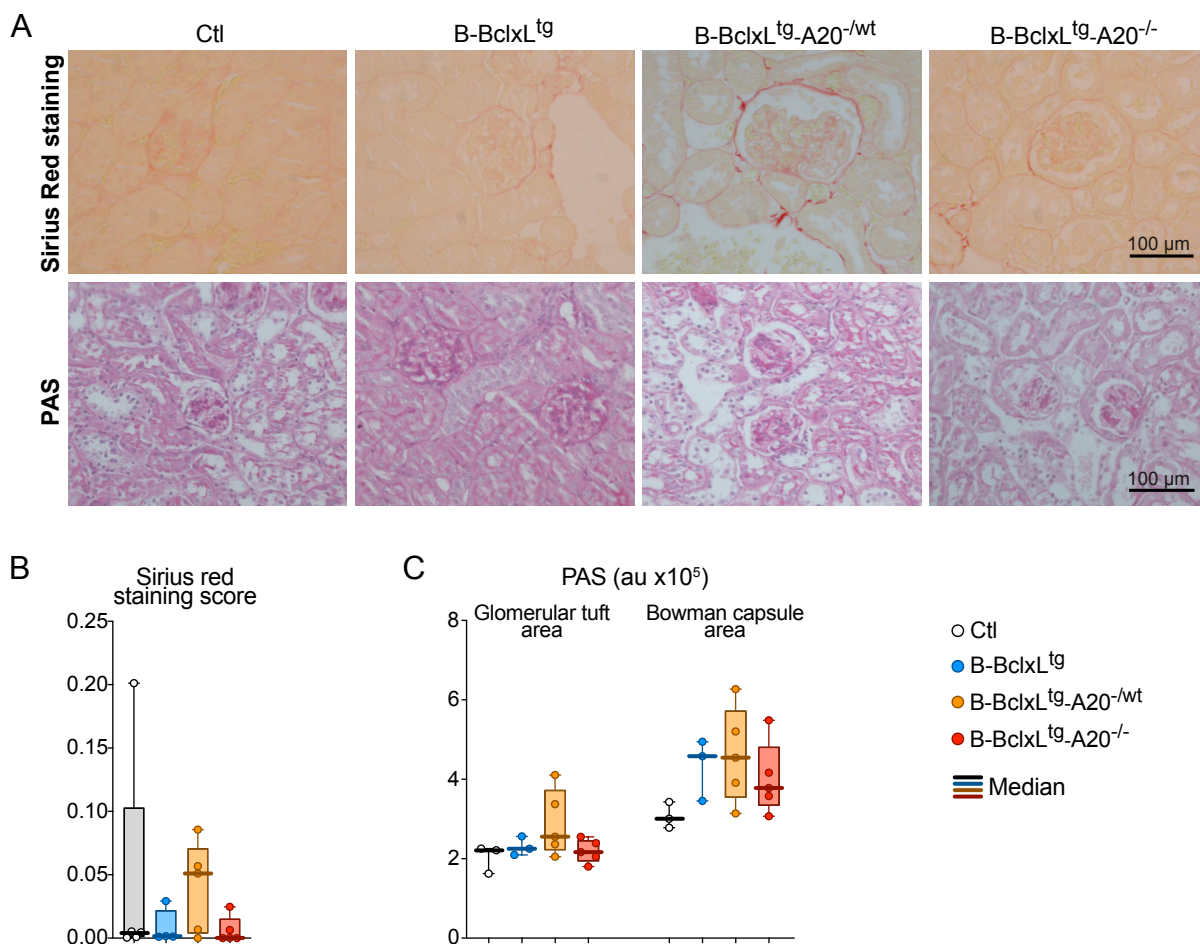


Figure 33. Kidney damage.

(A) Example pictures for confocal microscopy of Sirius Red (upper panel) and Periodic Acid Schiff (PAS) stained (lower panel) kidney slides. **(B)** Sirius Red staining score as measure for fibrotic tissue within the glomerular tuft area. **(C)** PAS quantification as area under the curve (au). (A-C) 4 or 5 kidneys were analyzed per genotype and 10 glomeruli were analyzed per kidney. Data is displayed as box-whisker-plots. Each dot represents the mean value for one kidney, thick lines highlight the median values per genotype. Assessment of normality and statistical testing were performed as described in the Methods section (chapter 3.11). No significant differences were detected. (A-B) Staining, confocal microscopy and quantification were performed by Prof. Dr. Maciej Lech (LMU, München).

Continuous inflammation can induce damage to the kidney tissue, mainly glomeruli, leading to lupus nephritis. While virtually all human SLE patients exhibit IC deposition, only about half of them develop glomerulonephritis (399), which strongly increases the risk of death (400). In nephritic kidneys, positive Sirius Red staining can be correlated with SLE disease activity (401).

In some but not all B-BclxL^{tg}-A20^{-/wt} mice, we detected signs of slight glomerular fibrosis apparent by positive Sirius Red staining on renal tissue sections (**Figure 33A, B**). Additional Periodic Acid Schiff (PAS) staining on the kidneys revealed no clear signs of glomerular damage (**Figure 33A, C**). This shows that despite strong IC deposition and considerable immune cell infiltration, the kidney tissue was not strongly damaged in young B-BclxL^{tg}-A20^{-/wt} mice.

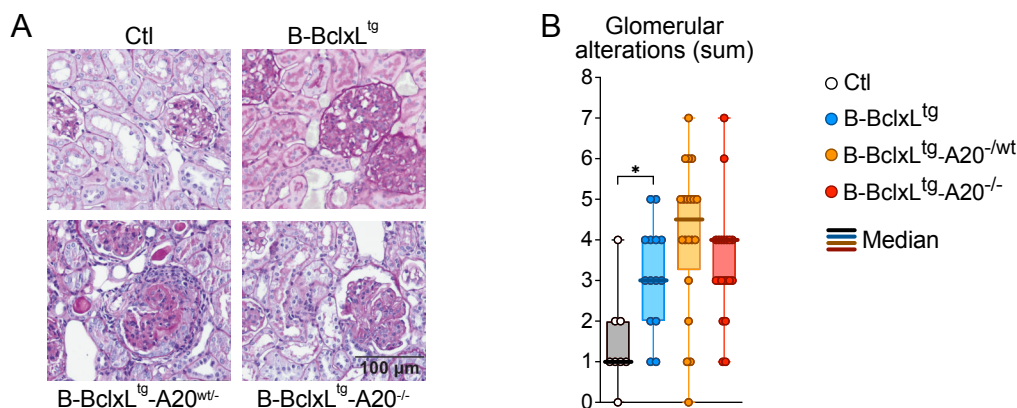


Figure 34. Glomerular alterations in aged mice.

(A) Representative pictures for H&E staining and **(B)** quantification of kidney pathology (hypercellularity, apoptosis, thrombi, thickened basement membrane, extracapillary proliferates, segmental sclerosis) in aged mice. Sum of pathological glomerular alterations per mouse is depicted. Data is displayed as box-whisker-plots. Each dot represents the mean value for one kidney, thick lines highlight the median values per genotype. Assessment of normality and statistical testing were performed as described in the Methods section (chapter 3.11). Only relevant comparisons are depicted on the graphs. Age range of the analyzed mice: Ctl 12 – 16 months, B-BclxL^{tg} 12 – 17 months, B-BclxL^{tg}-A20^{-/wt} 6 – 14 months, B-BclxL^{tg}-A20^{-/-} 13 – 16 months. *(A-B) Mice were analyzed by Dr. Yuanyuan Chu. H&E staining and evaluation of pathology were done by Prof. Dr. Christoph Daniel (FAU, Erlangen).*

The age range of the analyzed mice (3 – 5 months) was below the age range with the maximum death rate of B-BclxL^{tg}-A20^{-/wt} mice (6 – 8 months). In humans, the development of autoantibodies precedes fatal pathology (402). It was therefore likely that the kidney pathology of B-BclxL^{tg}-A20 mice increased over time. A more detailed analysis was performed in cooperation between Prof. Dr. Christoph Daniel (Erlangen) and Dr. Yuanyuan Chu to evaluate different pathological alterations in kidneys from aged (6 – 17 months old) mice. The analysis included changes in the glomerular basal membrane, mesenchymal matrix extension, hypercellularity, intracapillary thrombi, apoptotic events, extracapillary proliferation and segmentary sclerosis (**Figure 34A**). When the number of all glomerular alterations per sample was summed up, increased pathologic glomerular alterations were detected in the kidneys of all BclxL transgenic groups, where B-BclxL^{tg}-A20^{-/wt} mice had by tendency the strongest damage (**Figure 34B**).

4.2.3.3 Glomerular filtration rate

During lupus nephritis, IC deposition and kidney damage are followed by a reduced glomerular filtration rate, which can be measured by quantification of blood urea nitrogen (BUN) in serum. High levels of BUN were detectable in several mice with BclxL^{tg} A20^{-/wt} and BclxL^{tg} A20^{-/-} B cells, demonstrating defective glomerular filtration in a fraction of animals (**Figure 35A**).

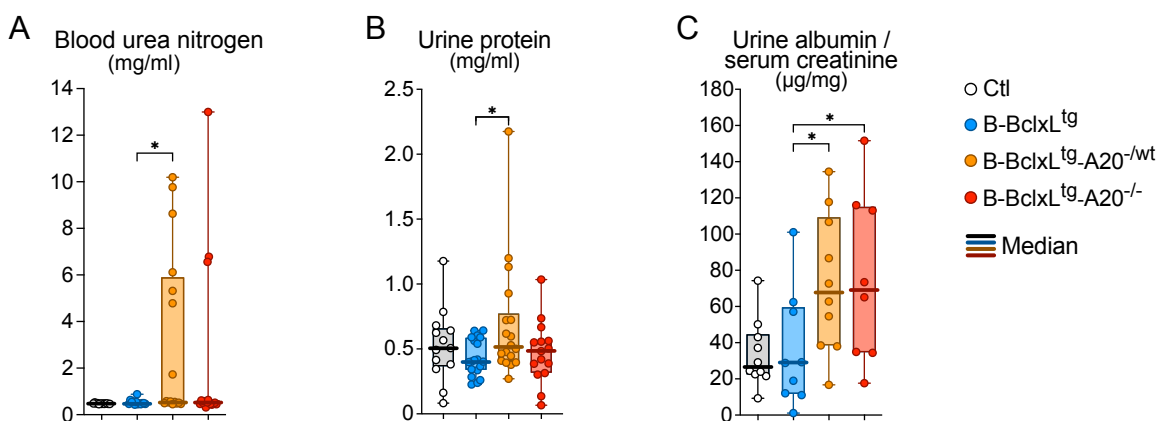


Figure 35. Glomerular filtration rate.

(A) Serum concentration (mg/ml) of blood urea nitrogen (BUN). **(B)** Total protein concentration (mg/ml) in urine, measured with BCA. **(C)** Ratio of urine albumin to serum creatinine concentration, measured with ELISA. Data is displayed as box-whisker-plot. Dots represent individual samples, and thick lines highlight the median value. Assessment of normality and statistical testing were performed as described in the Methods section (chapter 3.11). Only relevant comparisons are depicted on the graphs. (A, C) BUN and albumin/creatinine were measured by Prof. Dr. Maciej Lech (LMU, München).

Reduced glomerular filtration causes proteinuria, which can be measured either by quantification of whole protein in the urine or by measuring the concentration of urine albumin in relation to serum creatinine. I collected urine from 4 months old mice and measured the total protein content. While several B-BclxL^{tg}-A20^{-/wt} mice had slightly increased protein in the urine, there was no sign for strong proteinuria (**Figure 35B**). However, the albumin/creatinine ratio, determined in collaboration with the LMU department of medicine (Munich), appeared equally increased in both, B-BclxL^{tg}-A20^{-/wt} and B-BclxL^{tg}-A20^{-/-} mice, at the age of 4 months (**Figure 35C**). No signs of proteinuria could be detected in younger (2-3 months) and older (5-7 months) mice (total urine protein, data not shown).

Overall, the kidney analyses showed that despite the strong IC deposition, both young and aged B-BclxL^{tg}-A20^{-/wt} mice had only a rather mild renal pathology regarding nephritis and the glomerular filtration rate. Fatal kidney failure is typically preceded by a decline in the general condition of mice. Daily observation of B-BclxL^{tg}-A20^{-/wt} mice revealed no indication for suffering, such as malnutrition, reduced mobility or social isolation, prior to their death. Therefore, I suspected that apart from nephritis these mice may have experienced another, more acute, cause of death.

4.2.4 Heart and liver pathology

Since B-BclxL^{tg}-A20^{-/wt} mice frequently died abruptly without a preceding phase of obvious burden, I investigated other two other vital organs, heart and liver, for macroscopic and microscopic changes, respectively. In human SLE patients, the development of anti-cardiolipin autoantibodies can induce cardiac manifestations (403). Basic analysis of the heart weight did not reveal any general changes, but I observed an infrequent occurrence of hypertrophy in B-BclxL^{tg}-A20^{-/wt} mice (**Figure 36A**).

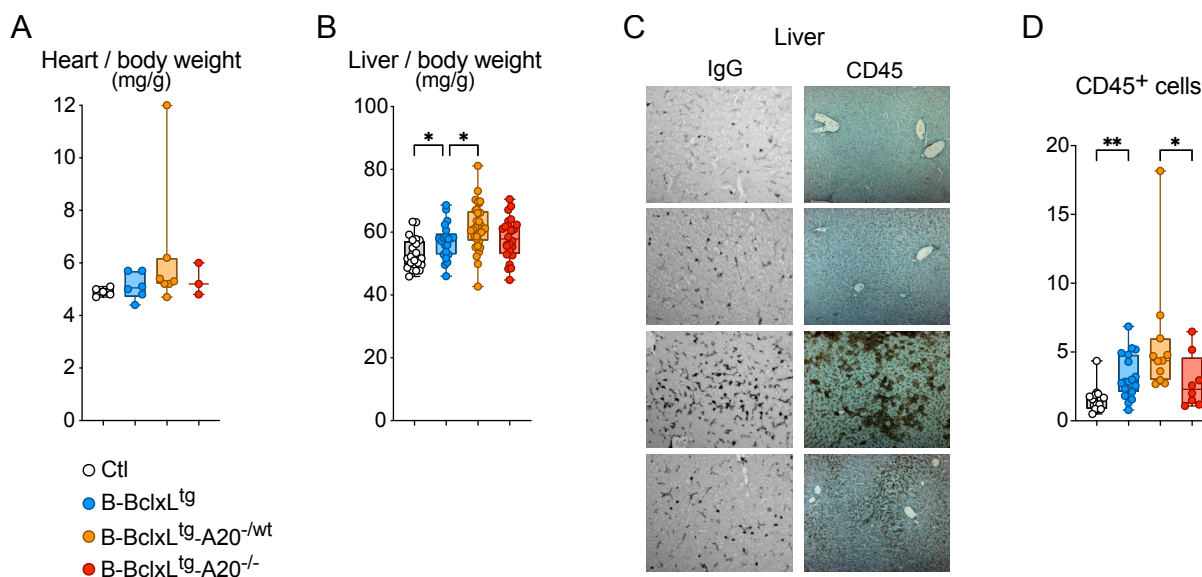


Figure 36. Heart and liver pathology.

(**A**) Weight of the heart divided by total body weight of the mouse. (**B**) Weight of the liver divided by total body weight of the mouse. (**C**) Representative pictures for confocal microscopy of kidney slides immunohistochemically stained for IgG (left) and CD45 (right). (**D**) Quantified cell count of CD45⁺ leukocytes per picture. Data is displayed as box-whisker-plot. Dots represent individual samples, and thick lines highlight the median value. Assessment of normality and statistical testing were performed as described in the Methods section (chapter 3.11). Only relevant comparisons are depicted on the graphs. (*C-D*) Staining, confocal microscopy and quantification were performed by Dr. Mohsen Honarpisheh and Prof. Dr. Maciej Lech (LMU, München).

Another, rather rare, complication in SLE patients is the development of autoimmune hepatitis (AIH) (404). To assess the involvement of liver damage in B-BclxL^{tg}-A20^{-/wt} mice, I investigated liver weight, IgG deposition and immune cell infiltration of the liver tissue in collaboration with the LMU department of medicine (Munich). The liver weight, which is increased in AIH mouse models (405), was significantly higher B-BclxL^{tg}-A20^{-/wt} mice, indicating liver inflammation in these mice (**Figure 36B**). Also, clear deposition of IgG could be detected in liver tissue of B-BclxL^{tg}-A20^{-/wt} mice (**Figure 36C**). Since a large amount of serum IgG in these mice binds to nuclear components, the attachment of IgG to liver tissue must not necessarily be caused by liver-specific antibodies. Instead, intracellular components might become exposed from disrupted cells and be targeted by anti-nuclear autoantibodies. Inflammation was evident by considerable infiltration of B-BclxL^{tg}-A20^{-/wt} livers by CD45⁺ immune cells (**Figure 36D**).

Together, autoantibody binding to and inflammation of the livers may enhance the morbidity of B-BclxL^{tg}-A20^{-/wt} mice but are probably not the main drivers of mortality.

4.2.5 Thymic B cells and salivary gland infiltration

B cells are a scarce population within the thymus and are involved in the negative selection of thymic autoreactive T cells (406). In lupus prone NZB/W mice, thymic B cells strongly expand upon disease development, form structures resembling ectopic germinal centers and induce the differentiation of thymocytes to T_{fh} cells. Additionally, autoreactive plasmacytic cells were detected in the thymi of these mice (407).

In B-BclxL^{tg}-A20^{-/wt} mice, the mean frequency of thymic B cells was only slightly increased (**Figure 37A**). However, in mice with a strong pathology, evident by enlargement of spleen and lymph nodes, large numbers of B and plasmacytic cells were present in the thymus (**Figure 37A, B**; correlation to organ size not shown). Among these B cells, a considerable fraction had a GCB-like phenotype (IgD⁺/CD38^{low}) and part of CD4 T cells were CXCR5⁺ PD-1⁺ T_{fh} cells (**Figure 37C**). This shows that regarding thymic B cells, B-BclxL^{tg}-A20^{-/wt} mice resemble the NZB/W lupus mouse model (407).

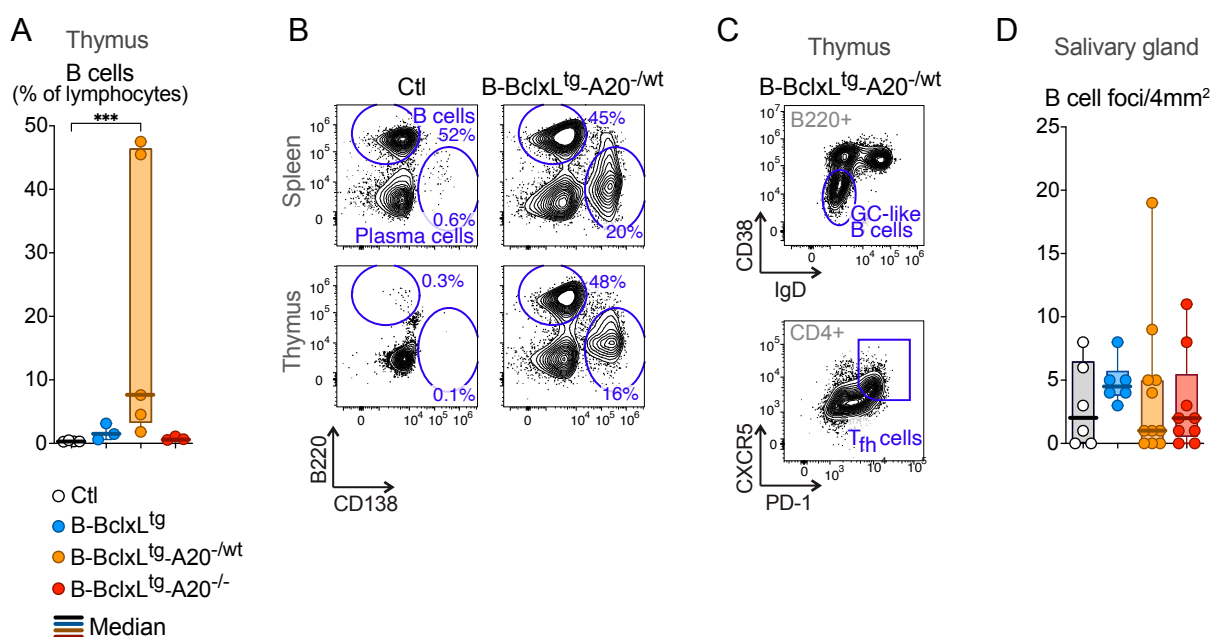


Figure 37. Thymic B cells and salivary gland infiltration.

(A) Fraction of B cells within thymic lymphocytes. **(B)** Flow cytometry plot depicting the fraction of B and plasma cells in spleen and thymus of one CD19Cre control mouse and one B-BclxL^{tg}-A20^{-/wt} mouse with high B cell content. **(C)** Flow cytometry plot depicting the fraction of Germinal center (GC)-like B cells and follicular helper (T_{fh}) cells in the thymus of the second B-BclxL^{tg}-A20^{-/wt} mouse with high B cell content. **(D)** Quantification of salivary gland infiltrating B cells (B cell foci per 4mm² area). (A, B) Data is displayed as box-whisker-plot. Dots represent individual samples, and thick lines highlight the median value. Assessment of normality and statistical testing were performed as described in the Methods section (chapter 3.11). Only relevant comparisons are depicted on the graphs. (A) Some samples were analyzed by Dr. Yuanyuan Chu. (D) Mice were analyzed by Dr. Yuanyuan Chu and B cell infiltrates were quantified by Prof. Dr. Martina Rudelius (LMU, München).

4.2.6 Thrombosis risk

4.2.6.1 Development of an antiphospholipid syndrome (APS)

Death of B-BclxL^{tg}-A20^{-/wt} mice seemed to be rather spontaneous and was impossible to be anticipated despite daily mouse observation in the facility. No signs of burden or suffering indicated vital organ failure as would be caused by fatal nephritis or hepatitis. I therefore expected another, rather sudden cause of mortality.

Human SLE often entails the development of a secondary anti-phospholipid syndrome (APS), which includes the generation of autoantibodies directed against cardiolipin, β_2 -glycoprotein or serine-prothrombin, and correlates with an increased risk for thromboembolic events. There is a variety of mechanisms by which these autoantibodies mediate thrombosis during APS, depending on their specificity, titer, affinity and avidity. Thereby, the autoantibodies induce a prothrombotic state in which thrombosis can be triggered by local stimuli that would not normally be sufficient to do so (408).

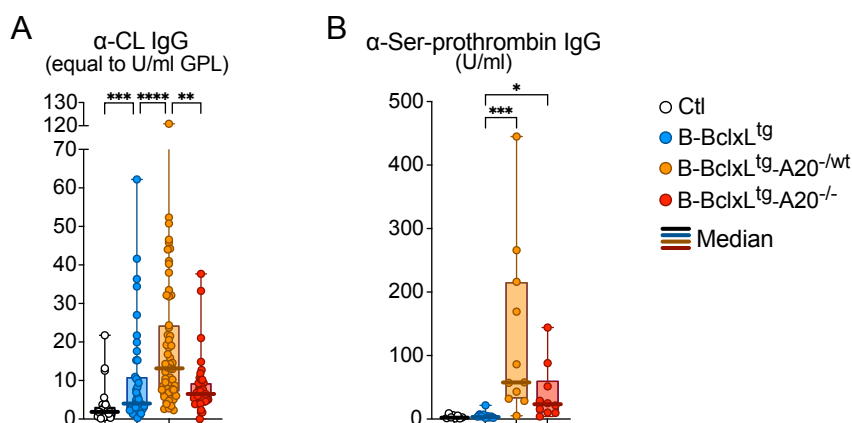


Figure 38. Autoantibodies indicative of APS.

Serum concentration of (A) anti-cardiolipin IgG (α -CL, equal to U/ml GPL) and (B) anti-serin-prothrombin IgG (α -Ser-prothrombin, U/ml) antibodies. Data is displayed as box-whisker-plot. Dots represent individual samples, and thick lines highlight the median value. Assessment of normality and statistical testing were performed as described in the Methods section (chapter 3.11). Only relevant comparisons are depicted on the graphs.

To investigate whether B-BclxL^{tg}-A20^{-/wt} mice develop an APS, I first analyzed the serum concentration of anti-cardiolipin (α -CL) and anti-serin-prothrombin (α -Ser-prothrombin) IgG autoantibodies. All analyzed B-BclxL^{tg}-A20^{-/wt} mice had detectable serum levels of α -CL IgG autoantibodies (Figure 38A). The median concentration was twice as high compared to B-BclxL^{tg}-A20^{-/-} mice. Additionally, in most B-BclxL^{tg}-A20^{-/wt} mice the serum concentration of α -Ser-prothrombin IgG was very high. Also in B-BclxL^{tg}-A20^{-/-} mice, α -Ser-prothrombin IgG was significantly increased compared to B-BclxL^{tg} control mice (Figure 38B).

4.2.6.2 Artificial vessel damage assay

The high serum concentrations of both α -CL and α -Ser-prothrombin autoantibodies were indicative of an APS in B-BclxL^{tg}-A20^{-/wt} mice. The kidney is a major target organ in APS and renal prognosis in SLE patients with lupus nephritis is negatively correlated to the presence of anti-phospholipid antibodies (409). We therefore investigated the occurrence of spontaneous thrombi in kidneys of B-BclxL^{tg}-A20 mice. Indeed, there was a higher incidence of intracapillary thrombi in the kidneys of aged B-BclxL^{tg}-A20^{-/wt} mice compared to all other groups (**Figure 39A**).

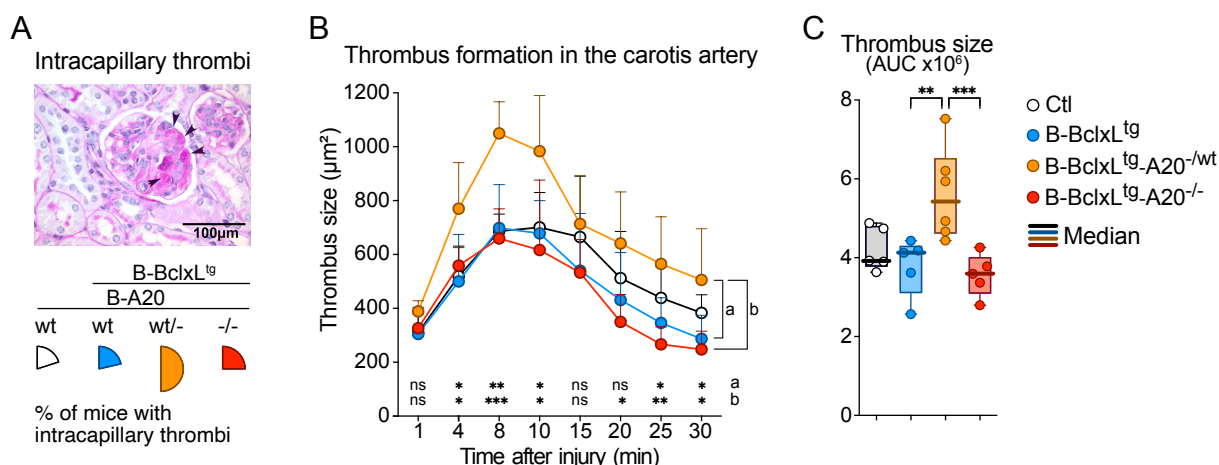


Figure 39. Increased thrombotic activity upon heterozygous and homozygous loss of A20.

(A) Exemplary picture for intracapillary thrombi (highlighted by arrows) in PAS-stained kidney from an aged B-BclxL^{tg}-A20^{wt/-} mouse. Pie charts depict the percentage of mice with intracapillary thrombi in kidneys. Intracapillary thrombi are also included in the sum of total glomerular alterations (Figure 34B). Age range of the analyzed mice: Ctl 12 – 16 months, B-BclxL^{tg} 12 – 17 months, B-BclxL^{tg}-A20^{-/wt} 6 – 14 months, B-BclxL^{tg}-A20^{-/-} 13 – 16 months. (B) Thrombus size over time after injury of the Carotis artery. Significant differences per timepoint depicted for B-BclxL^{tg}-A20^{wt/-} vs. B-BclxL^{tg}-A20^{-/-} and B-BclxL^{tg} mice. Mean values and SD are shown. (C) Cumulative thrombus size calculated as area under the curve (see (B)). Data is displayed as box-whisker-plot. Dots represent individual samples, and thick lines highlight the median value. Assessment of normality and statistical testing were performed as described in the Methods section (chapter 3.11). Only relevant comparisons are depicted on the graphs. (A) Mice were analyzed by Dr. Yuanyuan Chu. H&E staining and evaluation of pathology were done by Prof. Dr. Christoph Daniel (FAU, Erlangen). (B-C) Arterial vessel damage assay was performed by Ul Ain Qurrat and supervised by Dr. med. Joachim Pircher (LMU, München).

To verify if these anti-phospholipid antibodies cause a prothrombotic state, which might propagate thrombus formation, I performed an *in vivo* thrombosis assay in the Carotis artery in cooperation with the LMU Medical Clinic I (Munich). In the anesthetized animals, the vessel was laid open, injury was induced by FeCl₃ application and consecutive thrombus formation at the site of injury was monitored by intravital microscopy. In B-BclxL^{tg}-A20^{-/wt} mice we observed accelerated thrombus formation upon injury and the maximum thrombus size was observed already after 8 minutes, while this was the case only after 10 minutes in control groups. The specific thrombus size in B-BclxL^{tg}-A20^{-/wt} mice was significantly bigger compared to B-BclxL^{tg}-A20^{-/-}, B-BclxL^{tg} and control mice at

early timepoints of 4 to 10 minutes after injury (**Figure 39B**). Consequently, the cumulative thrombus size summed up over the observation time (area under the curve) was significantly higher in B-BclxL^{tg}-A20^{-/wt} mice than in all other groups (**Figure 39C**).

Interestingly, the arterial thrombi in B-BclxL^{tg}-A20^{-/} mice were rather instable: they degraded faster compared to the thrombi in control mice (**Figure 39B**) and had a significantly higher number of embolization events (detachment events of thrombus pieces) (**Supplementary Figure 4A**). Correspondingly, also the serum concentration of the fibrin degradation product D-dimer, which can be detected in blood after thrombus degradation (410), was a much higher in B-BclxL^{tg}-A20^{-/} mice compared to all other groups under steady state (**Supplementary Figure 4B**). This indicated the development of instable thrombi which are subject to steady embolization and degradation in B-BclxL^{tg}-A20^{-/} mice. Microembolizations from arterial thrombi can be beneficial and even life-saving, as they prohibit complete arterial occlusion. These detached thromboemboli are likely susceptible to lysis but might still induce downstream damage to distant tissues. The distal induced detrimental effect is, however, outweighed by the relief of fatal arterial thrombosis (411).

The increased thrombus incidence in the kidneys of B-BclxL^{tg}-A20^{-/wt} mice *in vivo* together with their hyper-coagulability in the vessel damage assay, is in line with the assumption that a secondary APS accompanies their SLE-like phenotype. Apart from anti-phospholipid autoantibodies (see **Figure 38**), B-BclxL^{tg}-A20^{-/wt} mice also had significantly higher serum levels of pro-inflammatory cytokines (see **Figure 28**). Specifically, membrane bound, as well as soluble CD40L can exert a pro-coagulant function through activation of tissue factor expression by endothelial cells (363). Since I detected an elevated serum concentration of sCD40L in B-BclxL^{tg}-A20^{-/wt} mice (see **Figure 28**, group 2), this effect might cooperate with the autoantibody-driven hyper-coagulability to induce lethal thrombosis.

In summary, the high concentration of anti-phospholipid autoantibodies in B-BclxL^{tg}-A20^{-/wt} mice correlated with increased induced thrombus formation and stability. In combination with the high level of systemic inflammation, this prothrombic state, reminiscent of anti-phospholipid syndrome, poses a considerable risk for thrombosis development *in vivo*. I therefore conclude that thrombosis is a potential cause of death and could contribute to the high and sudden mortality of B-BclxL^{tg}-A20^{-/wt} mice.

In conclusion, I was able to identify the lethal pathology in B-BclxL^{tg}-A20^{-/wt} mice as a systemic autoimmune disease resembling many features of human SLE. B cells are known key players in the progression of human SLE (412) and I demonstrated that genetic targeting of B cells alone is sufficient to initiate a full-blown disease in mice.

4.3 Mechanisms of the B cell-driven autoimmune pathology in B-BclxL^{tg} A20^{-/wt} mice

4.3.1 The B cell-driven autoimmune pathology depends on the signaling via MyD88

Turer et al. demonstrated that a body-wide complete knockout of A20 in mice induces systemic inflammation leading to premature death. This inflammatory phenotype was triggered by enhanced toll-like-receptor (TLR) signaling, induced by microbial PAMPs, and could be rescued by simultaneous knockout of the signaling mediator MyD88, which transfers signals downstream of almost all TLRs (235).

Since in SLE autoreactivity is directed against nuclear components, including dsDNA, DNA-sensing receptors like TLRs play a key role in disease initiation and progression. Enhanced TLR signaling predisposes for the development of SLE and in SLE mouse models carrying the Yaa susceptibility locus, an additional copy of the TLR7 gene induces a lupus-like disease development (199, 202). Additionally, TLR7 signaling enhances the expansion and diversification of B cells in the germinal center (200) and can induce the production of pathogenic autoantibodies in spontaneous germinal centers (201). Since combined TLR7 and TLR9 knockout as well as MyD88 knockout are sufficient to inhibit the lupus-like pathology in MRL/lpr mice and Lyn^{-/-} mice (413, 414), MyD88-dependent TLR signaling might also be involved in my A20-deficient B cell-driven autoimmune model. Therefore, I additionally deleted MyD88 specifically in B cells by use of a conditional MyD88 allele (289).

B cell numbers

The resulting B-BclxL^{tg}-MyD88^{-/-}-A20^{-/wt} mice had a significantly extended life span compared to B-BclxL^{tg}-A20^{-/wt} mice, with a median survival of 589 days, and did not die significantly earlier than CD19Cre control mice. Interestingly, in combination with complete loss of A20 in B cells (B-BclxL^{tg}-MyD88^{-/-}-A20^{-/-}), B-MyD88 knockout seemed to have a detrimental effect and significantly reduced the median survival to only 442 days (**Figure 40A**).

The average spleen size of B-BclxL^{tg}-MyD88^{-/-}-A20^{-/wt} mice was even smaller than that of CD19Cre control mice (data not shown). This went in hand with significantly reduced numbers of total splenocytes and splenic B as well as GCB cells. The fraction of GCB cells from all splenocytes was similar in B-BclxL^{tg}-MyD88^{-/-}-A20^{-/wt} and control mice (data not shown), demonstrating that the sustained massive expansion of BclxL^{tg} A20^{-/wt} GCB cells could be inhibited by ablation of B cell-intrinsic MyD88 signaling. In B-BclxL^{tg}-MyD88^{-/-}-A20^{-/-} mice, the loss of MyD88 signaling had no or only a minor effect on the spleen size and the number and total splenic B and GCB cells (**Figure 40B**).

The number of splenic plasmacytic cells was strongly reduced in both B-BclxL^{tg}-A20^{-/wt} and B-BclxL^{tg}-A20^{-/-} mice upon B-MyD88 knockout. In line with the reduction of GCB cells, the fraction of IgG⁺ class switched splenic BclxL^{tg} MyD88^{-/-} A20^{-/wt} plasmacytic cells was decreased, while the fraction of IgM⁺ and to a lesser extent IgA⁺ plasmacytic cells increased (**Figure 40B**). The same effect on isotype distribution, was seen in B-MyD88^{-/-} control mice, showing that this is a direct effect of defective MyD88 signaling in B cells.

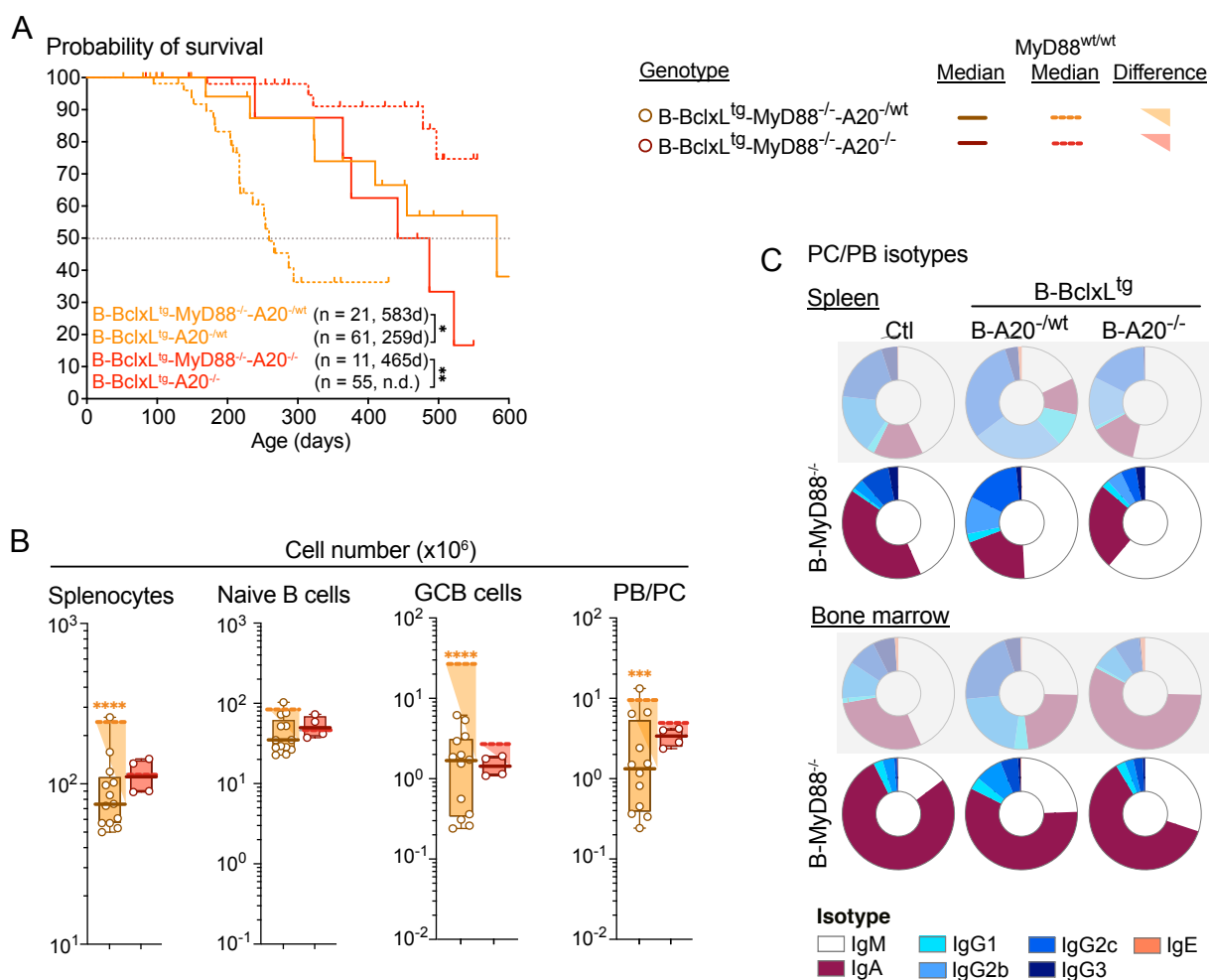


Figure 40. Lethality and B cell expansion of B-BclxL^{tg}-A20^{-/wt} mice are rescued by B cell-specific MyD88 knockout.

(A) Kaplan Meier survival curves of B cell-specific A20-deficient BclxLtg mice with (straight lines) and without (dotted lines) B-MyD88^{-/-}. Cohort sizes and median survival times are shown. Dotted lines were also depicted in Figure 27A. (B) Absolute numbers of total splenocytes, splenic naïve B (CD19⁺ B220⁺ CD95⁻ CD38⁺), germinal center B (GCB, CD19⁺ B220⁺ CD95⁺ CD38^{low}), plasma cells/plasmablasts (PC/PB, CD138⁺ IRF4⁺). Data is displayed as box-whisker-plots. Dots represent individual samples. Thick lines highlight the median values, dotted lines represent the median values of MyD88-sufficient mice. Shaded triangles highlight the difference between both medians and asterisks depict their statistical significance. Assessment of normality and statistical testing were performed as described in the Methods section (chapter 3.11). (C) Fraction of isotypes within PC/PB in spleen and mLN. Shaded pie charts are a repetition of data shown in Figure 13 and are shown here again for visualization of the respective changes upon B-MyD88^{-/-}.

In a bone marrow chimera model, IgG2c class switching was reported to be dependent on B cell-intrinsic MyD88 signaling, as it drives IFN γ production by T cells, while switching to IgG1, IgG3, IgG2b and IgA was less dependent on MyD88 (415). In all B-MyD88^{-/-} mice, switching to all IgG subclasses was uniformly reduced, while IgA switching was increased (**Figure 40C**) despite unchanged concentrations of serum IFN γ (see **Figure 42B**).

B cell-intrinsic MyD88 signaling is required for the production of NAAbs (415). Lack of NAAbs in B-BclxL^{tg}-MyD88^{-/-}-A20^{-/-} could therefore foil the protective effect these antibodies might exert against autoimmunity in B-BclxL^{tg}-A20^{-/-} mice, and thereby potentially contribute to their enhanced lethality.

B and T cell activation

In line with the fact that MyD88 dependent signaling can drive the downregulation of CD62L (313), B-MyD88 knockout leads to a higher CD62L surface expression in B cells. Consistently, BclxL^{tg} MyD88^{-/-} A20^{-/wt} and BclxL^{tg} MyD88^{-/-} A20^{-/-} B cells had more surface CD62L than their MyD88-sufficient counterparts (**Figure 41A**). Also, the expression of most other surface activation markers was reduced on BclxL^{tg} A20^{-/wt} B cells upon loss of MyD88. These included CD44, CD69, CD80 and CD86, although only the latter change was significant. Interestingly, the activation status of BclxL^{tg} A20^{-/-} B cells appeared to be unaffected by loss of MyD88 signaling, which is in line with their generally unchanged B cell numbers and the apparent enhanced capability to induce a fatal pathology. However, more biological replicates of B-BclxL^{tg}-MyD88^{-/-}-A20^{-/-} will be necessary to support this assumption (**Figure 41A**).

Activation of CD4 T cells by B cell APC function is dependent on B cell intrinsic MyD88 signaling (416). B cell specific MyD88 knockout reduced the effector phenotype of CD4 as well as CD8 T cells, apparent by elevated surface CD62L, in B-BclxL^{tg}-A20^{-/wt} but not B-BclxL^{tg}-A20^{-/-} mice (**Figure 41B**). However, more biological replicates of B-BclxL^{tg}-MyD88^{-/-}-A20^{-/-} will be necessary to support this assumption as well.

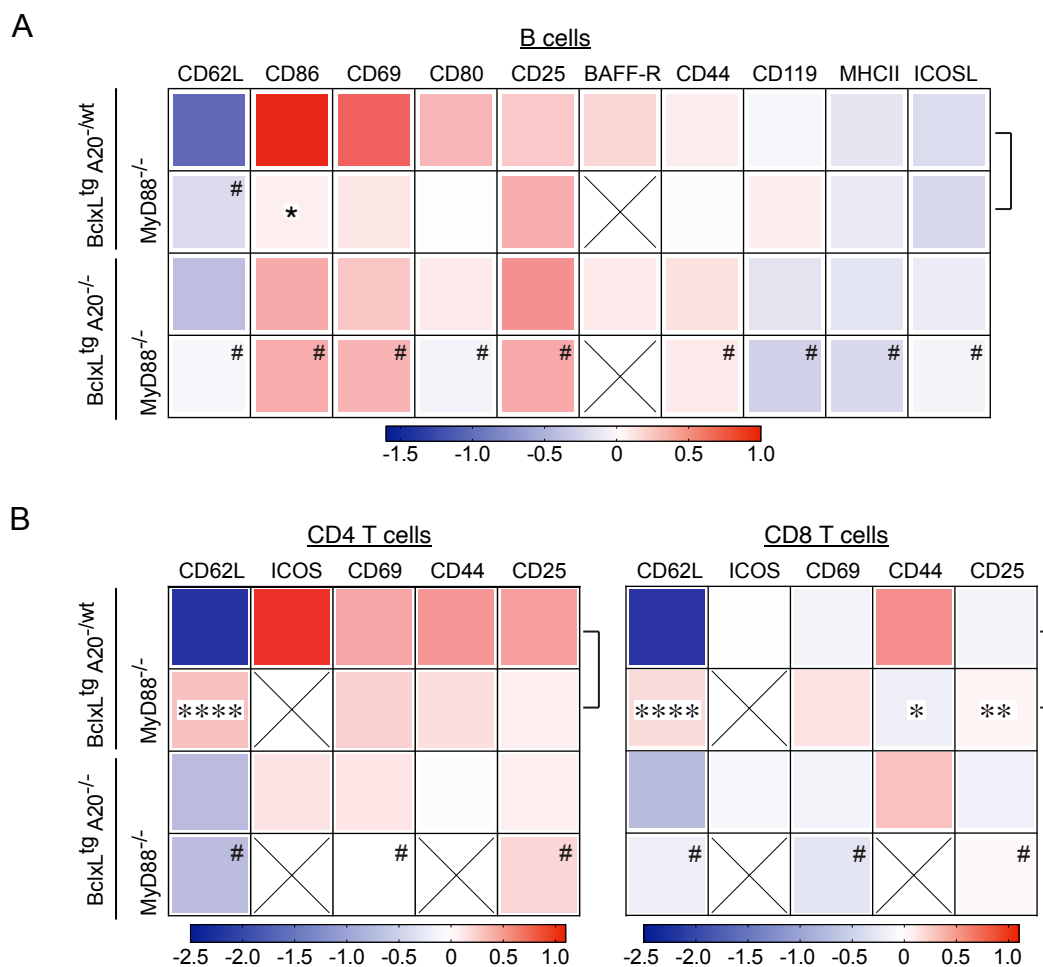


Figure 41. Activation marker expression on B and T cells upon B cell specific MyD88 knockout.

(A-B) Heatmaps representing the log₂-fold change of protein expression in (A) B cells and (B) CD4 or CD8 T cells from B-BclxL^{tg}-A20 and B-BclxL^{tg}-MyD88^{-/-}-A20 mice relative to CD19Cre control cells of the same cell type; measured with flow cytometry. #: value extracted from only 1 biological replicate. Asterisks mark significant differences between cells from B-BclxL^{tg}-A20^{-/wt} and B-BclxL^{tg}-MyD88^{-/-}-A20^{-/wt} mice. Values for MyD88-sufficient mice were shown before in Figure 18 and are included here again for visualization of the difference inferred by B-MyD88^{-/-}.

Pathology

Increased survival and normalization of B cell numbers indicated an alleviation of autoimmune pathology in B-BclxL^{tg}-MyD88^{-/-}-A20^{-/wt} mice. It was uncertain, however, if the increased mortality of B-BclxL^{tg}-MyD88^{-/-}-A20^{-/-} mice related to an increased autoreactivity. Interestingly, both B-BclxL^{tg}-MyD88^{-/-}-A20^{-/wt} and B-BclxL^{tg}-MyD88^{-/-}-A20^{-/-} mice developed no ANA IgG and only few B-BclxL^{tg}-MyD88^{-/-}-A20^{-/wt} mice had an increased amount of anti-cardiolipin IgG (Figure 42A). This clearly demonstrates that the development of autoreactive class-switched autoantibodies in my B-BclxL^{tg}-A20 mouse models depended on B cell-intrinsic signaling via MyD88.

Upon knockout of MyD88, a considerable number of IgG switched plasmacytic cells was still produced (see **Figure 40B, C**). This shows that the lack of autoreactive IgG antibodies in B-BclxL^{tg}-MyD88^{-/-}-A20^{-/wt} was not due to the absence of IgG-class plasmacytic cells but rather resulted from reduced development of autoreactivity upon impaired stimulation of TLRs by self-constituents.

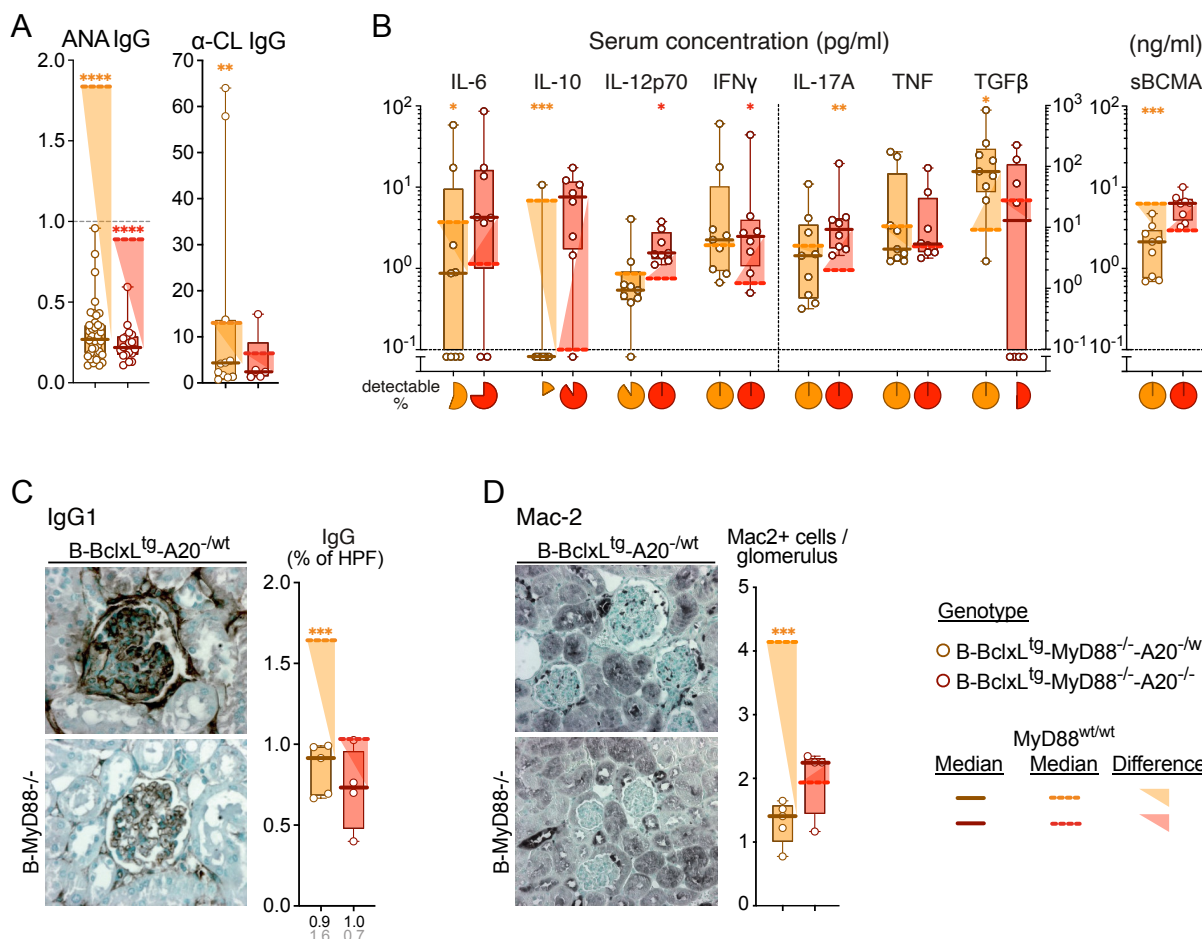


Figure 42. SLE-like pathology is rescued upon MyD88 knockout.

(A) Serum levels of anti-nuclear autoantibodies (ANA, normalized to positive control) and anti-cardiolipin IgG (α -CL, equal to U/ml GPL). **(B)** Serum concentration of IL-6, IL10, IL-12p70, IFN γ , IL-17A, TNF and TGF β (pg/ml) and of soluble BCMA (sBCMA, ng/ml). **(C)** Representative pictures and quantified IgG immune complex deposition (% of high-power field, HPF) in kidney glomeruli. Per genotype 15 - 56 glomeruli have been evaluated in a total of 4 to 5 kidneys. Quantitative data is displayed as box-whisker-plots. Each dot represents the mean %HPF value for one kidney, thick lines highlight the median values per genotype. **(D)** Representative pictures for confocal microscopy of immunohistochemical stained kidney slides and quantified cell count of Mac-2⁺ inflammatory macrophages per glomerulus. Per genotype 6 - 8 glomeruli were evaluated in a total of 4 to 5 kidneys. Data is displayed as box-whisker-plots. Each dot represents the mean value for one kidney. (A-D) Thick lines highlight the median values. dotted lines represent the median values of MyD88-sufficient mice. Shaded triangles highlight the difference between both medians and asterisks depict their statistical significance. Assessment of normality and statistical testing were performed as described in the Methods section (chapter 3.11). (B) Legendplex assay was performed by Julia Knogler. (C-D) Staining, confocal microscopy and quantification were performed by Dr. Mohsen Honarpisheh and Prof. Dr. Maciej Lech (LMU, München).

By multiplex analysis I investigated the serum concentration of inflammatory cytokines. B-MyD88 knockout did not reduce the serum concentration of IFN γ , and high levels of IL-6 and TNF still appeared in the serum of some B-BclxL^{tg}-MyD88^{-/-}-A20^{-/wt} mice, while the average concentration decreased (**Figure 42B**). BCMA levels, however, were reduced in correspondence to lower PC/PB numbers (see **Figure 40B**) and IL-10 was barely detectable in the serum of B-BclxL^{tg}-MyD88^{-/-}-A20^{-/wt} mice (**Figure 42B**). In addition, the serum concentration of TGF β increased in B-BclxL^{tg}-MyD88^{-/-}-A20^{-/wt} mice, which overall supported a normalization of the SLE-typical cytokine pattern (**Figure 42B**). On the contrary, B-MyD88 knockout in B-BclxL^{tg}-A20^{-/-} mice induced an increase of the SLE biomarkers IL-6, IL-10, IL-12p70 and IFN γ as well as the Th17-derived pro-inflammatory cytokine IL-17 (**Figure 42B**).

Kidney pathology was absent in both, B-BclxL^{tg}-MyD88^{-/-}-A20^{-/wt} and B-BclxL^{tg}-MyD88^{-/-}-A20^{-/-} mice: Renal IgG IC deposition was significantly reduced (**Figure 42C**) and no macrophage infiltration could be detected in the glomeruli of B-BclxL^{tg}-MyD88^{-/-}-A20^{-/wt} mice (**Figure 42D**). Furthermore, there was no elevated BUN in any of the B-BclxL^{tg}-MyD88^{-/-}-A20^{-/wt} samples (data not shown), underlining the absence of kidney damage.

Together, these observations clearly demonstrate that the development of the SLE-like autoimmune pathology, induced by heterozygous A20-deficiency in B cells, depends on signaling via MyD88. Therefore, the upstream activation of NF- κ B signaling leading to B cell hyperactivation in B-BclxL^{tg}-A20^{-/wt} mice is mainly transmitted via this adaptor molecule and likely affects mainly ssRNA and dsDNA sensing via TLR7 and TLR9, respectively. In absence of these signals autoreactivity is not initiated.

Fittingly, the combined loss of TLR7 and TLR9 as well as MyD88 knockout were reported to reduce total serum IgG and autoantibody production as well as kidney pathology in MRL/lpr mice (417).

4.3.2 The role of the germinal center for autoimmune pathology

The germinal center reaction seems to play a key role in the development of SLE-like pathology in B-BclxL^{tg}-A20^{-/wt} mice as their tremendous GCB cell expansion increases the chance to generate high affinity class-switched autoreactive antibodies through sustained SHM. We therefore aimed to examine whether a loss of A20 specifically in GCB cells is sufficient to initiate an equally strong autoimmune pathology.

4.3.2.1 Loss of A20 specifically in GCB cells (C γ 1Cre/AIDCre model)

Since the initiation of A20-deficiency by CD19Cre also affects non-GCB cell subsets I crossed the conditional A20 alleles with the C γ 1Cre and AIDCre mouse strains. C γ 1Cre activates Cre recombinase from the endogenous immunoglobulin heavy constant gamma 1 (Ighg1) locus, ablating A20 specifically in GCB cells upon onset of germline C γ 1 transcription (288). Thereby IgG1 switched, but also most of IgG3, IgG2b, IgG2c and IgA switched GCB cells as well as the subsequently generated memory B and plasma cells are targeted by Cre-mediated A20 ablation (288). AIDCre activates Cre recombinase from the endogenous Aicda locus, coding for AID, which is specifically activated in GCB cells to enable CSR and SHM (286). Low level AID expression, however, can also be found in BM immature and transitional B cells (418) as well as embryonic neuronal cells (419). Due to this background activity, we performed only few analyses with AIDCre (**Figure 43**). However, since the effect of AIDCre and C γ 1Cre driven A20 deletion in GCB cells was largely equal, the results of both lines were combined and are subsequently termed GCB-BclxL^{tg}-A20^{-/-}, GCB-BclxL^{tg}-A20^{-/wt} and GCB-BclxL^{tg}. Despite this annotation, the E μ -BclxL transgene was expressed in all B cell lineages, not only GCB cells.

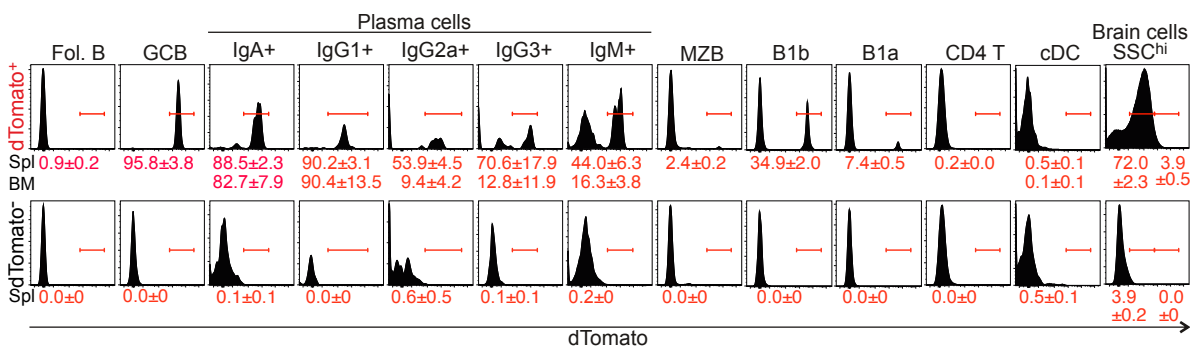


Figure 43. AIDCre activity.

Histograms depicting the expression of a conditional dTomato reporter upon AIDCre activity in different cell types. The fraction of dTomato-expressing cells per cell type is shown in red for spleen (Spl, first row) and bone marrow (BM, second row) in a mouse carrying one dTomato allele (upper panel) and a control mouse without dTomato allele (lower panel).

Heterozygous deletion of A20 at the GCB developmental stage was sufficient to recapitulate the pathology of B-BclxL^{tg}-A20^{-/wt} mice. GCB-BclxL^{tg}-A20^{-/wt} mice displayed substantial splenomegaly already at 3-5 months age. This was accompanied by a strong expansion of splenic GCB and plasmacytic cells. Simultaneously, the number of T_{fh} cells was increased similar to B-BclxL^{tg}-A20^{-/wt} mice (**Figure 44A-E**).

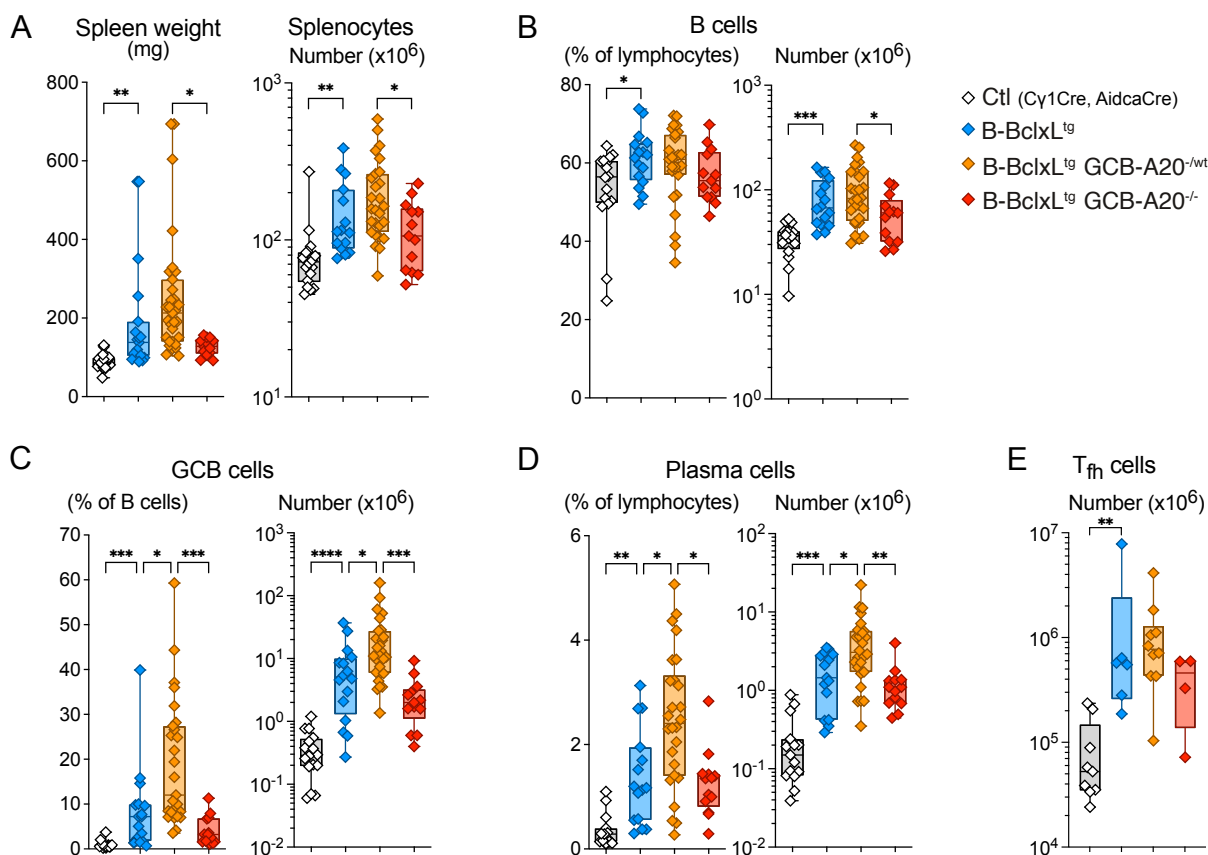


Figure 44. Splenic cell composition in GCB-BclxL^{tg}-A20 mice.

(A) Spleen weight and total number of splenocytes. (B-D) Fraction and total number of (B) B220⁺ CD19⁺ B cells, (C) B220⁺ CD19⁺ CD95⁺ CD38^{lo} GCB cells, (D) CD138⁺ CD38^{lo} plasma cells and (E) absolute number of CD4⁺ CDXCR5⁺ PD-1⁺ follicular helper T (T_{fh}) cells. (A-E) Data is displayed as box-whisker-plots. Diamonds represent individual samples. Assessment of normality and statistical testing were performed as described in the Methods section (chapter 3.11). Only relevant comparisons are depicted on the graphs. (A-D) Graphs include values of Cy1Cre mice, which were analyzed by Dr. Yuanyuan Chu and Dr. Valeria Soberón

Corresponding to the increase of germinal centers, an increased fraction of splenic plasma cells in GCB-BclxL^{tg}-A20^{-/wt} mice was switched, non-IgM⁺, and these mice contained elevated ANA IgG as well as anti-cardiolipin IgG autoantibodies at young age (**Figure 45A, B**). This demonstrates that the heterozygous loss of A20 specifically in GCB cells is sufficient to induce the development of systemic autoimmunity with an equally early disease onset as A20-deficiency in all B cells.

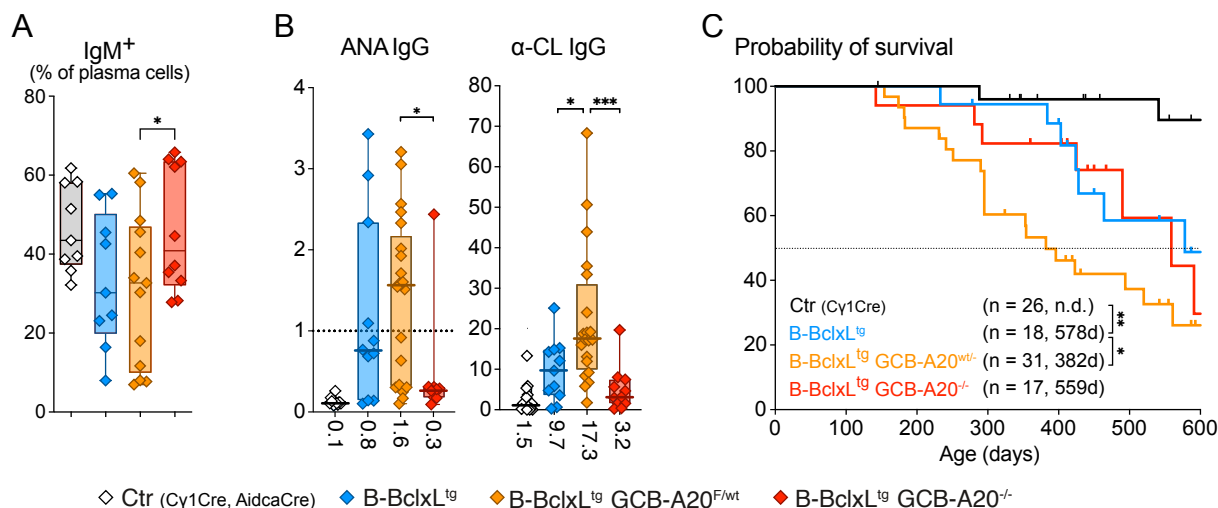


Figure 45. Autoimmune pathology in GCB-BclxL^{tg}-A20 mice.

(A) Fraction of IgM⁺ splenic plasma cells. (B) Serum levels of anti-nuclear IgG antibodies (ANA, normalized to positive control) in young mice, 3 - 6 months. (C) Serum concentration of anti-cardiolipin IgG (α-CL, equivalent to U/ml GPL). Data is displayed as box-whisker-plots. Diamonds represent individual samples. Assessment of normality and statistical testing were performed as described in the Methods section (chapter 3.11). Only relevant comparisons are depicted on the graphs. (A-C) Graphs include values of *Cy1Cre* mice, which were analyzed by Dr. Yuanyuan Chu and Dr. Valeria Soberón.

Disease progression, however, seemed to be slightly delayed (median survival 354 days in GCB-BclxL^{tg}-A20^{-/wt} vs. 259 days in B-BclxL^{tg}-A20^{-/wt} mice), but the survival difference was not statistically significant (**Figure 45C**). Consequently, I could show that heterozygous loss of A20 in GCB cells is sufficient to cause a deadly autoimmune pathology.

4.3.2.2 The autoimmune pathology depends on the generation of class-switched high-affinity autoantibodies through affinity maturation of autoreactive B cells within the germinal center

The germinal center reaction depends on the expression of activation-induced cytidine deaminase (*Aicda*/AID) to enable CSR and SHM (17). Through breeding of a Cre-recombinase knock-in into the *Aicda* gene locus (286) to homozygosity, I generated a complete AID knockout (AID^{Δ/Δ}).

AID knockout normalized the splenomegaly and reduced the absolute B cell numbers in B-BclxL^{tg}-A20^{-/wt} mice. While loss of AID is known to inhibit the development of affinity matured and class switched plasma cells, it is not disrupting the generation of Fas^{high} CD38^{low} GCB cells per se. Indeed, the total number of GCB cells was reported to be slightly elevated in AID knockout mouse models, compared to control mice, while the generation of class switched, affinity matured plasma cells was blocked (420-422). In line with these findings, blocking of CSR and SHM by AID knockout even increased the absolute number of splenic GCB cells in AID^{Δ/Δ} B-BclxL^{tg} control mice (**Figure 46A**).

In mice with heterozygous A20-deficiency in B cells ($AID^{\Delta/\Delta}$ B- $BclxL^{tg}$ - $A20^{-/wt}$), however, AID knockout significantly reduced the number of GCB cells and ameliorated splenomegaly, compared to B- $BclxL^{tg}$ - $A20^{-/wt}$ mice (**Figure 46A**). This demonstrates that the strong $BclxL^{tg}$ $A20^{-/wt}$ GCB cell expansion is not only driven by a lowered threshold for germinal center entry and increased proliferation inside the germinal center. Instead, B and GCB cell expansion are to a large extent secondary to events requiring class-switch recombination and somatic hypermutation, including the development of affinity-matured class-switched autoreactive plasma cells. The subsequent development of systemic inflammation sustains an on-going germinal center expansion.

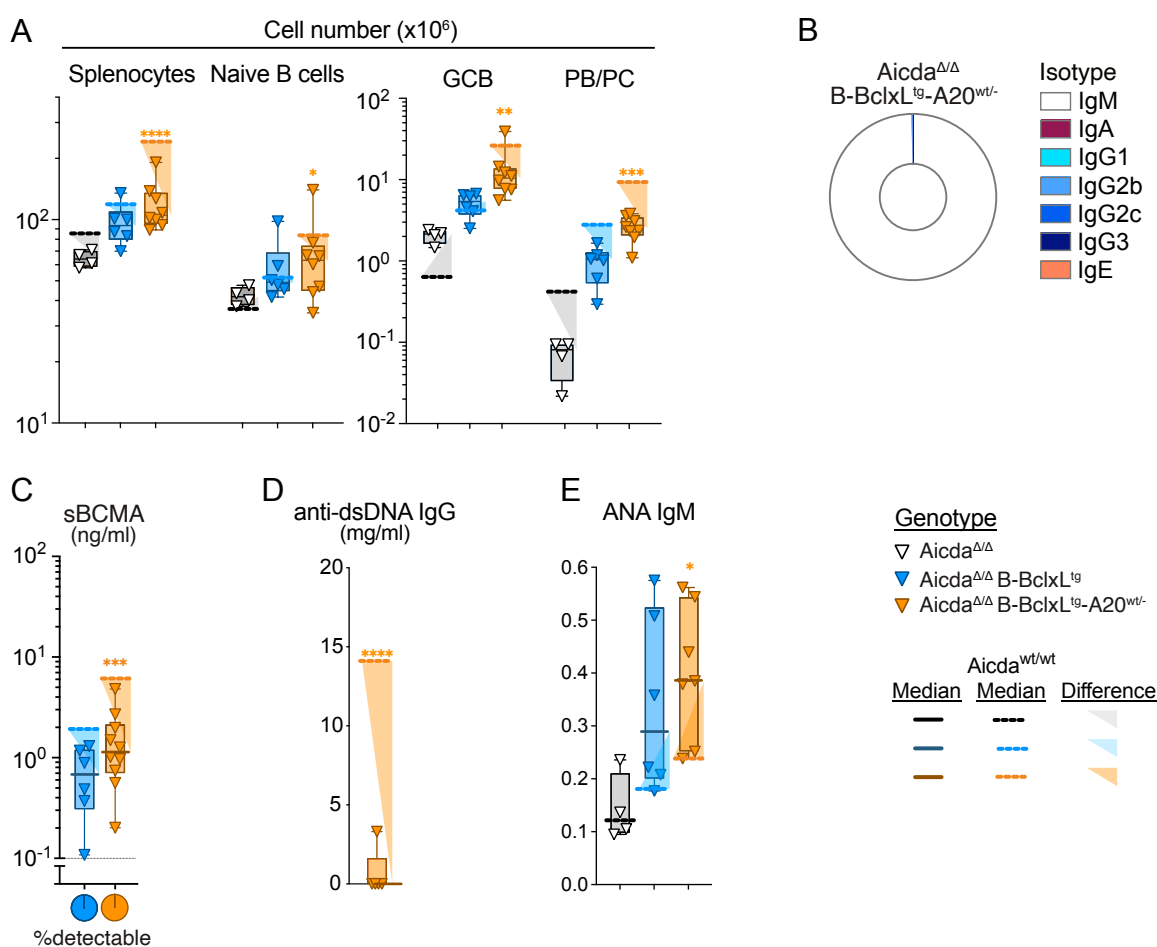


Figure 46. *Aicda* knockout inhibits the generation of class switched plasmacytic cells.

(A) Absolute numbers of total splenocytes, splenic naïve B ($CD19^+$ $B220^+$ $CD95^-$ $CD38^+$), germinal center B (GCB, $CD19^+$ $B220^+$ $CD95^+$ $CD38^{low}$), plasma cells/plasmablasts (PC/PB, $CD138^+$ $IRF4^+$). **(B)** Fraction of isotypes within splenic PC/PB of a $AID^{\Delta/\Delta}$ B- $BclxL^{tg}$ - $A20^{-/wt}$ mouse. **(C)** Serum concentration of soluble BCMA (sBCMA, ng/ml). **(D)** Serum concentration of anti-dsDNA IgG autoantibodies (mg/ml). **(E)** Serum levels of anti-nuclear IgM autoantibodies (ANA IgM, normalized to positive control). Data is displayed as box-whisker-plots. Dots represent individual samples. Thick lines highlight the median values, dotted lines represent the median values of AID-sufficient mice. Shaded triangles highlight the difference between both medians and asterisks depict their statistical significance. Assessment of normality and statistical testing were performed as described in the Methods section (chapter 3.11). *(C) Legendplex assay was performed by Julia Knogler. (D) anti-dsDNA ELISA was performed by Prof. Dr. Maciej Lech (LMU, München).*

The number of splenic plasmacytic cells was also significantly reduced in $AID^{\Delta/\Delta}$ B-BclxL^{tg}-A20^{-/wt} mice (**Figure 46A**) in line with reduced serum levels of sBCMA (**Figure 46C**). Due to the inhibition of CSR, all $AID^{\Delta/\Delta}$ mice were lacking class-switched plasma cells and all existing plasma cells were IgM⁺ (**Figure 46B**). Consequently, there were no ANA IgG (data not shown) and anti-dsDNA IgG (**Figure 46D**) autoantibodies detectable in the serum of $AID^{\Delta/\Delta}$ B-BclxL^{tg}-A20^{-/wt} mice.

Importantly, low level AID expression in bone marrow immature and transitional B cells was shown to suppress the development of autoreactivity (418). In addition, B-BclxL^{tg} expression increases the likelihood for autoreactive B cells to escape negative selection (423). In correlation to previously published $Aicda^{-/-}$ mice, which exhibit significantly increased serum autoantibody (418), also $AID^{\Delta/\Delta}$ B-BclxL^{tg}-A20^{-/wt} and of $AID^{\Delta/\Delta}$ B-BclxL^{tg} mice had higher serum levels of ANA IgM than AID wild type B-BclxL^{tg}-A20^{-/wt} and B-BclxL^{tg} mice (**Figure 46E**). However, these ANA IgM also comprise NAAbs with protective functions.

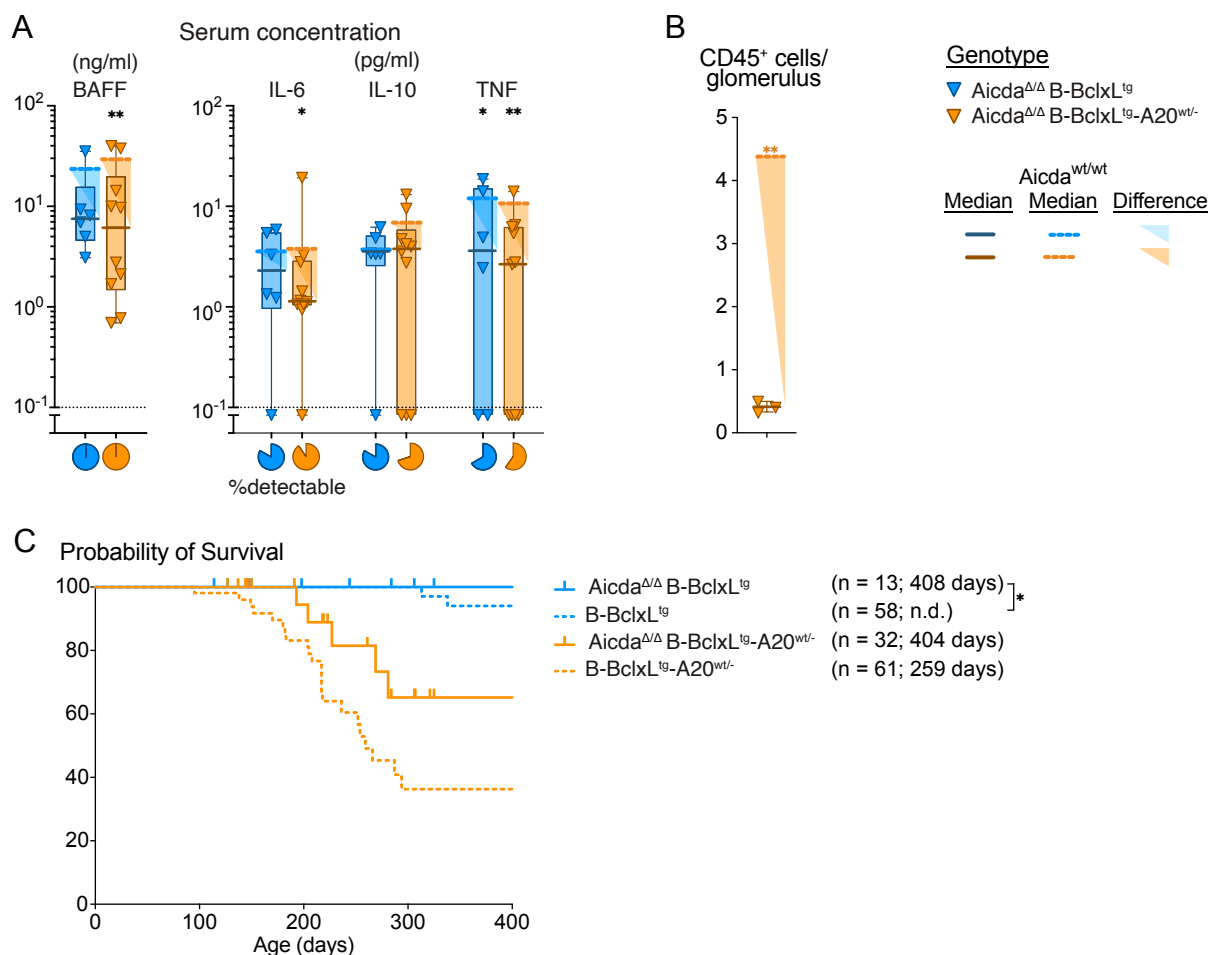


Figure 47. *Aicda* knockout ameliorates systemic inflammation and autoimmune pathology.

(A) Serum concentration of BAFF (ng/ml) and of IL-6, IL10 and TNF (pg/ml). Data is displayed as box-whisker-plots. Triangles represent individual values. (B) Cell count of CD45⁺ leukocytes per glomerulus. Per genotype 6 - 8 glomeruli were evaluated in a total of 4 to 5 kidneys. Data is displayed as box-whisker-plots. Each triangle represents the mean value for one kidney. (A-B) Thick lines highlight the median values, dotted lines represent the median values of AID-sufficient

mice. Shaded triangles highlight the difference between both medians and asterisks depict their statistical significance. Assessment of normality and statistical testing were performed as described in the Methods section (chapter 3.11). **(C)** Kaplan Meier survival curves of B cell-specific A20-deficient BclxLtg mice with (straight lines) and without (dotted lines) AID-knockout. Cohort sizes and median survival times are shown. Dotted lines were also depicted in Figure 27A. *(A) Legendplex assay was performed by Julia Knogler. (B) Staining, confocal microscopy and quantification were performed by Dr. Mohsen Honarpisheh and Prof. Dr. Maciej Lech (LMU, München).*

In addition to the decrease in autoreactive IgG, the serum levels of inflammatory cytokines BAFF, IL-10, IL-6 and TNF, observed in B-BclxL^{tg}-A20^{-/wt} mice, were reduced upon AID knockout to reach concentrations similar to B-BclxL^{tg} control mice, demonstrating the alleviation of systemic inflammation (**Figure 47A**).

In line with the reduced inflammation, AID knockout improved the kidney pathology (**Figure 47B**) and survival of B-BclxL^{tg}-A20^{-/wt} mice (**Figure 47C**). This effect persisted despite an undefined negative impact of AID^{ΔΔ} in control mice.

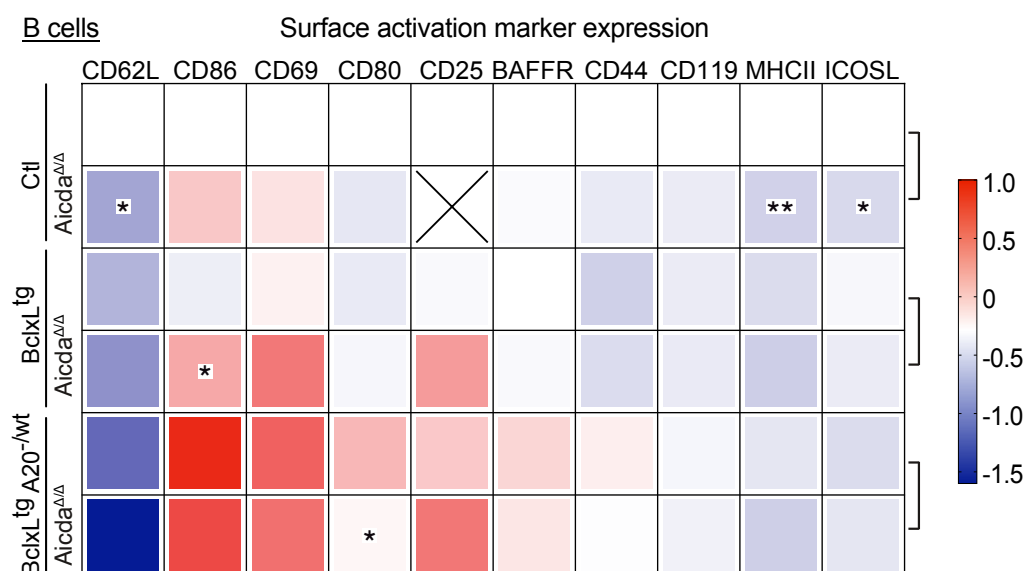


Figure 48. Aicda knockout does not reduce B cell activation.

Surface activation marker expression of B2 cells (B220⁺ CD19⁺). Geom. mean fluorescent intensity was extracted for the indicated surface marker proteins. MFI values were normalized to the MFI values of CD19Cre control cells within each experiment. Mean log₂ values were plotted. Asterisks depict significant differences between the indicated groups. Each value is the mean of at least 3 replicates from minimum 3 independent experiments. Values for AID-sufficient mice were shown before in Figure 18 and are included here again for visualization of the difference inferred by AID^{ΔΔ}.

I next investigated whether the loss of AID also rendered the B cells less hyperactive regarding their surface activation marker expression (**Figure 48**). Interestingly, the knockout of AID in control ($AID^{\Delta\Delta}$ control) and B-BclxL^{tg} mice increased the mean surface expression of the activation markers CD86 and CD69 in B cells, but reduced surface MHCII and ICOSL. Despite their lower fraction of GCB cells, mean surface expression of CD86 was not decreased in $AID^{\Delta\Delta}$ B-BclxL^{tg}-A20^{-/wt} mice. Among all analyzed activation markers, decreased surface expression was only detected for CD80. CD80 can be upregulated in CD86 expressing activated B cells upon contact to CD28 (424), indicating that contact to T cells might be reduced. Since CD80 expression on B cells is critical for germinal center stability, T_h differentiation and PC generation, the low CD80 levels correlate to the observed cellular composition in the spleen of $AID^{\Delta\Delta}$ B-BclxL^{tg}-A20^{-/wt} mice (425). This demonstrates that the intrinsic potential of BclxL^{tg} A20^{-/wt} B cells for strong activation is not reduced upon loss of AID-expression.

Overall, the inability to generate high-affinity class-switched plasma cells, protected $AID^{\Delta\Delta}$ B-BclxL^{tg}-A20^{-/wt} mice against the development of lethal systemic inflammation and SLE-like autoimmunity.

In summary, my data allows the conclusion that the development of a strong autoimmune pathology in B-BclxL^{tg}-A20^{-/wt} mice depends on the generation of class-switched high-affinity autoreactive plasma cells. The autoreactive B cells, giving rise to these plasma cells, likely stem from a pool of low-affinity autoreactive B cells, generated during B cell development in the bone marrow. Increased NF- κ B activation upon heterozygous loss of A20 might lower the threshold for the recruitment of low affinity autoreactive B cells into the germinal center, where the affinity towards self-antigen is enhanced through SHM. Additionally, de novo mutations transforming a non-autoreactive to an autoreactive B cell might occur during the germinal center reaction. However, we did not further investigate the influence of both, affinity maturation of autoreactive clones and de novo acquisition of autoreactivity, on the development of pathology.

The strong clonal expansion of autoreactive BclxL^{tg} A20^{-/wt} B cells in the germinal center is sustained by increased availability of T cell help from presumably autoreactive T_h cells, which were positively selected by antigen-presenting autoreactive B cells. The subsequent autoantibody production by class-switched plasma cells induces the generation of immune complex and the development of systemic inflammation. This boosts B cell hyperactivation as well as a sustained germinal center reaction through inflammatory cytokine signaling in a positive feedback loop. The cooperation of BCR and MyD88-mediated TLR signaling specifically drives the development of DNA-specific autoreactivity.

4.4 Homozygous A20 ablation induces contradictory effects *in vivo* and *in vitro*

B cell-specific BclxL^{tg} expression in combination with heterozygous loss of A20 in mice induces an autoimmune disease resembling many features of human SLE. Patients with SLE and other systemic autoimmune diseases including RA or SjS are frequently reported to carry inactivating mutations in *Tnfrif3/A20*, which were essentially always monoallelic (241).

More general, the haploinsufficiency of A20, defined as HA20 disease entity, causes a variety of autoinflammatory symptoms and new HA20 cases are being detected regularly. Since the complete loss of A20 in cells is known to be much more activating than its heterozygous deficiency, one would expect the complete B cell-specific A20 knockout to induce an even stronger pathology than its heterozygous ablation. Since, this seems not to be the case, there must be a yet undefined mechanism that prevents the pathological expansion and function of A20 knockout B cells.

4.4.1 Transcriptomics data reveals a high metabolic signature in A20^{-/-} B cells

To gain insight into the differences in gene expression between BclxL^{tg}, BclxL^{tg} A20^{-/wt} and BclxL^{tg} A20^{-/-} (\pm MyD88^{-/-}) B cells and to identify the effects counteracting BclxL^{tg} A20^{-/-} B cell expansion *in vivo*, I performed transcriptomic analyses on bulk sorted follicular B (FolB), GCB and plasma cells isolated from mice of the genotypes mentioned above. In collaboration with the Institute for Experimental Cancer Genetics, TUM, I first investigated the independent clustering of the samples by principal component analysis (PCA). When all samples were included, I observed a clear clustering of the samples by organ, demonstrating that the microenvironment imposed a stronger effect on the gene expression than the deficiencies for A20 and MyD88 (**Figure 49A**). Therefore, I next decided to investigate genotypic effects on the gene expression initially only in splenic samples. Within the spleen, only the plasma cell samples clustered according to their genotype. However, the knockout of MyD88 had a stronger effect on the gene expression than both BclxL^{tg} expression and hetero- or homozygous loss of A20 (**Figure 49B**, left panels). To detect the effect of A20 gene dosage on B and plasma cell gene expression, I performed a PCA including only MyD88-sufficient samples from spleen. This showed a clustering of BclxL^{tg} A20^{-/-} plasma cells away from BclxL^{tg} A20^{-/wt} and BclxL^{tg} plasma cells (**Figure 49B**, right panels).

In all instances, naïve B cells and GCB cells did not cluster according to genotype (**Figure 49B**), suggesting only very mild effects of the genetic alterations on their gene expression in the steady state.

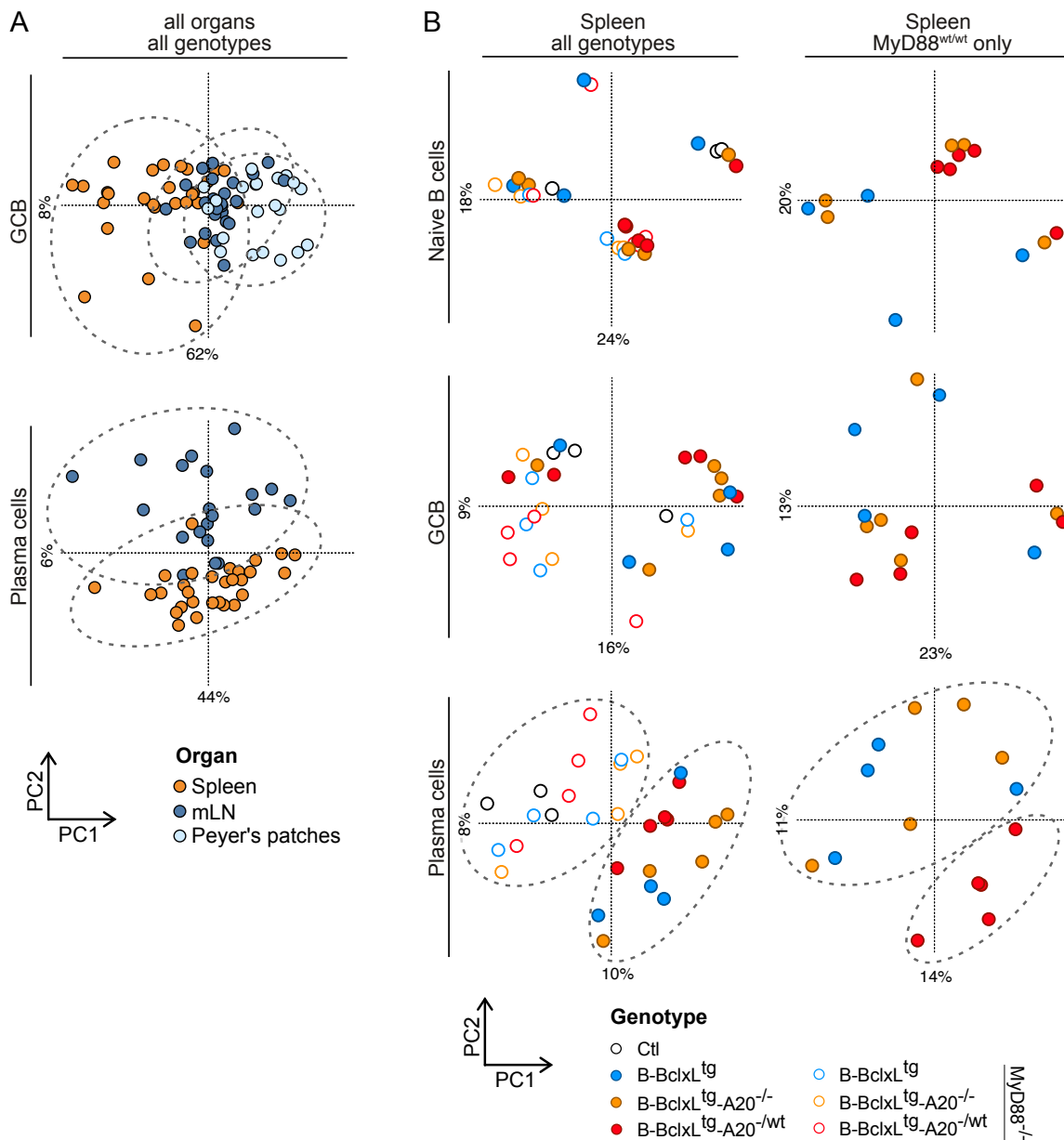


Figure 49. Principal component analysis of bulk RNA sequencing in B cells from B-BclxL^{tg}-A20 mice.

Clustering of the bulk RNA sequencing data set extracted from 1000 sorted **(A)** germinal center B cells (GCB, CD19⁺ B220⁺ CD95⁺ CD38^{low}) or plasma cells (CD138⁺ B220^{low}), including samples from all organs: spleen, mesenteric lymph nodes (mLN) and Peyer's patches and **(B)** naïve B cell (CD19⁺ B220⁺ CD95⁻ CD38⁺), GCB cell and plasma cell samples from spleen, including all genotypes (left panel) or only samples with the genotype B-MyD88^{wt/wt} (right panel). *(A, B) Cells were sorted by me. RNA sequencing was performed by Dr. Rupert Öllinger. Sequencing data was analyzed and heatmap was generated by Dr. Thomas Engleitner in accordance with my requests.*

Next, I analyzed the MyD88-sufficient samples from spleens for differentially expressed genes. Overall, there were only very few significantly regulated genes (**Figure 50A**, padj <0.05), in FolB, GC and PC. This suggested that, while A20-deficiency alters GC entry and exit as well as plasmacytic differentiation of B cells, it has no major impact on their steady state gene expression. To detect also trends for less pronounced expression differences between the genotypes, I lowered the significance threshold to normal pvalue <0.05.

Subsequent independent clustering separated the GCB cell samples by genotype and revealed an overall changed mRNA expression in $BclxL^{tg} A20^{-/-}$ compared to $BclxL^{tg} A20^{-/wt}$ and $BclxL^{tg}$ GCB cells. The latter two had a largely similar gene expression (**Figure 50B**).

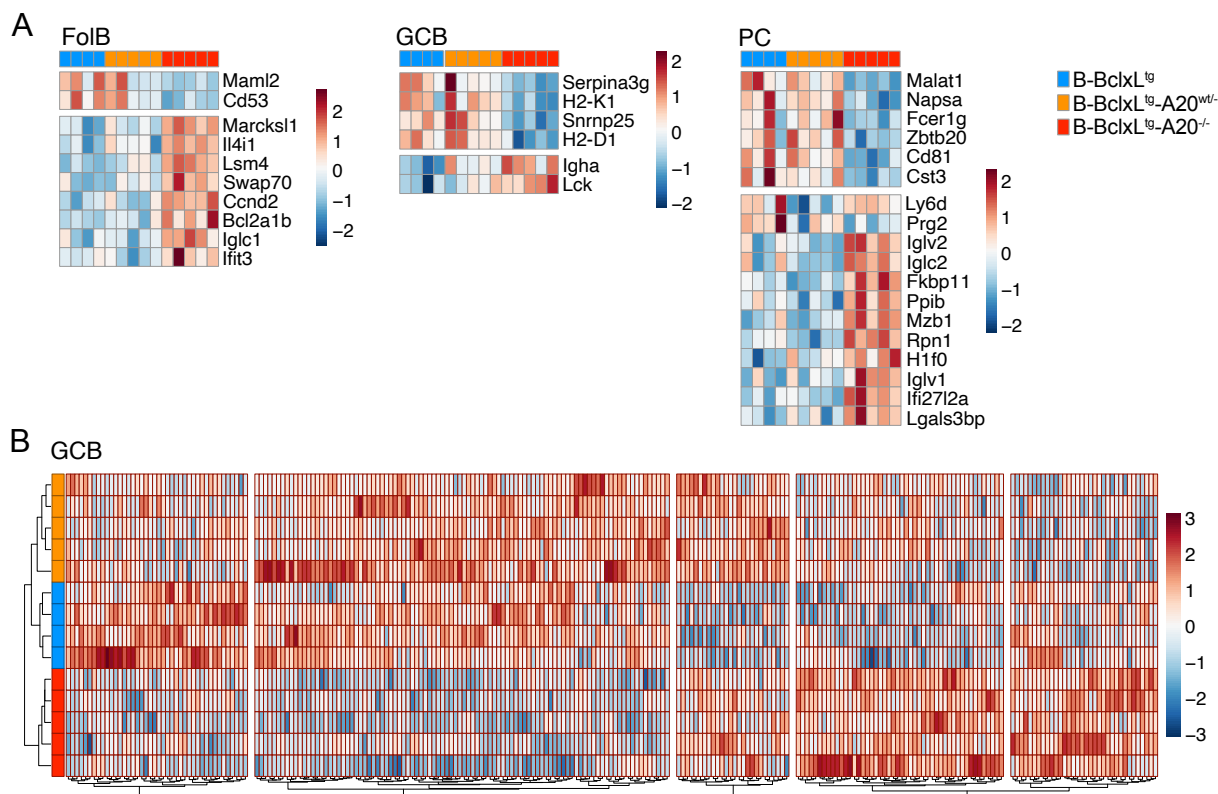


Figure 50. Differential gene expression in bulk RNA sequencing.

(A) ANOVA heatmap of differentially expressed genes in follicular B cells (FolB, AA4.1⁺ B220⁺ CD21⁻ CD1d^{low}), germinal center B cells (GCB, CD19⁺ B220⁺ CD95⁺ CD38^{low}) and plasma cells (PC, CD138⁺ B220^{low}) sorted from B- $BclxL^{tg}$, B- $BclxL^{tg}-A20^{wt/+}$ and B- $BclxL^{tg}-A20^{-/-}$ mice. Bulk RNA from 1000 sorted cells, adjusted p value (padj) <0.05, forced clustering by genotype. (B) ANOVA heatmap of differentially expressed genes in germinal center B cells (GCB) sorted from B- $BclxL^{tg}$, B- $BclxL^{tg}-A20^{wt/+}$ and B- $BclxL^{tg}-A20^{-/-}$ mice. Bulk RNA from 1000 sorted cells, normal pvalue <0.5, independent clustering. (A, B) Cells were sorted by me. RNA sequencing was performed by Dr. Rupert Öllinger. Sequencing data was analyzed by Dr. Thomas Engleitner (A) Heatmaps were generated by me. (B) Heatmap was generated by Dr. Thomas Engleitner in accordance with my requests.

Gene set enrichment analysis (GSEA) of FolB and GCB cell samples confirmed an increased expression of SLE-associated genes in $BclxL^{tg} A20^{-/wt}$ compared to $BclxL^{tg} A20^{-/-}$ cells, using two different genesets (1. KEGG database list for SLE: **Figure 51A** (GCB) and 2. SLE-associated geneset from Nehar-Belaid et al. (426): **Figure 51C** (FolB)). Furthermore, in line with the increased IgG class switching in B- $BclxL^{tg}-A20^{-/wt}$ mice (see **Figure 13**), their GCB cells showed an enhanced IFN γ signaling signature compared to B- $BclxL^{tg}-A20^{-/-}$ mice (**Figure 51A**), which contained a lower fraction of class-switched cells (see **Figure 13**).

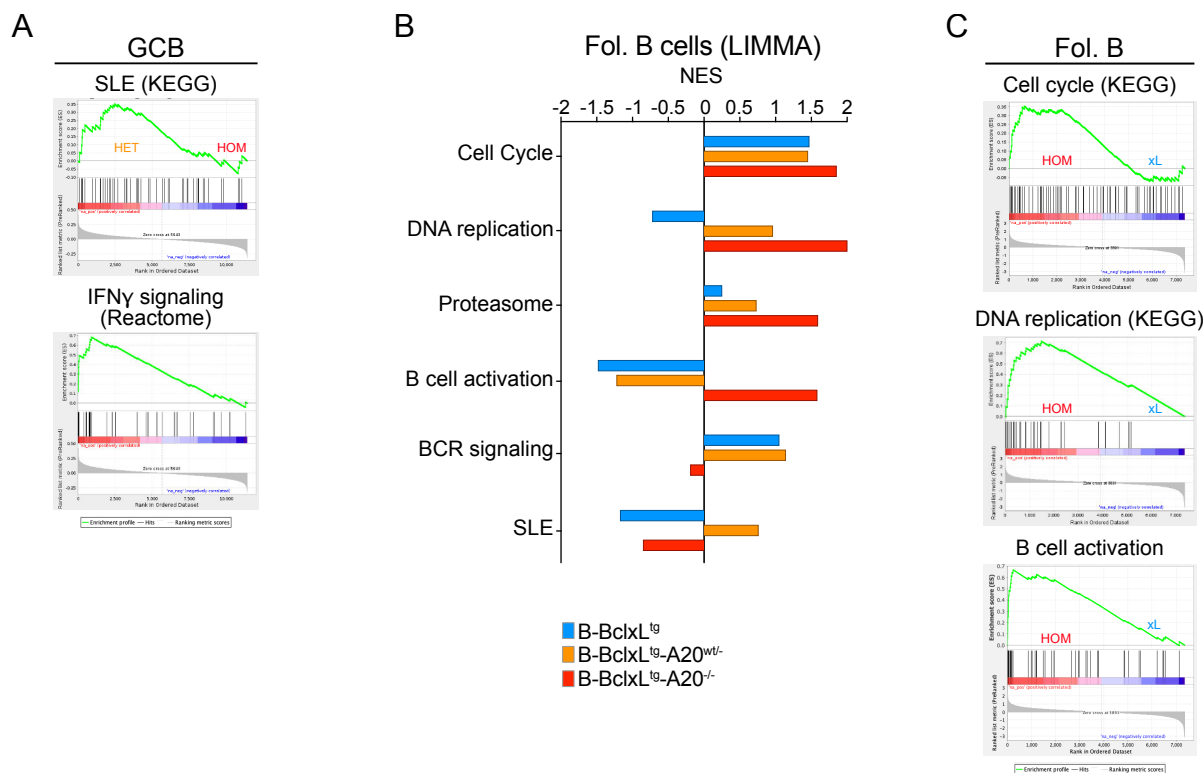


Figure 51. Gene set enrichment analysis.

(A) Gene set enrichment in B-BclxL^{tg}-A20^{-/-wt} compared to B-BclxL^{tg}-A20^{-/-}-GCB cells plotting genesets consisting of SLE-associated genes (left) or IFN γ signaling genes (right) from the KEGG database. (B) Normalized enrichment scores (NES, calculated with GSEA) for genesets for cell cycle, DNA replication, proteasome genes, genes describing B cell activation, BCR signaling genes and SLE-associated genes (Nehar-Belaid et al. (426), **Supplementary Table 2**). RNA sequencing data of BclxLtg, BclxLtg-A20wt/- and BclxLtg-A20/- compared to CD19Cre control follicular B cells. (C) Gene set enrichment in B-BclxL^{tg}-A20^{-/-} compared to B-BclxL^{tg} follicular B cells plotting genesets consisting of cell cycle-associated genes (left) or DNA replication genes (middle) from the KEGG database and a geneset describing B cell activation (right, hand curated gene list, **Supplementary Table 3**). (A -C) Cells were sorted by me and RNA sequencing was performed by Dr. Rupert Öllinger. Sequencing data was analyzed by Dr. Thomas Engleitner. GSEA was performed by me.

In BclxL^{tg} A20^{-/-} FolB cells, I found an enrichment of gene sets associated with proliferation, including cell cycle, DNA replication, RNA polymerase and amino acid metabolism (**Figure 51B, C** and data not shown), as well as a genes linked to proteasome function. Collectively, these gene expression profiles indicated an enhanced proliferative capacity of B cells with homozygous A20-deficiency. Intriguingly, this is in principle in line with previously published data, demonstrating a hyperreactivity of A20^{-/-} B cell *in vitro* (280-282), however seems to contradict my *in vivo* observation that B-BclxL^{tg}-A20^{-/-} mice do not contain higher but even a slightly reduced numbers of B cells compared to BclxL^{tg} control mice.

4.4.2 Proliferation in the iGB culture

To investigate the *in vitro* proliferative potential of B cells with homo- and heterozygous A20-deficiency in the context of BclxL^{tg} expression, I made use of the iGB culture system (302). iGB cells are highly proliferative. Since after day 8 the culture is comprised of two subpopulations, Pax5⁺ GCB-like and Blimp1⁺ PC-like iGB (see **Figure 12**), I analyzed the proliferative activity of both groups by DNA staining with DRAQ5 (**Figure 52A**). On day 4, Blimp1⁺ iGB cells had a bigger fraction in G2/M phase than Pax5⁺ iGB cells from the same culture (**Figure 52B**), which identified them as highly proliferative plasmablast-like cells. The expression of BclxL^{tg} did not affect the cycling of iGB cells. The knockout of A20, increased the fraction of Blimp1⁺ iGB cells in the G2/M phase (**Figure 52B**). Quantification of the cell cycle phases among total (Pax5⁺ and Blimp1⁺) iGB cells without BclxL^{tg} expression, revealed a stepwise increase of cells in G0 phase between days 4 and 12. From day 8 onwards most (> 80 %) iGB cells were Blimp1⁺ (see **Figure 12C**), demonstrating that PC-like iGB cells lose their high proliferative capacity (**Figure 52C**). Comparing genotypes, A20^{-/-} iGB cells consistently had a slightly higher fraction of cycling (G1 and G2/M) iGB cells, while the fraction of cycling cells was lowest in control and intermediate in A20^{-/wt} iGB cells.

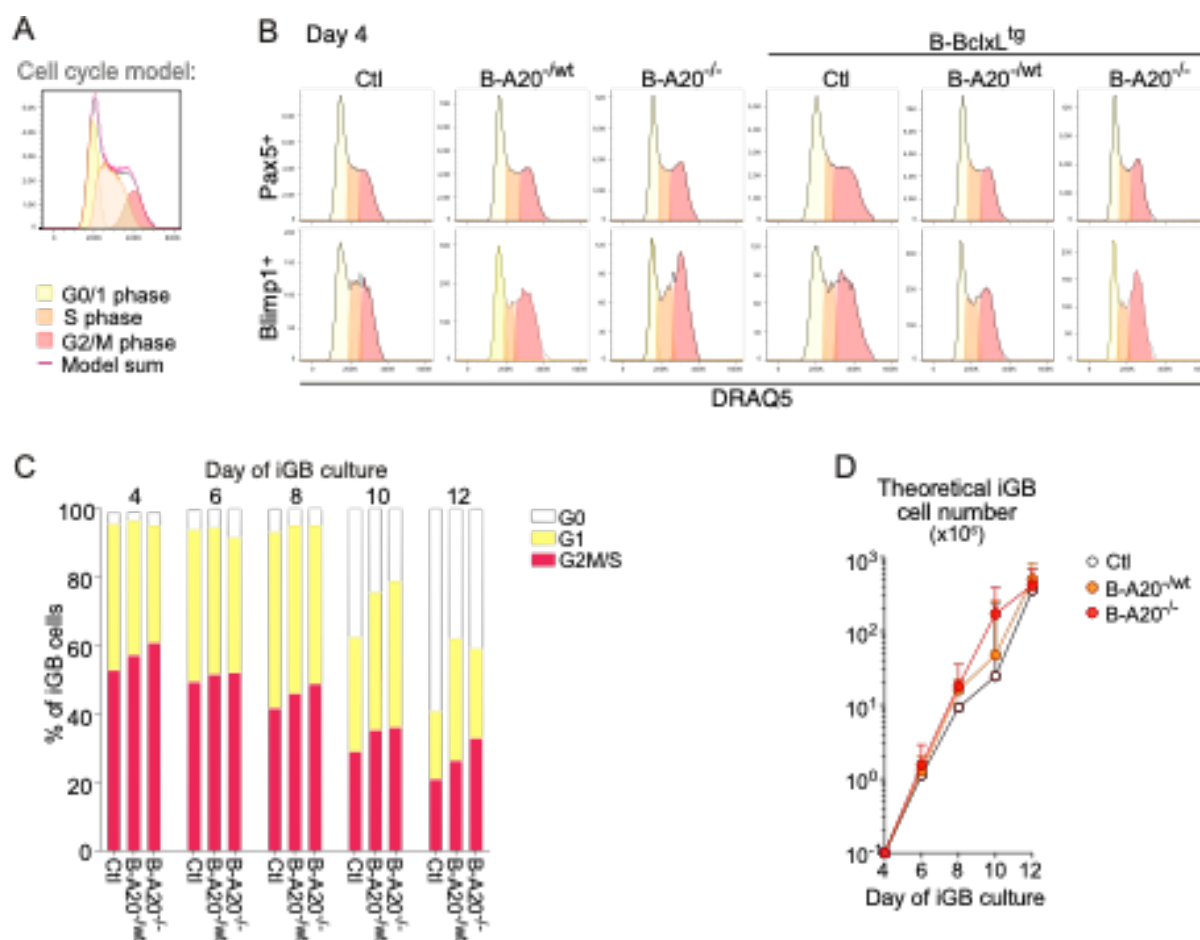


Figure 52. Proliferation in iGB cell culture.

Figure 52. Proliferation in iGB cell culture (Legend)

(A) Quantification of cell cycle stages on flow cytometry data with the Watson (pragmatic) cell cycle model. **(B)** Application of the Watson cell cycle model onto Pax5⁺ (upper panel) and Blimp1⁺ (lower panel) iGB cells with and without BclxL^{tg} expression on day 4 of culture. **(C)** Quantification of cells in G2M/S (sum of cells in G2/M and S phase), G1 (Ki67⁺ cells in G0/1 phase) or G0 (Ki67⁻ cells in G0/1 phase) as percent of all iGB cells. Data from 1 experiment. **(D)** Theoretical cell number in the iGB culture on days 4, 6, 8, 10 and 12. *(B-C) iGB culture and DRAQ5 staining as well as FACS analysis were performed by my supervised student Anna Sichler. I performed the data analysis. (E) Theoretical cell numbers were calculated by my supervised student Sophie Levantovsky.*

The tendency for increased cell cycling of A20^{-/-} iGB cells resulted in the highest cell accumulation for this genotype. Since the culture was serially diluted on every second day, a theoretical number of iGB cells was calculated, which would be generated within each culture without if no dilutions had been performed. To do so, I determined the number of cell divisions (n), which occurred within 48 hours, from the number of harvested cells (N_C) and the number of initially seeded cell (N_S). The theoretical cell number (N) was subsequently defined by multiplying the number of cell divisions (n) per 48 hours timeframe with the cell number that had been generated at the end of the preceding time frame (N_0). The calculation was performed as follows:

$$\log(N_C) = \log(N_S) + n \times \log(2)$$

$$n = \frac{\log(N_C) - \log(N_S)}{\log(2)}$$

N_C = counted cell number, N_S = seeded cell number, n = cell divisions

$$N = N_0 \times 2^n$$

N = theoretical cell number, N_0 = initial cell number, n = cell divisions

The proliferation between day 1 and day 4 was highly variable between different experiments, likely due to strong effects of the different IL-4 batches used for stimulation. Therefore, proliferation in the first 4 days was not considered for the calculation of total theoretical cell numbers.

A20^{-/-} iGB cell numbers increased rapidly until day 10 and stagnated afterwards, while A20^{-/wt} and control iGB cells still expanded after this time point (**Figure 52D**). Since the cell cycle data suggested still the highest cell division rate in A20^{-/-} cells on days 10 and 12, their expansion was likely counteracted by a high rate of apoptosis. Possibly, the earlier plasmacytic differentiation of A20^{-/-} iGB cells to short-lived plasmablast-like cells, implied their earlier termination of expansion. Indeed, the apoptosis rate of iGB cells increased after day 8 (**Supplementary Figure 2A**). However, I did not systematically compare the extent of apoptosis between the genotypes.

Of note, BclxL^{tg} expression did not change the cell cycle pattern of Pax5⁺ or Blimp1⁺ iGB cells, nor did it increase the total number of iGB cells generated in combination with all A20 zygosityes (**Figure 52B** and data not shown).

By use of the iGB culture system, I could demonstrate that the intrinsic proliferative potential upon stimulation with CD40L, BAFF and IL-4 is strongly increased in A20^{-/-} and mildly elevated in A20^{-/wt} GCB-like iGB cells. This *in vitro* result fits well with the gene expression pattern of *ex vivo* isolated BclxL^{tg} A20^{-/-} B cells, which indicated their enhanced proliferative activity. Together, these results are in line with previously published data, showing that A20 knockout in B cells renders them hyperproliferative towards various stimuli *in vitro*, while the heterozygous loss of A20 has intermediate effects on proliferation (280). Paradoxically, the *in vivo* B cell expansion as well as all aspects of systemic autoimmunity, including autoantibody production, kidney IC deposition and secondary APS development, were less pronounced in B-BclxL^{tg}-A20^{-/-} compared to B-BclxL^{tg}-A20^{-/wt} mice. I therefore aimed to identify the factors, which counteract the intrinsically strong BclxL^{tg} A20^{-/-} B cells hyperactivity and the development of lethal autoimmunity in the corresponding mice.

4.4.3 BCR stimulation and signaling strength

Since the high proliferative potential of A20^{-/-} B cells was not reflected by the respective B cell population sizes and responses *in vivo*, there should be counter-acting effects interfering with B cell maintenance and responses within the living animal. In the previously performed *in vitro* experiments (1, 5, 6), activating stimuli were uniformly applied to B cells of all genotypes, however, in the *in vivo* setting, availability of pro-inflammatory cytokines and stimulation by helper T cells depends on the microenvironment as well as the BCR specificity of the B cell. The iGB culture is independent of antigen recognition, while *in vivo*, the selection and expansion of GCB cells strongly depends on the BCR affinity. Interestingly, GSEA of transcriptomics data suggested that genes involved in BCR signaling had a reduced expression in BclxL^{tg} A20^{-/-} compared to BclxL^{tg} FolB cells (**Figure 53A**). To investigate whether this reflects a reduced ability of BclxL^{tg} A20^{-/-} B cells to transmit BCR signals *in vivo*, I employed a transgenic mouse strain, which expresses a GFP reporter under the control of the Nr4a1 promoter (Nur77^{GFP}) (290). The orphan nuclear hormone receptor *Nr4a1/Nur77* is rapidly expressed upon antigen receptor activation in B and T cells (427, 428). Nur77^{GFP} was bred into the B-BclxL^{tg}-A20 mouse lines, whose B and T cells express GFP upon BCR or TCR activation, respectively.

To judge the extent of antigen-induced B cell activation under steady-state conditions *in vivo*, I analyzed the GFP expression in *ex vivo* isolated B cell subsets. Despite the presumably lower expression of proteins involved in BCR signaling, *ex vivo* isolated BclxL^{tg} A20^{-/-} Nur77^{GFP} FolB and more specifically IgM⁺ FolB cells on average had the highest MFI of (Nur77-)eGFP compared to the other genotypes (**Figure 53B**). It has been shown that Nur77 is upregulated upon chronic antigen stimulation in self-reactive B2 cells and restricts their survival by promoting antigen-induced cell death (AICD). This renders them more dependent on BAFF and leads to their elimination in competition with non-autoreactive B cells (429). The strong GFP intensity in BclxL^{tg} A20^{-/-} FolB cells indicates more intense and/or prolonged BCR signals. In absence of activation by foreign antigens, this could indicate B cell autoreactivity. In the subset of B1 cells, those with heterozygous loss of A20 had the highest GFP expression (**Figure 53B**). Nur77 was shown to be upregulated in B1a cells by chronic self-antigen stimulation, limiting their differentiation to plasma cells secreting natural IgM (430). B1 cell-derived natural IgM with low affinity autoreactivity serves a protective function against autoimmunity (7). Consequently, high Nur77^{GFP} in BclxL^{tg} A20^{-/wt} B1 cells suggests their reduced generation of antibody secreting cells, which might additionally promote the autoimmune pathology. For both, GCB and plasma cells, the fraction of GFP⁺ cells was generally very low and no difference between the genotypes could be observed (**Figure 53B**).

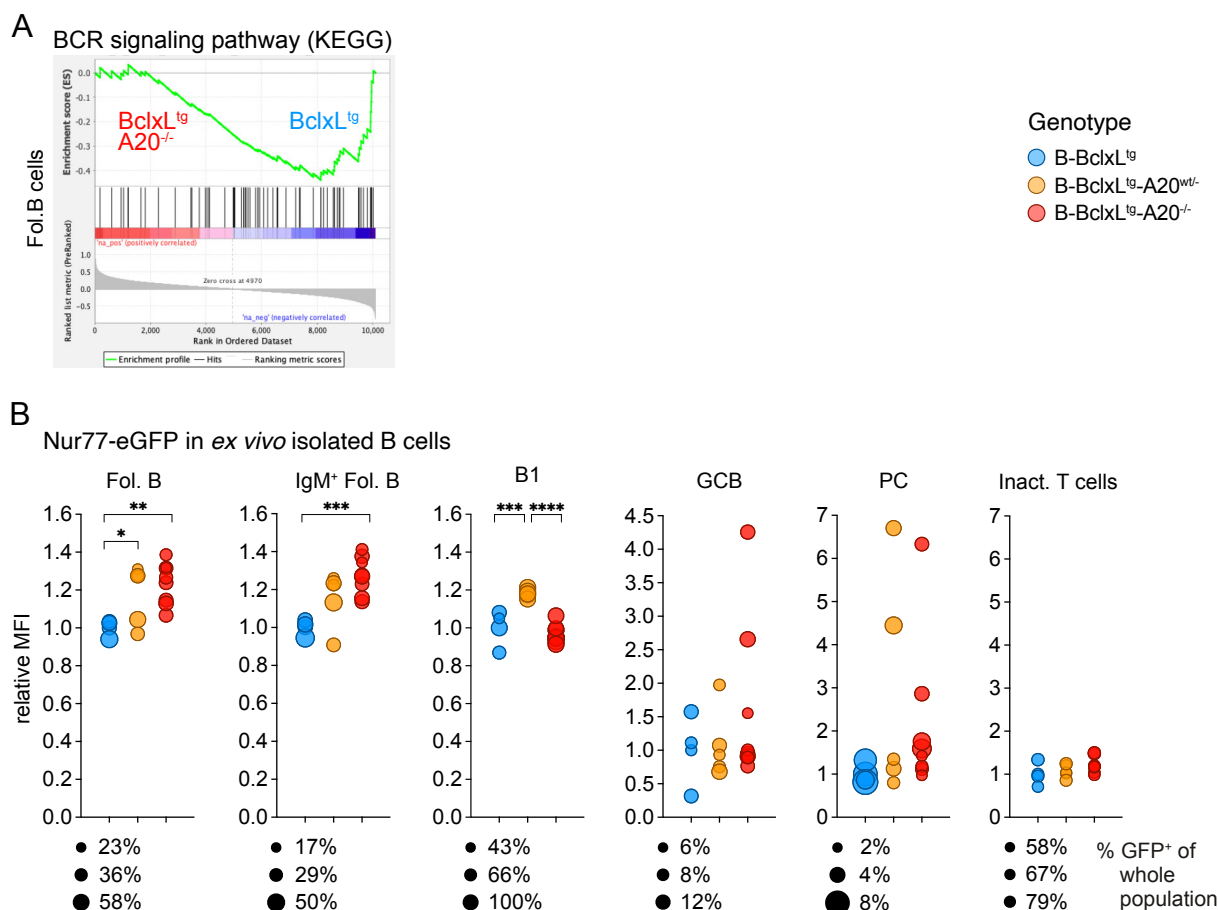


Figure 53. BCR signaling intensity.

(A) Gene set enrichment in B-BclxL^{tg}-A20^{-/-} compared to B-BclxL^{tg} B cells for BCR signaling pathway genes from the KEGG database. Normalized ranked expression list of pairwise from DESeq2 analyzed matrix containing data from B-BclxL^{tg}-A20^{-/-}, B-BclxL^{tg}-A20^{wt/-} and B-BclxL^{tg}. (B) GFP signal intensity, correlating to Nur77^{GFP} expression, measured by flow cytometry on *ex vivo* isolated splenocytes, normalized to GFP signal intensity in the corresponding cell type isolated from control mice. Follicular B (FolB, CD19⁺ B220⁺ CD38⁺ CD95⁻), B1 (CD19⁺ B220⁺), germinal center B (GCB, CD19⁺ B220⁺ CD38⁻ CD95⁺), plasma cells (PC, CD138⁺ B200^{low}) and inactive T cells (CD25⁻ CD44⁻). (A) Cells were sorted by me and RNA sequencing was performed by Dr. Rupert Öllinger. Sequencing data was analyzed by Dr. Thomas Englertner and GSEA was performed by me.

The high GFP levels of *ex vivo* isolated BclxL^{tg} A20^{-/-} and BclxL^{tg} A20^{wt/-} B cells indicated a high abundance of available (auto-)antigens, which might compensate for the lower expression of genes involved in BCR signaling. In B-BclxL^{tg}-A20^{wt/-} mice, autoantigen recognition triggers B cell expansion, likely through combined BCR and TLR signaling. In B-BclxL^{tg}-A20^{-/-} mice *in vivo* BCR stimulation, which is potentially also triggered by autoantigens, induced high Nur77^{GFP} expression in B2 but not B1 cells. However, the BCR stimulation in BclxL^{tg} A20^{-/-} B cells seemed to promote their elimination rather than inducing tolerance (429, 430).

4.4.4 Sensitivity towards TNF-induced apoptosis

One possible explanation for the reduced B cell numbers and responses in B-BclxL^{tg}-A20^{-/-} mice could be that A20 knockout renders B cells more susceptible to death signaling. Apart from negatively regulating NF-κB activation, A20 also protects cells from apoptotic cell death. A20^{-/-} thymocytes are more prone to die upon *in vitro* TNF stimulation through caspase-dependent pathways (234). The serum concentration of TNF was largely equal in B-BclxL^{tg}-A20^{-/-} and control mice under steady state conditions (see **Figure 28A**). Nevertheless, BclxL^{tg} A20^{-/-} B cells, might be triggered to undergo apoptosis by the available TNF. Consequently, increased TNF-induced apoptosis of BclxL^{tg} A20^{-/-} B cells could explain the relatively low B cell numbers in B-BclxL^{tg}-A20^{-/-} mice despite their highly proliferative potential (see **Figure 51** and **Figure 52**).

4.4.4.1 *In vivo* TNF depletion

By repeated intraperitoneal (i.p.) injection of α-TNF antibody *in vivo*, I neutralized TNF from the circulation for two weeks and investigated if this would increase the survival and thereby the total numbers of B cells in B-BclxL^{tg}-A20^{-/-} and control mice.

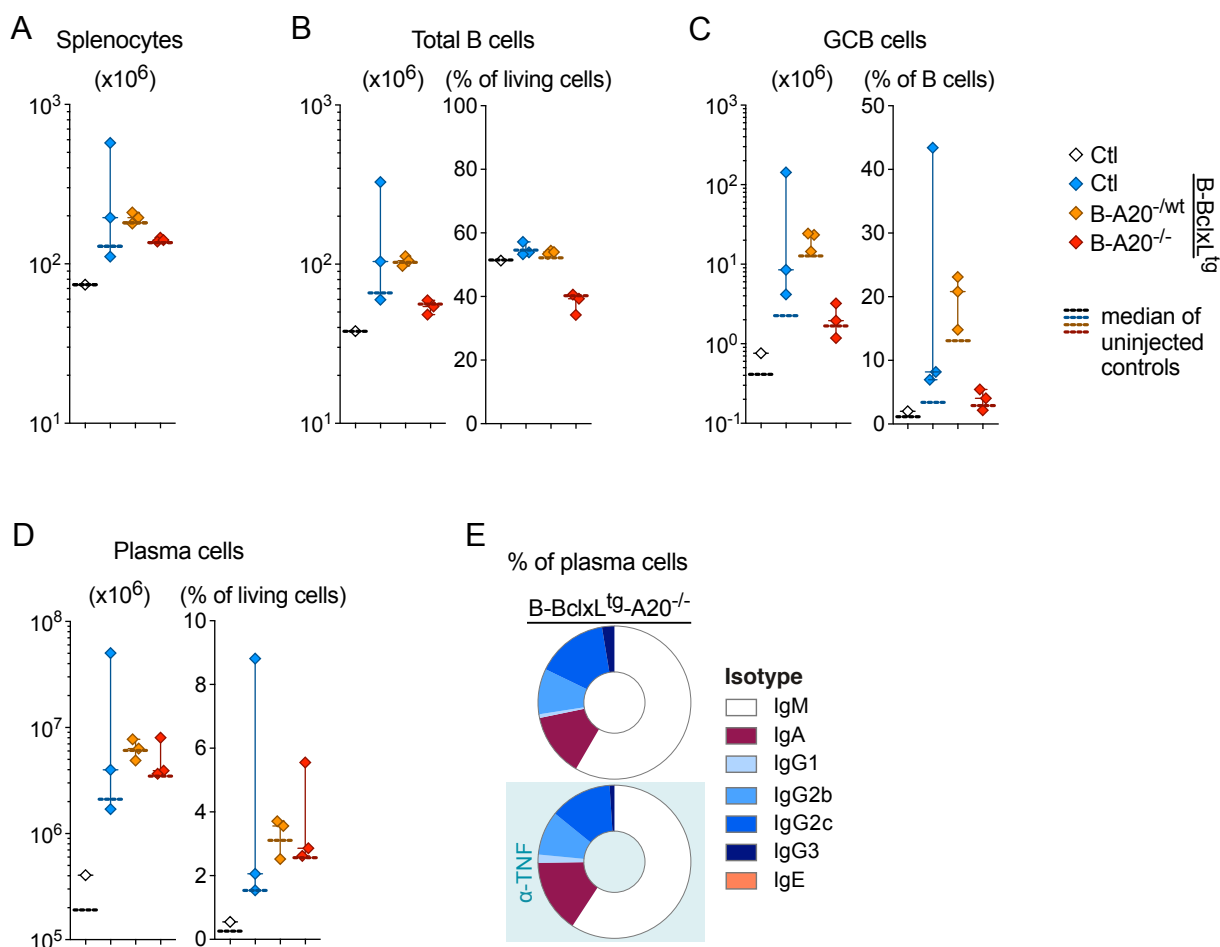


Figure 54. TNF-depletion *in vivo*.

Figure 54. TNF-depletion *in vivo* (Legend).

(A) Absolute numbers of splenocytes, (B-D) Fraction and absolute numbers of (B) total splenic B cells (B220⁺, CD138⁻), (C) germinal center B cells (GCB: B220⁺, CD38^{lo}, CD95^{hi}) and (D) plasma cells (CD138⁺, B220^{low}). (E) Percentage of isotypes in splenic plasma cells from B-BclxL^{tg}-A20^{-/-} mice. (A-D) Data from 1 or 3 anti-TNF injected mice is depicted as individual diamonds, including spread and median. Median from 1 or 3 PBS-injected control mice is shown as dotted line. (A-E) FACS data was analyzed by Francisco Osorio-Barrios.

TNF neutralization had essentially no effect on splenic and mLN absolute B, GCB and plasma cell numbers as well as class-switching in any of the mice analyzed, including B-BclxL^{tg}-A20^{-/-} mice (Figure 54A-E, mLN data not shown). I conclude that TNF-induced apoptosis does not explain the paucity of B cells in B-BclxL^{tg}-A20^{-/-} mice.

4.4.4.2 *In vitro* TNF stimulation

To directly test the sensitivity of BclxL^{tg} A20^{-/-} B cells towards TNF-induced apoptosis, I stimulated total splenocytes of B-BclxL^{tg}-A20^{-/-}, B-BclxL^{tg}-A20^{-/wt}, B-BclxL^{tg} and control mice with TNF *in vitro*. After 3 hours stimulation with 100ng/ml TNF, the fraction of dead, early and late apoptotic cells was equal for BclxL^{tg} A20^{-/-}, BclxL^{tg} and control plasma and B cell subsets, while slightly more apoptotic cells were detected in the BclxL^{tg}-A20^{-/wt} samples (Figure 55A). This suggests that BclxL^{tg} expression together with homozygous but not heterozygous loss of A20 had a protective effect against B cell apoptosis after 24 hours *in vitro*. However, more detailed analyses revealed that these differences in apoptosis were due to the genotype of the B cells and that TNF stimulation did not impact the apoptosis rate of B cells within each genotype (Figure 55B, left panel). After 24 hours in culture, the fraction of BclxL^{tg} A20^{-/-} B cells among all cells was strongly increased compared to their fraction within the originally seeded splenocytes and also this effect was independent of TNF stimulation (Figure 55B, right panel).

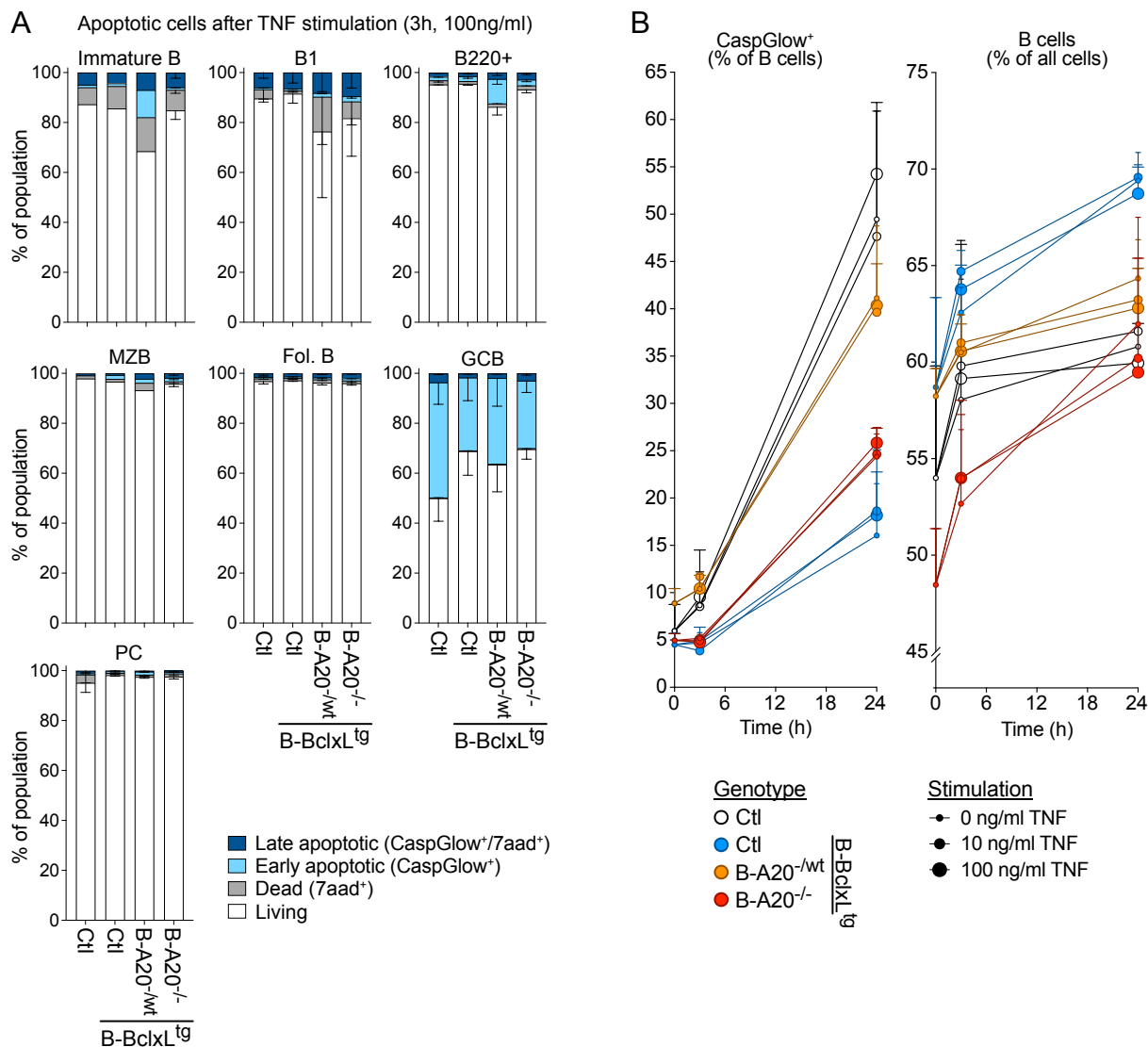


Figure 55. TNF stimulation *in vitro*.

(A) Fraction of late apoptotic (CaspGlow⁺, 7aad⁺), early apoptotic (CaspGlow⁺), dead (7aad⁺) and living immature B cells (AA4.1⁺, B220⁺), B1 cells (CD19⁺, B220^{low}), B220⁺ (AA4.1⁻) mature B cells, marginal zone B cells (MZB: CD1d⁺, CD21⁺), follicular B (Fol. B: B220⁺, CD38⁺, CD95^{lo}), germinal center B cells (GCB: B220⁺, CD38^{lo}, CD95^{hi}) and plasma cells (PC: CD138⁺, B220^{low}). Mean values and SEM from 1 or 3 biological replicates from up to 3 independent experiments are shown. (B) Fraction of CaspGlow⁺ apoptotic cells from total B220⁺ B cells after 0, 3 and 24 hours TNF stimulation in culture. Mean values and SEM from 3 biological replicates from 3 independent experiments are shown.

Overall, BclxL^{tg} expression and homozygous but to a lesser extent heterozygous loss of A20 had a protective effect against B cell apoptosis *in vitro*. Stimulation with TNF had neither a pro-apoptotic nor a protective effect on B cell survival. Overall, I concluded that the homozygous loss of A20 does not render B cells susceptible towards TNF-induced cell death. Independent of TNF stimulation, BclxL^{tg} A20^{-/-} B cells preferentially survived in the splenic cell mixture, further demonstrating that in general the lack of A20 imposes a survival advantage on B cells *in vitro*.

4.4.5 Competitive bone marrow transfer reveals a systemic effect counteracting the expansion of BclxL^{tg} A20^{-/-} B cells *in vivo*

B cells with a homozygous and heterozygous deletion of A20 have a clearly different capacity to expand *in vivo* and induce lethal autoimmunity. I therefore aimed to investigate whether the systemic inflammation induced in B-BclxL^{tg}-A20^{-/-} mice is sufficient to also drive the expansion of BclxL^{tg} A20^{-/-} B cells or whether, conversely, a systemic effect induced by BclxL^{tg} A20^{-/-} B cells *in vivo* would also counteract the expansion of BclxL^{tg} A20^{-/-} B cells. Since the hyperproliferation and hyperactivation of BclxL^{tg} A20^{-/-} cells could not be recapitulated *in vitro*, I performed mixed bone marrow transplantation, which enabled the direct competitive comparison of genotype effects on B cell expansion and disease development *in vivo*.

For this, I depleted the bone marrow of B-BclxL^{tg}, B-BclxL^{tg}-A20^{-/-} and B-BclxL^{tg}-A20^{-/-} donor mice from B and T cells by MACS and prepared pairwise 50:50 mixtures of the three genotypes (**Figure 56A**). Subsequently, 40,000 cells were transplanted into sublethally irradiated Rag2-knockout mice by injection into the tail vein. In each pairwise cell mix, the B cells from one donor mouse were conditionally expressing the CAR cell surface protein (301) to enable their identification by flow cytometry. CAR is a cell surface receptor and it cannot be excluded that its expression affects B lineage cells at some stage of their differentiation and/or expansion. I therefore used the CAR reporter in an equal number (six animals) of both genotypes per pairwise mix to account for possible effects of CAR expression (**Figure 56B**).

The initial plan foresaw analysis of the recipient mice three months after receiving the transplant, as I expected to detect a development of autoimmunity at this time. However, already six weeks after transplantation, a severe pathology, evident by reduced activity and lethargy, appeared in the group of mice, which received a mix of B-BclxL^{tg} and B-BclxL^{tg}-A20^{-/-} BM [Ctl / A20^{-/-}], and two mice were found dead (**Figure 56C**). For this reason, all remaining mice were analyzed regarding their immune cell competition, six weeks after the transplantation.

The median splenocyte number as well as B, GCB and plasma cell numbers of [Ctl / A20^{-/-}] chimeras were equal to [Ctl / Ctl] control chimeras (**Figure 56D-G**). This indicates that the time since transplant was not long enough to induce a pathologic expansion of BclxL^{tg} A20^{-/-} B cells. In line with this, the amount of ANA IgG was only slightly elevated in [Ctl / A20^{-/-}] chimeras (see **Figure 57A**). However, one animal showed high ANA, demonstrating that systemic autoimmunity can be induced by BclxL^{tg} A20^{-/-} B cells upon BM transfer, albeit requiring more than six weeks to fully develop disease (see **Figure 57A**).

The group of [Ctl / A20^{-/-}] chimeras and surprisingly also the group of [A20^{-/-} / A20^{-/-}] chimeras had a strong B cell deficiency (**Figure 56E**). GCB cells were almost completely absent in all [Ctl / A20^{-/-}] and most [A20^{-/-} / A20^{-/-}] chimeras (**Figure 56F**).

In those [A20^{-/-} / A20^{-/wt}] chimeras, which harbored GCB cells, the major fraction of B (84.1 %) and GCB (87.1 %) cells were A20^{-/wt}, in line with their capacity to expand in [Ctl / A20^{-/wt}] chimeras (**Figure 56E, F**).

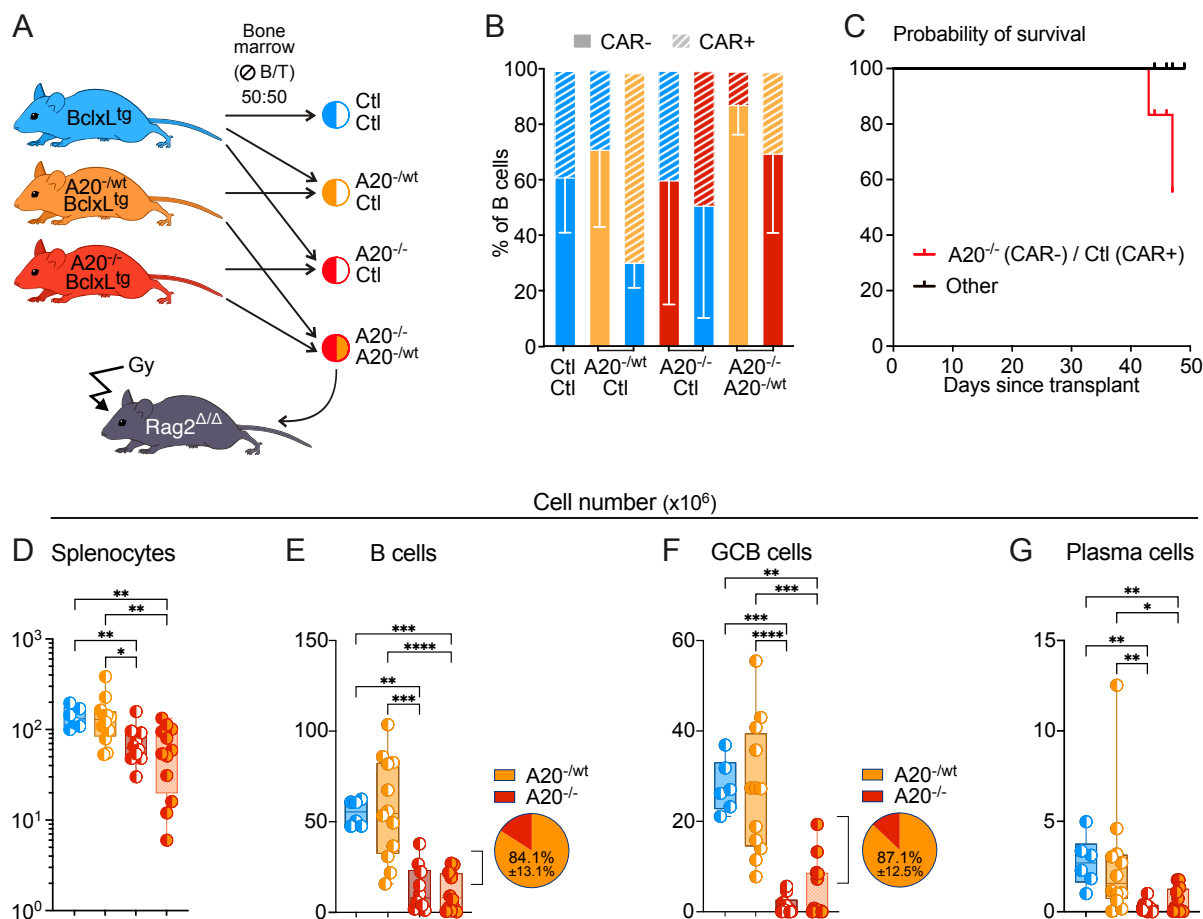


Figure 56. Competitive bone marrow chimeras.

(A) mixed Scheme of the generation of mixed bone marrow chimeras: B-BclxL^{tg}, B-BclxL^{tg}-A20^{-/wt} and B-BclxL^{tg}-A20^{-/-} bone marrow (BM) cells were mixed pairwise in equal numbers to generate four different mixtures ([Ctl / Ctl], [A20^{-/wt} / Ctl], [A20^{-/-} / Ctl] and [A20^{-/-} / A20^{-/wt}]). The BM mixtures were then injected into sublethally irradiated female Rag2^{-/-} recipients. (B) Fraction of CAR⁻ (clear bars) and CAR⁺ (striped bars) cells in each chimera group at time of analysis. Bar color represents the donor BM genotype. Each group contained six mice, except the group [A20^{-/-} CAR⁻ / Ctl CAR⁺] (bar 4), which contained only four mice. Mean fraction and SD are depicted. (C) Kaplan-Meier survival curve since transplant of [A20^{-/-} CAR⁻ / Ctl CAR⁺] chimeras (red line) and all other chimeras (black line). (D-G) Absolute number of (D) splenocytes, (E) CD19⁺ B220⁺ B cells, (F) CD19⁺ B220⁺ CD95⁺ CD38^{low} germinal center B (GCB) cells and (G) CD138⁺ B220^{low} plasma cells in the four chimera groups [Ctl / Ctl], [A20^{-/wt} / Ctl], [A20^{-/-} / Ctl] and [A20^{-/-} / A20^{-/wt}]. Data is displayed as box-whisker-plots. Dots represent individual mice, irrespective of the CAR⁻ / CAR⁺ mixture. (E, F) Pie charts display the mean fraction plus SD of A20^{-/wt} and A20^{-/-} cells within the respective population. Mice of the BM chimera experiment were analyzed in cooperation with Dr. Maike Kober, Dr. Valeria Soberon, Dr. Sabrina Bortoluzzi and Julia Knogler.

Corresponding to the strongly reduced number of total splenocytes (**Figure 56D**), also the numbers other immune cell types, including CD4 and CD8 T cells were slightly reduced in [Ctl / A20^{-/-}] and [A20^{-/-} / A20^{-/wt}] chimeras (**Figure 57B**). T_{reg} cells and, corresponding to the low GCB cell numbers, especially T_{FH} cells were diminished in [Ctl / A20^{-/-}] and [A20^{-/-}

/ A20^{-/wt}] chimeras (**Figure 57C**). Macrophages and monocytes also had the lowest numbers in the group of [A20^{-/} / A20^{-/wt}] chimeras (**Figure 57D**). The very small spleens with sometimes only few living cells in this group possibly indicated acute organ failure.

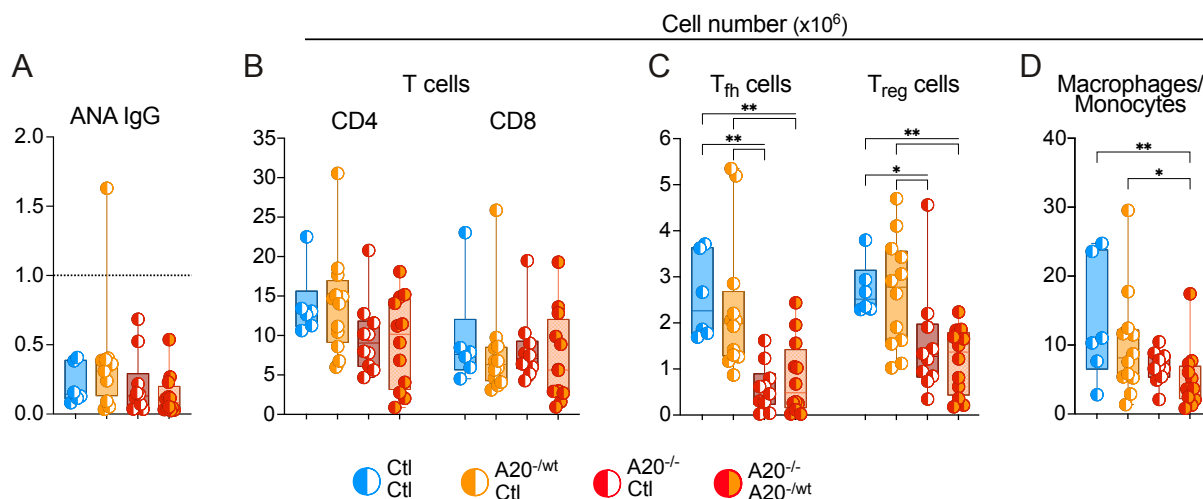


Figure 57. T cells in competitive BM chimeras.

(A) Serum levels of anti-nuclear IgG antibodies (ANA, normalized by positive control). (B-D) Absolute numbers of (B) CD4 and CD8 TCR β ⁺ T cells, (C) Follicular helper T (T_{fh}) cells and regulatory T (T_{reg}) cells and (D) Gr1⁺ CD11b⁺ macrophages and monocytes in the four chimera groups [Ctl / Ctl], [A20^{-/wt} / Ctl], [A20^{-/} / Ctl] and [A20^{-/} / A20^{-/wt}]. Data is displayed as box-whisker-plots. Dots represent individual mice, irrespective of the CAR⁻ / CAR⁺ mixture. *Mice of the BM chimera experiment were analyzed in cooperation with Dr. Maike Kober, Dr. Valeria Soberon, Dr. Sabrina Bortoluzzi and Julia Knogler.*

To evaluate within each chimera group how strongly the B cells of the two mixed genotypes expanded, the frequency of CAR⁺ and CAR⁻ cells per mouse was extracted and normalized by the mean CAR⁺/CAR⁻ ratio of [Ctl / Ctl] control chimeras for B cells (40:60, see **Figure 56B**) and similarly for GCB (35:65, not shown) and plasma cells (13:87, not shown) (**Figure 58A**).

Six weeks after transfer, the median number of A20^{-/wt} B cells in the spleens of [Ctl / A20^{-/wt}] chimeras was equal to their number in mice, which received pure B-BclxL^{tg}-A20^{-/wt} BM [A20^{-/wt}]. Simultaneously, the number of Ctl B cells in [Ctl / A20^{-/wt}] chimeras was largely comparable to the number in mice, which received [Ctl / Ctl] control BM (**Figure 58B**). Within the [Ctl / A20^{-/wt}] chimeras, A20^{-/wt} B cells had an expansion benefit over the competing Ctl B cells, evident from a 70:30 ratio (normalized) (**Figure 58A**).

The advantage of A20^{-wt} over Ctl cells became even more apparent in GCB and plasma cells, where the ratio was equally 76:24. When comparing the expansion of A20^{-/-} B cells with Ctl B cells, there seemed to be no strong competitive advantage or disadvantage regarding the B and GCB cell expansion, however, within the plasma cells, a higher fraction (71%) was A20^{-/-} in [Ctl / A20^{-/-}] chimeras (**Figure 58A**). In [A20^{-/-} / A20^{-wt}] chimeras, A20^{-wt} cells made up the greatest fraction (76-78%) within all analyzed B cell subsets (**Figure 58A**).

Overall, the genotype ratios revealed a strong competitive advantage of A20^{-wt} cells over Ctl and A20^{-/-} cells and a minor competitive advantage of A20^{-/-} cells over Ctl cells, which was strongest with regards to plasmacytic differentiation (**Figure 58A**).

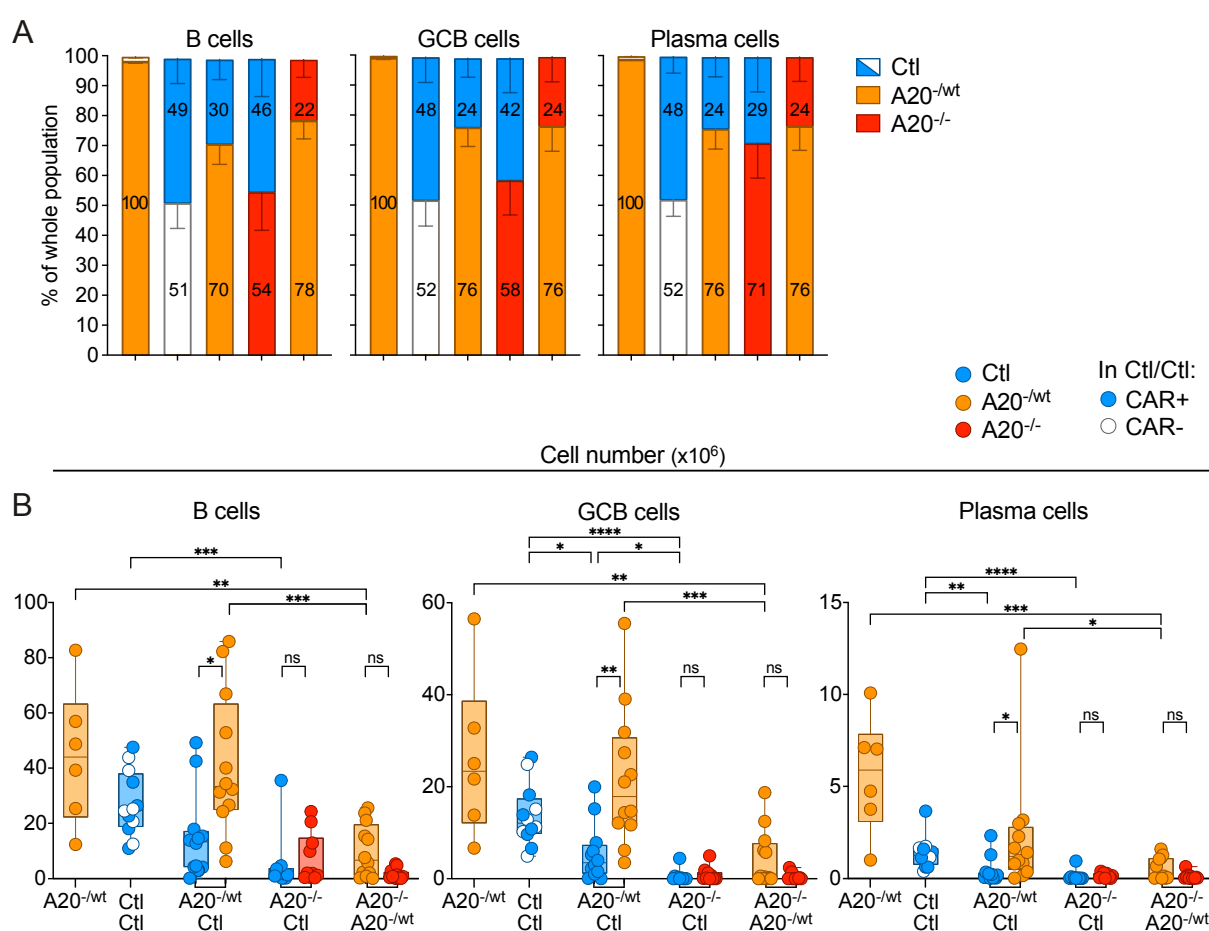


Figure 58. Genotype fractions in the bone marrow chimeras.

(A) Normalized fraction of the two mixed genotypes within CD19⁺ B220⁺ B cells (left), CD19⁺ B220⁺ CD95⁺ CD38^{low} germinal center B (GCB) cells (middle) and CD138⁺ B220^{low} plasma cells (right) in the spleen. The fraction detected by flow cytometry was normalized by division by the mean ratio of CAR⁺/CAR⁻ cells in [Ctl / Ctl] chimeras. (B) Total number of B, GCB or plasma cells splitted by genotype for the four chimeras and mice that were transplanted only with [A20^{-wt}] BM. Data is displayed as box-whisker-plots. Dots represent individual mice. In most groups, colors are irrespective of the CAR⁻ / CAR⁺ mixture, except [Ctl / Ctl] chimeras, in which white dots represent CAR⁻ cells and blue dots represent CAR⁺ cells. Mice of the BM chimera experiment were analyzed in cooperation with Dr. Maike Kober, Dr. Valeria Soberón, Dr. Sabrina Bortoluzzi and Julia Knogler.

Remarkably, the absolute number of Ctl as well as A20^{-/-wt} B, GCB and plasma cells was strongly reduced in all chimeras, which simultaneously received B-A20^{-/-} BM (**Figure 58B**). This clearly demonstrates that a systemic effect, hindering B cell expansion and differentiation, is evoked by the presence of A20^{-/-} B cells. A similar effect may be in place in (non-chimeric) B-BclxL^{tg}-A20^{-/-} mice to counteract the pathological expansion of A20^{-/-} B cells. However, in the setting of this BM chimera experiment, the effect was likely over-amplified due to the induction of an inflammatory setting through sublethal irradiation of the recipient mice. Since the transplanted BM had only been depleted from B and T cells, stem cells were transplanted together with other BM resident cells, which might have participated in the inflammatory response, counteracting B cell expansion. Indeed, inflammatory cytokines like TNF were elevated in the sera of [Ctl / A20^{-/-}] and [A20^{-/-} / A20^{-/-wt}] chimeras (**Figure 59D**).

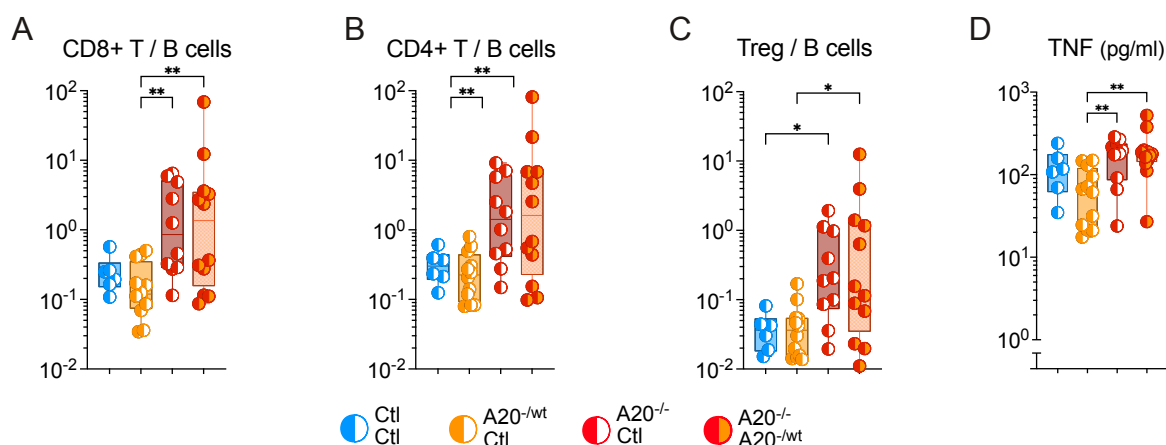


Figure 59. Ratio of B and T cells in bone marrow chimeras.

(A-C) Ratio of splenic (A) CD8 T cells, (B) CD4 T cells and (C) regulatory T cells (T_{reg}) numbers and total B cell numbers per recipient mouse. (D) Serum concentration (pg/ml) of TNF. Data is displayed as box-whisker-plots. Dots represent individual mice irrespective of the CAR⁻ / CAR⁺ mixture. Mice of the BM chimera experiment were analyzed in cooperation with Dr. Maike Kober, Dr. Valeria Soberon, Dr. Sabrina Bortoluzzi and Julia Knogler.

Importantly, the [Ctl / A20^{-/-}] and [A20^{-/-} / A20^{-/-wt}] chimeras, were not devoid of T cells. Therefore, specifically the expansion B cell lineage cells was inhibited in these mice, indicating a precise mechanism to be at hand. I therefore suspected a cell-driven rather than cytokine-driven effect. The ratio of CD8, CD4 and especially T_{reg} cell numbers to B cell numbers was increased in those chimeras containing A20^{-/-} B cells (**Figure 59A-C**). This indicated a potential role of T cells in the counter-selection of A20^{-/-} B cells and I therefore decided to investigate a potential cytotoxic targeting of B cells by T lineage cells.

4.5 T cell immune surveillance

The concept of immune surveillance, meaning the cytotoxic targeting of rogue endogenous cells, has been described for aberrantly transformed cancer cells. During tumor immune surveillance, CTL activity is triggered by and directed against cells expressing tumor-associated (auto-)antigens or tumor specific (neo-)antigens (431).

4.5.1 *In vivo* T cell activation

In the competitive bone marrow chimeras, the transfer of B-BclxL^{tg}-A20^{-/-} bone marrow correlated with a strong relative increase of CD8⁺ T cell numbers (**Figure 60A**), implying that cytotoxic CD8 T cells might be involved in the lethal inflammation and elimination of B cells in these mice. An activation of T cells from B-BclxL^{tg}-A20^{-/-} mice is additionally indicated by their increased fraction of effector-memory-like CD8⁺ T cells (see **Figure 22B**).

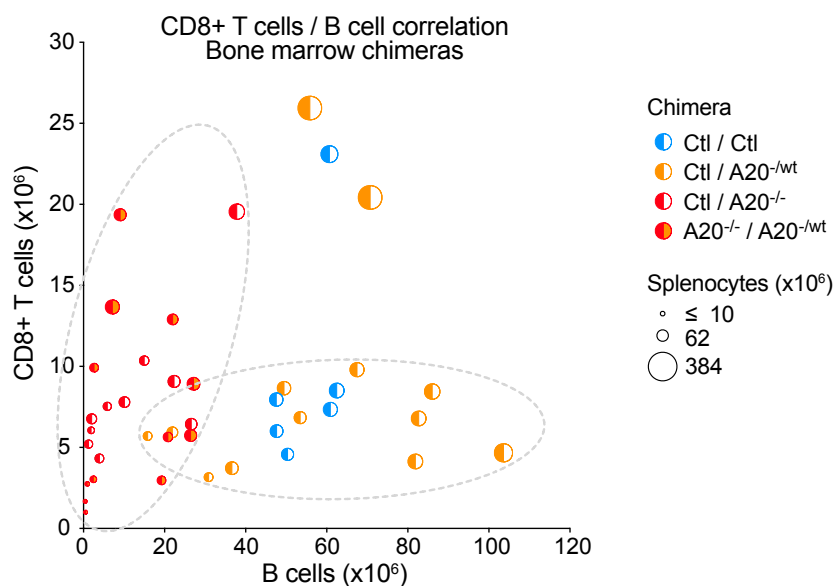


Figure 60. CD8 T cell expansion.

x-y-plot depicting the absolute number of splenic B cells and CD8⁺ T cells per recipient mouse, which received bone marrow transfer of the indicated mixture (color) 6 weeks before. The dot size corresponds to the absolute number of living cells per spleen.

4.5.2 Investigating the effects of T cell depletion

This *in vivo* data strongly suggested that T cells could contribute somehow to the observed counter-selection of BclxL^{tg} A20^{-/-} B cells under steady state conditions and even more pronounced in the competitive BM chimeras. To investigate the effects of a temporary loss of T cells, I depleted T cells through repeated antibody injection *in vivo* over a time span of two weeks.

4.5.2.1 CD8⁺ T cell depletion

T cell cytotoxicity is exerted mainly by CD8 T cells (126), while the positive selection and expansion of B cells in the germinal center depends on the support from CD4 Th and T_{FH} cells. Since I aimed to not disrupt the germinal center-dependent potential of B cells to initiate autoimmunity, I depleted only CD8⁺ T cells subset by repeated injection of anti-CD8 antibody *in vivo*.

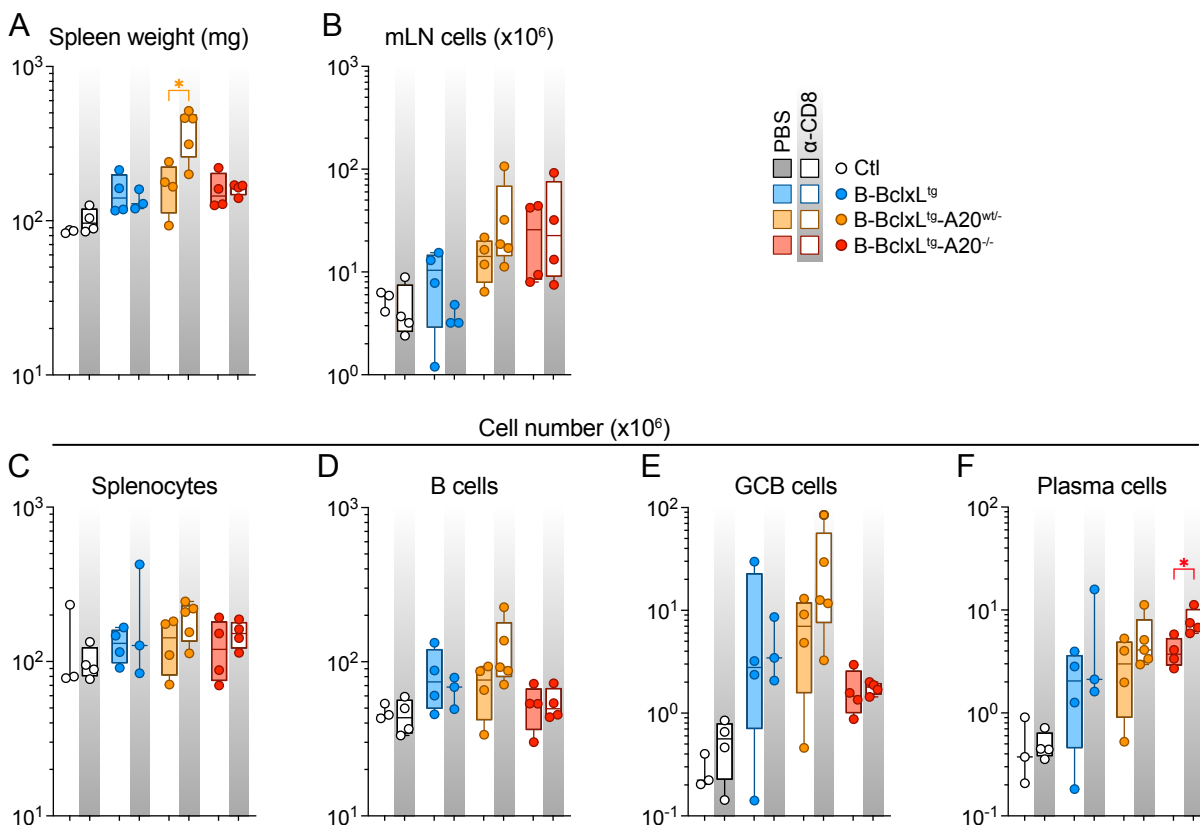


Figure 61. CD8⁺ T cell depletion.

(A) Spleen weight upon 2 weeks anti-CD8 or PBS (control) injections. (B) Absolute numbers of living cells in mesenteric lymph nodes (mLN) upon 2 weeks anti-CD8 or PBS (control) injections. (C-F) Absolute numbers of (C) splenocytes (D) splenic B, (E) germinal center B (GCB) and (F) plasma cells (IRF4⁺, CD138⁺) upon 2 weeks anti-CD8 or PBS (control) injections. (A-F) Shaded areas highlight the anti-CD8-injected group. Stars mark significant differences by two-tailed t-test between anti-CD8 injected and PBS-injected control group. (A-F) Mice were injected by Sabrina Bortoluzzi, Francisco Osorio-Barrios, Sabine Helmraht, Seren Baygün and Julia Knogler. FACS data was analyzed by Francisco Osorio-Barrios.

CD8⁺ T cell-depleted B-BclxL^{tg}-A20^{-/wt} mice had a significantly higher spleen weight compared to the PBS injected control group (**Figure 61A**). However, given the very high variability of spleen weights, which was generally observed in B-BclxL^{tg}-A20^{-/wt} mice (see **Figure 7A**, median spleen weight 300 mg), it is possibly only coincidence that the cohort selected as PBS-injected controls in the T cell depletion assay had only comparably mild splenomegaly (median spleen weight 150 mg). The cell number in mLNs was equal between CD8⁺ T cell-depleted and control mice for all genotypes (**Figure 61B**). Consistent with the bigger spleen size, also the total number of splenocytes as well as splenic B, GCB and plasmacytic cells was slightly higher in CD8⁺ T cell-depleted B-BclxL^{tg}-A20^{-/wt} mice compared to the PBS injected control group, however, the difference was not significant (**Figure 61C-F**). While CD8⁺ T cell depletion had no effect on the absolute number of splenic B or GCB cells in B-BclxL^{tg}-A20^{-/-} mice, it led to a significant expansion of their plasmacytic cells. The fractions of Ig subsets within the plasmacytic cells remained unchanged (data not shown). In mLN, no significant differences were detected for total B, GCB and plasmacytic cell numbers between CD8⁺ T cell-depleted mice and control mice for all groups (data not shown).

4.5.2.2 Depletion of all T cell subsets

Zhang et al. demonstrated that LMP1-driven B cell lymphomas were completely suppressed by cytotoxic T cells in mice. Outgrowth of LMP1⁺ B cells in vivo only occurred upon depletion of all T cell subsets as well as Thy1.1⁺ NK cell subsets using a combination of anti-CD8, anti-CD4 and anti-Thy1 antibodies and not by using either of these antibodies alone (432). Since the depletion of CD8⁺ T cells induced an expansion of plasmacytic cells in B-BclxL^{tg}-A20^{-/-} mice, I decided to use the approach of Zhang et al. and depleted all mature T cells, including $\gamma\delta$ T cells and natural killer T (NKT) cells as well as activated NK cells (432), by combined injection of anti-CD8, anti-CD4 and anti-Thy1 (α -CD8/CD4/Thy1) antibodies for 16 days.

T cell depletion was efficiently established starting at day 5 after α -CD8/CD4/Thy1 treatment (**Figure 62A**). However, in contrast to CD19Cre control mice, all B-BclxL^{tg} containing groups retained considerably more T cells compared to CD19Cre controls after 16 days of the depletion regimen (**Figure 62A**).

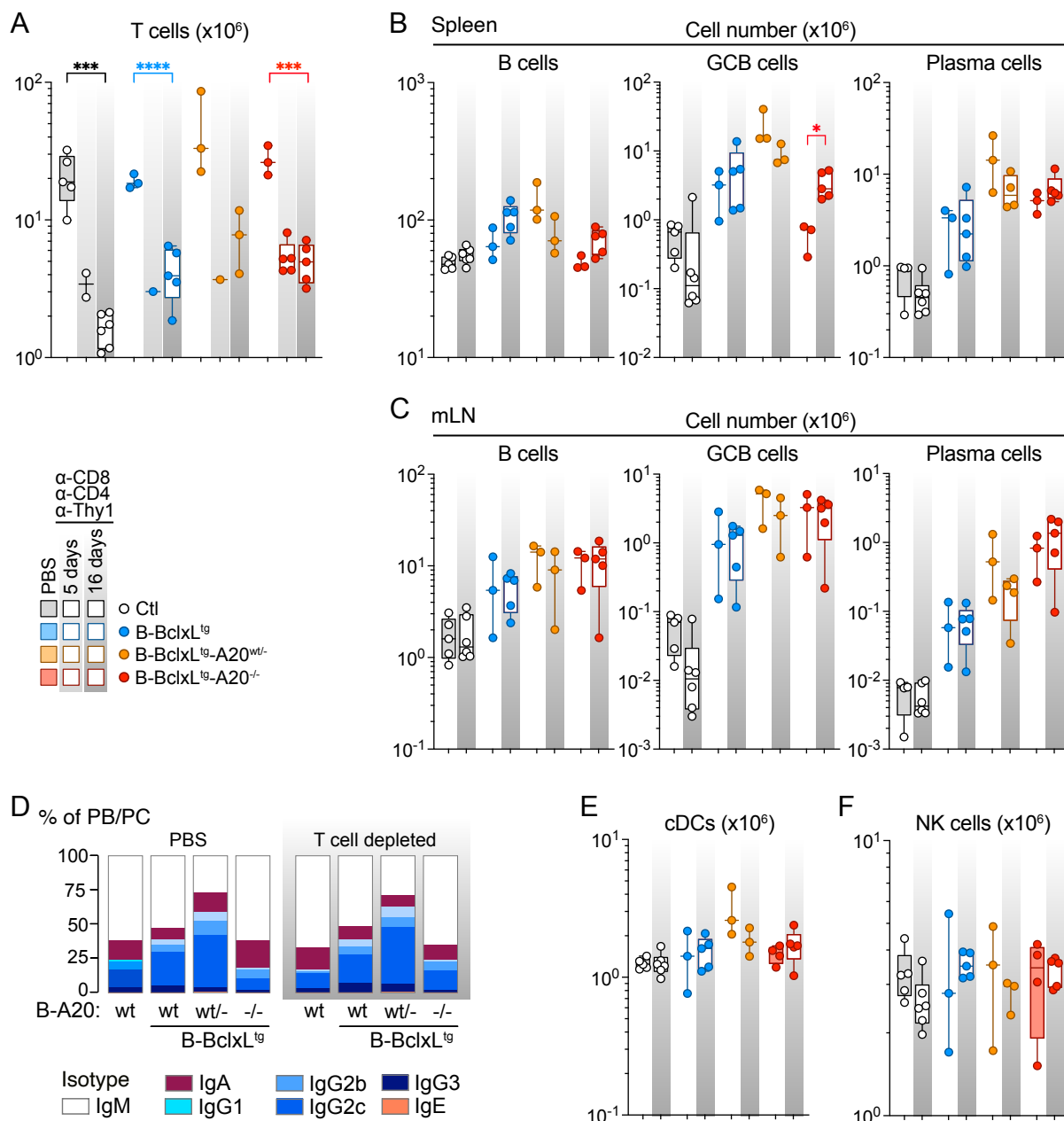


Figure 62. Whole T cell depletion.

(A) Absolute numbers of total splenic T cells after 5 or 16 days of T cell depletion through anti-CD8/anti-CD4/anti-Thy1 or after PBS (control) injections. (B-C) Absolute numbers of (B) splenic and (C) mLN B cells (B220⁺ CD19⁺), germinal center B cells (GCB, CD95⁺ CD38⁻) and plasma cells (CD138⁺, B220^{low}) after 16 days T cell depletion through anti-CD8/anti-CD4/anti-Thy1 or after PBS (control) injections. (D) Isotype distribution of splenic plasma cells after 16 days T cell depletion through anti-CD8/anti-CD4/anti-Thy1 or PBS (control) injections. (E-F) Absolute numbers of splenic (E) conventional dendritic cells (cDC, CD11c^{hi}) and (F) natural killer cells (NK, NK1.1⁺, TCR β) after 16 days T cell depletion through anti-CD8/anti-CD4/anti-Thy1 or after PBS (control) injections. (A-F) Shaded areas highlight the T cell depleted groups. Stars mark significant differences by two-tailed t-test between 16 days T cell-depleted and PBS-injected control group. (A-F) Mice were partially injected by Monika Mittermeier. FACS data was analyzed by Francisco Osorio-Barrios.

The expansion of autoreactive B cells in B-BclxL^{tg}-A20^{-/wt} mice is highly dependent on T cell help in the germinal center. This could explain why the depletion of T cells in these mice led to a slight reduction of total B, as well as GCB and plasma cell numbers in spleen and mLN (**Figure 62B, C**). Interestingly, the opposite effect was observed in B-BclxL^{tg}-A20^{-/-} mice, where T cell depletion led to an increase of the absolute splenic B, GCB and plasmacytic cell numbers (**Figure 62B**). The isotype distribution of splenic plasmacytic cells remained unaffected by the T cell depletion, indicating that the majority of previously generated GCB and plasmacytic cells remained in the spleen for more than 16 days (**Figure 62D**). The depletion regimen had no significant effect on the number of conventional dendritic (cDC) and natural killer (NK) cells as well as other myeloid lineage cells (**Figure 62E, F** and data not shown).

In CD19Cre control mice, T cell depletion was much more efficient and their spleens were essentially devoid of CD4⁺ T cells (**Figure 62A**). Consequently, due to the lack of T cell help they lost most GCB cells, resulting in a reduced fraction of class-switched plasmacytic cells (**Figure 62B-D**).

Overall, this data indicate that T cells are required to support (autoimmune) B cell expansion and differentiation in the context of A20 heterozygosity in BclxL^{tg} B cells. In striking contrast, T cell depletion significantly counteracted the differentiation and/or expansion of B cells, especially GCB cells, in the context of complete loss of A20.

4.5.3 T cell knockout in A20-deficient mice

Based on the effects of the incomplete antibody-mediated T cell depletion, I decided to investigate the effects complete T cell deficiency, introduced by genetic knockout of CD3 ϵ (CD3 $\epsilon^{\Delta\Delta}$), a central mediator of TCR signals (287).

4.5.3.1 BclxL^{tg} A20^{-/-} plasmacytic cells expand in the absence of T cells

As expected and suggested by the temporary T cell depletion experiments (see **Figure 61** and **Figure 62**), I observed a decrease of B and plasmacytic cells in CD3 $\epsilon^{\Delta\Delta}$ B-BclxL^{tg} and especially in CD3 $\epsilon^{\Delta\Delta}$ B-BclxL^{tg}-A20^{-/wt} mice (**Figure 63A, B**). In striking contrast, in B-BclxL^{tg}-A20^{-/-} mice, T cell-deficiency significantly increased B cell (3-fold) and PC/PB (10-fold) numbers in the spleen compared to their T cell containing counterparts (**Figure 63A**). Consistently, all CD3 $\epsilon^{\Delta\Delta}$ B-BclxL^{tg}-A20^{-/-} mice had more plasmacytic cells in spleen and mLN than both CD3 $\epsilon^{\Delta\Delta}$ B-BclxL^{tg} and CD3 $\epsilon^{\Delta\Delta}$ B-BclxL^{tg}-A20^{-/wt} mice (**Figure 63A, B**, right panels).

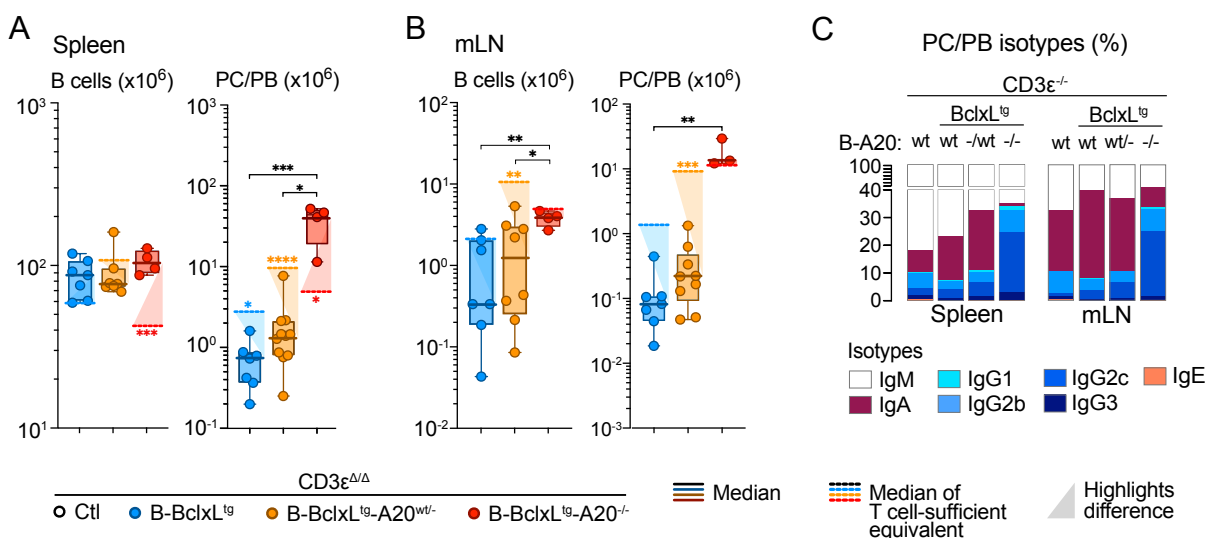


Figure 63. B and plasmacytic cells expand in T cell-deficient B-BclxL^{tg}-A20 mice.

(A-B) Absolute number of B and plasmacytic cells (PC/PB) in (A) spleen and (B) mesenteric lymph nodes (mLN) of T cell deficient (CD3 $\epsilon^{\Delta\Delta}$) B-BclxL^{tg}-A20 mice. Data is displayed as box-whisker-plots. Dots represent individual mice. Continuous lines depict medians, dotted lines depict medians of the corresponding T cell-sufficient equivalents, shaded triangles highlight the difference between medians. (C) Isotype distribution of plasmacytic cells in spleen and mLN in CD3 $\epsilon^{\Delta\Delta}$ B-BclxL^{tg}-A20 mice. (A-C) Some mice were analyzed by Valeria Soberón and Seren Baygün. Data was analyzed and plotted by me.

The lack of T cells in CD3 $\epsilon^{\Delta\Delta}$ mice allows only T cell-independent class switching, which can be triggered by TACI, BCR and TLR stimulation and mainly produces IgA switched plasma cells (433-435). Correspondingly, Ctl, BclxL^{tg} and BclxL^{tg} A20^{-/wt} PC/PB in the spleen and even more prominently in the mLN of CD3 $\epsilon^{\Delta\Delta}$ mice were mainly of the IgA isotype (**Figure 63C**). In stark contrast, BclxL^{tg} A20^{-/-} PC/PB had a high prevalence for the IgG2b and IgG2c classes in the context of T cell-deficiency (**Figure 63C**). This demonstrates a highly unusual capacity of these cells for T cell-independent CSR.

4.5.3.2 The development of autoimmunity in B-BclxL^{tg}-A20^{-wt} mice is T cell dependent

Class switching occurs preferentially early in the germinal center reaction but can also be initiated extrafollicularly. Especially in autoimmune B-BclxL^{tg}-A20^{-wt} mice, the immense number GCB cells indicated that the vast majority of class-switched PB/PC is germinal center-derived and therefore generated in dependence of T cell help.

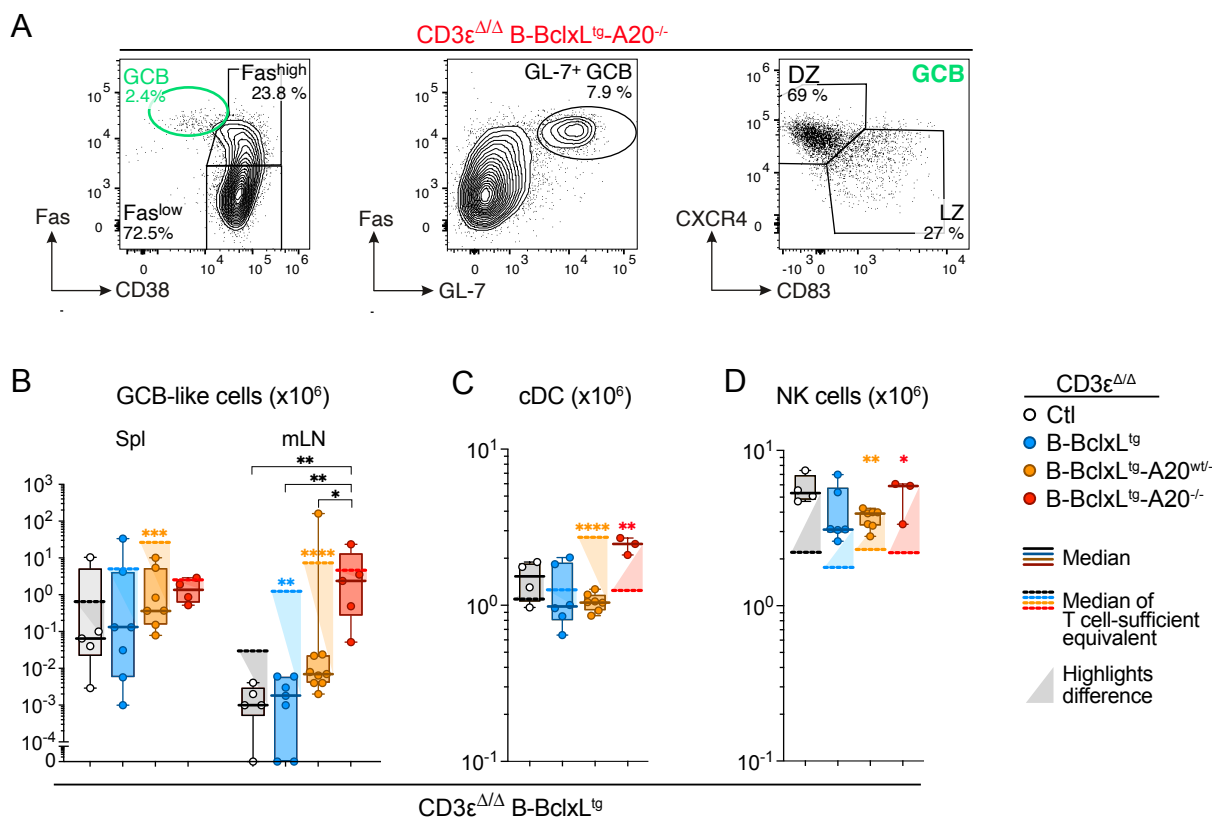


Figure 64. Immune cell composition in spleens of T cell deficient B-BclxL^{tg}-A20 mice.

(A) Representative flow cytometry plots depicting the Fas and CD38 expression (left), Fas and GL-7 expression (middle) in B220⁺ CD19⁺ B cells and the expression of CXCR4 and CD83 on Fas^{high} CD38^{low} GCB cells (right) from the spleen of a CD3 $\epsilon^{\Delta/\Delta}$ B-BclxL^{tg}-A20^{-/-} mouse. (B-D) Absolute number of (B) B220⁺ CD19⁺ CD95⁺ CD38^{low} germinal center B (GCB)-like cells (C) CD11c^{hi} conventional dendritic cells (cDC) and (D) NK1.1⁺ TCR β ⁻ natural killer (NK) cells spleens of CD3 $\epsilon^{\Delta/\Delta}$ B-BclxL^{tg}-A20 mice.

In line with the lack of T cell help, the number of Fas^{high} CD38^{low} B cells phenotypically resembling GCB cells (GCB-like) was strongly reduced in the spleen and even more in the mLN of CD3 $\epsilon^{\Delta/\Delta}$, CD3 $\epsilon^{\Delta/\Delta}$ B-BclxL^{tg} and CD3 $\epsilon^{\Delta/\Delta}$ B-BclxL^{tg}-A20^{-wt} animals. In CD3 $\epsilon^{\Delta/\Delta}$ B-BclxL^{tg}-A20^{-/-} mice, however, T cell deficiency did not strongly affect the numbers of GCB-like cells (**Figure 64B**). A Fas^{high} CD38^{low} GCB cell-reminiscent phenotype developed in BclxL^{tg} A20^{-/-} B cells independent of T cell help. GCB-like cells also expressed the GCB cell marker GL-7 and the LZ / DZ markers CXCR4 and CD83 in common ratios (**Figure 64**).

Also splenic conventional dendritic (cDC) cell numbers were significantly decreased in $CD3\epsilon^{\Delta\Delta}$ B-BclxL^{tg}-A20^{-wt} but significantly increased in $CD3\epsilon^{\Delta\Delta}$ B-BclxL^{tg}-A20^{-/-} mice (**Figure 64C**).

While the CD3 ϵ protein is expressed in the cytoplasm of fetal thymic T/NK bipotential progenitor cells and activated NK cells, no functional CD3 is detectable on their surface (436, 437). This suggests that the genetic disruption of CD3 ϵ exon 5 does not inhibit NK cell development and function (437). In line with this, also $CD3\epsilon^{\Delta\Delta}$ mice had no defect regarding their NK cell development. Instead, splenic NK cells were more abundant in all $CD3\epsilon^{\Delta\Delta}$ B-BclxL^{tg}-A20 mice compared to their T cell sufficient counterparts (**Figure 64C**). This suggests that NK cell cytotoxicity is still functional in $CD3\epsilon^{\Delta\Delta}$ mice and is therefore not directed against or not sufficient to eradicate A20-deficient B cells.

Corresponding to the observation that autoimmune B cell differentiation in B-BclxL^{tg}-A20^{-wt} mice strongly depended on T cell help, ANA as well as anti-cardiolipin (α -CL) IgG autoantibodies were essentially reduced to background levels in the serum of $CD3\epsilon^{\Delta\Delta}$ B-BclxL^{tg}-A20^{-wt} and $CD3\epsilon^{\Delta\Delta}$ B-BclxL^{tg} mice (**Figure 65A**). Strikingly, $CD3\epsilon^{\Delta\Delta}$ B-BclxL^{tg}-A20^{-/-} mice retained significantly higher serum levels of ANA as well as α -CL IgG compared to the other $CD3\epsilon^{\Delta\Delta}$ groups. Still, the comparably low absolute autoantibody concentration was likely not pathological in $CD3\epsilon^{\Delta\Delta}$ B-BclxL^{tg}-A20^{-/-} mice (**Figure 65A**).

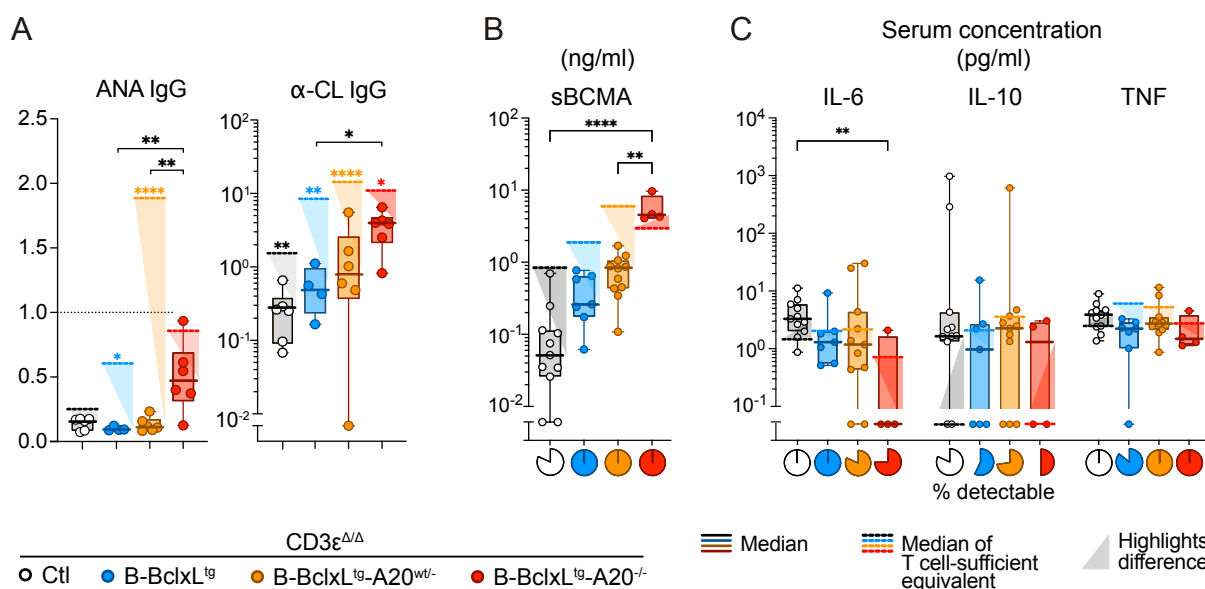


Figure 65. Lack of autoimmune manifestations in T cell-deficient B-BclxL^{tg}-A20 mice.

(A) Serum levels of anti-nuclear IgG autoantibodies (ANA, normalized to positive control) and anti-cardiolipin IgG (α -CL, equal to U/ml GPL) in $CD3\epsilon^{\Delta\Delta}$ B-BclxL^{tg}-A20 mice. **(B-C)** Serum concentration of **(B)** sBCMA and **(C)** IL-6, IL-10 and TNF in $CD3\epsilon^{\Delta\Delta}$ B-BclxL^{tg}-A20 mice measured with Legendplex kit. Pie charts depict the percentage of samples above the minimum detection value. Data is displayed as box-whisker-plots. Dots represent individual mice. Continuous lines depict medians, dotted lines depict medians of the corresponding T cell-sufficient equivalents, shaded triangles highlight the difference between the medians. *(A-C) Some mice were analyzed by Valeria Soberón and Seren Baygün. ANA and α -CL ELISAs and Legendplex assay were performed by Julia Knogler and data was plotted by me.*

Corresponding to the relative changes in PC/PB numbers, the concentration of serum sBCMA increased in $CD3\epsilon^{\Delta\Delta}$ B-BclxL^{tg}-A20^{-/-} mice, while it decreased in all other groups (**Figure 65B**). The absence of autoimmunity was also reflected by a decrease in the levels of SLE-associated cytokines in $CD3\epsilon^{\Delta\Delta}$ B-BclxL^{tg} and $CD3\epsilon^{\Delta\Delta}$ B-BclxL^{tg}-A20^{-/wt} mice, compared to their T cell sufficient counterparts (**Figure 65B**).

4.5.3.3 T cell deficiency allows the lymphoproliferative expansion of A20-deficient B cells

When combined with B-BclxL^{tg} expression and B cell-specific A20-deficiency, the survival of $CD3\epsilon^{\Delta\Delta}$ mice decreased in direct correlation with the A20 gene dose: B-BclxL^{tg}-A20^{-/-} > B-BclxL^{tg}-A20^{wt/-} > B-BclxL^{tg} > Ctl (**Figure 66A**). The premature death went in hand with a massive lymphoproliferation, which also corresponded to the A20 zygosity and BclxL^{tg} expression (**Figure 66B and Supplementary Table 4**).

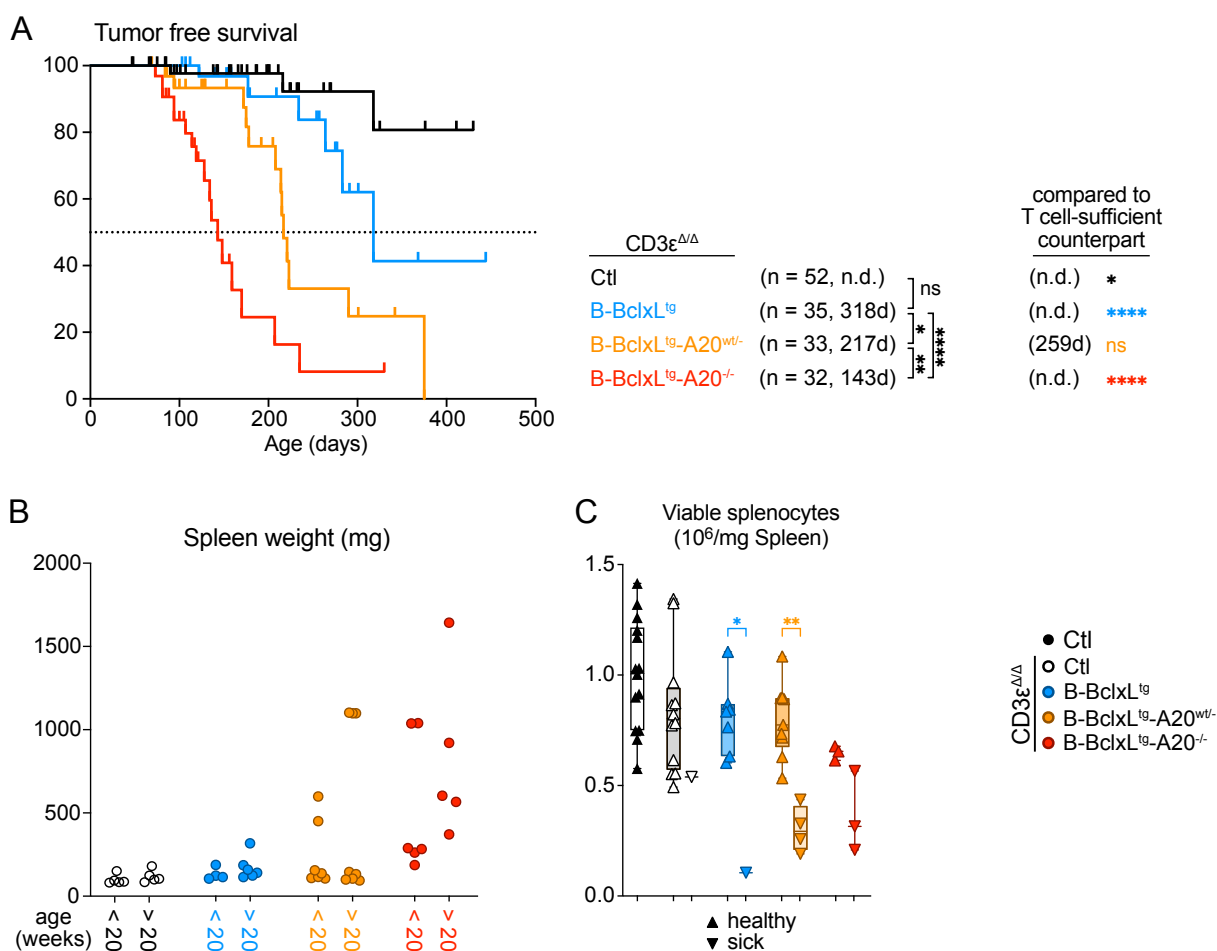


Figure 66. Lethality and lymphoproliferation in $CD3\epsilon^{\Delta\Delta}$ B-BclxL^{tg}-A20 mice.

Figure 66. Lethality and lymphoproliferation in CD3 $\epsilon^{\Delta\Delta}$ B-BclxL^{tg}-A20 mice (Legend)

(A) Kaplan Meier survival curves for CD3 $\epsilon^{\Delta\Delta}$ B-BclxL^{tg} mice with B cell-specific A20-deficiency. Cohort sizes and median survival times are shown. **(B)** Spleen weights of CD3 $\epsilon^{\Delta\Delta}$ B-BclxL^{tg} mice of the different A20 genotypes, divided by age: CD3 $\epsilon^{\Delta\Delta}$ Ctl: 9-20 and 20-54 weeks; CD3 $\epsilon^{\Delta\Delta}$ BclxL^{tg}: 15-20 and 20-41 weeks; CD3 $\epsilon^{\Delta\Delta}$ BclxL^{tg}-A20^{-wt}: 12-20 and 20-48 weeks; CD3 $\epsilon^{\Delta\Delta}$ BclxL^{tg}-A20^{-/-}: 12-20 and 20-24 weeks. **(C)** Ratio of viable cell number ($\times 10^6$) and weight per spleen for healthy (upward triangle) and sick (downward triangle) CD3 $\epsilon^{\Delta\Delta}$ B-BclxL^{tg}-A20 and control mice. (A-C) Some mice were analyzed by Valeria Soberón (VS) and Seren Baygün. (B) Data was plotted by VS.

In all CD3 $\epsilon^{\Delta\Delta}$ B-BclxL^{tg}-A20 groups, some mice became macroscopically “sick” – judged by visible ill-being or palpable tumor-like spleen expansion – and were immediately analyzed. In parallel, cohorts of age-matched mice were analyzed, which did not yet show macroscopical signs of ill-being. If no tumors could be identified within these mice upon analysis, they were classified as “healthy”. In all genotype groups, “sick” mice had a consistently reduced number of viable cells per splenic weight compared to their healthy” counterparts, which indicated an on-going inflammation (**Figure 66C**).

Lethal lymphoproliferations also developed in CD3 $\epsilon^{\Delta\Delta}$ B-A20^{wt/-} and CD3 $\epsilon^{\Delta\Delta}$ B-A20^{-/-} mice without BclxL^{tg} transgene expression (**Supplementary Figure 5A, B**) and resembled neoplasms in approximately 25% and 40% of cases, respectively (**Supplementary Figure 5C**). This demonstrates that mutations leading to the loss of A20 can act as oncogenic hits driving B cell lymphomagenesis. The mono- and bi-allelic loss of A20 were reported in human lymphoma patients but the tumor-driving effect A20-deficiency had not yet been demonstrated in mouse models (270, 271, 438). Here, I show that the B cell specific mono- and bi- allelic loss of A20 act oncogenic in the context of defective T cell immune surveillance.

4.5.3.4 A20 knockout induces an aberrant surface marker expression on BclxL^{tg} B cells

The lymphoproliferations in CD3 $\epsilon^{\Delta\Delta}$ B-BclxL^{tg}-A20 mice consisted mainly of CD19⁺ B cells, which frequently lost B220 expression. Afshar-Sterle et al. (133) observed lymphomagenesis in CD3 $\epsilon^{\Delta\Delta}$ mice with B cell specific knockout of Blimp1 (B-Blimp1 $\Delta\Delta$). They defined two subtypes: “A” with mainly CD19⁺ B220⁺ cells and “B” with reduced B220 expression. All B-Blimp1 $\Delta\Delta$ lymphomas were IgM⁺ but expressed low levels of the mature B cell markers IgD and CD23, and sometimes were CD43⁺. Importantly, B-Blimp1 $\Delta\Delta$ lymphomas expressed high levels of Fas which rendered them susceptible to FasL induced cell death *in vitro* (133). Among the CD3 $\epsilon^{\Delta\Delta}$ B-BclxL^{tg}-A20^{/wt} lymphoproliferations two samples were examined for the expression of these markers and both contained a B220^{low} CD19⁺ population but most cells expressed both surface markers. Therefore, these lymphoproliferations did not fit either sub-classification observed by Afshar-Sterle et al., (133) (**Figure 67A**). B220^{low} and B220^{high} lymphoproliferative B cells were mainly IgM⁺ but IgD^{low} and CD23^{low}, and a large fraction of them expressed high levels of Fas (**Figure 67A** and **Supplementary Figure 6**). Importantly, the expression of Fas was highly heterogeneous among the B cells from different CD3 $\epsilon^{\Delta\Delta}$ B-BclxL^{tg}-A20 mice (**Supplementary Figure 7**). Whether or not Fas expression marks premalignant lymphoproliferations, early neoplasms and/or malignant cells remains to be clarified in future studies.

Flow cytometric profiling of splenic B cells from “healthy” mice revealed that B cells from all CD3 $\epsilon^{\Delta\Delta}$ B-BclxL^{tg}-A20 mice had a generally low expression of surface activation markers, demonstrating that their activated phenotypes in T cell sufficient mice were largely T cell-dependent. Exceptions were a very high expression of CD86 and low surface CD62L on BclxL^{tg} A20^{-/-} B cells in absence of T cells (**Figure 67B**). Comparing CD3 $\epsilon^{\Delta\Delta}$ with T cell sufficient mice, I found that the loss of surface CD62L on BclxL^{tg} A20^{-/-} B cells was strongly enhanced in the absence of T cells (**Figure 67C**, turquoise vs. red histograms). Furthermore, the fraction of CD62L^{low} cells was bigger in Fas^{high} compared to Fas^{low} BclxL^{tg} A20^{-/-} B cells (**Figure 67C**). This demonstrates a strong T cell-independent activation of BclxL^{tg} A20^{-/-} B cells, which induces Fas upregulation and shedding of CD62L, potentially induced via stimulation and/or BCR signals (4, 439). Low surface CD62L also fits with the strong plasmacytic differentiation of BclxL^{tg}-A20^{-/-} B cells (440).

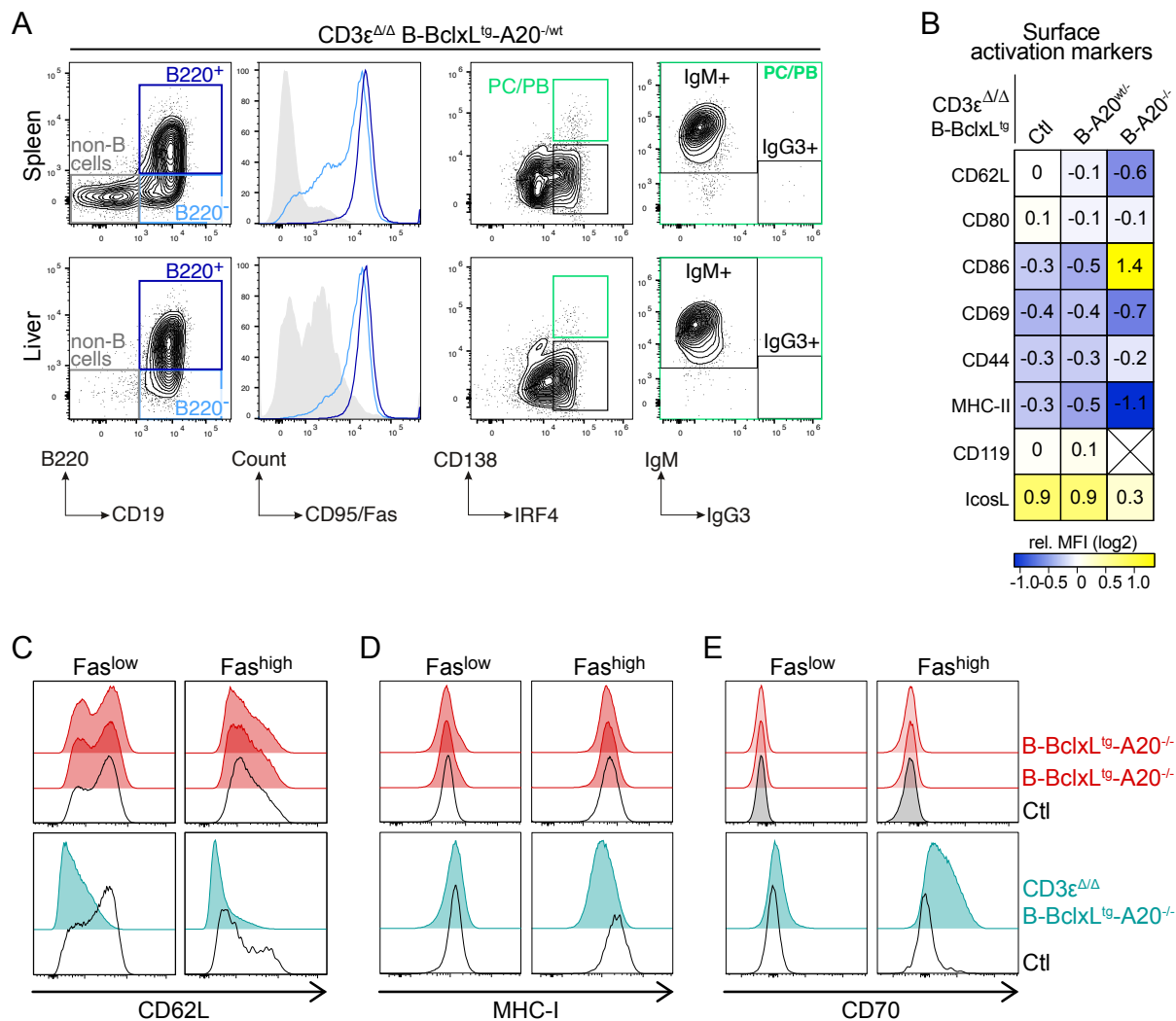


Figure 67. Marker expression on B cells from $CD3\epsilon^{\Delta/\Delta}$ mice.

(A) FACS plots depicting B220 and CD19 expression on lymphocytes (1st panels); histograms depicting Fas signal intensity on B220⁺ (dark blue) and B220^{low} (light blue) CD19⁺ B cells as well as non-B cells (grey) (2nd panels); FACS plot depicting the expression of IRF4 and CD138 on lymphocytes (3rd panels); FACS plot depicting the expression of IgM and IgG3 on CD138⁺ IRF4⁺ plasmacytic cells (PC/PC) (4th panels) in the spleen and the liver of a sick $CD3\epsilon^{\Delta/\Delta}$ B-BclxLtg-A20^{-/wt} mouse. (B) Heatmap representing the log2fold change of protein expression in splenic B cells from $CD3\epsilon^{\Delta/\Delta}$ B-BclxLtg-A20 mice relative to CD19Cre control B cells measured with flow cytometry. Mean values from at least 3 biological replicates are shown. (C-E) Histograms depicting (C) CD62L, (D) MHC-I and (E) CD70 protein expression on BclxL^{tg} A20^{-/-} B cells from T cell sufficient (upper panel, red) or $CD3\epsilon^{\Delta/\Delta}$ mice (lower panel, green) and control B cells (both panels (black)) by flow cytometry. Data from the upper and lower panel was acquired in different experiments. (C-D) Mice were analyzed and flow cytometric analysis was performed by Seren Baygün and Valeria Soberón. The data is used with the consent of the contributing scientists.

ICOSL is being shed from B cells upon interaction with ICOS on T cells (441). Consistently, B cells from CD3 $\epsilon^{\Delta\Delta}$ mice retained higher surface ICOSL than B cells from T cell-sufficient mice (**Figure 67B** and see **Figure 18**). Surface ICOSL had the lowest MFI on BclxL^{tg} A20^{-/-} B cells.

Surface MHCII was also lowest in BclxL^{tg} A20^{-/-} B cells, suggesting a reduced potential for antigen presentation. This further supports the apparently reduced prevalence of A20^{-/-} B cells for T cell interaction (**Figure 67B**). Consistently, also a slight downregulation of MHC I was visible in Fas^{high} BclxL^{tg} A20^{-/-} B cells from CD3 $\epsilon^{\Delta\Delta}$ compared to CD3 $\epsilon^{\Delta\Delta}$ control mice (**Figure 67D**).

Intriguingly, activated (Fas^{high}) B cells from CD3 $\epsilon^{\Delta\Delta}$ B-BclxL^{tg}-A20^{-/-} but not from T cell-sufficient mice expressed strongly elevated levels of CD70 (**Figure 67E**). This co-stimulatory ligand was reported to be upregulated in malignant B cells upon CD40 engagement. CD70 co-stimulation of T cells is critical to induce their cytotoxic antileukemic activity (442). In the T cell-sufficient setting, CD70 expressing aberrant B cells seem to be efficiently eradicated (**Figure 67E**).

4.5.3.5 Initial characterization of the lymphoproliferative expansions

The lymphoproliferations in $CD3\epsilon^{\Delta\Delta}$ B-BclxL^{tg}-A20 mice were detected mainly in the spleen but sporadically also in LNs and mLNs (**Supplementary Table 1**). Frequently, these lymphoproliferative cells also infiltrated other organs, most prominently the liver (**Figure 67A**, **Supplementary Table 1**). To date, histopathological analysis was performed for one BclxL^{tg} A20^{-/-} and one BclxL^{tg} A20^{wt/-} sample, which revealed a phenotype resembling diffuse large B cell lymphoma (**Figure 68A**). To assess the clonality of the lymphoma from the different $CD3\epsilon^{\Delta\Delta}$ B-BclxL^{tg}-A20 mice, the results from three different PCR assays were combined. This revealed that most lymphoproliferations were (oligo-)clonal (**Figure 68B**).

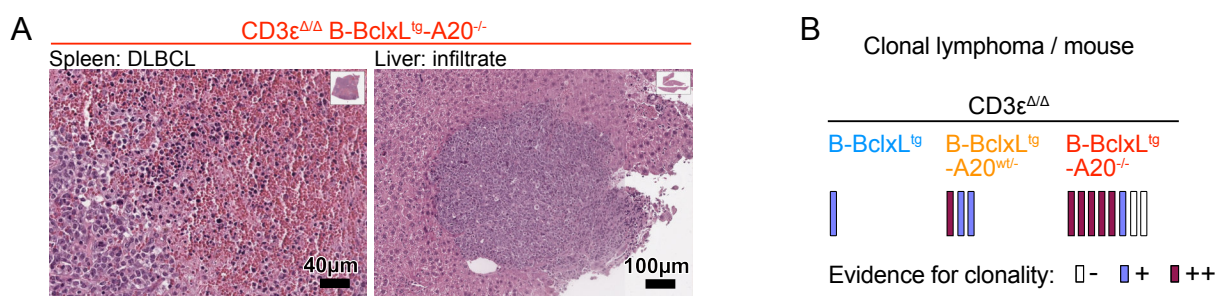


Figure 68. Lymphoma type and clonality.

(A) Representative pictures for H&E staining of a DLBCL lymphoma in the spleen (left) and malignant infiltrate in the liver (right) of a $CD3\epsilon^{\Delta\Delta}$ B-BclxL^{tg}-A20^{wt/-} mouse. (B) Tumor clonality classified based on the amplification of the BCR heavy-(JH1-4) and kappa-light chain rearrangements (Vκdeg-Jκ5BR, Jκdeg-Jκ5AR). - no evidence for clonality, + polyclonal, ++ clonal. (A, B) Valeria Soberón (VS) and Seren Baygün (SB) harvested the organs. (A) Histopathological analysis was performed by Prof. Dr. Katja Steiger in collaboration with VS. (B) Clonality PCRs were run and pictures taken by Laura Kraus (LK) and classified by LK in cooperation with SB, Prof. Marc Schmidt-Supprian (MSS) and me. The data is used with the consent of the contributing scientists.

Collectively, the knockout of T cells revealed a linear correlation between the A20 gene dose in B cells and their capacity to induce a lethal pathology. This effect had been concealed in T cell sufficient mice, demonstrating that the expansion of A20-deficient B cells can be efficiently suppressed by T cell-mediated immune surveillance.

Altogether, my work demonstrates that mildly hyperreactive BclxL^{tg} A20^{wt/-} B cells have the capacity to induce a lethal autoimmune pathology, which is fully dependent on the support by helper T cells. On the contrary, strongly hyperreactive BclxL^{tg} A20^{-/-} B cells fail to receive proper T cell help and instead induce their own elimination by cytotoxic T cells.

5 DISCUSSION

The tight regulation of immune responses is crucial, since uncontrolled activation and failure to terminate an ongoing immune reaction can induce a variety of threatening effects: lymphoma development through uncontrolled expansion of immune cells and autoimmunity through development of autoreactive lymphocytes. One critical player mediating immune cell activation is the canonical NF- κ B signaling pathway and its shutdown requires the expression of the negative feedback regulator A20 (443). Defects of A20 expression and function entail an inefficient shutdown of the immune cell activation. Consequently, mutations in the *A20/TNFAIP3* gene locus are frequently detected in various human blood cancers and autoimmune diseases, including SLE (241, 245, 246).

B cells are central to the development of human SLE and targeting of B cells can be used as efficient treatment for this disease (180, 412). The key role of A20 in B cell biology and the strong implication of B cells in autoimmunity and lymphomagenesis underline the relevance to investigate the role of A20-deficiency in these B cell-driven diseases. More than 10 years ago, three mouse models were published, in which A20 was ablated specifically in the B cell lineage (280-282). A20 knockout in B cells induced a strong hyperreactivity towards NF- κ B activating stimuli *in vitro*. These B-A20^{-/-} mice developed mild autoimmune manifestations, evident by the development of anti-nuclear and anti-cardiolipin as well as tissue-specific autoantibodies, increased pro-inflammatory IL-6, and immune complex deposition in the kidneys. The pathology, however, was rather mild and only appeared in mice older than one year. Subsequently, it was suggested that mice with reduced A20 expression instead of complete loss of A20 may provide a closer genetic approximation to the human condition (241). Data on mice with heterozygous A20-deficiency in B cells (B-A20^{-/wt}) indicated an expansion of germinal center B cells and class-switched autoantibody production (280, 281). However, no follow-up-study has been published, which investigates the extent of autoimmunity in B-A20^{-/wt} mice.

Our laboratory continued the analysis B cell-specific A20-deficient mice and found that indeed, the heterozygous deletion of A20 had a more detrimental effect than its complete knockout. Still, heterozygous A20-deficiency by itself was a rather weak driver of B cell hyperactivation and required the additive effect of other autoimmunity pre-disposing effects, including female sex or elevated levels of BAFF, to initiate a strong pathology (unpublished data). This fits with the concept that the development of autoimmunity depends on environmental triggers as well as the breakdown of several checkpoints, which protect against disease development (43). One disease-driving alteration is the enhancement of anti-apoptotic proteins. In mice, B cell-specific overexpression of anti-apoptotic BclxL (E μ -BclxL^{tg}) leads to an accumulation of autoreactive clones in the peripheral B cell pool (117, 152).

Furthermore, it was proposed that increased expression of BclxL by A20-deficient B cells increases their resistance towards Fas-induced cell death in the germinal center (281). Supporting this notion, *ex vivo* isolated total A20-deficient B cells were stimulated with anti-CD40 and subsequently treated with anti-Fas *in vitro*. BclxL expression as well as survival against anti-Fas stimulation increased with decreasing A20 gene dose (281). I was able to confirm enhanced BclxL expression in A20-deficient B cells upon CD40 stimulation by use of an *in vitro* derived germinal center B (iGB) cell culture system. However, I demonstrated that neither the loss of A20 nor BclxL^{tg} expression protected GCB-like iGB cells against apoptosis induced by membrane-bound FasL. This suggests that GCB cells transmit Fas-induced apoptosis signal via the mitochondria-independent type I pathway. While B cells have been reported to exert Fas-induced apoptosis via the type II pathway (444), to my knowledge no study had previously been performed to investigate the type of Fas-induced apoptosis pathway in GCB cells. The iGB system potentially poses a more suitable model for Fas-stimulation in the germinal center than previous studies (281, 445), as the iGB cells have a GCB-like phenotype and are stimulated by membrane-bound Fas instead of anti-Fas ligation.

Although BclxL^{tg} expression does not protect A20-deficient B cells against FasL-induced cell death, it does protect GCB cells against apoptosis induced by intrinsic triggers. To evaluate the combined effect of heterozygous A20 deletion together with E μ -BclxL^{tg} expression, I generated an intercross between both lines and analyzed the developing autoimmune phenotype.

5.1 B-BclxL^{tg}-A20^{-/wt} mice as a model for human SLE

The combination of B cell-specific heterozygous A20 deletion with E μ -BclxL^{tg} expression promoted the generation and expansion of autoreactive B cells and their differentiation to autoantibody-secreting plasmacytic cells. This entailed the development of a systemic autoimmune pathology, which faithfully recapitulates many features of human SLE.

5.1.1 Similarities between B-BclxL^{tg}-A20^{-/wt} mice and other SLE mouse models

In the following chapter I compare and contrast my new SLE mouse model to existing mouse models for this disease.

The mean survival of B-BclxL^{tg}-A20^{-/wt} mice (50 % survival after 8 months) was equal to the mean survival of the congenic B6.NZMSle1/Sle2/Sle3 strain, which carries the SLE risk loci sle1, 2, 3 from inbred NZM mice (192, 193) on the C57BL/6 genetic background (198, 446). Inbred lupus mouse strains, like NZB/NZWF1 and NZM (192, 193) mice have a prevalence for autoimmunity development in females (193), while MRL/lpr mice, a genetic model of a generalized autoimmune disease, carrying a single-allele Fas mutation

and sharing many features with systemic lupus erythematosus (SLE), disease develops equally in males and females (193). Also in the B-BclxL^{tg}-A20^{-wt} model, the occurrence and severity of the autoimmune pathology was independent of the mouse sex. This indicates that increased resistance against apoptosis (via Fas^{-/-} or BclxL^{tg}) overrides disease predisposing factors which are imposed by female sex.

BSXB male mice, which carry an additional copy of the *Tlr7* gene locus develop a SLE-like disease (199). In addition, TLR7 knockout in lupus-prone mice was shown to ameliorate the disease severity. Consistently, the B cell-specific knockout of MyD88 in B-BclxL^{tg}-A20^{-wt} mice rescued them from the SLE-like pathology. This suggests that TLR signaling in BclxL^{tg} A20^{-wt} B cells plays a pivotal role in driving their autoreactivity, although I cannot formally exclude a role for IL-1 signaling, which is also dependent on MyD88 (447). TLR sensing of nucleic acids is essential for the generation of ANA and anti-dsDNA autoantibodies, which are the predominant autoantibody type in most SLE mouse models (448). In line with this, these and other SLE-related autoantibodies were strongly enriched in B-BclxL^{tg}-A20^{-wt} mice.

With regards to strong IFN γ signaling, B-BclxL^{tg}-A20^{-wt} mice are highly similar to other SLE mouse models, in which, unlike the situation in human SLE patients, the disease is not primarily driven by IFN α but rather IFN γ (448).

Cutaneous manifestations are a common symptom of human SLE patients, occurring in 70% to 85% of individuals over the course of the disease (449). In contrast, skin pathology appears only in very few of the commonly used SLE mouse models (448). I have not systematically evaluated a potential skin pathology in B-BclxL^{tg}-A20^{-wt} mice, however, no obvious cutaneous changes came to my attention during all analyses.

The development of immune complex glomerulonephritis is a common feature of essentially all SLE mouse models, while the extent and onset of symptoms is highly variable (448). While immune complex deposition was highly prevalent in B-BclxL^{tg}-A20^{-wt} mice, their nephritis symptoms were rather mild. I identified the development of an antiphospholipid syndrome (APS) in B-BclxL^{tg}-A20^{-wt} mice, which might contribute to their high mortality in absence of strong kidney pathology in most mice. Consistently, APS was shown to develop also in other SLE mouse models (450-452).

The genetic modifications of most inbred and single-gene SLE strains are germline-encoded and thereby affect all somatic cell types. In contrast, in the B-BclxL^{tg}-A20^{-wt} mice the loss of A20 and anti-apoptotic BclxL overexpression affect only B cells. Thereby this mouse model more closely recapitulates the cumulated acquisition of somatic mutations predisposing for autoimmunity (18, 43). Importantly, in MRL-lpr mice, B cells were shown to play a key role in driving the autoimmune pathology. The involved B cell function exceeded autoantibody production but also included their cytokine secretion and antibody presenting function (205, 453-455). With the B-BclxL^{tg}-A20^{-wt} mouse model, I was able to demonstrate that somatic mutations, affecting only B cells, suffice to induce a SLE-like pathology.

The B-BclxL^{tg}-A20^{-wt} mice showed also similarities to a mouse model with B cell-specific Fas deficiency (B-Fas^{-/-}) (150). These mice also developed splenomegaly with an increased proliferation and cross-activation of B and T cells, as well as elevated serum IFN γ , TNF, IL-6 and IL-10 (150). The close resemblance to B-Fas^{-/-} mice supports the notion that the pathology in B-BclxL^{tg}-A20^{-wt} mice is germinal center driven.

Overall, I was able to demonstrate that the combination of B cell-specific heterozygous A20-deficiency with E μ -BclxL^{tg} expression in mice can induce a lethal autoimmune pathology with a great similarity to other SLE mouse models and, more importantly, to the human SLE pathology.

5.1.2 The stochastic nature of autoimmunity

While heterozygous A20-deficiency in combination with BclxL overexpression in B cells posed a high risk for the development of autoimmunity, the timepoint of disease development and the disease severity, were not uniform among all mice. For analysis, mice of a certain age were selected without prior screening for disease parameters and therefore represented a mix of strong and mild pathology. Anti-nuclear autoantibodies (ANAs) were detectable at similar rates in young and aged mice, demonstrating that pathology also develops at higher age in some mice. In a large proportion of B-BclxL^{tg}-A20^{-wt} mice, the genetic alteration did not lead to lethal disease, as one third of these mice survived for more than 400 days in our facility. This is in line with inbred lupus-prone mouse strains, which also vary considerably in the time of disease onset as well as the severity and the type of pathology (456, 457). Due to this great variability of disease severity in B-BclxL^{tg}-A20^{-wt} mice, analyses of many disease parameters, including inflammatory cytokines and organ involvement, resulted in a high variability of measured values. The pathology and lethality likely depended on various parameters, including the type of autoantigen targeted and the extent of systemic inflammation, driving organ pathology.

In humans, apart from the genetic background, autoimmunity depends also on environmental factors including the individual's lifestyle. All B-BclxL^{tg}-A20^{-wt} mice harbored the same genetic background and experienced equal living conditions under SPF (specific pathogen free) or SOPF (specific and opportunistic pathogen free) hygiene standards and with regards to housing and food. Therefore, the variation of disease severity could mostly reflect the complicated cellular network, which prohibits autoimmunity by nature but can fail to do so in numerous steps. While BclxL overexpression and heterozygous A20-deficiency increase the likelihood for the generation, selection and expansion of autoreactive B cells, the initial development of strong autoreactivity remains an element of chance.

5.1.3 Why are BclxL^{tg} A20^{-wt} B cells such potent inducers of systemic autoimmunity?

Central tolerance eliminates high-affinity autoreactive lymphocytes, while lower-affinity autoreactive T, but especially B cells can become part of the normal peripheral immune repertoire. These autoreactive peripheral B cells are either subject to regulatory mechanisms, including the induction of anergy and activation-induced cell death (AICD) through Fas or TNFR signaling, or they remain quiescent owing to the lack of appropriate T cell help (457). In order for autoimmunity to develop, several tolerance mechanisms need to be broken down. Unlike other autoimmunity-predisposing genetic alterations, including Fas-deficiency or TLR7-amplification, NF-κB overactivation through heterozygous loss of A20 may act on many tolerance checkpoints simultaneously: Various stimuli required for the positive selection of B cells could be over-amplified, including BAFFR-, CD40- and TLR-engagement, and an enhanced expression of anti-apoptotic proteins could protect the cells from BIM induced apoptosis (43). The additional inhibition of apoptosis through BclxL^{tg} expression leads to an increased pool of peripheral autoreactive B cells (152) and furthermore supports the survival of autoreactive B cells independent of NF-κB activation.

The initial loss of self-tolerance presumably occurs in peripheral B cells with low, but relevant, affinity for self. Upon positive selection of an autoreactive B cell into the germinal center, SHM can result in the generation of high affinity towards self-antigens, provided that T cell help is available. Importantly, hyperactivated autoreactive B cells can break tolerance of low affinity autoreactive T cells (458) and also induce help from initially foreign-reactive T cells (459, 460). In a process termed “epitope spreading”, certain autoreactive B cells can present foreign antigens that complex with autoantigens, and thereby get help from foreign-reactive T cells (457). In the context of systemic autoimmunity, the production of autoantibodies can be induced by DNA-peptide-complexes or DNA-containing immune-complexes (105, 461). Under physiological circumstances, nuclear autoantigens, including dsDNA, can become exposed due to uncontrolled cell death. The sensing of nuclear autoantigens occurs MyD88-dependently via TLRs. DNA-peptide- as well as DNA-immune-complexes can activate both, TLR and BCR signaling, which were shown to have a synergistic effect on autoreactive B cell activation (105). In TI responses, CD40L-CD40 engagement can be substituted by B cell TLR engagement to induce AID activity (435) and it has recently been shown that TLR-BCR co-engagement can potently induce the generation of class-switched, hypermutated antibodies in absence of T cells (462). In B-BclxL^{tg}-A20^{-wt} mice, the initiation of autoimmunity depended completely on MyD88. The initial activation of autoreactive DNA-binding B cells in these mice might therefore happen independent of T cell help through combined BCR and TLR7 stimulation. Antigen processing and MHCII presentation subsequently initiates T cell help to support the positive selection of the autoreactive B cell and potentially involves epitope spreading.

The entry of the autoreactive B cell into the germinal center marks the initiation of a positive feedback loop of self-sustaining inflammation and enhanced autoreactivity: Through SHM the affinity of the B cell towards the autoantigen increases. The subsequent generation of high-affinity autoantibodies by plasma cells leads to immune complex development, which induces inflammation and end organ damage. Cytokine production by the activated B and T cells can also activate other immune cell types to sustain the inflammatory response. Once established, the high inflammatory state boosts T cell help for the autoreactive B cells, which further increases autoreactivity and enables the generation of refined autoantibodies, including those targeting phospholipids. The further enhanced systemic inflammation accelerates the organ pathology and drives a lethal APS in some mice. In line with previously published concepts that B cells can initiate an autoimmune pathology by shaping the T cell repertoire (457), I have shown here that autoreactive BclxL^{tg} A20^{-/wt} B cells have the capacity to autonomously recruit T cell help and induce an early-onset SLE-like pathology in mice.

The unaccompanied heterozygous loss of A20 in B cells caused mostly only a mild and late-onset autoimmunity/autoinflammation. However, corresponding to the highly diverse genetic background of human SLE, the B cell-specific heterozygous loss of A20 in mice cooperates with other autoimmunity-predisposing alterations to promote an enhanced autoimmune pathology, as shown here for enhanced B cell survival through enhanced BclxL expression in B cells.

5.1.4 The clinical relevance of heterozygous A20-deficiency

Several autoinflammatory conditions are known to be caused by the haploinsufficiency of A20 (HA20), and the number of patients diagnosed with this genetic alteration is rising steadily (see chapter 1.4.3). The symptoms of the HA20 disease entity are highly diverse. This is likely due to the variable extent of the loss of A20 function and its impact on different cell types. The genetic alterations causing HA20 are hereditary only in 50% of cases. In all other patients *TNFAIP3* mutations arise *de novo* (259) and might therefore be somatic mutations, affecting only one or several cell types. Most reported *TNFAIP3* variants in HA20 patients were identified by whole-exome sequencing of peripheral blood mononuclear cells (PBMC). Therefore, the genetic alteration could be restricted to blood-resident immune cells in some patients. This is supported by a few reports of remission after autologous hematopoietic stem cell transplantation (266).

5.2 The A20-knockout paradox

Interestingly, while HA20 is a potent inducer of various autoimmune phenotypes, the bi-allelic loss of A20 was basically never detected in somatic cells of HA20 patients or human autoimmune patients. Two examples for bi-allelic *TNFAIP3* alterations in these disease entities, were reported in a patient with early-onset inflammatory and autoimmune manifestations, carrying one *TNFAIP3* loss of function allele and one Denisovan *TNFAIP3* allele with a subtle loss of function (237, 463), and in a patient with Sjögren's syndrome, carrying a frameshift mutation on the first and a splice donor mutation on the second *TNFAIP3* allele (211). In both instances, the amount of remaining functional A20 is unclear.

Intuitively, B cells which completely lack A20 expression ($A20^{-/-}$) should be even more hyperreactive than B cells which retained one functional *TNFAIP3* allele ($A20^{-/wt}$). Consequently, one would expect $A20^{-/-}$ B cells to have a competitive advantage and induce an even stronger pathology. A dominance of homozygous loss-of-function mutations has for example been reported for *FAS*. In patients with Autoimmune lymphoproliferative syndrome (ALPS), inherited *FAS* germline mutations are frequently accompanied by somatic events impacting the second allele of *FAS* (464).

Stronger hyperreactivity of $A20^{-/-}$ B cells towards various *in vitro* stimuli had previously been reported by us and others (280-282). In this thesis, I confirmed the superior reactivity of $A20^{-/-}$ B cells in the *in vitro*-derived germinal center B cell (iGB) culture system (302). In stark contrast, the severity of the systemic autoimmune pathology in the *in vivo* setting was much stronger in B-BclxL^{tg}- $A20^{-/wt}$ compared to B-BclxL^{tg}- $A20^{-/-}$ mice. B-BclxL^{tg}- $A20^{-/-}$ mice developed no lethal pathology even at old age. Still, they developed autoreactive plasma cells and some autoimmune manifestations. The total IgG concentration in the serum of B-BclxL^{tg}- $A20^{-/-}$ mice was similar to that in BclxL^{tg} control mice. Simultaneously, the amount of several autoreactive antibodies, including anti-Smith, anti-cardiolipin and ANA IgG (but not anti-dsDNA IgG) were slightly higher in B-BclxL^{tg}- $A20^{-/-}$ mice compared to BclxL^{tg} control mice and they developed a rather strong kidney immune complex deposition. This indicates that BclxL^{tg} $A20^{-/-}$ B cells have an enhanced tendency to develop into autoreactive plasma cells, which produce autoantibodies, subsequently depositing in the kidney. This is in line with an intrinsically increased plasmacytic differentiation of $A20^{-/-}$ B cells, which I was able to demonstrate *in vitro*. Their concomitant premature exit from the germinal center, and consequent lower antibody affinity, might partially explain the absence of lethal pathology in B-BclxL^{tg}- $A20^{-/-}$ mice.

5.2.1 A20^{-/-} B cells trigger T cell immune surveillance

In accordance with the mild phenotype in B-BclxL^{tg}-A20^{-/-} mice, the complete loss of A20 in somatic cells is barely detected in human autoimmune patients. Using competitive bone marrow chimeras, I was able to demonstrate that the complete lack of A20 in B cells induced a detrimental effect, which led to their elimination *in vivo*. I showed that transient as well as complete depletion of T cells in B-BclxL^{tg}-A20^{-/-} mice allowed the expansion of A20^{-/-} plasma cells. This demonstrates that T cells exert immune surveillance mechanisms counteracting aberrant A20^{-/-} B cell expansion in the context of autoreactivity. In future studies, it remains to be investigated, which molecular triggers initiate the targeting of hyperreactive B cells by T cells. Potentially, aberrantly activated A20^{-/-} B cells express specific antigens, which pose an alarm signal to induce T cell cytotoxicity.

However, competitive B-BclxL^{tg}-A20 BM chimeras have shown that while being induced specifically by the presence of BclxL^{tg}-A20^{-/-} B cells, B cell counterselection affected also “mildly hyperactive” BclxL^{tg}-A20^{-/wt} and BclxL^{tg} B cells present in the same animals. Therefore, once B cell pathogenicity has been sensed by CTLs, the molecular target for T cell cytotoxicity might also be a B cell-ubiquitous molecule. Potentially, also “off-target effects” were responsible for the removal of the BclxL^{tg}-A20^{-/wt} and BclxL^{tg} B cells in the bone marrow chimeras. It has been reported that during the antigen-specific T cell targeting of B cell lymphoma cells, also antigen-negative bystander cells can be eliminated by Fas-mediated killing (465).

Still, the question remains, which antigens on BclxL^{tg}-A20^{-/-} B cells initiate the T cell cytotoxicity. The expansion of BclxL^{tg} A20^{-/-} B cells in the absence of T cells, evident by the occurrence of lymphoproliferations, and the targeting of BclxL^{tg} and BclxL^{tg} A20^{-/wt} bystander B cells in competitive chimeras, strongly suggests that the antigens, which trigger T cell cytotoxicity are autoantigens, rather than specific (neo-)antigens (466). The elimination of hyperactivated B cells by T cells bearing low-avidity TCRs for self-antigen has been suggested as a mechanism protecting against B cell lymphoma (133).

The aberrant activation state and strong cell cycle activity, as suggested by transcriptomics data, likely poses stress on BclxL^{tg} A20^{-/-} B cells, which could entail the expression of NKG2D ligands (467, 468). Triggering of the respective NKG2D could alert CD8 T cells to eliminate the aberrant stressed BclxL^{tg} A20^{-/-} B cells. NKG2D ligands are expressed on the surface of tumor cells and NKG2D was shown to be critical for the immunosurveillance lymphoid malignancies (469). Consistently, chimeric NKG2D-expressing T cells were found to target multiple myeloma cells (470). The expression of NKG2D ligands on BclxL^{tg} A20^{-/-} B cells could be investigated using a simple, flow cytometry-based approach. This promises insights into the triggers, which initiate their cytotoxic elimination.

The full activation of NKG2D-stimulated CD8 T cells requires concurrent TCR stimulation (468). Consequently, the full activation of CD8 T cell cytotoxicity would require antigen-MHCI presentation by BclxL^{tg} A20^{-/-} B cells. It would be highly interesting to evaluate, which molecules on aberrant B cells trigger the T cell immune surveillance in B-BclxL^{tg}-A20^{-/-} mice. Recently published advanced methods promise the prediction of TCR-specificities, based on either sequence similarity to previously characterized receptors or computational approaches, which predict the binding TCR-peptide-MHC binding energy, using protein structural information (471, 472).

Next to CD8 T cells, the immune surveillance of BclxL^{tg} A20^{-/-} B cells likely also involves cytotoxic CD4 T cells, as their numbers were strongly increased in relation to the B cell numbers. Therefore, analysis of TCR specificity should optimally include both CD8 and CD4 T cells.

5.2.2 Initiation of the T cell immune surveillance depends on the extent of B cell hyperactivation

Intriguingly, mildly hyperreactive BclxL^{tg} A20^{-/wt} B cells manage to not only escape negative selection but to also shape the T cell repertoire to provide optimal support to foster autoimmunity. While there was a great amount of potentially cytotoxic (preliminary data, not shown) and regulatory T cells in B-BclxL^{tg}-A20^{-/wt} mice, these cells did not sufficiently detain or eliminate the autoreactive B cells. Cytotoxicity might even promote autoimmunity in B-BclxL^{tg}-A20^{-/wt} mice: through generating additional autoantigens, cleavage by granzyme B is implicated in the initiation and propagation of autoreactivity. (473-475).

To gain a clearer picture of the specific T cell populations, which are enriched in B-BclxL^{tg}-A20^{-/-} and B-BclxL^{tg}-A20^{-/wt} mice, respectively, and to understand, which functions they have, a single cell RNA sequencing approach should be performed as a next step. In addition, this could shed light on the mechanisms, which BclxL^{tg} A20^{-/wt} B cells employ to shape the immune cell repertoire and drive an autoimmune pathology. Furthermore, it needs to be clarified, which modes of cytotoxicity are used for the elimination of BclxL^{tg} A20^{-/-} B cells. Since a strong upregulation of Fas went in hand with the lymphoproliferative expansion of B-BclxL^{tg}-A20 B cells in CD3e^{ΔΔ} mice, Fas-mediated killing might play a key role in the elimination of aberrantly activated B cells. A blockade of Fas-FasL interactions in vivo could clarify to which extent Fas-mediated killing is involved in diminishing the numbers of BclxL^{tg} A20^{-/-} B cells.

5.2.3 Malignant expansion of A20-deficient B cells requires their escape from T cell cytotoxicity

In contrast to human autoimmune patients, in B cell lymphoma, also the bi-allelic loss of A20 can be commonly detected (270-274). In some cases of MZL (270), Hodgkin lymphoma, primary mediastinal B cell lymphoma (271), MALT lymphoma (272) and DLBCL (273), A20 is also mono-allelically mutated/inactivated. Together with my colleagues, I was able to show that in the absence of T cells, homo- and heterozygous loss of A20 led to a malignant expansion of A20^{-/-} as well as A20^{-/wt} B cells. This demonstrates that A20 acts as homo- and heterozygous tumor suppressor. The time of onset and extent of B cell lymphomagenesis was even more enhanced upon simultaneous B-BclxL^{tg} expression. Clonal lymphomagenesis of A20-deficient and BclxL^{tg} A20-deficient B cells occurred only in the absence of T cells. This demonstrates that naturally, B cell lymphomagenesis is efficiently suppressed by T cell immune surveillance.

Diminished A20 function is strongly implicated in autoimmune diseases as well as B cell lymphoma and autoimmune patients have a higher risk for lymphomagenesis (210, 241). Most prominently, A20-deficiency is involved in the connection of Sjögren's Syndrome and MALT lymphoma (276). This concurrency underlines concepts proposing similar genesis of autoimmune diseases and lymphoma (43). In most cases, autoimmunity precedes lymphomagenesis (43, 210, 276). As initiating genetic alteration, HA20 enables the emergence of autoinflammatory symptoms. The high prevalence of bi-allelic A20-deficiency in B cell lymphoma suggests that malignant transformation is strongly enhanced when B cells acquire an additional loss-of function mutation in the second *Tnfrsf18* allele. Since A20 knockout in B cells provokes T cell cytotoxicity, these A20^{-/-} lymphoma cells need to acquire additional mutations, enabling their escape from T cell immune surveillance.

Overall, my results indicate that the initiation of a T cell immune surveillance corresponds to the extent of A20 loss of function, which reflects B cell hyperactivation. The initial T cell sensing of pathogenicity likely depends on the B cell hyperactivation status. Once the activation passes a certain threshold, T cells switch from a helper towards a cytotoxic function to eliminate the aberrant B cells. This critical activation threshold seems to be reached upon complete lack of A20 in the context of B-BclxL^{tg} expression.

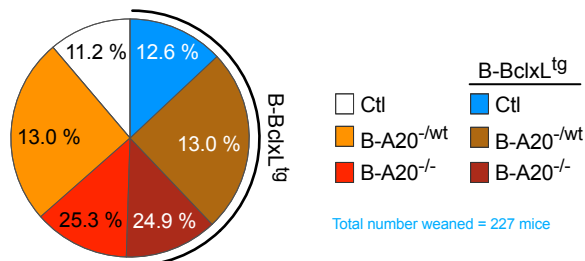
B cells with lower activation did not induce their own counterselection. This seems to be the case for BclxL^{tg} A20^{-/wt} B cells but also for BclxL^{tg} A20^{-/-} B cells with simultaneous lack of MyD88 signaling (B-MyD88^{-/-}). Strikingly, lethality was enhanced in B-BclxL^{tg}-A20^{-/-} mice with B-MyD88^{-/-}. Potentially, defective TLR signaling in MyD88^{-/-} B cells reduced their overall hyperactivation or their expression of NKG2D ligands (468), which consequently spared them from cytotoxic action. B-MyD88^{-/-}-BclxL^{tg}-A20^{-/-} mice retained high numbers of mainly IgM⁺ plasmacytic cells. Since MyD88 signaling is dispensable for the development of IgM autoreactive B cells (476), it is worth to further investigate if autoreactive IgM plasma cells induce an autoimmune pathology in B-MyD88^{-/-}-BclxL^{tg}-A20^{-/-} mice.

This suggests that the T cell mediated elimination of aberrant B cells in correspondence to their intrinsic hyperreactivity might be a universal concept that protects mice and men from B cell lymphomagenesis. To a certain extent, the same mechanism could protect from the development of lethal B cell-driven autoimmunity, as is the case for B-BclxL^{tg}-A20^{-/-} mice.

In summary, in this thesis, I created a novel mouse model for B cell-driven autoimmunity. I demonstrated that the heterozygous loss of A20 and the overexpression of anti-apoptotic BclxL in B cells cooperate to induce a lethal autoimmune phenotype, resembling many features of human SLE. Paradoxically, mice with a complete knockout of A20 in their B cells were consistently spared from lethal pathology, despite an enhanced *in vivo* and *in vivo* hyperreactivity of BclxL^{tg} A20^{-/-} B cells. In the absence of T cells, B-BclxL^{tg} mice developed clonal lymphoproliferations in direct correlation to the A20 gene dose, demonstrating T cell immune surveillance is instructed by and eliminates strongly hyperreactive BclxL^{tg} A20^{-/-} B cells *in vivo*. Less hyperreactive B cells fail to induce immune surveillance and can thereby induce an autoimmune pathology.

SUPPLEMENTARY FIGURES

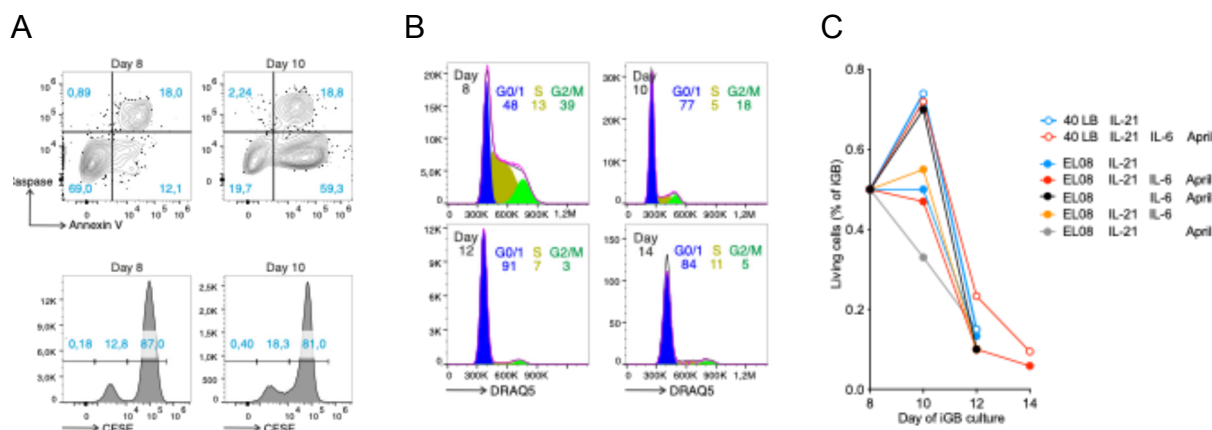
S1



Supplementary Figure 1. Genotype ratio in newborn mice with B cell specific A20-deficiency and BclxL^{tg} expression.

To exclude that mice with heterozygous and homozygous A20 deletion in B cells or E μ -BclxL transgene expression have defects in embryonal development, we evaluated the Mendelian ratio of genotypes after weaning. For the offspring from A20^{F/wt} X A20^{F/wt} breedings, resulting in heterozygous CD19Cre expression and potential BclxL transgene expression, the ratio of genotype was analyzed in all weaned mice. Only mice that reached weaning age (21-24 days) were being genotyped, so mice that died prematurely are not considered in this calculation. However, premature death was not observed frequently. The BclxL transgene was inherited by 50% of the offspring and the A20-floxed allele was expressed heterozygous in approximately 50% and homozygous in approximately 12.5% of all weaned mice (Figure 2). We can therefore conclude that B cell specific BclxL transgene expression combined with heterozygous as well as homozygous deletion of A20 in B cells does not affect embryonal development.

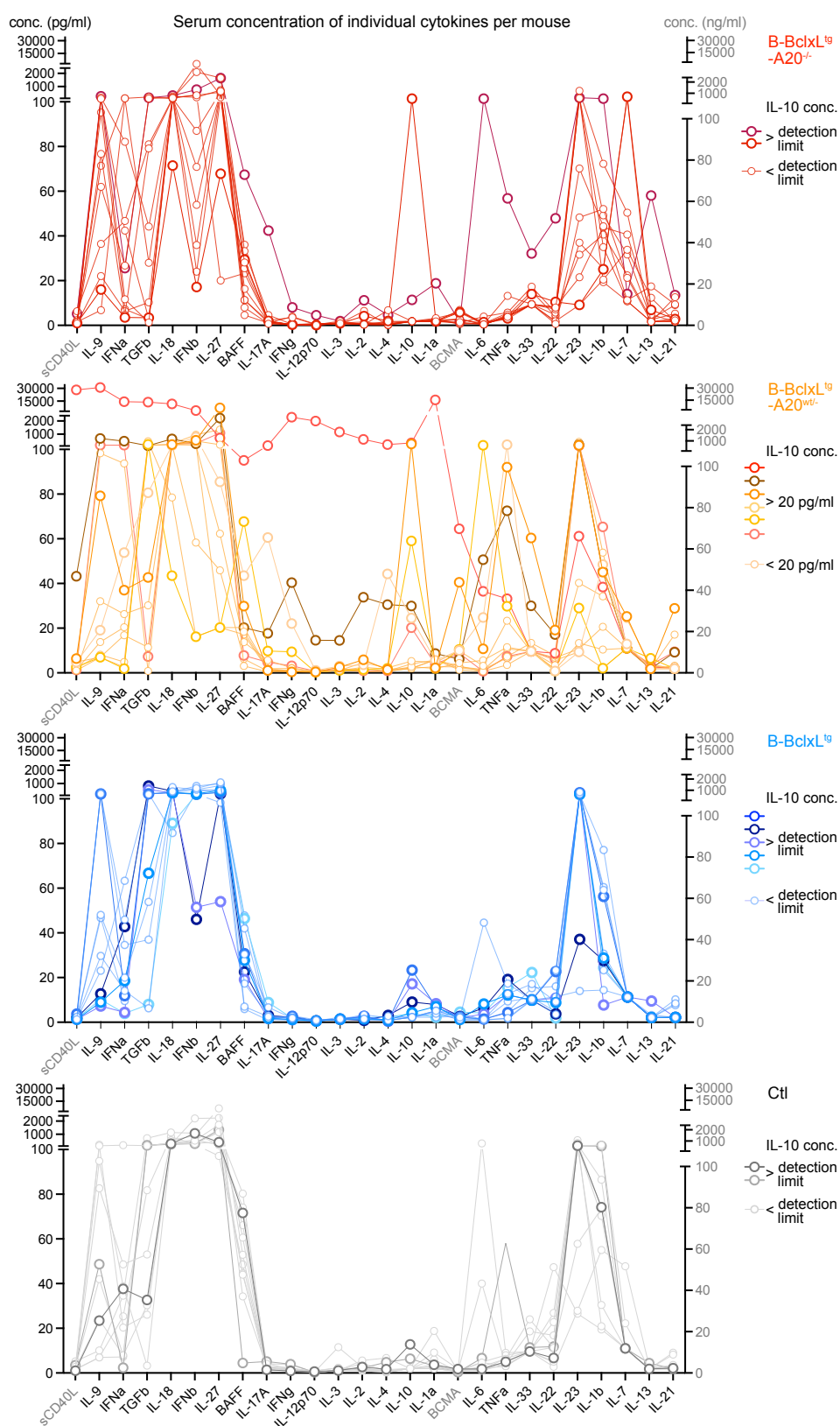
S2



Supplementary Figure 2. Survival of PC-like iGB cells.

(A) Fraction of apoptotic cells detected by Caspase and Annexin V staining (upper panel) and Proliferative capacity detected by CFSE signal 4 hours after staining on day 8 and day 10 of iGB culture. (B) Cell cycle analysis of B-A20^{-/wt} on days 8, 10, 12 and 14 of iGB culture. (C) Fraction of living cells in among iGB cells stimulated with IL-21, IL-6 and/or April and co-cultured with either 40LB or EL08 cells after day 8 of culture. (A-C) iGB cultures and FACS analysis were performed by my supervised student Anna Sichler.

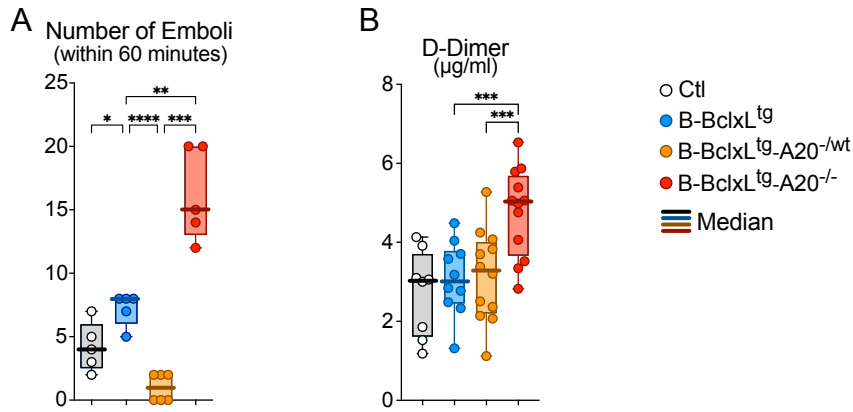
S3



Supplementary Figure 3. Serum cytokine concentration in individual mice.

Individual serum concentration (pg/ml: black or ng/ml: grey) of 26 analytes per mouse. The geom. mean values of these samples were depicted in Figure 28). Samples from each individual mouse are connected with a line. Colorized are the 2 to 6 samples from those mice with the highest IL-10 serum concentration; the remaining samples are depicted in faint color.

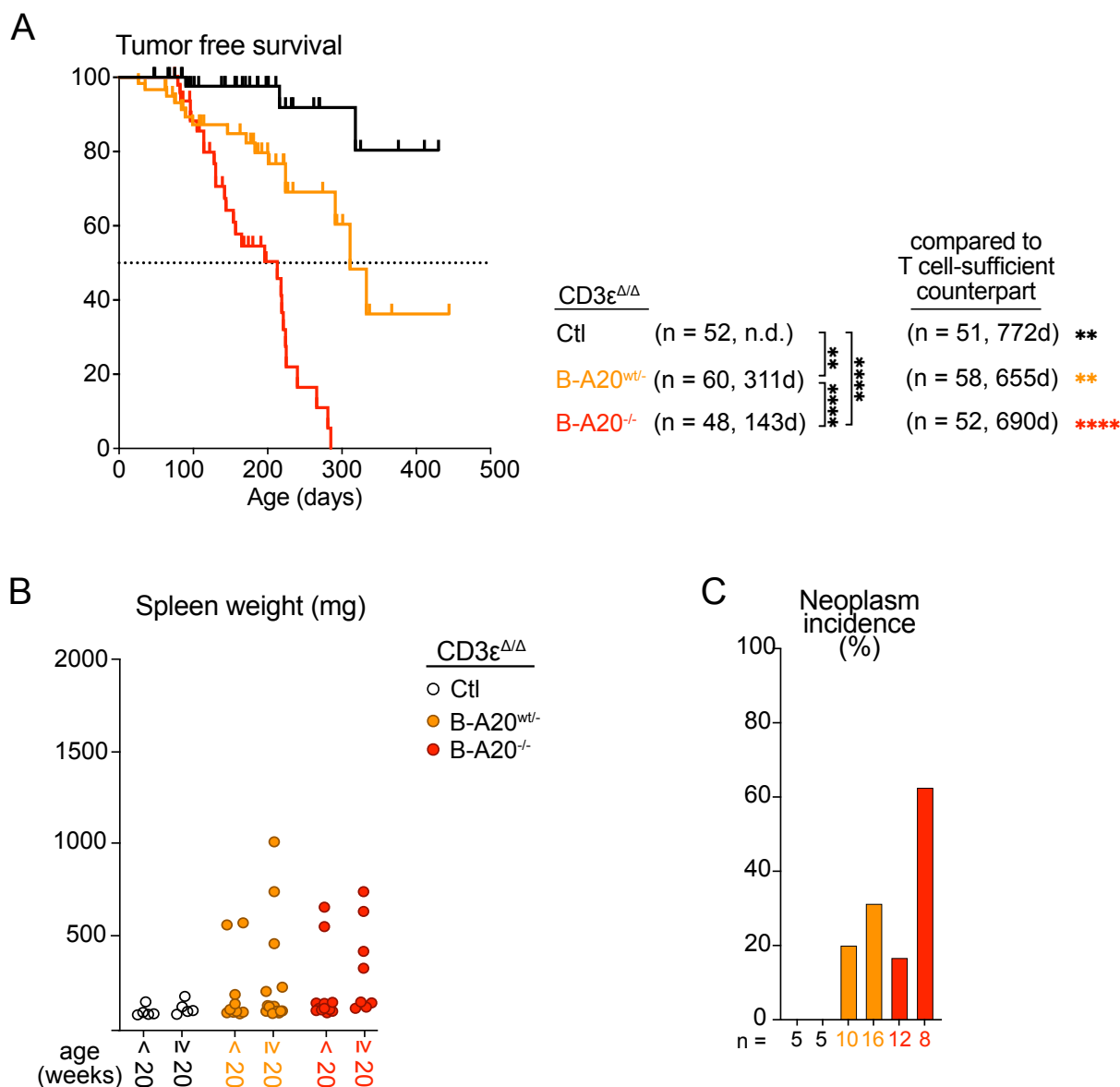
S4



Supplementary Figure 4. Thrombus stability.

(A) Number of emboli appearing within 60 minutes after vessel damage. (B) Serum concentration of D-dimer (µg/ml). (A-B) Data is displayed as box-whisker-plot. Dots represent individual samples, and thick lines highlight the median value. (A) Arterial vessel damage assay was performed by Ul Ain Qurrat and supervised by Dr. med. Joachim Pircher (LMU, München). (B) D-Dimer ELISA was performed by Julia Knogler.

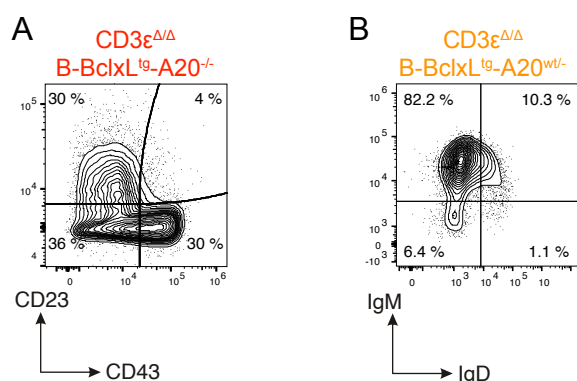
S5



Supplementary Figure 5. Lethality and lymphoproliferation in CD3 $\epsilon^{\Delta/\Delta}$ B-A20 mice.

(A) Kaplan Meier survival curves for CD3 $\epsilon^{\Delta/\Delta}$ mice with B cell-specific A20-deficiency. Cohort sizes and median survival times are shown. **(B)** Spleen weights of CD3 $\epsilon^{\Delta/\Delta}$ mice of the different A20 genotypes, divided by age: CD3 $\epsilon^{\Delta/\Delta}$ Ctl: 9-20 and 20-54 weeks (data also shown in Figure 66, depicted here again for comparison); CD3 $\epsilon^{\Delta/\Delta}$ B-A20^{wt/-}: 12-20 and 20-48 weeks; CD3 $\epsilon^{\Delta/\Delta}$ B-A20^{-/-}: 12-20 and 20-34 weeks. **(C)** Incidence of lymphoma-like pathology in all analyzed spleens of CD3 $\epsilon^{\Delta/\Delta}$ B-A20^{wt/-} (orange) and CD3 $\epsilon^{\Delta/\Delta}$ B-A20^{-/-} (red) mice. Lymphoma cases were categorized by spleen size (≥ 200 mg) in combination with flow cytometry analysis (data not shown) and/or initial histological assessment (H&E, data not shown) and PCR clonality (data not shown). *(B-C) Mice were analyzed and by Seren Baygün (SB) and Valeria Soberón. (B) Data was plotted by SB. (C) Data was plotted by VS.*

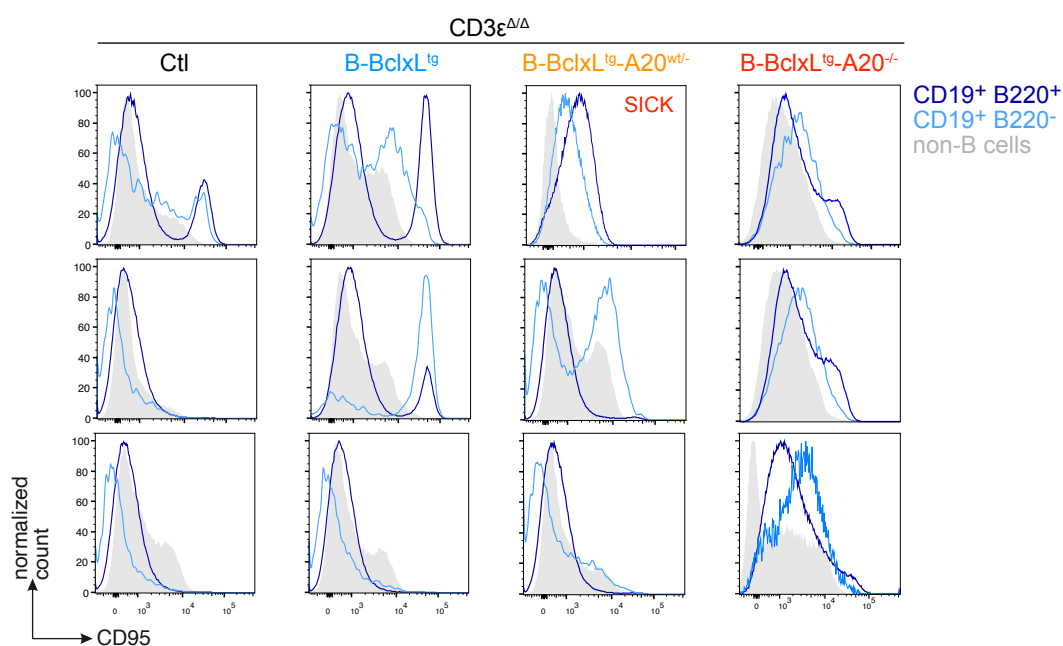
S6



Supplementary Figure 6. Marker expression on B cells from $CD3\epsilon^{\Delta\Delta}$ B-BclxL^{tg}-A20 mice.

Example flow cytometry plots depicting (A) the expression of CD43 and CD23 on all splenocytes of a $CD3\epsilon^{\Delta\Delta}$ B-BclxL^{tg}-A20^{-/-} mouse and (B) the expression of IgM and IgD on all splenocytes of a $CD3\epsilon^{\Delta\Delta}$ B-BclxL^{tg}-A20^{-/wt} mouse.

S7



Supplementary Figure 7. Variability of Fas expression of B cells from different mice.

Fas expression on B220⁺ and B220⁻ B cells and non-B cells from $CD3\epsilon^{\Delta\Delta}$ mice. Three samples are depicted per genotype. One mouse had a lymphoma-like expansion (labelled SICK).

SUPPLEMENTARY TABLES

Supplementary Table 1. Genome-wide association studies (GWAS) catalog for TNFAIP3 associations: <https://www.ebi.ac.uk/gwas/genes/TNFAIP3> (accessed on 16.07.2021 / 23.05.2023).

Variant and risk allele	Mapped gene	Reported trait	Study accession	First Author	Location	Access Date
rs5029937- G	TNFAIP3	Allergy (hay fever, asthma, or eczema)	GCST005038	Ferreira MA	6:137874014	16.7.21
rs5029937- T	TNFAIP3	SLE	GCST004867	Gateva V	6:137874014	16.7.21
rs643177- ?	TNFAIP3	Inflammatory skin disease	GCST002740	Baurecht H	6:137874556	16.7.21
rs643177- C	TNFAIP3	Neutrophil count	GCST90002351	Chen MH	6:137874556	16.7.21
rs643177- C	TNFAIP3	Neutrophil count	GCST90002355	Chen MH	6:137874556	16.7.21
rs643177- T	TNFAIP3	Psoriasis	GCST002874	Yin X	6:137874556	16.7.21
rs643177- T	TNFAIP3	Psoriasis	GCST002874	Yin X	6:137874556	16.7.21
rs5029939- ?	TNFAIP3	SLE	GCST005752	Langefeld CD	6:137874586	16.7.21
rs5029939- ?	TNFAIP3	SLE	GCST000216	Graham RR	6:137874586	16.7.21
rs5029939- G	TNFAIP3	Non-albumin protein levels	GCST90019515	Sinnott-Armstrong N	6:137874586	16.7.21
rs5029939- G	TNFAIP3	Sjögren's syndrome	GCST002217	Li Y	6:137874586	16.7.21
rs2230926- ?	TNFAIP3	SLE	GCST003622	Morris DL	6:137874929	16.7.21
rs2230926- ?	TNFAIP3	SLE	GCST003599	Lessard CJ	6:137874929	16.7.21
rs2230926- ?	TNFAIP3	SLE	GCST003622	Morris DL	6:137874929	16.7.21
rs2230926- C	TNFAIP3	RA	GCST000677	Kochi Y	6:137874929	16.7.21
rs2230926- C	TNFAIP3	SLE	GCST000507	Han JW	6:137874929	16.7.21
rs2230926- G	TNFAIP3	SLE	GCST001795	Yang W	6:137874929	16.7.21
rs2230926- G	TNFAIP3	Systemic sclerosis	GCST004202	Terao C	6:137874929	16.7.21
rs2230926- G	TNFAIP3	Systemic sclerosis	GCST004202	Terao C	6:137874929	16.7.21
rs5029949- ?	TNFAIP3	Eczema	GCST007075	Kichaev G	6:137876369	16.7.21
rs610604- ?	TNFAIP3	Psoriasis	GCST000833	Strange A	6:137878280	16.7.21
rs610604- G	TNFAIP3	Cutaneous psoriasis	GCST003269	Stuart PE	6:137878280	16.7.21
rs610604- G	TNFAIP3	Psoriasis	GCST000322	Nair RP	6:137878280	16.7.21
rs610604- G	TNFAIP3	Psoriasis vulgaris	GCST003268	Stuart PE	6:137878280	16.7.21
rs610604- G	TNFAIP3	Psoriasis or type 2 diabetes	GCST011990	Patrick MT	6:137878280	16.7.21
rs610604- T	TNFAIP3	White blood cell count	GCST90002374	Chen MH	6:137878280	16.7.21

rs1082428- ?	TNFAIP3, LINC02528	White blood cell count	GCST007070	Kichaev G	6:137886592	16.7.21
rs674451- C	LINC02528, TNFAIP3	White blood cell count	GCST90002378	Chen MH	6:137895651	16.7.21
rs9494892- ?	LINC02528, TNFAIP3	Respiratory diseases	GCST007076	Kichaev G	6:137902352	16.7.21
rs9494893- ?	TNFAIP3, LINC02528	RA	GCST011389	Kwon YC	6:137902353	16.7.21
rs57245978 6-?	LINC02528, TNFAIP3	Malaria	GCST010725	MGEN	6:137904008	16.7.21
rs57245978 6-?	LINC02528, TNFAIP3	Malaria	GCST010725	MGEN	6:137904008	16.7.21
rs57245978 6-?	LINC02528, TNFAIP3	Malaria	GCST010725	MGEN	6:137904008	16.7.21
rs7752903- G	LINC02528, TNFAIP3	RA	GCST002318	Okada Y	6:137906227	16.7.21
rs7752903- G	LINC02528, TNFAIP3	RA	GCST002318	Okada Y	6:137906227	16.7.21
rs7752903- G	LINC02528, TNFAIP3	RA	GCST002318	Okada Y	6:137906227	16.7.21
rs7752903- T	LINC02528, TNFAIP3	RA	GCST006959	Laufer VA	6:137906227	16.7.21
rs7752903- T	LINC02528, TNFAIP3	RA	GCST006959	Laufer VA	6:137906227	16.7.21
rs7752903- T	LINC02528, TNFAIP3	RA	GCST006959	Laufer VA	6:137906227	16.7.21
rs9494894- T	TNFAIP3, LINC02528	SLE	GCST011956	Yin X	6:137907383	16.7.21
rs7749323- A	LINC02528, TNFAIP3	RA	GCST90013534	Ha E	6:137909252	16.7.21
rs72980770- C	TNFAIP3, LINC02528	Primary sclerosing cholangitis	GCST004030	Ji SG	6:137913152	16.7.21
rs77000060- ?	LINC02528, TNFAIP3	SLE	GCST007400	Langefeld CD	6:137916852	16.7.21
rs6932056- ?	LINC02528, TNFAIP3	Eosinophil counts	GCST007065	Kichaev G	6:137921300	16.7.21
rs6932056- C	LINC02528, TNFAIP3	SLE	GCST003155	Bentham J	6:137921300	16.7.21
rs13929935 0-A	TNFAIP3, LINC02528	White blood cell count	GCST90002407	Vuckovic D	6:137921487	16.7.21
rs13929935 0-A	TNFAIP3, LINC02528	Neutrophil count	GCST90002398	Vuckovic D	6:137921487	16.7.21
rs58721818- A	TNFAIP3, LINC02528	RA (ACPA- positive)	GCST006048	Kim K	6:137922602	16.7.21
rs58721818- T	TNFAIP3, LINC02528	Autoimmune traits (pleiotropy)	GCST009873	Márquez A	6:137922602	16.7.21
rs58721818- T	TNFAIP3, LINC02528	RA	GCST009877	Márquez A	6:137922602	16.7.21
rs58721818- T	TNFAIP3, LINC02528	SLE	GCST003156	Bentham J	6:137922602	16.7.21
rs58721818- T	TNFAIP3, LINC02528	Systemic seropositive rheumatic diseases	GCST007278	Acosta- Herrera M	6:137922602	16.7.21
rs67297943- A	TNFAIP3, LINC02528	Multiple sclerosis	GCST005531	Beecham AH	6:137923679	16.7.21
rs17781283- ?	LINC02528, TNFAIP3	Ejection fraction in T. cruzi seropositivity	GCST002281	Deng X	6:137941636	16.7.21
rs17781283- A	LINC02528, TNFAIP3	Eosinophil counts	GCST90002298	Chen MH	6:137941636	16.7.21

rs17781283- A	LINC02528, TNFAIP3	Eosinophil counts	GCST90002381	Vuckovic D	6:137941636	16.7.21
rs17781283- A	LINC02528, TNFAIP3	Eosinophil percentage of white cells	GCST90002382	Vuckovic D	6:137941636	16.7.21
rs610604- G	TNFAIP3	Psoriatic arthritis	GCST90243956	Soomro M	6:137878280	23.5.23
rs7752903- G	TNFAIP3, LINC02528	Eosinophil counts	GCST90018953	Sakaue S	6:137906227	23.5.23
rs9494894- C	TNFAIP3, LINC02528	RA	GCST90018910	Sakaue S	6:137907383	23.5.23
rs9494895- T	TNFAIP3, LINC02528	SLE	GCST90018917	Sakaue S	6:137913641	23.5.23
rs6933987- T	TNFAIP3, LINC02528	Psoriasis vulgaris	GCST90018907	Sakaue S	6:137918297	23.5.23
rs6932056- C	LINC02528, TNFAIP3	RA	GCST90132222	Ishigaki K	6:137921300	23.5.23

MGEN = Malaria Genomic Epidemiology Network; RA = Rheumatoid arthritis; SLE = Systemic Lupus Erythematosus.

Supplementary Table 2: Gene list for SLE-associated genes used for GSEA on bulk RNAseq data. From Nehar-Belaid et al. (426)

Gene name		
B2M	GRN	EPSTI1
TMSB4X	HLA-DQB1	CD97
EMP3	UBC	ISCU
LY6E	GPR183	OST4
CIB1	CYBA	DAPP1
MALAT1	HLA-DRA	HLA-E
HLA-C	TNFRSF1B	POU2F2
ISG15	ZBTB32	ANXA2
HLA-A	CALM2	FCRL3
NEAT1	TYMP	SUB1
RGS2	ARPC2	ZEB2
CLECL1	SEC61B	FCRL2
MS4A1	ATP5E	OAS1
FGR	VOPP1	MAP3K8
HLA-DPA1	GAPDH	RHOA
SAT1	IFI6	UQCR11-1
HLA-B	PTPRCAP	
SRGN	HCK	
HSPB1	CLIC1	
HLA-DPB1	HLA-DQA1	
FCRL5	CD52	
CD74	ACTB	
GABARAPL2	LITAF	
S100A6	YWHAH	
HLA-DRB1	ITGB7	
ATP6V0E1	ACP5	
S100A11	PLEK	
COTL1	PSMB9	
PSAP	PPDPF	
IFI44L	MYL6	
SH3BGRL3	THEMIS2	
CRIP1	RNASET2	
IFITM2	CFL1	
MCL1	ARPC1B	
OAZ1	MT2A	
LGALS1	MIR142	
PFN1	CD99	
RHOB	CD19	
PPP1R14A	SERF2	
MX1	LRMP	
LSP1	IFI27	
TNFRSF13B	LY96	

Supplementary Table 3: Gene list for B cell activation signature used for GSEA on bulk RNAseq data. Adapted from Shen et al., 2014 (477): The activated B cell signature represents 200 genes with the highest significant (padj <0.05) fold change enriched in B cells activated 24h with LPS and anti-CD40 compared to naive B cells.

Gene name				
Il6	Pgk1	Chac1	Tpi1	Stil
Ccl22	Rad51ap1	Diaph3	Spag5	Cdca7
Ak4	Syde2	Elovl7	Ska1	Car13
Cth	Csf2	Gins2	Plod2	Psmc3ip
Ccl5	Melk	Mnd1	Bag2	Eif4ebp1
Fam129a	Dtl	Zbtb46	D13Ert37e	Mthfd1
Fabp5	Slco3a1	Tex15	Ms4a6c	Ccna2
Sgol1	Atp10a	Ncapg2	Ccne2	Pkp4
Bcat1	Nupr1	Spc24	Chchd6	Ifnz
Asns	Dlgap5	Ttc39c	Mlk1	Eme1
Fads2	Mem10	Atf3	Cdc25c	Pkdec
Zbtb32	Hacd1	Plagl1	Dhfr	Batf3
Slc1a4	Gpt2	Ccnd2	Txlnb	Cyp51
Esco2	Cmss1	Top2a	Traf1	Ticrr
Orc1	Dscc1	Tcte3	Bub1b	Ung
Tubb6	Ifih1	Aunip	Sqle	Cenph
Ankrd33b	Gapdh	Kntc1	Cd70	Ybx3
Mir155hg	Mpzl1	Fads1	Gins1	Lrp8
Nasp	Fscn1	Sept3	Smyd2	Clspn
Rad54b	Lrr1	Figl1	Rad54l	Bnip3
Nfil3	Rad51	Sapcd2	Cdc45	Basp1
Pla1a	Trip13	Cd80	Rfc4	Eef1d
Ier3	Psat1	Shcbp1	Cep55	Slc43a3
Mfsd2a	Mthfd2	Slc25a13	Cenpp	Cks1b
Il2ra	Rad51b	Hells	Hpd1	Timm8a1
Trib3	Slc16a1	D12Ert123e	Flt3	Aurkb
Spire1	Exo1	Tpx2	Suv39h2	Lap3
Eno2	Ttk	Chst7	Isg15	Ppa1
Egln3	Ska3	Tspan33	Taf1d	Socs2
Cdc6	Gbp2b	Cenpi	Mcm3	Spata6
Nt5dc2	Plscr1	Cenpk	Lss	Oip5
Dhcr24	Ifit1	Cdca5	Nek2	Mpp6
Hnf1b	Tiam1	Ncapg	Bcl2l1	
Slc7a5	Shmt1	Pycr1	Ldlr	
Uhrf1	Pter	Rrm2	Tmem97	
Mybl2	Hk2	Cdk1	Zwilch	
Tyms	Pbk	Tyms	Adk	
Bub1	Syce2	Sowahc	Uck2	
Vegfa	Idi1	Rad54l	Cenb1	
Chek1	Sh3rf1	Cdc20	Cdca8	
Cxcl10	Plpp1	Vldlr	Fdps	
Slc7a3	Armcx4	Ebi3	Coprs	

Supplementary Table 4: Tumor incidence and phenotype in CD3 $\epsilon^{\Delta/\Delta}$ mice

Sex	Mouse ID	Genotype	Age (days)	Macroscopic examination	Histology
M	90650	CD3 $\epsilon^{\Delta/\Delta}$ B-BclxLtg-A20-/-	105	healthy	
M	90670	CD3 $\epsilon^{\Delta/\Delta}$ B-BclxLtg-A20-/-	85	healthy	
M	90672	CD3 $\epsilon^{\Delta/\Delta}$ B-BclxLtg-A20-/-	85	healthy	
F	14001	CD3 $\epsilon^{\Delta/\Delta}$ B-BclxLtg-A20-/-	100	healthy	
M	13995	CD3 $\epsilon^{\Delta/\Delta}$ B-BclxLtg-A20-/-	135	Sick: very enlarged spleen with bulb-shaped areas	Spl: Centroblastic DLBCL, fully infiltrated; liver infiltration (1%)
M	14741	CD3 $\epsilon^{\Delta/\Delta}$ B-BclxLtg-A20-/-	134	Sick: LN enlargement, no obvious tumor	
F	90924	CD3 $\epsilon^{\Delta/\Delta}$ B-BclxLtg-A20-/-	114	Sick: Euthanized due to obvious burden	
M	15868	CD3 $\epsilon^{\Delta/\Delta}$ B-BclxLtg-A20-/-	170	Sick: Spl & mLN tumorigenic	
M	90922	CD3 $\epsilon^{\Delta/\Delta}$ B-BclxLtg-A20-/-	148	Sick: Spl & mLN tumorigenic	
F	90959	CD3 $\epsilon^{\Delta/\Delta}$ B-BclxLtg-A20-/-	148	Sick: enlarged Spl & mLN & LN & PP	
F	90960	CD3 $\epsilon^{\Delta/\Delta}$ B-BclxLtg-A20-/-	148	Sick: Spl & mLN tumorigenic, enlarged LN	
F	91006	CD3 $\epsilon^{\Delta/\Delta}$ B-BclxLtg-A20-/-	94	Sick: tumors in Spl, Liver, Pancreas; LN enlarged	
F	90985	CD3 $\epsilon^{\Delta/\Delta}$ B-BclxLtg-A20-/-	128	Sick: White nodules in spleen & liver	
F	90917	CD3 $\epsilon^{\Delta/\Delta}$ B-BclxLtg-A20-/-	107	Sick: died; Spl & mLN tumorigenic	
F	90003	CD3 $\epsilon^{\Delta/\Delta}$ B-BclxLtg-A20/wt	84	Sick: enlarged spleen	
M	2739	CD3 $\epsilon^{\Delta/\Delta}$ B-BclxLtg-A20/wt	100	healthy	
M	64554	CD3 $\epsilon^{\Delta/\Delta}$ B-BclxLtg-A20/wt	128	healthy	
M	3288	CD3 $\epsilon^{\Delta/\Delta}$ B-BclxLtg-A20/wt	142	healthy	
M	90076	CD3 $\epsilon^{\Delta/\Delta}$ B-BclxLtg-A20/wt	146	healthy	
F	4188	CD3 $\epsilon^{\Delta/\Delta}$ B-BclxLtg-A20/wt	156	healthy	
F	4717	CD3 $\epsilon^{\Delta/\Delta}$ B-BclxLtg-A20/wt	116	healthy	
F	4718	CD3 $\epsilon^{\Delta/\Delta}$ B-BclxLtg-A20/wt	116	healthy	
F	5570	CD3 $\epsilon^{\Delta/\Delta}$ B-BclxLtg-A20/wt	217	Sick: Tumors in Spl, Liver & Ovary	
F	14000	CD3 $\epsilon^{\Delta/\Delta}$ B-BclxLtg-A20/wt	100	healthy	
M	14744	CD3 $\epsilon^{\Delta/\Delta}$ B-BclxLtg-A20/wt	93	Sick: enlarged spleen	Sple: Immunoblastic DLBCL lymphoma; liver infiltration (5%)
M	13998	CD3 $\epsilon^{\Delta/\Delta}$ B-BclxLtg-A20/wt	192	healthy	no lymphoma
F	90926	CD3 $\epsilon^{\Delta/\Delta}$ B-BclxLtg-A20/wt	178	Sick: weight loss	
F	90939	CD3 $\epsilon^{\Delta/\Delta}$ B-BclxLtg-A20/wt	175	Sick: Tumors in Spl, Liver & Pancreas	
F	15753	CD3 $\epsilon^{\Delta/\Delta}$ B-BclxLtg-A20/wt	418	Found dead	
F	90946	CD3 $\epsilon^{\Delta/\Delta}$ B-BclxLtg-A20/wt	358	Sick: Anemic	
F	16326	CD3 $\epsilon^{\Delta/\Delta}$ B-BclxLtg-A20/wt	362	Found dead	
F	90944	CD3 $\epsilon^{\Delta/\Delta}$ B-BclxLtg-A20/wt	358	healthy	
F	90875	CD3 $\epsilon^{\Delta/\Delta}$ B-BclxLtg-A20/wt	342	healthy	
F	64553	CD3 $\epsilon^{\Delta/\Delta}$ B-BclxLtg	139	healthy	
F	90005	CD3 $\epsilon^{\Delta/\Delta}$ B-BclxLtg	155	healthy	
M	3287	CD3 $\epsilon^{\Delta/\Delta}$ B-BclxLtg	142	healthy	
F	4187	CD3 $\epsilon^{\Delta/\Delta}$ B-BclxLtg	156	healthy	
M	4712	CD3 $\epsilon^{\Delta/\Delta}$ B-BclxLtg	116	healthy	
F	4714	CD3 $\epsilon^{\Delta/\Delta}$ B-BclxLtg	116	healthy	
F	14031	CD3 $\epsilon^{\Delta/\Delta}$ B-BclxLtg	103	healthy	
F	15281	CD3 $\epsilon^{\Delta/\Delta}$ B-BclxLtg	264	Sick: enlarged right brachial and axillary LN	

F	15280	CD3 ϵ $\Delta\Delta$ B-BclxLtg	291	healthy	
M	15870	CD3 ϵ $\Delta\Delta$ B-BclxLtg	234	Sick: Tumors in Spl	
F	16330	CD3 ϵ $\Delta\Delta$ B-BclxLtg	362	healthy (wounded neck)	
M	3285	CD3 ϵ $\Delta\Delta$	142	healthy	
F	4186	CD3 ϵ $\Delta\Delta$	156	healthy	
M	4711	CD3 ϵ $\Delta\Delta$	116	healthy	
F	4716	CD3 ϵ $\Delta\Delta$	116	healthy	
M	13900	CD3 ϵ $\Delta\Delta$	66	Healthy	no lymphoma
M	13901	CD3 ϵ $\Delta\Delta$	66	Healthy	no lymphoma
M	13979	CD3 ϵ $\Delta\Delta$	84	healthy	no lymphoma
F	14632	CD3 ϵ $\Delta\Delta$	68	healthy	
F	14634	CD3 ϵ $\Delta\Delta$	74	healthy	no lymphoma
F	90696	CD3 ϵ $\Delta\Delta$	318	Sick: Tumor in Spl	
M	13981	CD3 ϵ $\Delta\Delta$	224	healthy	
M	14624	CD3 ϵ $\Delta\Delta$	187	healthy, slightly enlarged mLN	
M	14740	CD3 ϵ $\Delta\Delta$	270	healthy	
M	14742	CD3 ϵ $\Delta\Delta$	270	healthy	
M	15869	CD3 ϵ $\Delta\Delta$	234	healthy	
M	15873	CD3 ϵ $\Delta\Delta$	234	healthy	
F	15876	CD3 ϵ $\Delta\Delta$	406	healthy	
F	16328	CD3 ϵ $\Delta\Delta$	362	healthy	
M	13978	CD3 ϵ $\Delta\Delta$ B-A20-/wt	84	Sick: Enlarged spleen	Lymphoma
F	14746	CD3 ϵ $\Delta\Delta$ B-A20-/wt	99	Sick: tumorigenic spleen, pale kidneys	Lymphoma & necrosis in spleen, spleen fully infiltrated; liver (25%)
M	90693	CD3 ϵ $\Delta\Delta$ B-A20-/wt	291	Sick: weight loss; enlarged liver; white nodules in spleen	
F	14030	CD3 ϵ $\Delta\Delta$ B-A20-/wt	172	Sick	
M	13898	CD3 ϵ $\Delta\Delta$ B-A20-/wt	224	Sick: mLN enlarged or tumorigenic (440mg)	
M	14026	CD3 ϵ $\Delta\Delta$ B-A20-/wt	222	Enlarged/tumorigenic spleen, LN normal, mLN maybe a little enlarged	
M	90708	CD3 ϵ $\Delta\Delta$ B-A20-/-	114	Sick: spleen tumor	red pulp hyperplasia
M	13985	CD3 ϵ $\Delta\Delta$ B-A20-/-	79	Sick	Lymphoma and necrosis: DLBCL-like lymphoma
M	13908	CD3 ϵ $\Delta\Delta$ B-A20-/-	83	Sick: enlarged spleen	Lymphoma and necrosis in spleen; pancreas infiltrated, aggressive type
M	13989	CD3 ϵ $\Delta\Delta$ B-A20-/-	142	Sick: mouse pale and weak; spleen tumor; enlarged mLN	
F	14631	CD3 ϵ $\Delta\Delta$ B-A20-/-	105	Sick: spleen tumor, mLN-pancreas tumor	
F	13992	CD3 ϵ $\Delta\Delta$ B-A20-/-	197	Sick: mLN tumor	
M	13909	CD3 ϵ $\Delta\Delta$ B-A20-/-	224	Sick: spleen tumorigenic with white structures; intestines a little enlarged	
F	14027	CD3 ϵ $\Delta\Delta$ B-A20-/-	221	Sick: enlarged spleen, LNs and mLN	
F	13914	CD3 ϵ $\Delta\Delta$ B-A20-/-	225	Sick: One mLN was enlarged/tumorigenic, the other one was a slightly enlarged, liver was pale	

Spl = Spleen, LN = lymph nodes, mLN = mesenteric lymph nodes

REFERENCES

1. Nemazee D. Mechanisms of central tolerance for B cells. *Nat Rev Immunol.* 2017;17(5):281-94.
2. Bassing CH, Swat W, Alt FW. The mechanism and regulation of chromosomal V(D)J recombination. *Cell.* 2002;109 Suppl:S45-55.
3. Reth M. Antigen receptors on B lymphocytes. *Annu Rev Immunol.* 1992;10:97-121.
4. Morrison VL, Barr TA, Brown S, Gray D. TLR-Mediated Loss of CD62L Focuses B Cell Traffic to the Spleen during Salmonella typhimurium Infection. *The Journal of Immunology.* 2010;185(5):2737-46.
5. Enders A, Short A, Miosge LA, Bergmann H, Sontani Y, Bertram EM, et al. Zinc-finger protein ZFP318 is essential for expression of IgD, the alternatively spliced Igh product made by mature B lymphocytes. *Proceedings of the National Academy of Sciences of the United States of America.* 2014;111(12):4513-8.
6. Sindhava VJ, Bondada S. Multiple regulatory mechanisms control B-1 B cell activation. *Front Immunol.* 2012;3:372.
7. Reyneveld GI, Savelkoul HFJ, Parmentier HK. Current Understanding of Natural Antibodies and Exploring the Possibilities of Modulation Using Veterinary Models. A Review. *Front Immunol.* 2020;11:2139.
8. Wong JB, Hewitt SL, Heltemes-Harris LM, Mandal M, Johnson K, Rajewsky K, et al. B-1a cells acquire their unique characteristics by bypassing the pre-BCR selection stage. *Nature Communications.* 2019;10(1):4768.
9. Cerutti A, Cols M, Puga I. Marginal zone B cells: virtues of innate-like antibody-producing lymphocytes. *Nat Rev Immunol.* 2013;13(2):118-32.
10. Fasnacht N, Huang HY, Koch U, Favre S, Auderset F, Chai Q, et al. Specific fibroblastic niches in secondary lymphoid organs orchestrate distinct Notch-regulated immune responses. *J Exp Med.* 2014;211(11):2265-79.
11. Hampel F, Ehrenberg S, Hojer C, Draeseke A, Marschall-Schröter G, Kühn R, et al. CD19-independent instruction of murine marginal zone B-cell development by constitutive Notch2 signaling. *Blood.* 2011;118(24):6321-31.
12. Lechner M, Engleitner T, Babushku T, Schmidt-Supprian M, Rad R, Strobl LJ, et al. Notch2-mediated plasticity between marginal zone and follicular B cells. *Nature Communications.* 2021;12(1):1111.
13. Elsner RA, Shlomchik MJ. Germinal Center and Extrafollicular B Cell Responses in Vaccination, Immunity, and Autoimmunity. *Immunity.* 2020;53(6):1136-50.
14. De Silva NS, Klein U. Dynamics of B cells in germinal centres. *Nat Rev Immunol.* 2015;15(3):137-48.
15. Stebeegg M, Kumar SD, Silva-Cayetano A, Fonseca VR, Linterman MA, Graca L. Regulation of the Germinal Center Response. *Front Immunol.* 2018;9.
16. Victora GD, Nussenzweig MC. Germinal centers. *Annu Rev Immunol.* 2012;30:429-57.
17. Victora GD, Nussenzweig MC. Germinal Centers. *Annual Review of Immunology.* 2022;40(1):413-42.
18. Goodnow CC, Vinuesa CG, Randall KL, Mackay F, Brink R. Control systems and decision making for antibody production. *Nature immunology.* 2010;11(8):681-8.
19. Heesters BA, Myers RC, Carroll MC. Follicular dendritic cells: dynamic antigen libraries. *Nat Rev Immunol.* 2014;14(7):495-504.
20. Balogh A, Ádori M, Török K, Matko J, László G. A closer look into the GL7 antigen: Its spatio-temporally selective differential expression and localization in lymphoid cells and organs in human. *Immunology letters.* 2010;130(1):89-96.
21. Chen ST, Oliveira TY, Gazumyan A, Cipolla M, Nussenzweig MC. B cell receptor signaling in germinal centers prolongs survival and primes B cells for selection. *Immunity.* 2023.
22. Bélanger S, Crotty S. Dances with cytokines, featuring TFH cells, IL-21, IL-4 and B cells. *Nature immunology.* 2016;17(10):1135-6.
23. Dominguez-Sola D, Victora GD, Ying CY, Phan RT, Saito M, Nussenzweig MC, et al. The proto-oncogene MYC is required for selection in the germinal center and cyclic reentry. *Nature immunology.* 2012;13(11):1083-91.
24. Stavnezer J, Guikema JE, Schrader CE. Mechanism and regulation of class switch recombination. *Annu Rev Immunol.* 2008;26:261-92.

25. Victora GD, Schwickert TA, Fooksman DR, Kamphorst AO, Meyer-Hermann M, Dustin ML, et al. Germinal Center Dynamics Revealed by Multiphoton Microscopy with a Photoactivatable Fluorescent Reporter. *Cell*. 2010;143(4):592-605.
26. Shulman Z, Gitlin AD, Weinstein JS, Lainez B, Esplugues E, Flavell RA, et al. Dynamic signaling by T follicular helper cells during germinal center B cell selection. *Science*. 2014;345(6200):1058-62.
27. Shlomchik MJ, Luo W, Weisel F. Linking signaling and selection in the germinal center. *Immunological reviews*. 2019;288(1):49-63.
28. Zhang Y, Meyer-Hermann M, George LA, Figge MT, Khan M, Goodall M, et al. Germinal center B cells govern their own fate via antibody feedback. *J Exp Med*. 2013;210(3):457-64.
29. Lu LL, Suscovich TJ, Fortune SM, Alter G. Beyond binding: antibody effector functions in infectious diseases. *Nature Reviews Immunology*. 2018;18(1):46-61.
30. Slomp A, Peperzak V. Role and Regulation of Pro-survival BCL-2 Proteins in Multiple Myeloma. *Front Oncol*. 2018;8:533.
31. Radbruch A, Muehlinghaus G, Luger EO, Inamine A, Smith KG, Dörner T, et al. Competence and competition: the challenge of becoming a long-lived plasma cell. *Nat Rev Immunol*. 2006;6(10):741-50.
32. Nguyen DC, Joyner CJ, Sanz I, Lee FE-H. Factors Affecting Early Antibody Secreting Cell Maturation Into Long-Lived Plasma Cells. *Front Immunol*. 2019;10.
33. Malkiel S, Barlev AN, Atisha-Fregoso Y, Suurmond J, Diamond B. Plasma Cell Differentiation Pathways in Systemic Lupus Erythematosus. *Front Immunol*. 2018;9.
34. Rastogi I, Jeon D, Moseman JE, Muralidhar A, Potluri HK, McNeel DG. Role of B cells as antigen presenting cells. *Front Immunol*. 2022;13:954936.
35. Elgueta R, Benson MJ, de Vries VC, Wasiuk A, Guo Y, Noelle RJ. Molecular mechanism and function of CD40/CD40L engagement in the immune system. *Immunological reviews*. 2009;229(1):152-72.
36. Alberts B JA, Lewis J, et al. Helper T Cells and Lymphocyte Activation. *Molecular Biology of the Cell*. 4th Edition ed. New York: Garland Science; 2002.
37. Chester C, Sanmamed MF, Wang J, Melero I. Immunotherapy targeting 4-1BB: mechanistic rationale, clinical results, and future strategies. *Blood*. 2018;131(1):49-57.
38. Carrasco YR, Fleire SJ, Cameron T, Dustin ML, Batista FD. LFA-1/ICAM-1 interaction lowers the threshold of B cell activation by facilitating B cell adhesion and synapse formation. *Immunity*. 2004;20(5):589-99.
39. Goodnow CC, Sprent J, Fazekas de St Groth B, Vinuesa CG. Cellular and genetic mechanisms of self tolerance and autoimmunity. *Nature*. 2005;435(7042):590-7.
40. Amanna IJ, Dingwall JP, Hayes CE. Enforced bcl-xL gene expression restored splenic B lymphocyte development in BAFF-R mutant mice. *J Immunol*. 2003;170(9):4593-600.
41. Tanaka S, Ise W, Baba Y, Kurosaki T. Silencing and activating anergic B cells*. *Immunological reviews*. 2022;307(1):43-52.
42. Cambier JC, Gauld SB, Merrell KT, Vilen BJ. B-cell anergy: from transgenic models to naturally occurring anergic B cells? *Nature Reviews Immunology*. 2007;7(8):633-43.
43. Goodnow CC. Multistep pathogenesis of autoimmune disease. *Cell*. 2007;130(1):25-35.
44. Cyster JG, Goodnow CC. Antigen-induced exclusion from follicles and anergy are separate and complementary processes that influence peripheral B cell fate. *Immunity*. 1995;3(6):691-701.
45. Ekland EH, Forster R, Lipp M, Cyster JG. Requirements for follicular exclusion and competitive elimination of autoantigen-binding B cells. *J Immunol*. 2004;172(8):4700-8.
46. Paul E, Nelde A, Verschoor A, Carroll MC. Follicular exclusion of autoreactive B cells requires FcγRIIb. *International Immunology*. 2007;19(4):365-73.
47. Kwak K, Akkaya M, Pierce SK. B cell signaling in context. *Nature immunology*. 2019;20(8):963-9.
48. Brink R, Phan TG. Self-Reactive B Cells in the Germinal Center Reaction. *Annu Rev Immunol*. 2018;36:339-57.
49. Rui L, Vinuesa CG, Blasioli J, Goodnow CC. Resistance to CpG DNA-induced autoimmunity through tolerogenic B cell antigen receptor ERK signaling. *Nature immunology*. 2003;4(6):594-600.
50. Rui L, Healy JI, Blasioli J, Goodnow CC. ERK signaling is a molecular switch integrating opposing inputs from B cell receptor and T cell cytokines to control TLR4-driven plasma cell differentiation. *J Immunol*. 2006;177(8):5337-46.

51. Kim JM, Rasmussen JP, Rudensky AY. Regulatory T cells prevent catastrophic autoimmunity throughout the lifespan of mice. *Nature immunology*. 2007;8(2):191-7.
52. Chen JW, Schickel J-N, Tsakiris N, Sng J, Arbogast F, Bouis D, et al. Positive and negative selection shape the human naive B cell repertoire. *The Journal of Clinical Investigation*. 2022;132(2).
53. Seo S-j, Fields ML, Buckler JL, Reed AJ, Mandik-Nayak L, Nish SA, et al. The Impact of T Helper and T Regulatory Cells on the Regulation of Anti-Double-Stranded DNA B Cells. *Immunity*. 2002;16(4):535-46.
54. Meffre E, O'Connor KC. Impaired B-cell tolerance checkpoints promote the development of autoimmune diseases and pathogenic autoantibodies. *Immunological reviews*. 2019;292(1):90-101.
55. Owen DL, Sjaastad LE, Farrar MA. Regulatory T Cell Development in the Thymus. *J Immunol*. 2019;203(8):2031-41.
56. Starr TK, Jameson SC, Hogquist KA. Positive and Negative Selection of T Cells. *Annual Review of Immunology*. 2003;21(1):139-76.
57. Chopp L, Redmond C, O'Shea JJ, Schwartz DM. From thymus to tissues and tumors: A review of T-cell biology. *Journal of Allergy and Clinical Immunology*. 2023;151(1):81-97.
58. Golubovskaya V, Wu L. Different Subsets of T Cells, Memory, Effector Functions, and CAR-T Immunotherapy. *Cancers (Basel)*. 2016;8(3).
59. Snapper CM, Peschel C, Paul WE. IFN-gamma stimulates IgG2a secretion by murine B cells stimulated with bacterial lipopolysaccharide. *J Immunol*. 1988;140(7):2121-7.
60. Stevens TL, Bossie A, Sanders VM, Fernandez-Botran R, Coffman RL, Mosmann TR, et al. Regulation of antibody isotype secretion by subsets of antigen-specific helper T cells. *Nature*. 1988;334(6179):255-8.
61. Crotty S. T follicular helper cell differentiation, function, and roles in disease. *Immunity*. 2014;41(4):529-42.
62. Sakaguchi S, Mikami N, Wing JB, Tanaka A, Ichiyama K, Ohkura N. Regulatory T Cells and Human Disease. *Annu Rev Immunol*. 2020;38:541-66.
63. Chung Y, Tanaka S, Chu F, Nurieva RI, Martinez GJ, Rawal S, et al. Follicular regulatory T cells expressing Foxp3 and Bcl-6 suppress germinal center reactions. *Nat Med*. 2011;17(8):983-8.
64. Cenerenti M, Saillard M, Romero P, Jandus C. The Era of Cytotoxic CD4 T Cells. *Front Immunol*. 2022;13.
65. Cassioli C, Baldari CT. The Expanding Arsenal of Cytotoxic T Cells. *Front Immunol*. 2022;13.
66. He JS, Ostergaard HL. CTLs contain and use intracellular stores of FasL distinct from cytolytic granules. *J Immunol*. 2007;179(4):2339-48.
67. Barry M, Bleackley RC. Cytotoxic T lymphocytes: all roads lead to death. *Nature Reviews Immunology*. 2002;2(6):401-9.
68. Prager I, Watzl C. Mechanisms of natural killer cell-mediated cellular cytotoxicity. *Journal of Leukocyte Biology*. 2019;105(6):1319-29.
69. Sterner RC, Sterner RM. CAR-T cell therapy: current limitations and potential strategies. *Blood Cancer Journal*. 2021;11(4):69.
70. June CH, O'Connor RS, Kawalekar OU, Ghassemi S, Milone MC. CAR T cell immunotherapy for human cancer. *Science*. 2018;359(6382):1361-5.
71. Benmeharek MR, Karches CH, Cadilha BL, Lesch S, Endres S, Kobold S. Killing Mechanisms of Chimeric Antigen Receptor (CAR) T Cells. *Int J Mol Sci*. 2019;20(6).
72. Gao Z, Feng Y, Xu J, Liang J. T-cell exhaustion in immune-mediated inflammatory diseases: New implications for immunotherapy. *Front Immunol*. 2022;13.
73. McLane LM, Abdel-Hakeem MS, Wherry EJ. CD8 T Cell Exhaustion During Chronic Viral Infection and Cancer. *Annual Review of Immunology*. 2019;37(1):457-95.
74. Liu J, Chen Z, Li Y, Zhao W, Wu J, Zhang Z. PD-1/PD-L1 Checkpoint Inhibitors in Tumor Immunotherapy. *Frontiers in Pharmacology*. 2021;12.
75. D'Arcy MS. Cell death: a review of the major forms of apoptosis, necrosis and autophagy. *Cell Biology International*. 2019;43(6):582-92.
76. Czabotar PE, Lessene G, Strasser A, Adams JM. Control of apoptosis by the BCL-2 protein family: implications for physiology and therapy. *Nature Reviews Molecular Cell Biology*. 2014;15(1):49-63.

77. Singh R, Letai A, Sarosiek K. Regulation of apoptosis in health and disease: the balancing act of BCL-2 family proteins. *Nature Reviews Molecular Cell Biology*. 2019;20(3):175-93.
78. Yoshino T, Kondo E, Cao L, Takahashi K, Hayashi K, Nomura S, et al. Inverse expression of bcl-2 protein and Fas antigen in lymphoblasts in peripheral lymph nodes and activated peripheral blood T and B lymphocytes. *Blood*. 1994;83(7):1856-61.
79. Razzaghi R, Agarwal S, Kotlov N, Plotnikova O, Nomie K, Huang DW, et al. Compromised counterselection by FAS creates an aggressive subtype of germinal center lymphoma. *J Exp Med*. 2021;218(3).
80. Mintz MA, Cyster JG. T follicular helper cells in germinal center B cell selection and lymphomagenesis. *Immunological reviews*. 2020;296(1):48-61.
81. Kotov DI, Kotov JA, Goldberg MF, Jenkins MK. Many Th Cell Subsets Have Fas Ligand-Dependent Cytotoxic Potential. *J Immunol*. 2018;200(6):2004-12.
82. Hsu S-C, Gavrilin MA, Lee H-H, Wu C-C, Han S-H, Lai M-Z. NF- κ B-dependent Fas ligand expression. *European journal of immunology*. 1999;29(9):2948-56.
83. Krammer PH. CD95's deadly mission in the immune system. *Nature*. 2000;407(6805):789-95.
84. Kägi D, Vignaux F, Ledermann B, Bürki K, Depraetere V, Nagata S, et al. Fas and perforin pathways as major mechanisms of T cell-mediated cytotoxicity. *Science*. 1994;265(5171):528-30.
85. Scaffidi C, Fulda S, Srinivasan A, Friesen C, Li F, Tomaselli KJ, et al. Two CD95 (APO-1/Fas) signaling pathways. *The EMBO Journal*. 1998;17(6):1675-87.
86. Yamada A, Arakaki R, Saito M, Kudo Y, Ishimaru N. Dual Role of Fas/FasL-Mediated Signal in Peripheral Immune Tolerance. *Front Immunol*. 2017;8:403.
87. Schattner EJ, Elkon KB, Yoo DH, Tumang J, Krammer PH, Crow MK, et al. CD40 ligation induces Apo-1/Fas expression on human B lymphocytes and facilitates apoptosis through the Apo-1/Fas pathway. *J Exp Med*. 1995;182(5):1557-65.
88. Figgett William A, Fairfax K, Vincent Fabien B, Le Page Mélanie A, Katik I, Deliyanti D, et al. The TACI Receptor Regulates T-Cell-Independent Marginal Zone B Cell Responses through Innate Activation-Induced Cell Death. *Immunity*. 2013;39(3):573-83.
89. Rathmell JC, Townsend SE, Xu JC, Flavell RA, Goodnow CC. Expansion or elimination of B cells in vivo: dual roles for CD40- and Fas (CD95)-ligands modulated by the B cell antigen receptor. *Cell*. 1996;87(2):319-29.
90. Catlett IM, Bishop GA. Cutting Edge: A Novel Mechanism for Rescue of B Cells from CD95/Fas-Mediated Apoptosis1. *The Journal of Immunology*. 1999;163(5):2378-81.
91. Donjerković D, Scott DW. Activation-induced cell death in B lymphocytes. *Cell Res*. 2000;10(3):179-92.
92. Akkaya M, Traba J, Roesler AS, Miozzo P, Akkaya B, Theall BP, et al. Second signals rescue B cells from activation-induced mitochondrial dysfunction and death. *Nature immunology*. 2018;19(8):871-84.
93. Takahashi Y, Ohta H, Takemori T. Fas Is Required for Clonal Selection in Germinal Centers and the Subsequent Establishment of the Memory B Cell Repertoire. *Immunity*. 2001;14(2):181-92.
94. Karin M, Lin A. NF- κ B at the crossroads of life and death. *Nature immunology*. 2002;3(3):221-7.
95. Lawrence T. The nuclear factor NF-kappaB pathway in inflammation. *Cold Spring Harbor perspectives in biology*. 2009;1(6):a001651.
96. Sun SC. The non-canonical NF- κ B pathway in immunity and inflammation. *Nat Rev Immunol*. 2017;17(9):545-58.
97. Yu H, Lin L, Zhang Z, Zhang H, Hu H. Targeting NF- κ B pathway for the therapy of diseases: mechanism and clinical study. *Signal Transduction and Targeted Therapy*. 2020;5(1):209.
98. Bolduc A, Long E, Stapler D, Cascalho M, Tsubata T, Koni PA, et al. Constitutive CD40L Expression on B Cells Prematurely Terminates Germinal Center Response and Leads to Augmented Plasma Cell Production in T Cell Areas. *The Journal of Immunology*. 2010;185(1):220-30.
99. Wykes M. Why do B cells produce CD40 ligand? *Immunol Cell Biol*. 2003;81(4):328-31.
100. Duan T, Du Y, Xing C, Wang HY, Wang RF. Toll-Like Receptor Signaling and Its Role in Cell-Mediated Immunity. *Front Immunol*. 2022;13:812774.

101. Isaza-Correa JM, Liang Z, van den Berg A, Diepstra A, Visser L. Toll-like receptors in the pathogenesis of human B cell malignancies. *Journal of Hematology & Oncology*. 2014;7(1):57.
102. Kawai T, Akira S. Signaling to NF- κ B by Toll-like receptors. *Trends in Molecular Medicine*. 2007;13(11):460-9.
103. Blasius AL, Beutler B. Intracellular toll-like receptors. *Immunity*. 2010;32(3):305-15.
104. Pasare C, Medzhitov R. Control of B-cell responses by Toll-like receptors. *Nature*. 2005;438(7066):364-8.
105. Suthers AN, Sarantopoulos S. TLR7/TLR9- and B Cell Receptor-Signaling Crosstalk: Promotion of Potentially Dangerous B Cells. *Front Immunol*. 2017;8.
106. Poovassery JS, Vanden Bush TJ, Bishop GA. Antigen Receptor Signals Rescue B Cells from TLR Tolerance. *The Journal of Immunology*. 2009;183(5):2974-83.
107. Hua Z, Hou B. TLR signaling in B-cell development and activation. *Cell Mol Immunol*. 2013;10(2):103-6.
108. Leadbetter EA, Rifkin IR, Hohlbaum AM, Beaudette BC, Shlomchik MJ, Marshak-Rothstein A. Chromatin-IgG complexes activate B cells by dual engagement of IgM and Toll-like receptors. *Nature*. 2002;416(6881):603-7.
109. Soni C, Wong EB, Domeier PP, Khan TN, Satoh T, Akira S, et al. B cell-intrinsic TLR7 signaling is essential for the development of spontaneous germinal centers. *J Immunol*. 2014;193(9):4400-14.
110. Hoffmann FS, Kuhn PH, Laurent SA, Hauck SM, Berer K, Wendlinger SA, et al. The immunoregulator soluble TACI is released by ADAM10 and reflects B cell activation in autoimmunity. *J Immunol*. 2015;194(2):542-52.
111. Laurent SA, Hoffmann FS, Kuhn P-H, Cheng Q, Chu Y, Schmidt-Supprian M, et al. γ -secretase directly sheds the survival receptor BCMA from plasma cells. *Nature Communications*. 2015;6(1):7333.
112. Smulski CR, Eibel H. BAFF and BAFF-Receptor in B Cell Selection and Survival. *Front Immunol*. 2018;9.
113. Liu Z, Davidson A. BAFF and selection of autoreactive B cells. *Trends Immunol*. 2011;32(8):388-94.
114. Webster JD, Vucic D. The Balance of TNF Mediated Pathways Regulates Inflammatory Cell Death Signaling in Healthy and Diseased Tissues. *Frontiers in Cell and Developmental Biology*. 2020;8.
115. Saito M, Novak U, Piovan E, Basso K, Sumazin P, Schneider C, et al. BCL6 suppression of BCL2 via Miz1 and its disruption in diffuse large B cell lymphoma. *Proceedings of the National Academy of Sciences of the United States of America*. 2009;106(27):11294-9.
116. Boise LH, Gonzalez-Garcia M, Postema CE, Ding L, Lindsten T, Turka LA, et al. bcl-x, a bcl-2-related gene that functions as a dominant regulator of apoptotic cell death. *Cell*. 1993;74(4):597-608.
117. Grillot DA, Merino R, Pena JC, Fanslow WC, Finkelman FD, Thompson CB, et al. Bcl-x exhibits regulated expression during B cell development and activation and modulates lymphocyte survival in transgenic mice. *J Exp Med*. 1996;183(2):381-91.
118. Zhang L, Dong X, Lee M, Maslov AY, Wang T, Vijg J. Single-cell whole-genome sequencing reveals the functional landscape of somatic mutations in B lymphocytes across the human lifespan. *Proceedings of the National Academy of Sciences of the United States of America*. 2019;116(18):9014-9.
119. Machado HE, Mitchell E, Øbro NF, Kübler K, Davies M, Leongamornlert D, et al. Diverse mutational landscapes in human lymphocytes. *Nature*. 2022;608(7924):724-32.
120. Jaffe ES, Pittaluga S. Aggressive B-cell lymphomas: a review of new and old entities in the WHO classification. *Hematology Am Soc Hematol Educ Program*. 2011;2011:506-14.
121. Soberón VRL. Mouse models for aberrant NF- κ B activation in B-cell development and lymphomagenesis: LMU München; 2018.
122. Hömig-Hölzel C, Hojer C, Rastelli J, Casola S, Strobl LJ, Müller W, et al. Constitutive CD40 signaling in B cells selectively activates the noncanonical NF- κ B pathway and promotes lymphomagenesis. *J Exp Med*. 2008;205(6):1317-29.
123. Jost PJ, Ruland Jr. Aberrant NF- κ B signaling in lymphoma: mechanisms, consequences, and therapeutic implications. *Blood*. 2006;109(7):2700-7.
124. Calado DP, Zhang B, Srinivasan L, Sasaki Y, Seagal J, Unitt C, et al. Constitutive canonical NF- κ B activation cooperates with disruption of BLIMP1 in the pathogenesis of activated B cell-like diffuse large cell lymphoma. *Cancer Cell*. 2010;18(6):580-9.

125. Zhang B, Calado DP, Wang Z, Fröhler S, Köchert K, Qian Y, et al. An oncogenic role for alternative NF- κ B signaling in DLBCL revealed upon deregulated BCL6 expression. *Cell Rep.* 2015;11(5):715-26.
126. Raskov H, Orhan A, Christensen JP, Gögenur I. Cytotoxic CD8⁺ T cells in cancer and cancer immunotherapy. *British Journal of Cancer.* 2021;124(2):359-67.
127. Coté TR, Biggar RJ, Rosenberg PS, Devesa SS, Percy C, Yellin FJ, et al. Non-Hodgkin's lymphoma among people with AIDS: incidence, presentation and public health burden. AIDS/Cancer Study Group. *Int J Cancer.* 1997;73(5):645-50.
128. Grulich AE, van Leeuwen MT, Falster MO, Vajdic CM. Incidence of cancers in people with HIV/AIDS compared with immunosuppressed transplant recipients: a meta-analysis. *The Lancet.* 2007;370(9581):59-67.
129. Schreiber RD, Old LJ, Smyth MJ. Cancer Immunoediting: Integrating Immunity's Roles in Cancer Suppression and Promotion. *Science.* 2011;331(6024):1565-70.
130. Challa-Malladi M, Lieu YK, Califano O, Holmes AB, Bhagat G, Murty VV, et al. Combined genetic inactivation of β 2-Microglobulin and CD58 reveals frequent escape from immune recognition in diffuse large B cell lymphoma. *Cancer Cell.* 2011;20(6):728-40.
131. Basso K, Dalla-Favera R. Germinal centres and B cell lymphomagenesis. *Nature Reviews Immunology.* 2015;15(3):172-84.
132. Choi I-K, Wang Z, Ke Q, Hong M, Qian Y, Zhao X, et al. Signaling by the Epstein–Barr virus LMP1 protein induces potent cytotoxic CD4⁺ and CD8⁺ T cell responses. *Proceedings of the National Academy of Sciences.* 2018;115(4):E686-E95.
133. Afshar-Sterle S, Zotos D, Bernard NJ, Scherger AK, Rödling L, Alsop AE, et al. Fas ligand-mediated immune surveillance by T cells is essential for the control of spontaneous B cell lymphomas. *Nat Med.* 2014;20(3):283-90.
134. Bouska A, McKeithan TW, Deffenbacher KE, Lachel C, Wright GW, Iqbal J, et al. Genome-wide copy-number analyses reveal genomic abnormalities involved in transformation of follicular lymphoma. *Blood.* 2014;123(11):1681-90.
135. Bolitho P, Street SE, Westwood JA, Edelmann W, Macgregor D, Waring P, et al. Perforin-mediated suppression of B-cell lymphoma. *Proceedings of the National Academy of Sciences of the United States of America.* 2009;106(8):2723-8.
136. Miller FW. The increasing prevalence of autoimmunity and autoimmune diseases: an urgent call to action for improved understanding, diagnosis, treatment, and prevention. *Current Opinion in Immunology.* 2023;80:102266.
137. Hayter SM, Cook MC. Updated assessment of the prevalence, spectrum and case definition of autoimmune disease. *Autoimmunity Reviews.* 2012;11(10):754-65.
138. Dinse GE, Parks CG, Weinberg CR, Co CA, Wilkerson J, Zeldin DC, et al. Increasing Prevalence of Antinuclear Antibodies in the United States. *Arthritis Rheumatol.* 2020;72(6):1026-35.
139. Rosenblum MD, Remedios KA, Abbas AK. Mechanisms of human autoimmunity. *J Clin Invest.* 2015;125(6):2228-33.
140. Zenewicz LA, Abraham C, Flavell RA, Cho JH. Unraveling the genetics of autoimmunity. *Cell.* 2010;140(6):791-7.
141. Conrad N, Misra S, Verbakel JY, Verbeke G, Molenberghs G, Taylor PN, et al. Incidence, prevalence, and co-occurrence of autoimmune disorders over time and by age, sex, and socioeconomic status: a population-based cohort study of 22 million individuals in the UK. *The Lancet.*
142. Klein SL, Flanagan KL. Sex differences in immune responses. *Nature Reviews Immunology.* 2016;16(10):626-38.
143. Kronzer VL, Bridges Jr SL, Davis III JM. Why women have more autoimmune diseases than men: An evolutionary perspective. *Evolutionary Applications.* 2021;14(3):629-33.
144. Jiwrajka N, Anguera MC. The X in seX-biased immunity and autoimmune rheumatic disease. *Journal of Experimental Medicine.* 2022;219(6).
145. Souyris M, Cenac C, Azar P, Daviaud D, Canivet A, Grunenwald S, et al. TLR7 escapes X chromosome inactivation in immune cells. *Science Immunology.* 2018;3(19):eaap8855.
146. Mackay F, Woodcock SA, Lawton P, Ambrose C, Baetscher M, Schneider P, et al. Mice transgenic for BAFF develop lymphocytic disorders along with autoimmune manifestations. *J Exp Med.* 1999;190(11):1697-710.
147. Schweighoffer E, Tybulewicz VL. BAFF signaling in health and disease. *Curr Opin Immunol.* 2021;71:124-31.

148. Butt D, Chan TD, Bourne K, Hermes JR, Nguyen A, Statham A, et al. FAS Inactivation Releases Unconventional Germinal Center B Cells that Escape Antigen Control and Drive IgE and Autoantibody Production. *Immunity*. 2015;42(5):890-902.
149. Rathmell JC, Cooke MP, Ho WY, Grein J, Townsend SE, Davis MM, et al. CD95 (Fas)-dependent elimination of self-reactive B cells upon interaction with CD4+ T cells. *Nature*. 1995;376(6536):181-4.
150. Hao Z, Duncan GS, Seagal J, Su Y-W, Hong C, Haight J, et al. Fas Receptor Expression in Germinal-Center B Cells Is Essential for T and B Lymphocyte Homeostasis. *Immunity*. 2008;29(4):615-27.
151. Merino R, Grillot DA, Simonian PL, Muthukkumar S, Fanslow WC, Bondada S, et al. Modulation of anti-IgM-induced B cell apoptosis by Bcl-xL and CD40 in WEHI-231 cells. Dissociation from cell cycle arrest and dependence on the avidity of the antibody-IgM receptor interaction. *J Immunol*. 1995;155(8):3830-8.
152. Fang W, Weintraub BC, Dunlap B, Garside P, Pape KA, Jenkins MK, et al. Self-Reactive B Lymphocytes Overexpressing Bcl-xL Escape Negative Selection and Are Tolerized by Clonal Anergy and Receptor Editing. *Immunity*. 1998;9(1):35-45.
153. Vinuesa CG, Cook MC, Angelucci C, Athanasopoulos V, Rui L, Hill KM, et al. A RING-type ubiquitin ligase family member required to repress follicular helper T cells and autoimmunity. *Nature*. 2005;435(7041):452-8.
154. Kinnunen T, Chamberlain N, Morbach H, Choi J, Kim S, Craft J, et al. Accumulation of peripheral autoreactive B cells in the absence of functional human regulatory T cells. *Blood*. 2013;121(9):1595-603.
155. Sng J, Ayoglu B, Chen JW, Schickel JN, Ferre EMN, Glauzy S, et al. AIRE expression controls the peripheral selection of autoreactive B cells. *Sci Immunol*. 2019;4(34).
156. van Beers J, Schreurs MWJ. Anti-Sm antibodies in the classification criteria of systemic lupus erythematosus. *J Transl Autoimmun*. 2022;5:100155.
157. Migliorini P, Baldini C, Rocchi V, Bombardieri S. Anti-Sm and anti-RNP antibodies. *Autoimmunity*. 2005;38(1):47-54.
158. Schroeder K, Herrmann M, Winkler TH. The role of somatic hypermutation in the generation of pathogenic antibodies in SLE. *Autoimmunity*. 2013;46(2):121-7.
159. Suurmond J, Diamond B. Autoantibodies in systemic autoimmune diseases: specificity and pathogenicity. *The Journal of Clinical Investigation*. 2015;125(6):2194-202.
160. Davis LS, Hutcheson J, Mohan C. The role of cytokines in the pathogenesis and treatment of systemic lupus erythematosus. *J Interferon Cytokine Res*. 2011;31(10):781-9.
161. Biswas S, Bieber K, Manz RA. IL-10 revisited in systemic lupus erythematosus. *Front Immunol*. 2022;13:970906.
162. Viglianti GA, Lau CM, Hanley TM, Miko BA, Shlomchik MJ, Marshak-Rothstein A. Activation of Autoreactive B Cells by CpG dsDNA. *Immunity*. 2003;19(6):837-47.
163. Mohammad Hosseini A, Majidi J, Baradaran B, Yousefi M. Toll-Like Receptors in the Pathogenesis of Autoimmune Diseases. *Adv Pharm Bull*. 2015;5(Suppl 1):605-14.
164. Lyn-Cook BD, Xie C, Oates J, Treadwell E, Word B, Hammons G, et al. Increased expression of Toll-like receptors (TLRs) 7 and 9 and other cytokines in systemic lupus erythematosus (SLE) patients: Ethnic differences and potential new targets for therapeutic drugs. *Molecular Immunology*. 2014;61(1):38-43.
165. Reppe Moe SE, Molberg Ø, Strøm EH, Lerang K. Assessing the relative impact of lupus nephritis on mortality in a population-based systemic lupus erythematosus cohort. *Lupus*. 2019;28(7):818-25.
166. Mok CC, Kwok RC, Yip PS. Effect of renal disease on the standardized mortality ratio and life expectancy of patients with systemic lupus erythematosus. *Arthritis Rheum*. 2013;65(8):2154-60.
167. Almaani S, Meara A, Rovin BH. Update on lupus nephritis. *Clinical Journal of the American Society of Nephrology*. 2017;12(5):825-35.
168. Cameron JS, Frampton G. The 'antiphospholipid syndrome' and the 'lupus anticoagulant'. *Pediatr Nephrol*. 1990;4(6):663-78.
169. Bazzan M, Vaccarino A, Marletto F. Systemic lupus erythematosus and thrombosis. *Thromb J*. 2015;13:16.
170. Al-Homood IA. Thrombosis in systemic lupus erythematosus: a review article. *ISRN Rheumatol*. 2012;2012:428269.

171. Nojima J, Suehisa E, Kuratsune H, Machii T, Koike T, Kitani T, et al. Platelet activation induced by combined effects of anticardiolipin and lupus anticoagulant IgG antibodies in patients with systemic lupus erythematosus--possible association with thrombotic and thrombocytopenic complications. *Thromb Haemost.* 1999;81(3):436-41.
172. Brake MA, Ivanciu L, Maroney SA, Martinez ND, Mast AE, Westrick RJ. Assessing Blood Clotting and Coagulation Factors in Mice. *Current Protocols in Mouse Biology.* 2019;9(2):e61.
173. Horbach DA, van Oort E, Donders RC, Derksen RH, de Groot PG. Lupus anticoagulant is the strongest risk factor for both venous and arterial thrombosis in patients with systemic lupus erythematosus. Comparison between different assays for the detection of antiphospholipid antibodies. *Thromb Haemost.* 1996;76(6):916-24.
174. Afeltra A, Vadacca M, Conti L, Galluzzo S, Mitterhofer AP, Ferri GM, et al. Thrombosis in systemic lupus erythematosus: congenital and acquired risk factors. *Arthritis Rheum.* 2005;53(3):452-9.
175. Ponticelli C, Moroni G. Monoclonal Antibodies for Systemic Lupus Erythematosus (SLE). *Pharmaceuticals (Basel).* 2010;3(1):300-22.
176. Navarra SV, Guzmán RM, Gallacher AE, Hall S, Levy RA, Jimenez RE, et al. Efficacy and safety of belimumab in patients with active systemic lupus erythematosus: a randomised, placebo-controlled, phase 3 trial. *The Lancet.* 2011;377(9767):721-31.
177. Ostendorf L, Burns M, Durek P, Heinz GA, Heinrich F, Garantziotis P, et al. Targeting CD38 with Daratumumab in Refractory Systemic Lupus Erythematosus. *New England Journal of Medicine.* 2020;383(12):1149-55.
178. Rozkiewicz D, Hermanowicz JM, Kwiatkowska I, Krupa A, Pawlak D. Bruton's Tyrosine Kinase Inhibitors (BTKIs): Review of Preclinical Studies and Evaluation of Clinical Trials. *Molecules.* 2023;28(5).
179. Kansal R, Richardson N, Neeli I, Khawaja S, Chamberlain D, Ghani M, et al. Sustained B cell depletion by CD19-targeted CAR T cells is a highly effective treatment for murine lupus. *Science Translational Medicine.* 2019;11(482):eaav1648.
180. Mackensen A, Müller F, Mougiakakos D, Böltz S, Wilhelm A, Aigner M, et al. Anti-CD19 CAR T cell therapy for refractory systemic lupus erythematosus. *Nat Med.* 2022;28(10):2124-32.
181. Teruel M, Alarcón-Riquelme ME. The genetic basis of systemic lupus erythematosus: What are the risk factors and what have we learned. *Journal of Autoimmunity.* 2016;74:161-75.
182. Yin X, Kim K, Suetsugu H, Bang SY, Wen L, Koido M, et al. Meta-analysis of 208370 East Asians identifies 113 susceptibility loci for systemic lupus erythematosus. *Ann Rheum Dis.* 2020;80(5):632-40.
183. Brown GJ, Cañete PF, Wang H, Medhavy A, Bones J, Roco JA, et al. TLR7 gain-of-function genetic variation causes human lupus. *Nature.* 2022;605(7909):349-56.
184. Wu J, Wilson J, He J, Xiang L, Schur PH, Mountz JD. Fas ligand mutation in a patient with systemic lupus erythematosus and lymphoproliferative disease. *J Clin Invest.* 1996;98(5):1107-13.
185. Singh R, Pradhan V, Patwardhan M, Ghosh K. APO-1/Fas gene: Structural and functional characteristics in systemic lupus erythematosus and other autoimmune diseases. *Indian J Hum Genet.* 2009;15(3):98-102.
186. Barber MRW, Falasinnu T, Ramsey-Goldman R, Clarke AE. The global epidemiology of SLE: narrowing the knowledge gaps. *Rheumatology (Oxford).* 2023;62(Suppl 1):i4-i9.
187. García-Ortiz H, Velázquez-Cruz R, Espinosa-Rosales F, Jiménez-Morales S, Baca V, Orozco L. Association of TLR7 copy number variation with susceptibility to childhood-onset systemic lupus erythematosus in Mexican population. *Ann Rheum Dis.* 2010;69(10):1861-5.
188. Pacheco GV, Nakazawa Ueji YE, Bello JR, Barbosa Cobos RE, Jiménez Becerra ED, González Herrera LJ, et al. Copy Number Variation and Frequency of rs179008 in TLR7 Gene Associated with Systemic Lupus Erythematosus in Two Mexican Populations. *J Immunol Res.* 2022;2022:2553901.
189. Mehrian R, Quismorio FP, Jr., Strassmann G, Stimmler MM, Horwitz DA, Kitridou RC, et al. Synergistic effect between IL-10 and bcl-2 genotypes in determining susceptibility to systemic lupus erythematosus. *Arthritis Rheum.* 1998;41(4):596-602.
190. Batten M, Groom J, Cachero TG, Qian F, Schneider P, Tschopp J, et al. BAFF mediates survival of peripheral immature B lymphocytes. *J Exp Med.* 2000;192(10):1453-66.
191. Moudi B, Salimi S, Farajian Mashhadi F, Sandoughi M, Zakeri Z. Association of FAS and FAS Ligand Genes Polymorphism and Risk of Systemic Lupus Erythematosus. *The Scientific World Journal.* 2013;2013:176741.

192. Andrews BS, Eisenberg RA, Theofilopoulos AN, Izui S, Wilson CB, McConahey PJ, et al. Spontaneous murine lupus-like syndromes. Clinical and immunopathological manifestations in several strains. *J Exp Med*. 1978;148(5):1198-215.
193. Dixon FJ, Andrews BS, Eisenberg RA, McConahey PJ, Theofilopoulos AN, Wilson CB. Etiology and pathogenesis of a spontaneous lupus-like syndrome in mice. *Arthritis Rheum*. 1978;21(5 Suppl):S64-7.
194. Morel L, Mohan C, Yu Y, Croker BP, Tian N, Deng A, et al. Functional dissection of systemic lupus erythematosus using congenic mouse strains. *The Journal of Immunology*. 1997;158(12):6019-28.
195. Morel L, Blenman KR, Croker BP, Wakeland EK. The major murine systemic lupus erythematosus susceptibility locus, *Sle1*, is a cluster of functionally related genes. *Proceedings of the National Academy of Sciences of the United States of America*. 2001;98(4):1787-92.
196. Mohan C, Morel L, Yang P, Wakeland EK. Genetic dissection of systemic lupus erythematosus pathogenesis: *Sle2* on murine chromosome 4 leads to B cell hyperactivity. *The Journal of Immunology*. 1997;159(1):454-65.
197. Mohan C, Yu Y, Morel L, Yang P, Wakeland EK. Genetic dissection of *Sle* pathogenesis: *Sle3* on murine chromosome 7 impacts T cell activation, differentiation, and cell death. *J Immunol*. 1999;162(11):6492-502.
198. Morel L, Croker BP, Blenman KR, Mohan C, Huang G, Gilkeson G, et al. Genetic reconstitution of systemic lupus erythematosus immunopathology with polycongenic murine strains. *Proceedings of the National Academy of Sciences*. 2000;97(12):6670-5.
199. Izui S, Higaki M, Morrow D, Merino R. The Y chromosome from autoimmune BXSB/MpJ mice induces a lupus-like syndrome in (NZW x C57BL/6)F1 male mice, but not in C57BL/6 male mice. *European journal of immunology*. 1988;18(6):911-5.
200. Boneparth A, Huang W, Bethunaickan R, Woods M, Sahu R, Arora S, et al. TLR7 Influences Germinal Center Selection in Murine SLE. *PloS one*. 2015;10(3):e0119925.
201. Soni C, Wong EB, Domeier PP, Khan TN, Satoh T, Akira S, et al. B Cell–Intrinsic TLR7 Signaling Is Essential for the Development of Spontaneous Germinal Centers. *The Journal of Immunology*. 2014;193(9):4400.
202. Deane JA, Pisitkun P, Barrett RS, Feigenbaum L, Town T, Ward JM, et al. Control of toll-like receptor 7 expression is essential to restrict autoimmunity and dendritic cell proliferation. *Immunity*. 2007;27(5):801-10.
203. Rauch J, Murphy E, Roths JB, Stollar BD, Schwartz RS. A high frequency idiotypic marker of anti-DNA autoantibodies in MRL-Ipr/Ipr mice. *J Immunol*. 1982;129(1):236-41.
204. Wu J, Zhou T, He J, Mountz JD. Autoimmune disease in mice due to integration of an endogenous retrovirus in an apoptosis gene. *J Exp Med*. 1993;178(2):461-8.
205. Chan O, Shlomchik MJ. A new role for B cells in systemic autoimmunity: B cells promote spontaneous T cell activation in MRL-lpr/lpr mice. *J Immunol*. 1998;160(1):51-9.
206. Ramsdell F, Seaman MS, Miller RE, Tough TW, Alderson MR, Lynch DH. *gld/gld* mice are unable to express a functional ligand for Fas. *European journal of immunology*. 1994;24(4):928-33.
207. Bouillet P, Metcalf D, Huang DC, Tarlinton DM, Kay TW, Köntgen F, et al. Proapoptotic Bcl-2 relative Bim required for certain apoptotic responses, leukocyte homeostasis, and to preclude autoimmunity. *Science*. 1999;286(5445):1735-8.
208. Strasser A, Whittingham S, Vaux DL, Bath ML, Adams JM, Cory S, et al. Enforced BCL2 expression in B-lymphoid cells prolongs antibody responses and elicits autoimmune disease. *Proceedings of the National Academy of Sciences of the United States of America*. 1991;88(19):8661-5.
209. Smedby KE, Hjalgrim H, Askling J, Chang ET, Gregersen H, Porwit-MacDonald A, et al. Autoimmune and chronic inflammatory disorders and risk of non-Hodgkin lymphoma by subtype. *J Natl Cancer Inst*. 2006;98(1):51-60.
210. Miller B. Autoimmunity and Lymphoma: A Brief Review. *Journal of Rheumatic Diseases and Treatment*. 2018;4.
211. Singh M, Jackson KJL, Wang JJ, Schofield P, Field MA, Koppstein D, et al. Lymphoma Driver Mutations in the Pathogenic Evolution of an Iconic Human Autoantibody. *Cell*. 2020;180(5):878-94.e19.
212. Opipari AW, Jr., Boguski MS, Dixit VM. The A20 cDNA induced by tumor necrosis factor alpha encodes a novel type of zinc finger protein. *J Biol Chem*. 1990;265(25):14705-8.

213. Dixit VM, Green S, Sarma V, Holzman LB, Wolf FW, O'Rourke K, et al. Tumor necrosis factor- α induction of novel gene products in human endothelial cells including a macrophage-specific chemotaxin. *J Biol Chem*. 1990;265(5):2973-8.
214. Krikos A, Laherty CD, Dixit VM. Transcriptional activation of the tumor necrosis factor α -inducible zinc finger protein, A20, is mediated by kappa B elements. *J Biol Chem*. 1992;267(25):17971-6.
215. Cooper JT, Stroka DM, Brostjan C, Palmetshofer A, Bach FH, Ferran C. A20 blocks endothelial cell activation through a NF- κ B-dependent mechanism. *J Biol Chem*. 1996;271(30):18068-73.
216. Sarma V, Lin Z, Clark L, Rust BM, Tewari M, Noelle RJ, et al. Activation of the B-cell surface receptor CD40 induces A20, a novel zinc finger protein that inhibits apoptosis. *J Biol Chem*. 1995;270(21):12343-6.
217. Das T, Chen Z, Hendriks RW, Kool M. A20/Tumor Necrosis Factor α -Induced Protein 3 in Immune Cells Controls Development of Autoinflammation and Autoimmunity: Lessons from Mouse Models. *Front Immunol*. 2018;9:104.
218. Bai W, Huo S, Li J, Shao J. Advances in the Study of the Ubiquitin-Editing Enzyme A20. *Frontiers in Pharmacology*. 2022;13.
219. Wertz IE, O'Rourke KM, Zhou H, Eby M, Aravind L, Seshagiri S, et al. De-ubiquitination and ubiquitin ligase domains of A20 downregulate NF- κ B signalling. *Nature*. 2004;430(7000):694-9.
220. Harhaj EW, Dixit VM. Regulation of NF- κ B by deubiquitinases. *Immunological reviews*. 2012;246(1):107-24.
221. Sasaki K, Iwai K. Roles of linear ubiquitylation, a crucial regulator of NF- κ B and cell death, in the immune system. *Immunological reviews*. 2015;266(1):175-89.
222. Sun SC. A20 restricts inflammation via ubiquitin binding. *Nature immunology*. 2020;21(4):362-4.
223. Draber P, Kupka S, Reichert M, Draberova H, Lafont E, de Miguel D, et al. LUBAC-Recruited CYLD and A20 Regulate Gene Activation and Cell Death by Exerting Opposing Effects on Linear Ubiquitin in Signaling Complexes. *Cell Reports*. 2015;13(10):2258-72.
224. Polykratis A, Martens A, Eren RO, Shirasaki Y, Yamagishi M, Yamaguchi Y, et al. A20 prevents inflammasome-dependent arthritis by inhibiting macrophage necroptosis through its ZnF7 ubiquitin-binding domain. *Nat Cell Biol*. 2019;21(6):731-42.
225. Priem D, van Loo G, Bertrand MJM. A20 and Cell Death-driven Inflammation. *Trends Immunol*. 2020;41(5):421-35.
226. Razani B, Whang MI, Kim FS, Nakamura MC, Sun X, Advincula R, et al. Non-catalytic ubiquitin binding by A20 prevents psoriatic arthritis-like disease and inflammation. *Nature immunology*. 2020;21(4):422-33.
227. Martens A, van Loo G. A20 phosphorylation controls A20 function. *Nature immunology*. 2019;20(10):1261-2.
228. Hutti JE, Turk BE, Asara JM, Ma A, Cantley LC, Abbott DW. IkappaB kinase beta phosphorylates the K63 deubiquitinase A20 to cause feedback inhibition of the NF-kappaB pathway. *Mol Cell Biol*. 2007;27(21):7451-61.
229. Wertz IE, Newton K, Seshasayee D, Kusam S, Lam C, Zhang J, et al. Phosphorylation and linear ubiquitin direct A20 inhibition of inflammation. *Nature*. 2015;528(7582):370-5.
230. Malinverni C, Unterreiner A, Staal J, Demeyer A, Galaup M, Luyten M, et al. Cleavage by MALT1 induces cytosolic release of A20. *Biochemical and Biophysical Research Communications*. 2010;400(4):543-7.
231. Coornaert B, Baens M, Heyninck K, Bekaert T, Haegman M, Staal J, et al. T cell antigen receptor stimulation induces MALT1 paracaspase-mediated cleavage of the NF-kappaB inhibitor A20. *Nature immunology*. 2008;9(3):263-71.
232. Kulathu Y, Garcia FJ, Mevissen TET, Busch M, Arnaudo N, Carroll KS, et al. Regulation of A20 and other OTU deubiquitinases by reversible oxidation. *Nature Communications*. 2013;4(1):1569.
233. Shrikhande GV, Scali ST, da Silva CG, Damrauer SM, Csizmadia E, Putheti P, et al. O-Glycosylation Regulates Ubiquitination and Degradation of the Anti-Inflammatory Protein A20 to Accelerate Atherosclerosis in Diabetic ApoE-Null Mice. *PloS one*. 2010;5(12):e14240.
234. Lee EG, Boone DL, Chai S, Libby SL, Chien M, Lodolce JP, et al. Failure to regulate TNF-induced NF- κ B and cell death responses in A20-deficient mice. *Science*. 2000;289(5488):2350-4.

235. Turer EE, Tavares RM, Mortier E, Hitotsumatsu O, Advincula R, Lee B, et al. Homeostatic MyD88-dependent signals cause lethal inflammation in the absence of A20. *J Exp Med*. 2008;205(2):451-64.
236. Boone DL, Turer EE, Lee EG, Ahmad RC, Wheeler MT, Tsui C, et al. The ubiquitin-modifying enzyme A20 is required for termination of Toll-like receptor responses. *Nature immunology*. 2004;5(10):1052-60.
237. Zammit NW, Siggs OM, Gray PE, Horikawa K, Langley DB, Walters SN, et al. Denisovan, modern human and mouse TNFAIP3 alleles tune A20 phosphorylation and immunity. *Nature immunology*. 2019;20(10):1299-310.
238. Martens A, Priem D, Hoste E, Vettters J, Rennen S, Catrysse L, et al. Two distinct ubiquitin-binding motifs in A20 mediate its anti-inflammatory and cell-protective activities. *Nature immunology*. 2020;21(4):381-7.
239. Lu TT, Onizawa M, Hammer GE, Turer EE, Yin Q, Damko E, et al. Dimerization and ubiquitin mediated recruitment of A20, a complex deubiquitinating enzyme. *Immunity*. 2013;38(5):896-905.
240. De A, Dainichi T, Rathinam CV, Ghosh S. The deubiquitinase activity of A20 is dispensable for NF- κ B signaling. *EMBO reports*. 2014;15(7):775-83.
241. Ma A, Malynn BA. A20: linking a complex regulator of ubiquitylation to immunity and human disease. *Nat Rev Immunol*. 2012;12(11):774-85.
242. Wu Y, He X, Huang N, Yu J, Shao B. A20: a master regulator of arthritis. *Arthritis Res Ther*. 2020;22(1):220.
243. Khatri B, Tessneer KL, Rasmussen A, Aghakhanian F, Reksten TR, Adler A, et al. Genome-wide association study identifies Sjögren's risk loci with functional implications in immune and glandular cells. *Nat Commun*. 2022;13(1):4287.
244. Musone SL, Taylor KE, Lu TT, Nititham J, Ferreira RC, Ortmann W, et al. Multiple polymorphisms in the TNFAIP3 region are independently associated with systemic lupus erythematosus. *Nat Genet*. 2008;40(9):1062-4.
245. Graham RR, Cotsapas C, Davies L, Hackett R, Lessard CJ, Leon JM, et al. Genetic variants near TNFAIP3 on 6q23 are associated with systemic lupus erythematosus. *Nat Genet*. 2008;40(9):1059-61.
246. Liu X, Qin H, Wu J, Xu J. Association of TNFAIP3 and TNIP1 polymorphisms with systemic lupus erythematosus risk: A meta-analysis. *Gene*. 2018;668:155-65.
247. Bates JS, Lessard CJ, Leon JM, Nguyen T, Battiest LJ, Rodgers J, et al. Meta-analysis and imputation identifies a 109 kb risk haplotype spanning TNFAIP3 associated with lupus nephritis and hematologic manifestations. *Genes Immun*. 2009;10(5):470-7.
248. Adrianto I, Wen F, Templeton A, Wiley G, King JB, Lessard CJ, et al. Association of a functional variant downstream of TNFAIP3 with systemic lupus erythematosus. *Nat Genet*. 2011;43(3):253-8.
249. Sokhi UK, Liber MP, Frye L, Park S, Kang K, Pannellini T, et al. Dissection and function of autoimmunity-associated TNFAIP3 (A20) gene enhancers in humanized mouse models. *Nature Communications*. 2018;9(1):658.
250. Wang S, Wen F, Wiley GB, Kinter MT, Gaffney PM. An enhancer element harboring variants associated with systemic lupus erythematosus engages the TNFAIP3 promoter to influence A20 expression. *PLoS Genet*. 2013;9(9):e1003750.
251. Zhang C, Han X, Sun L, Yang S, Peng J, Chen Y, et al. Novel loss-of-function mutations in TNFAIP3 gene in patients with lupus nephritis. *Clin Kidney J*. 2022;15(11):2027-38.
252. Mele A, Cervantes JR, Chien V, Friedman D, Ferran C. Single nucleotide polymorphisms at the TNFAIP3/A20 locus and susceptibility/resistance to inflammatory and autoimmune diseases. *Adv Exp Med Biol*. 2014;809:163-83.
253. Housley WJ, Fernandez SD, Vera K, Murikinati SR, Grutzendler J, Cuerdon N, et al. Genetic variants associated with autoimmunity drive NF κ B signaling and responses to inflammatory stimuli. *Science Translational Medicine*. 2015;7(291):291ra93-ra93.
254. Wang Z, Zhang Z, Yuan J, Li L. Altered TNFAIP3 mRNA expression in peripheral blood mononuclear cells from patients with rheumatoid arthritis. *Biomed Rep*. 2015;3(5):675-80.
255. Zhou Q, Wang H, Schwartz DM, Stoffels M, Park YH, Zhang Y, et al. Loss-of-function mutations in TNFAIP3 leading to A20 haploinsufficiency cause an early-onset autoinflammatory disease. *Nature genetics*. 2016;48(1):67-73.

256. Takagi M, Ogata S, Ueno H, Yoshida K, Yeh T, Hoshino A, et al. Haploinsufficiency of TNFAIP3 (A20) by germline mutation is involved in autoimmune lymphoproliferative syndrome. *J Allergy Clin Immunol*. 2017;139(6):1914-22.
257. Duncan CJA, Dinnigan E, Theobald R, Grainger A, Skelton AJ, Hussain R, et al. Early-onset autoimmune disease due to a heterozygous loss-of-function mutation in *TNFAIP3* (A20). *Annals of the Rheumatic Diseases*. 2018;77(5):783-6.
258. Sato S, Fujita Y, Shigemura T, Matoba H, Agematsu K, Sumichika Y, et al. Juvenile onset autoinflammatory disease due to a novel mutation in TNFAIP3 (A20). *Arthritis Research & Therapy*. 2018;20(1):274.
259. Yu MP, Xu XS, Zhou Q, Deutch N, Lu MP. Haploinsufficiency of A20 (HA20): updates on the genetics, phenotype, pathogenesis and treatment. *World J Pediatr*. 2020;16(6):575-84.
260. He T, Huang Y, Luo Y, Xia Y, Wang L, Zhang H, et al. Haploinsufficiency of A20 Due to Novel Mutations in TNFAIP3. *Journal of Clinical Immunology*. 2020;40(5):741-51.
261. Zhang D, Su G, Zhou Z, Lai J. Clinical characteristics and genetic analysis of A20 haploinsufficiency. *Pediatr Rheumatol Online J*. 2021;19(1):75.
262. Shimizu M, Matsubayashi T, Ohnishi H, Nakama M, Izawa K, Honda Y, et al. Haploinsufficiency of A20 with a novel mutation of deletion of exons 2–3 of TNFAIP3. *Modern Rheumatology*. 2021;31(2):493-7.
263. Shaheen ZR, Williams SJA, Binstadt BA. Case Report: A Novel TNFAIP3 Mutation Causing Haploinsufficiency of A20 With a Lupus-Like Phenotype. *Front Immunol*. 2021;12:629457-.
264. Hautala T, Vähäsalo P, Kuismin O, Keskitalo S, Rajamäki K, Väänänen A, et al. A Family With A20 Haploinsufficiency Presenting With Novel Clinical Manifestations and Challenges for Treatment. *J Clin Rheumatol*. 2021;27(8):e583-e7.
265. Aslani N, Asnaashari K, Parvaneh N, Shahrooei M, Sotoudeh-Anvari M, Shahram F, et al. TNFAIP3 mutation causing haploinsufficiency of A20 with a hemophagocytic lymphohistiocytosis phenotype: a report of two cases. *Pediatr Rheumatol Online J*. 2022;20(1):78.
266. Liu J, Lin Y, Li X, Ba H, He X, Peng H, et al. Haploinsufficiency of A20 in a Chinese child caused by loss-of-function mutations in TNFAIP3: A case report and review of the literature. *Front Pediatr*. 2022;10:990008.
267. Rossi MN, Federici S, Uva A, Passarelli C, Celani C, Caiello I, et al. Identification of a Novel Mutation in TNFAIP3 in a Family With Poly-Autoimmunity. *Front Immunol*. 2022;13:804401.
268. Zanatta L, Biscaro F, Bresolin S, Marzaro M, Sarcognato S, Cataldo I, et al. Case Report: An early-onset inflammatory colitis due to a variant in TNFAIP3 causing A20 haploinsufficiency. *Front Pediatr*. 2022;10:1044007.
269. Wakatsuki R, Hatai Y, Okamoto K, Kaneko S, Shimbo A, Irabu H, et al. An infant with A20 haploinsufficiency presenting with periodic fever syndrome: A case report. *Int J Rheum Dis*. 2023;26(5):973-6.
270. Novak U, Rinaldi A, Kwee I, Nandula SV, Rancoita PM, Compagno M, et al. The NF- κ B negative regulator TNFAIP3 (A20) is inactivated by somatic mutations and genomic deletions in marginal zone lymphomas. *Blood*. 2009;113(20):4918-21.
271. Schmitz R, Hansmann ML, Bohle V, Martin-Subero JI, Hartmann S, Mechttersheimer G, et al. TNFAIP3 (A20) is a tumor suppressor gene in Hodgkin lymphoma and primary mediastinal B cell lymphoma. *J Exp Med*. 2009;206(5):981-9.
272. Kato M, Sanada M, Kato I, Sato Y, Takita J, Takeuchi K, et al. Frequent inactivation of A20 in B-cell lymphomas. *Nature*. 2009;459(7247):712-6.
273. Compagno M, Lim WK, Grunn A, Nandula SV, Brahmachary M, Shen Q, et al. Mutations of multiple genes cause deregulation of NF- κ B in diffuse large B-cell lymphoma. *Nature*. 2009;459(7247):717-21.
274. Honma K, Tsuzuki S, Nakagawa M, Tagawa H, Nakamura S, Morishima Y, et al. TNFAIP3/A20 functions as a novel tumor suppressor gene in several subtypes of non-Hodgkin lymphomas. *Blood*. 2009;114(12):2467-75.
275. Alhanafy AM, Elshafie M, Abou Elnour ES, Genena S. MALT1- A20 and NF- κ B expression pattern in patients with non-Hodgkin lymphomas. *Annals of Oncology*. 2019;30:ix93.
276. Nocturne G, Boudaoud S, Miceli-Richard C, Viengchareun S, Lazure T, Nititham J, et al. Germline and somatic genetic variations of TNFAIP3 in lymphoma complicating primary Sjögren's syndrome. *Blood*. 2013;122(25):4068-76.

277. Heger K, Fierens K, Vahl JC, Aszodi A, Peschke K, Schenten D, et al. A20-deficient mast cells exacerbate inflammatory responses in vivo. *PLoS Biol.* 2014;12(1):e1001762.
278. Rickert RC, Roes J, Rajewsky K. B lymphocyte-specific, Cre-mediated mutagenesis in mice. *Nucleic acids research.* 1997;25(6):1317-8.
279. Vereecke L, Sze M, Guire CM, Rogiers B, Chu Y, Schmidt-Supprian M, et al. Enterocyte-specific A20 deficiency sensitizes to tumor necrosis factor-induced toxicity and experimental colitis. *The Journal of Experimental Medicine.* 2010;207(7):1513-23.
280. Chu Y, Vahl JC, Kumar D, Heger K, Bertossi A, Wójtowicz E, et al. B cells lacking the tumor suppressor TNFAIP3/A20 display impaired differentiation and hyperactivation and cause inflammation and autoimmunity in aged mice. *Blood.* 2011;117(7):2227-36.
281. Tavares RM, Turer EE, Liu CL, Advincula R, Scapini P, Rhee L, et al. The Ubiquitin Modifying Enzyme A20 Restricts B cell Survival and Prevents Autoimmunity. *Immunity.* 2010;33(2):181-91.
282. Hövelmeyer N, Reissig S, Xuan NT, Adams-Quack P, Lukas D, Nikolaev A, et al. A20 deficiency in B cells enhances B-cell proliferation and results in the development of autoantibodies. *European journal of immunology.* 2011;41(3):595-601.
283. Rubin SJS, Bloom MS, Robinson WH. B cell checkpoints in autoimmune rheumatic diseases. *Nature Reviews Rheumatology.* 2019;15(5):303-15.
284. Çakan E, Gunaydin G. Activation induced cytidine deaminase: An old friend with new faces. *Front Immunol.* 2022;13.
285. Hillion S, Youinou P, Jamin C. Peripheral expression of RAG in human B lymphocytes in normal and pathological conditions is dependent on interleukin-6. *Autoimmunity Reviews.* 2007;6(6):415-20.
286. Robbiani DF, Bothmer A, Callen E, Reina-San-Martin B, Dorsett Y, Difilippantonio S, et al. AID Is Required for the Chromosomal Breaks in c-myc that Lead to c-myc/IgH Translocations. *Cell.* 2008;135(6):1028-38.
287. Malissen M, Gillet A, Ardouin L, Bouvier G, Trucy J, Ferrier P, et al. Altered T cell development in mice with a targeted mutation of the CD3-epsilon gene. *The EMBO Journal.* 1995;14(19):4641-53.
288. Casola S, Cattoretti G, Uyttersprot N, Koralov SB, Seagal J, Hao Z, et al. Tracking germinal center B cells expressing germ-line immunoglobulin gamma1 transcripts by conditional gene targeting. *Proceedings of the National Academy of Sciences of the United States of America.* 2006;103(19):7396-401.
289. Schenten D, Nish SA, Yu S, Yan X, Lee HK, Brodsky I, et al. Signaling through the adaptor molecule MyD88 in CD4+ T cells is required to overcome suppression by regulatory T cells. *Immunity.* 2014;40(1):78-90.
290. Zikherman J, Parameswaran R, Weiss A. Endogenous antigen tunes the responsiveness of naive B cells but not T cells. *Nature.* 2012;489(7414):160-4.
291. Shinkai Y, Rathbun G, Lam KP, Oltz EM, Stewart V, Mendelsohn M, et al. RAG-2-deficient mice lack mature lymphocytes owing to inability to initiate V(D)J rearrangement. *Cell.* 1992;68(5):855-67.
292. Morse HC, 3rd, Anver MR, Fredrickson TN, Haines DC, Harris AW, Harris NL, et al. Bethesda proposals for classification of lymphoid neoplasms in mice. *Blood.* 2002;100(1):246-58.
293. Rehg JE, Bush D, Ward JM. The utility of immunohistochemistry for the identification of hematopoietic and lymphoid cells in normal tissues and interpretation of proliferative and inflammatory lesions of mice and rats. *Toxicol Pathol.* 2012;40(2):345-74.
294. Willard-Mack CL, Elmore SA, Hall WC, Harleman J, Kuper CF, Losco P, et al. Nonproliferative and Proliferative Lesions of the Rat and Mouse Hematolymphoid System. *Toxicol Pathol.* 2019;47(6):665-783.
295. Parekh S, Ziegenhain C, Vieth B, Enard W, Hellmann I. The impact of amplification on differential expression analyses by RNA-seq. *Sci Rep.* 2016;6:25533.
296. Macosko EZ, Basu A, Satija R, Nemesh J, Shekhar K, Goldman M, et al. Highly Parallel Genome-wide Expression Profiling of Individual Cells Using Nanoliter Droplets. *Cell.* 2015;161(5):1202-14.
297. Love MI, Huber W, Anders S. Moderated estimation of fold change and dispersion for RNA-seq data with DESeq2. *Genome Biology.* 2014;15(12):550.
298. Subramanian A, Tamayo P, Mootha VK, Mukherjee S, Ebert BL, Gillette MA, et al. Gene set enrichment analysis: A knowledge-based approach for interpreting genome-wide expression profiles. *Proceedings of the National Academy of Sciences.* 2005;102(43):15545-50.

299. Schenten D, Egert A, Pasparakis M, Rajewsky K. M17, a gene specific for germinal center (GC) B cells and a prognostic marker for GC B-cell lymphomas, is dispensable for the GC reaction in mice. *Blood*. 2006;107(12):4849-56.
300. Maccarthy T, Roa S, Scharff MD, Bergman A. SHMTool: a webserver for comparative analysis of somatic hypermutation datasets. *DNA Repair (Amst)*. 2009;8(1):137-41.
301. Heger K, Kober M, Rieß D, Drees C, de Vries I, Bertossi A, et al. A novel Cre recombinase reporter mouse strain facilitates selective and efficient infection of primary immune cells with adenoviral vectors. *European journal of immunology*. 2015;45(6):1614-20.
302. Nojima T, Haniuda K, Moutai T, Matsudaira M, Mizokawa S, Shiratori I, et al. In-vitro derived germinal centre B cells differentially generate memory B or plasma cells in vivo. *Nat Commun*. 2011;2:465.
303. Oostendorp RAJ, Harvey KN, Kusadasi N, de Bruijn MFTR, Saris C, Ploemacher RE, et al. Stromal cell lines from mouse aorta-gonads-mesonephros subregions are potent supporters of hematopoietic stem cell activity. *Blood*. 2002;99(4):1183-9.
304. Moutai T, Yamana H, Nojima T, Kitamura D. A novel and effective cancer immunotherapy mouse model using antigen-specific B cells selected in vitro. *PloS one*. 2014;9(3):e92732.
305. Andre J, Cimaz R, Ranchin B, Galambrun C, Bertrand Y, Bouvier R, et al. Overexpression of the antiapoptotic gene Bfl-1 in B cells from patients with familial systemic lupus erythematosus. *Lupus*. 2007;16(2):95-100.
306. Huang DCS, Hahne M, Schroeter M, Frei K, Fontana A, Villunger A, et al. Activation of Fas by FasL induces apoptosis by a mechanism that cannot be blocked by Bcl-2 or Bcl-xL. *Proceedings of the National Academy of Sciences of the United States of America*. 1999;96(26):14871-6.
307. Gerondakis S, Siebenlist U. Roles of the NF-kappaB pathway in lymphocyte development and function. *Cold Spring Harbor perspectives in biology*. 2010;2(5):a000182.
308. Nikolaou C, Muehle K, Schlickeiser S, Japp AS, Matzmohr N, Kunkel D, et al. High-dimensional single cell mass cytometry analysis of the murine hematopoietic system reveals signatures induced by ageing and physiological pathogen challenges. *Immunity & Ageing*. 2021;18(1):20.
309. Naito Y, Takematsu H, Koyama S, Miyake S, Yamamoto H, Fujinawa R, et al. Germinal center marker GL7 probes activation-dependent repression of N-glycolylneuraminic acid, a sialic acid species involved in the negative modulation of B-cell activation. *Mol Cell Biol*. 2007;27(8):3008-22.
310. Pracht K, Meininger J, Daum P, Schulz SR, Reimer D, Hauke M, et al. A new staining protocol for detection of murine antibody-secreting plasma cell subsets by flow cytometry. *European journal of immunology*. 2017;47(8):1389-92.
311. Bergqvist P, Stensson A, Lycke NY, Bemark M. T cell-independent IgA class switch recombination is restricted to the GALT and occurs prior to manifest germinal center formation. *J Immunol*. 2010;184(7):3545-53.
312. Keppler SJ, Goess MC, Heinze JM. The Wanderings of Gut-Derived IgA Plasma Cells: Impact on Systemic Immune Responses. *Front Immunol*. 2021;12:670290.
313. Morrison VL, Barr TA, Brown S, Gray D. TLR-Mediated Loss of CD62L Focuses B Cell Traffic to the Spleen during *Salmonella typhimurium* Infection. *The Journal of Immunology*. 2010;185(5):2737-46.
314. Camp RL, Kraus TA, Birkeland ML, Puré E. High levels of CD44 expression distinguish virgin from antigen-primed B cells. *Journal of Experimental Medicine*. 1991;173(3):763-6.
315. Zimmermann M, Rose N, Lindner JM, Kim H, Gonçalves AR, Callegari I, et al. Antigen Extraction and B Cell Activation Enable Identification of Rare Membrane Antigen Specific Human B Cells. *Front Immunol*. 2019;10.
316. Rau FC, Dieter J, Luo Z, Priest SO, Baumgarth N. B7-1/2 (CD80/CD86) direct signaling to B cells enhances IgG secretion. *Journal of immunology (Baltimore, Md : 1950)*. 2009;183(12):7661-71.
317. Victora GD, Dominguez-Sola D, Holmes AB, Deroubaix S, Dalla-Favera R, Nussenzweig MC. Identification of human germinal center light and dark zone cells and their relationship to human B-cell lymphomas. *Blood*. 2012;120(11):2240-8.
318. Logue EC, Bakkour S, Murphy MM, Nolla H, Sha WC. ICOS-induced B7h shedding on B cells is inhibited by TLR7/8 and TLR9. *J Immunol*. 2006;177(4):2356-64.

319. Linterman MA, Pierson W, Lee SK, Kallies A, Kawamoto S, Rayner TF, et al. Foxp3+ follicular regulatory T cells control the germinal center response. *Nat Med.* 2011;17(8):975-82.
320. Wing JB, Kitagawa Y, Locci M, Hume H, Tay C, Morita T, et al. A distinct subpopulation of CD25(-) T-follicular regulatory cells localizes in the germinal centers. *Proceedings of the National Academy of Sciences of the United States of America.* 2017;114(31):E6400-e9.
321. Wing JB, Tekgüç M, Sakaguchi S. Control of Germinal Center Responses by T-Follicular Regulatory Cells. *Front Immunol.* 2018;9(1910).
322. Yang S, Liu F, Wang QJ, Rosenberg SA, Morgan RA. The shedding of CD62L (L-selectin) regulates the acquisition of lytic activity in human tumor reactive T lymphocytes. *PloS one.* 2011;6(7):e22560.
323. McDaniel MM, Chawla AS, Jain A, Meibers HE, Saha I, Gao Y, et al. Effector memory CD4(+) T cells induce damaging innate inflammation and autoimmune pathology by engaging CD40 and TNFR on myeloid cells. *Sci Immunol.* 2022;7(67):eabk0182.
324. Wan YY, Flavell RA. How diverse--CD4 effector T cells and their functions. *J Mol Cell Biol.* 2009;1(1):20-36.
325. Bassler K, Schulte-Schrepping J, Warnat-Herresthal S, Aschenbrenner AC, Schultze JL. The Myeloid Cell Compartment—Cell by Cell. *Annual Review of Immunology.* 2019;37(1):269-93.
326. Kawamoto H, Minato N. Myeloid cells. *The International Journal of Biochemistry & Cell Biology.* 2004;36(8):1374-9.
327. Galli SJ, Borregaard N, Wynn TA. Phenotypic and functional plasticity of cells of innate immunity: macrophages, mast cells and neutrophils. *Nature immunology.* 2011;12(11):1035-44.
328. Song L, Dong G, Guo L, Graves DT. The function of dendritic cells in modulating the host response. *Mol Oral Microbiol.* 2018;33(1):13-21.
329. Colonna M, Trinchieri G, Liu Y-J. Plasmacytoid dendritic cells in immunity. *Nature immunology.* 2004;5(12):1219-26.
330. Rönnblom L, Pascual V. The innate immune system in SLE: type I interferons and dendritic cells. *Lupus.* 2008;17(5):394-9.
331. Zhou Z, Ma J, Xiao C, Han X, Qiu R, Wang Y, et al. Phenotypic and functional alterations of pDCs in lupus-prone mice. *Sci Rep.* 2016;6:20373.
332. Scott JL, Wirth JR, EuDaly JG, Gilkeson GS, Cunningham MA. Plasmacytoid dendritic cell distribution and maturation are altered in lupus prone mice prior to the onset of clinical disease. *Clin Immunol.* 2017;175:109-14.
333. Wen T, Rothenberg ME. The Regulatory Function of Eosinophils. *Microbiol Spectr.* 2016;4(5).
334. Abel AM, Yang C, Thakar MS, Malarkannan S. Natural Killer Cells: Development, Maturation, and Clinical Utilization. *Front Immunol.* 2018;9.
335. Swirski FK, Nahrendorf M, Etzrodt M, Wildgruber M, Cortez-Retamozo V, Panizzi P, et al. Identification of splenic reservoir monocytes and their deployment to inflammatory sites. *Science.* 2009;325(5940):612-6.
336. Zheng B, Marinova E, Switzer K, Wansley D, He H, Bheekha-Escura R, et al. Overexpression of Bcl(XL) in B cells promotes Th1 response and exacerbates collagen-induced arthritis. *J Immunol.* 2007;179(10):7087-92.
337. Hochberg MC. Updating the American college of rheumatology revised criteria for the classification of systemic lupus erythematosus. *Arthritis & Rheumatism.* 1997;40(9):1725-.
338. Petri M, Orbai A-M, Alarcón GS, Gordon C, Merrill JT, Fortin PR, et al. Derivation and validation of the Systemic Lupus International Collaborating Clinics classification criteria for systemic lupus erythematosus. *Arthritis & Rheumatism.* 2012;64(8):2677-86.
339. Rönnblom L, Leonard D. Interferon pathway in SLE: one key to unlocking the mystery of the disease. *Lupus Sci Med.* 2019;6(1):e000270.
340. Vincent FB, Kandane-Rathnayake R, Koelmeyer R, Hoi AY, Harris J, Mackay F, et al. Analysis of serum B cell-activating factor from the tumor necrosis factor family (BAFF) and its soluble receptors in systemic lupus erythematosus. *Clin Transl Immunology.* 2019;8(4):e01047.
341. Ruchakorn N, Ngamjanyaporn P, Suangtamai T, Kafaksom T, Polpanumas C, Petpisit V, et al. Performance of cytokine models in predicting SLE activity. *Arthritis Research & Therapy.* 2019;21(1):287.
342. Tsantikos E, Maxwell MJ, Putoczki T, Ernst M, Rose-John S, Tarlinton DM, et al. Interleukin-6 Trans-Signaling Exacerbates Inflammation and Renal Pathology in Lupus-Prone Mice. *Arthritis & Rheumatism.* 2013;65(10):2691-702.

343. Arkatkar T, Du SW, Jacobs HM, Dam EM, Hou B, Buckner JH, et al. B cell-derived IL-6 initiates spontaneous germinal center formation during systemic autoimmunity. *J Exp Med*. 2017;214(11):3207-17.
344. Niewold TB, Hua J, Lehman TJA, Harley JB, Crow MK. High serum IFN- α activity is a heritable risk factor for systemic lupus erythematosus. *Genes & Immunity*. 2007;8(6):492-502.
345. Bengtsson AA, Sturfelt G, Truedsson L, Blomberg J, Alm G, Vallin H, et al. Activation of type I interferon system in systemic lupus erythematosus correlates with disease activity but not with antiretroviral antibodies. *Lupus*. 2000;9(9):664-71.
346. Keller EJ, Patel NB, Patt M, Nguyen JK, Jørgensen TN. Partial Protection From Lupus-Like Disease by B-Cell Specific Type I Interferon Receptor Deficiency. *Front Immunol*. 2021;11(3371).
347. Munroe ME, Lu R, Zhao YD, Fife DA, Robertson JM, Guthridge JM, et al. Altered type II interferon precedes autoantibody accrual and elevated type I interferon activity prior to systemic lupus erythematosus classification. *Ann Rheum Dis*. 2016;75(11):2014-21.
348. Chun HY, Chung JW, Kim HA, Yun JM, Jeon JY, Ye YM, et al. Cytokine IL-6 and IL-10 as biomarkers in systemic lupus erythematosus. *J Clin Immunol*. 2007;27(5):461-6.
349. Finkelman FD, Katona IM, Mosmann TR, Coffman RL. IFN-gamma regulates the isotypes of Ig secreted during in vivo humoral immune responses. *J Immunol*. 1988;140(4):1022-7.
350. Attridge K, Kenefeck R, Wardzinski L, Qureshi OS, Wang CJ, Manzotti C, et al. IL-21 Promotes CD4 T Cell Responses by Phosphatidylinositol 3-Kinase-Dependent Upregulation of CD86 on B Cells. *The Journal of Immunology*. 2014:1302082.
351. Salazar-Camarena DC, Palafox-Sánchez CA, Cruz A, Marín-Rosales M, Muñoz-Valle JF. Analysis of the receptor BCMA as a biomarker in systemic lupus erythematosus patients. *Scientific Reports*. 2020;10(1):6236.
352. Houssiau F, Lefebvre C, Vanden Berghe M, Lambert M, Devogelaer J-P, Renaud J-C. Serum interleukin 10 titers in systemic lupus erythematosus reflect disease activity. *Lupus*. 1995;4(5):393-5.
353. Malisan F, Brière F, Bridon JM, Harindranath N, Mills FC, Max EE, et al. Interleukin-10 induces immunoglobulin G isotype switch recombination in human CD40-activated naive B lymphocytes. *J Exp Med*. 1996;183(3):937-47.
354. Llorente L, Zou W, Levy Y, Richaud-Patin Y, Wijdenes J, Alcocer-Varela J, et al. Role of interleukin 10 in the B lymphocyte hyperactivity and autoantibody production of human systemic lupus erythematosus. *J Exp Med*. 1995;181(3):839-44.
355. Rousset F, Garcia E, Defrance T, Péronne C, Vezzio N, Hsu DH, et al. Interleukin 10 is a potent growth and differentiation factor for activated human B lymphocytes. *Proceedings of the National Academy of Sciences*. 1992;89(5):1890-3.
356. Peçanha LM, Snapper CM, Lees A, Yamaguchi H, Mond JJ. IL-10 inhibits T cell-independent but not T cell-dependent responses in vitro. *J Immunol*. 1993;150(8 Pt 1):3215-23.
357. Heine G, Drozdenko G, Grün JR, Chang HD, Radbruch A, Worm M. Autocrine IL-10 promotes human B-cell differentiation into IgM- or IgG-secreting plasmablasts. *European journal of immunology*. 2014;44(6):1615-21.
358. Foy TM, Laman JD, Ledbetter JA, Aruffo A, Claassen E, Noelle RJ. gp39-CD40 interactions are essential for germinal center formation and the development of B cell memory. *J Exp Med*. 1994;180(1):157-63.
359. Foy TM, Shepherd DM, Durie FH, Aruffo A, Ledbetter JA, Noelle RJ. In vivo CD40-gp39 interactions are essential for thymus-dependent humoral immunity. II. Prolonged suppression of the humoral immune response by an antibody to the ligand for CD40, gp39. *J Exp Med*. 1993;178(5):1567-75.
360. Callard RE, Armitage RJ, Fanslow WC, Spriggs MK. CD40 ligand and its role in X-linked hyper-IgM syndrome. *Immunol Today*. 1993;14(11):559-64.
361. Armitage RJ, Fanslow WC, Strockbine L, Sato TA, Clifford KN, Macduff BM, et al. Molecular and biological characterization of a murine ligand for CD40. *Nature*. 1992;357(6373):80-2.
362. Armitage RJ, Sato TA, Macduff BM, Clifford KN, Alpert AR, Smith CA, et al. Identification of a source of biologically active CD40 ligand. *European journal of immunology*. 1992;22(8):2071-6.
363. Schönbeck U, Libby P. The CD40/CD154 receptor/ligand dyad. *Cellular and Molecular Life Sciences*. 2001;58(1):4-43.

364. Grammer AC, Bergman MC, Miura Y, Fujita K, Davis LS, Lipsky PE. The CD40 ligand expressed by human B cells costimulates B cell responses. *J Immunol.* 1995;154(10):4996-5010.
365. Wykes M, Poudrier J, Lindstedt R, Gray D. Regulation of cytoplasmic, surface and soluble forms of CD40 ligand in mouse B cells. *European journal of immunology.* 1998;28(2):548-59.
366. Graf D, Müller S, Korthäuer U, van Kooten C, Weise C, Kroczeck RA. A soluble form of TRAP (CD40 ligand) is rapidly released after T cell activation. *European journal of immunology.* 1995;25(6):1749-54.
367. Wu C, Liu Y, Zhao Q, Chen G, Chen J, Yan X, et al. Soluble CD40 ligand-activated human peripheral B cells as surrogated antigen presenting cells: A preliminary approach for anti-HBV immunotherapy. *Virology.* 2010;7:370-.
368. Kato K, Santana-Sahagún E, Rassenti LZ, Weisman MH, Tamura N, Kobayashi S, et al. The soluble CD40 ligand sCD154 in systemic lupus erythematosus. *J Clin Invest.* 1999;104(7):947-55.
369. Goules A, Tzioufas AG, Manousakis MN, Kirou KA, Crow MK, Routsias JG. Elevated levels of soluble CD40 ligand (sCD40L) in serum of patients with systemic autoimmune diseases. *J Autoimmun.* 2006;26(3):165-71.
370. Desai-Mehta A, Lu L, Ramsey-Goldman R, Datta SK. Hyperexpression of CD40 ligand by B and T cells in human lupus and its role in pathogenic autoantibody production. *The Journal of Clinical Investigation.* 1996;97(9):2063-73.
371. Perazzio SF, Soeiro-Pereira PV, dos Santos VC, de Brito MV, Salu B, Oliva MLV, et al. Soluble CD40L is associated with increased oxidative burst and neutrophil extracellular trap release in Behçet's disease. *Arthritis Research & Therapy.* 2017;19(1):235.
372. Zickert A, Amoudruz P, Sundström Y, Rönnelid J, Malmström V, Gunnarsson I. IL-17 and IL-23 in lupus nephritis - association to histopathology and response to treatment. *BMC Immunology.* 2015;16(1):7.
373. Bruey J-M, Bruey-Sedano N, Luciano F, Zhai D, Balpai R, Xu C, et al. Bcl-2 and Bcl-XL Regulate Proinflammatory Caspase-1 Activation by Interaction with NALP1. *Cell.* 2007;129(1):45-56.
374. Voronov E, Dayan M, Zinger H, Gayvoronsky L, Lin JP, Iwakura Y, et al. IL-1 beta-deficient mice are resistant to induction of experimental SLE. *Eur Cytokine Netw.* 2006;17(2):109-16.
375. Mende R, Vincent FB, Kandane-Rathnayake R, Koelmeyer R, Lin E, Chang J, et al. Analysis of Serum Interleukin (IL)-1 β and IL-18 in Systemic Lupus Erythematosus. *Front Immunol.* 2018;9(1250).
376. Becker-Merok A, Eilertsen G, Nossent JC. Levels of transforming growth factor-beta are low in systemic lupus erythematosus patients with active disease. *J Rheumatol.* 2010;37(10):2039-45.
377. Yang X, Gao Y, Wang H, Zhao X, Gong X, Wang Q, et al. Increased Urinary Interleukin 22 Binding Protein Levels Correlate with Lupus Nephritis Activity. *The Journal of Rheumatology.* 2014;41(9):1793-800.
378. Pan HF, Zhao XF, Yuan H, Zhang WH, Li XP, Wang GH, et al. Decreased serum IL-22 levels in patients with systemic lupus erythematosus. *Clin Chim Acta.* 2009;401(1-2):179-80.
379. Li TT, Zhang T, Chen GM, Zhu QQ, Tao JH, Pan HF, et al. Low level of serum interleukin 27 in patients with systemic lupus erythematosus. *J Investig Med.* 2010;58(5):737-9.
380. Pan HF, Tao JH, Ye DQ. Therapeutic potential of IL-27 in systemic lupus erythematosus. *Expert Opin Ther Targets.* 2010;14(5):479-84.
381. Dauba A, Braikia F-Z, Oudinet C, Khamlichi AA. Interleukin 7 regulates switch transcription in developing B cells. *Cellular & Molecular Immunology.* 2021;18(3):776-8.
382. Chen C, Zhou M, Yan X-g, Chen Y-x, Cui M, Chen H-c, et al. A recombinant canine distemper virus expressing interleukin-7 enhances humoral immunity. *Journal of General Virology.* 2019;100(4):602-15.
383. Defrance T, Carayon P, Billian G, Guillemot JC, Minty A, Caput D, et al. Interleukin 13 is a B cell stimulating factor. *J Exp Med.* 1994;179(1):135-43.
384. Hajoui O, Janani R, Tulic M, Joubert P, Ronis T, Hamid Q, et al. Synthesis of IL-13 by human B lymphocytes: regulation and role in IgE production. *J Allergy Clin Immunol.* 2004;114(3):657-63.
385. Minty A, Chalon P, Derocq JM, Dumont X, Guillemot JC, Kaghad M, et al. Interleukin-13 is a new human lymphokine regulating inflammatory and immune responses. *Nature.* 1993;362(6417):248-50.

386. Ozaki K, Spolski R, Ettinger R, Kim H-P, Wang G, Qi C-F, et al. Regulation of B Cell Differentiation and Plasma Cell Generation by IL-21, a Novel Inducer of Blimp-1 and Bcl-6. *The Journal of Immunology*. 2004;173(9):5361-71.
387. Jankovic D, Kugler DG, Sher A. IL-10 production by CD4+ effector T cells: a mechanism for self-regulation. *Mucosal Immunology*. 2010;3(3):239-46.
388. Trinchieri G. Regulatory role of T cells producing both interferon gamma and interleukin 10 in persistent infection. *J Exp Med*. 2001;194(10):F53-7.
389. Lan RY, Ansari AA, Lian ZX, Gershwin ME. Regulatory T cells: development, function and role in autoimmunity. *Autoimmun Rev*. 2005;4(6):351-63.
390. Gocher AM, Handu S, Workman CJ, Vignali DAA. Interferon gamma production by regulatory T cells is required for response to cancer immunotherapy. *The Journal of Immunology*. 2020;204(1 Supplement):244.8-8.
391. Fuschioti P, Larregina AT, Ho J, Feghali-Bostwick C, Medsger TA, Jr. Interleukin-13-producing CD8+ T cells mediate dermal fibrosis in patients with systemic sclerosis. *Arthritis Rheum*. 2013;65(1):236-46.
392. Bao Y, Cao X. The immune potential and immunopathology of cytokine-producing B cell subsets: A comprehensive review. *Journal of Autoimmunity*. 2014;55:10-23.
393. de Gruijter NM, Jebson B, Rosser EC. Cytokine production by human B cells: role in health and autoimmune disease. *Clin Exp Immunol*. 2022;210(3):253-62.
394. Saraiva M, O'Garra A. The regulation of IL-10 production by immune cells. *Nat Rev Immunol*. 2010;10(3):170-81.
395. Baldwin DS, Gluck MC, Lowenstein J, Gallo GR. Lupus nephritis. Clinical course as related to morphologic forms and their transitions. *Am J Med*. 1977;62(1):12-30.
396. Dong S, Hughes RC. Macrophage surface glycoproteins binding to galectin-3 (Mac-2-antigen). *Glycoconj J*. 1997;14(2):267-74.
397. Chalmers SA, Chitu V, Ramanujam M, Putterman C. Therapeutic targeting of macrophages in lupus nephritis. *Discov Med*. 2015;20(108):43-9.
398. Espeli M, Bökers S, Giannico G, Dickinson HA, Bardsley V, Fogo AB, et al. Local renal autoantibody production in lupus nephritis. *J Am Soc Nephrol*. 2011;22(2):296-305.
399. Flores-Mendoza G, Sansón SP, Rodríguez-Castro S, Crispín JC, Rosetti F. Mechanisms of Tissue Injury in Lupus Nephritis. *Trends in Molecular Medicine*. 2018;24(4):364-78.
400. Hanly JG, O'Keefe AG, Su L, Urowitz MB, Romero-Diaz J, Gordon C, et al. The frequency and outcome of lupus nephritis: results from an international inception cohort study. *Rheumatology (Oxford)*. 2016;55(2):252-62.
401. Hunter MG, Hurwitz S, Bellamy COC, Duffield JS. Quantitative morphometry of lupus nephritis: The significance of collagen, tubular space, and inflammatory infiltrate. *Kidney International*. 2005;67(1):94-102.
402. Arbuckle MR, McClain MT, Rubertone MV, Scofield RH, Dennis GJ, James JA, et al. Development of Autoantibodies before the Clinical Onset of Systemic Lupus Erythematosus. *New England Journal of Medicine*. 2003;349(16):1526-33.
403. Kolitz T, Shiber S, Sharabi I, Winder A, Zandman-Goddard G. Cardiac Manifestations of Antiphospholipid Syndrome With Focus on Its Primary Form. *Front Immunol*. 2019;10:941.
404. Lai W-T, Cho W-H, Eng H-L, Kuo M-H, Huang F-C. Overlap Syndrome Involving Systemic Lupus Erythematosus and Autoimmune Hepatitis in Children: A Case Report and Literature Review. *Frontiers in Pediatrics*. 2019;7(310).
405. Kang Y, Kuang X, Yan H, Ren P, Yang X, Liu H, et al. A Novel Synbiotic Alleviates Autoimmune Hepatitis by Modulating the Gut Microbiota-Liver Axis and Inhibiting the Hepatic TLR4/NF- κ B/NLRP3 Signaling Pathway. *mSystems*. 0(0):e01127-22.
406. Frommer F, Waisman A. B Cells Participate in Thymic Negative Selection of Murine Auto-reactive CD4+ T Cells. *PloS one*. 2010;5(10):e15372.
407. Hidalgo Y, Núñez S, Fuenzalida MJ, Flores-Santibáñez F, Sáez PJ, Dorner J, et al. Thymic B Cells Promote Germinal Center-Like Structures and the Expansion of Follicular Helper T Cells in Lupus-Prone Mice. *Front Immunol*. 2020;11:696.
408. Roubey RA. Mechanisms of autoantibody-mediated thrombosis. *Lupus*. 1998;7 Suppl 2:S114-9.
409. Sciascia S, Cuadrado MJ, Khamashta M, Roccatello D. Renal involvement in antiphospholipid syndrome. *Nature Reviews Nephrology*. 2014;10(5):279-89.
410. Khan F, Tritschler T, Kahn SR, Rodger MA. Venous thromboembolism. *The Lancet*. 2021;398(10294):64-77.

411. Gorog DA, Fayad ZA, Fuster V. Arterial Thrombus Stability: Does It Matter and Can We Detect It? *Journal of the American College of Cardiology*. 2017;70(16):2036-47.
412. Canny SP, Jackson SW. B Cells in Systemic Lupus Erythematosus: From Disease Mechanisms to Targeted Therapies. *Rheum Dis Clin North Am*. 2021;47(3):395-413.
413. Nickerson KM, Christensen SR, Shupe J, Kashgarian M, Kim D, Elkon K, et al. TLR9 regulates TLR7- and MyD88-dependent autoantibody production and disease in a murine model of lupus. *J Immunol*. 2010;184(4):1840-8.
414. Hua Z, Gross AJ, Lamagna C, Ramos-Hernández N, Scapini P, Ji M, et al. Requirement for MyD88 signaling in B cells and dendritic cells for germinal center anti-nuclear antibody production in Lyn-deficient mice. *J Immunol*. 2014;192(3):875-85.
415. Barr TA, Brown S, Mastroeni P, Gray D. B cell intrinsic MyD88 signals drive IFN-gamma production from T cells and control switching to IgG2c. *J Immunol*. 2009;183(2):1005-12.
416. Hong S, Zhang Z, Liu H, Tian M, Zhu X, Zhang Z, et al. B Cells Are the Dominant Antigen-Presenting Cells that Activate Naive CD4(+) T Cells upon Immunization with a Virus-Derived Nanoparticle Antigen. *Immunity*. 2018;49(4):695-708.e4.
417. Christensen SR, Shupe J, Nickerson K, Kashgarian M, Flavell RA, Shlomchik MJ. Toll-like receptor 7 and TLR9 dictate autoantibody specificity and have opposing inflammatory and regulatory roles in a murine model of lupus. *Immunity*. 2006;25(3):417-28.
418. Kuraoka M, Holl TM, Liao D, Womble M, Cain DW, Reynolds AE, et al. Activation-induced cytidine deaminase mediates central tolerance in B cells. *Proceedings of the National Academy of Sciences of the United States of America*. 2011;108(28):11560-5.
419. Rommel PC, Bosque D, Gitlin AD, Croft GF, Heintz N, Casellas R, et al. Fate mapping for activation-induced cytidine deaminase (AID) marks non-lymphoid cells during mouse development. *PloS one*. 2013;8(7):e69208.
420. Hogenbirk MA, Heideman MR, Velds A, van den Berk PC, Kerkhoven RM, van Steensel B, et al. Differential programming of B cells in AID deficient mice. *PloS one*. 2013;8(7):e69815.
421. Ratiu JJ, Racine JJ, Hasham MG, Wang Q, Branca JA, Chapman HD, et al. Genetic and Small Molecule Disruption of the AID/RAD51 Axis Similarly Protects Nonobese Diabetic Mice from Type 1 Diabetes through Expansion of Regulatory B Lymphocytes. *J Immunol*. 2017;198(11):4255-67.
422. Muramatsu M, Kinoshita K, Fagarasan S, Yamada S, Shinkai Y, Honjo T. Class switch recombination and hypermutation require activation-induced cytidine deaminase (AID), a potential RNA editing enzyme. *Cell*. 2000;102(5):553-63.
423. Fang W, Mueller DL, Pennell CA, Rivard JJ, Li YS, Hardy RR, et al. Frequent aberrant immunoglobulin gene rearrangements in pro-B cells revealed by a bcl-xL transgene. *Immunity*. 1996;4(3):291-9.
424. Sahoo NC, Rao KV, Natarajan K. CD80 expression is induced on activated B cells following stimulation by CD86. *Scand J Immunol*. 2002;55(6):577-84.
425. Good-Jacobson KL, Song E, Anderson S, Sharpe AH, Shlomchik MJ. CD80 expression on B cells regulates murine T follicular helper development, germinal center B cell survival, and plasma cell generation. *J Immunol*. 2012;188(9):4217-25.
426. Nehar-Belaid D, Hong S, Marches R, Chen G, Bolisetty M, Baisch J, et al. Mapping systemic lupus erythematosus heterogeneity at the single-cell level. *Nature immunology*. 2020;21(9):1094-106.
427. Ashouri JF, Weiss A. Endogenous Nur77 Is a Specific Indicator of Antigen Receptor Signaling in Human T and B Cells. *J Immunol*. 2017;198(2):657-68.
428. Mittelstadt PR, DeFranco AL. Induction of early response genes by cross-linking membrane Ig on B lymphocytes. *The Journal of Immunology*. 1993;150(11):4822-32.
429. Tan C, Mueller JL, Noviski M, Huizar J, Lau D, Dubinin A, et al. Nur77 Links Chronic Antigen Stimulation to B Cell Tolerance by Restricting the Survival of Self-Reactive B Cells in the Periphery. *J Immunol*. 2019;202(10):2907-23.
430. Huizar J, Tan C, Noviski M, Mueller JL, Zikherman J. Nur77 Is Upregulated in B-1a Cells by Chronic Self-Antigen Stimulation and Limits Generation of Natural IgM Plasma Cells. *Immunohorizons*. 2017;1(9):188-97.
431. Apavaloaei A, Hardy MP, Thibault P, Perreault C. The Origin and Immune Recognition of Tumor-Specific Antigens. *Cancers (Basel)*. 2020;12(9).
432. Zhang B, Kracker S, Yasuda T, Casola S, Vanneman M, Hömig-Hölzel C, et al. Immune Surveillance and Therapy of Lymphomas Driven by Epstein-Barr Virus Protein LMP1 in a Mouse Model. *Cell*. 2012;148(4):739-51.

433. Xu Z, Zan H, Pone EJ, Mai T, Casali P. Immunoglobulin class-switch DNA recombination: induction, targeting and beyond. *Nature Reviews Immunology*. 2012;12(7):517-31.
434. Grasset EK, Chorny A, Casas-Recasens S, Gutzeit C, Bongers G, Thomsen I, et al. Gut T cell-independent IgA responses to commensal bacteria require engagement of the TACI receptor on B cells. *Sci Immunol*. 2020;5(49).
435. Pone EJ, Zhang J, Mai T, White CA, Li G, Sakakura JK, et al. BCR-signalling synergizes with TLR-signalling for induction of AID and immunoglobulin class-switching through the non-canonical NF- κ B pathway. *Nature Communications*. 2012;3(1):767.
436. Lanier LL, Chang C, Spits H, Phillips JH. Expression of cytoplasmic CD3 epsilon proteins in activated human adult natural killer (NK) cells and CD3 gamma, delta, epsilon complexes in fetal NK cells. Implications for the relationship of NK and T lymphocytes. *J Immunol*. 1992;149(6):1876-80.
437. Renard V, Ardouin L, Malissen M, Milon G, Lebastard M, Gillet A, et al. Normal development and function of natural killer cells in CD3 epsilon delta 5/delta 5 mutant mice. *Proceedings of the National Academy of Sciences of the United States of America*. 1995;92(16):7545-9.
438. Malynn BA, Ma A. A20 takes on tumors: tumor suppression by an ubiquitin-editing enzyme. *J Exp Med*. 2009;206(5):977-80.
439. Vlad A, Deglesne P-A, Letestu R, Chevallier N, Baran-Marszak F, Varin-Blank N, et al. CXCR4 and CD62L Down-Regulation Following B-Cell Receptor Ligation Is Restricted to Progressive Chronic Lymphocytic Leukemia (CLL) Cases. *Blood*. 2007;110(11):1122-.
440. Scharer CD, Patterson DG, Mi T, Price MJ, Hicks SL, Boss JM. Antibody-secreting cell destiny emerges during the initial stages of B-cell activation. *Nature Communications*. 2020;11(1):3989.
441. Lownik JC, Luker AJ, Damle SR, Cooley LF, El Sayed R, Hutloff A, et al. ADAM10-Mediated ICOS Ligand Shedding on B Cells Is Necessary for Proper T Cell ICOS Regulation and T Follicular Helper Responses. *J Immunol*. 2017;199(7):2305-15.
442. Glouchkova L, Ackermann B, Zibert A, Meisel R, Siepermann M, Janka-Schaub GE, et al. The CD70/CD27 pathway is critical for stimulation of an effective cytotoxic T cell response against B cell precursor acute lymphoblastic leukemia. *J Immunol*. 2009;182(1):718-25.
443. Shembade N, Harhaj EW. Regulation of NF- κ B signaling by the A20 deubiquitinase. *Cell Mol Immunol*. 2012;9(2):123-30.
444. Koncz G, Hueber A-O. The Fas/CD95 Receptor Regulates the Death of Autoreactive B Cells and the Selection of Antigen-Specific B Cells. *Front Immunol*. 2012;3.
445. Lee HH, Dadgostar H, Cheng Q, Shu J, Cheng G. NF-kappaB-mediated up-regulation of Bcl-x and Bfl-1/A1 is required for CD40 survival signaling in B lymphocytes. *Proceedings of the National Academy of Sciences of the United States of America*. 1999;96(16):9136-41.
446. Morel L, Yu Y, Blenman KR, Caldwell RA, Wakeland EK. Production of congenic mouse strains carrying genomic intervals containing SLE-susceptibility genes derived from the SLE-prone NZM2410 strain. *Mamm Genome*. 1996;7(5):335-9.
447. Medzhitov R, Preston-Hurlburt P, Kopp E, Stadlen A, Chen C, Ghosh S, et al. MyD88 is an adaptor protein in the hToll/IL-1 receptor family signaling pathways. *Mol Cell*. 1998;2(2):253-8.
448. Richard ML, Gilkeson G. Mouse models of lupus: what they tell us and what they don't. *Lupus Sci Med*. 2018;5(1):e000199-e.
449. Stull C, Sprow G, Werth VP. Cutaneous Involvement in Systemic Lupus Erythematosus: A Review for the Rheumatologist. *The Journal of Rheumatology*. 2023;50(1):27-35.
450. Gharavi AE, Mellors RC, Elkon KB. IgG anti-cardiolipin antibodies in murine lupus. *Clin Exp Immunol*. 1989;78(2):233-8.
451. Smith HR, Hansen CL, Rose R, Canoso RT. Autoimmune MRL-1 pr/1pr mice are an animal model for the secondary antiphospholipid syndrome. *J Rheumatol*. 1990;17(7):911-5.
452. Hashimoto Y, Kawamura M, Ichikawa K, Suzuki T, Sumida T, Yoshida S, et al. Anticardiolipin antibodies in NZW x BXSB F1 mice. A model of antiphospholipid syndrome. *J Immunol*. 1992;149(3):1063-8.
453. Chan OT, Madaio MP, Shlomchik MJ. B cells are required for lupus nephritis in the polygenic, Fas-intact MRL model of systemic autoimmunity. *J Immunol*. 1999;163(7):3592-6.
454. Chan OTM, Hannum LG, Haberman AM, Madaio MP, Shlomchik MJ. A Novel Mouse with B Cells but Lacking Serum Antibody Reveals an Antibody-independent Role for B Cells in Murine Lupus. *Journal of Experimental Medicine*. 1999;189(10):1639-48.

455. Chan OTM, Madaio MR, Shlomchik MJ, Chan OIM, Madaio MP, Shlomchik MJ. The central and multiple roles of B cells in lupus pathogenesis. *Immunological reviews*. 1999;169(1):107-21.
456. Eisenberg RA, Craven SY, Warren RW, Cohen PL. Stochastic control of anti-Sm autoantibodies in MRL/Mp-lpr/lpr mice. *J Clin Invest*. 1987;80(3):691-7.
457. Shlomchik MJ, Craft JE, Mamula MJ. From T to B and back again: positive feedback in systemic autoimmune disease. *Nat Rev Immunol*. 2001;1(2):147-53.
458. Rathmell JC, Fournier S, Weintraub BC, Allison JP, Goodnow CC. Repression of B7.2 on self-reactive B cells is essential to prevent proliferation and allow Fas-mediated deletion by CD4(+) T cells. *J Exp Med*. 1998;188(4):651-9.
459. Yan J, Mamula MJ. B and T cell tolerance and autoimmunity in autoantibody transgenic mice. *Int Immunol*. 2002;14(8):963-71.
460. Shinde S, Gee R, Santulli-Marotto S, Bockenstedt LK, Clarke SH, Mamula MJ. T cell autoimmunity in Ig transgenic mice. *J Immunol*. 1999;162(12):7519-24.
461. Desai DD, Marion TN. Induction of anti-DNA antibody with DNA-peptide complexes. *International Immunology*. 2000;12(11):1569-78.
462. Rivera CE, Zhou Y, Chupp DP, Yan H, Fisher AD, Simon R, et al. Intrinsic B cell TLR-BCR linked coengagement induces class-switched, hypermutated, neutralizing antibody responses in absence of T cells. *Sci Adv*. 2023;9(17):eade8928.
463. Zammit NW, Gray PE, Siggs OM, Yap JY, Russell A, Cultrone D, et al. Environmental and genetic disease modifiers of haploinsufficiency of A20. *bioRxiv*. 2022:2022.03.19.485004.
464. Magerus A, Bercher-Brayer C, Rieux-Laucat F. The genetic landscape of the FAS pathway deficiencies. *Biomed J*. 2021;44(4):388-99.
465. Upadhyay R, Boiarsky JA, Pantsulaia G, Svensson-Arvelund J, Lin MJ, Wroblewska A, et al. A Critical Role for Fas-Mediated Off-Target Tumor Killing in T-cell Immunotherapy. *Cancer Discov*. 2021;11(3):599-613.
466. Ilyas S, Yang JC. Landscape of Tumor Antigens in T Cell Immunotherapy. *J Immunol*. 2015;195(11):5117-22.
467. Schmiedel D, Mandelboim O. NKG2D Ligands—Critical Targets for Cancer Immune Escape and Therapy. *Front Immunol*. 2018;9.
468. Prajapati K, Perez C, Rojas LBP, Burke B, Guevara-Patino JA. Functions of NKG2D in CD8+ T cells: an opportunity for immunotherapy. *Cellular & Molecular Immunology*. 2018;15(5):470-9.
469. Guerra N, Tan YX, Joncker NT, Choy A, Gallardo F, Xiong N, et al. NKG2D-deficient mice are defective in tumor surveillance in models of spontaneous malignancy. *Immunity*. 2008;28(4):571-80.
470. Barber A, Zhang T, Megli CJ, Wu J, Meehan KR, Sentman CL. Chimeric NKG2D receptor-expressing T cells as an immunotherapy for multiple myeloma. *Exp Hematol*. 2008;36(10):1318-28.
471. Chronister WD, Crinklaw A, Mahajan S, Vita R, Koşaloğlu-Yalçın Z, Yan Z, et al. TCRMatch: Predicting T-Cell Receptor Specificity Based on Sequence Similarity to Previously Characterized Receptors. *Front Immunol*. 2021;12.
472. Lin X, George JT, Schafer NP, Ng Chau K, Birnbaum ME, Clementi C, et al. Rapid assessment of T-cell receptor specificity of the immune repertoire. *Nature Computational Science*. 2021;1(5):362-73.
473. Casciola-Rosen L, Andrade F, Ulanet D, Wong WB, Rosen A. Cleavage by granzyme B is strongly predictive of autoantigen status: implications for initiation of autoimmunity. *J Exp Med*. 1999;190(6):815-26.
474. Darrah E, Rosen A. Granzyme B cleavage of autoantigens in autoimmunity. *Cell death and differentiation*. 2010;17(4):624-32.
475. Rosen A, Casciola-Rosen L. Autoantigens as Partners in Initiation and Propagation of Autoimmune Rheumatic Diseases. *Annu Rev Immunol*. 2016;34:395-420.
476. Ehlers M, Fukuyama H, McGaha TL, Aderem A, Ravetch JV. TLR9/MyD88 signaling is required for class switching to pathogenic IgG2a and 2b autoantibodies in SLE. *J Exp Med*. 2006;203(3):553-61.
477. Shen P, Roch T, Lampropoulou V, O'Connor RA, Stervbo U, Hilgenberg E, et al. IL-35-producing B cells are critical regulators of immunity during autoimmune and infectious diseases. *Nature*. 2014;507(7492):366-70.

LIST OF FIGURES

Figures

Figure 1. Early B cell development and central tolerance in the bone marrow.....	2
Figure 2. The germinal center reaction.....	4
Figure 3. Inhibition of NF- κ B signaling, inflammasome activation and cell death by A20.....	27
Figure 4. Loss of function mutations of A20 are linked to the development of auto-inflammatory diseases and lymphomagenesis.....	29
Figure 5. BclxL expression in A20-deficient B cells.....	54
Figure 6. BclxL expression does not protect iGB cells against Fas-induced cell death.....	54
Figure 7. Spleen weight and cellularity in B-BclxL ^{tg} -A20 mice.....	56
Figure 8. Splenic B cell subsets in B-BclxL ^{tg} -A20 mice.....	57
Figure 9. Marginal zone B cells in B-BclxL ^{tg} -A20 mice.....	58
Figure 10. Splenic GCB cells in B-BclxL ^{tg} -A20 mice.....	59
Figure 11. Light zone / dark zone distribution.....	61
Figure 12. Premature exit of A20 homozygous B cells from the germinal center.....	62
Figure 13. Class switching in the spleen of B-BclxL ^{tg} -A20 mice.....	64
Figure 14. Class switching in the iGB culture.....	65
Figure 15. B cell differentiation in GALT of B-BclxL ^{tg} -A20 mice.....	66
Figure 16. Long-lived plasma cells in the bone marrow.....	68
Figure 17. Serum immunoglobulin in B-BclxL ^{tg} -A20 mice.....	69
Figure 18. Surface activation markers on B cells.....	70
Figure 19. CD4 and CD8 T cells in the spleen of B-BclxL ^{tg} -A20 mice.....	72
Figure 20. CD4 T cell subsets in B-BclxL ^{tg} -A20 mice.....	74
Figure 21. T cell activation in B-BclxL ^{tg} -A20 mice.....	76
Figure 22. Effector and memory T cell differentiation in B-BclxL ^{tg} -A20 mice.....	77
Figure 23. T cell exhaustion in B-BclxL ^{tg} -A20 mice.....	78
Figure 24. Dendritic cells in the spleen.....	79
Figure 25. Granulocytes and NK cells in the spleen.....	80
Figure 26: Macrophages and monocytes in the spleen.....	81
Figure 27. Systemic autoantibodies and survival.....	83
Figure 28. Serum cytokine concentration quantified with multiplexed FACS analysis.....	85
Figure 29. Serum concentration of BAFF and TGF β	88
Figure 30. Cytokine producers.....	90
Figure 31. Renal immune complex deposition.....	92
Figure 32. Kidney immune cell infiltration.....	93
Figure 33. Kidney damage.....	94
Figure 34. Glomerular alterations in aged mice.....	95
Figure 35. Glomerular filtration rate.....	96
Figure 36. Heart and liver pathology.....	97
Figure 37. Thymic B cells and salivary gland infiltration.....	98
Figure 38. Autoantibodies indicative of APS.....	99
Figure 39. Increased thrombotic activity upon heterozygous and homozygous loss of A20.....	100
Figure 40. Lethality and B cell expansion of B-BclxL ^{tg} - A20 ^{-wt} mice are rescued by B cell-specific MyD88 knockout.....	103
Figure 41. Activation marker expression on B and T cells upon B cell specific MyD88 knockout.....	105
Figure 42. SLE-like pathology is rescued upon MyD88 knockout.....	106
Figure 43. AIDCre activity.....	108
Figure 44. Splenic cell composition in GCB-BclxL ^{tg} -A20 mice.....	109
Figure 45. Autoimmune pathology in GCB-BclxL ^{tg} -A20 mice.....	110
Figure 46. Aicda knockout inhibits the generation of class switched plasmacytic cells.....	111
Figure 47. Aicda knockout ameliorates systemic inflammation and autoimmune pathology.....	112
Figure 48. Aicda knockout does not reduce B cell activation.....	113
Figure 49. Principal component analysis of bulk RNA sequencing in B cells from B-BclxL ^{tg} -A20 mice.....	116
Figure 50. Differential gene expression in bulk RNA sequencing.....	117
Figure 51. Gene set enrichment analysis.....	118

Figure 52. Proliferation in iGB cell culture.....	119
Figure 53. BCR signaling intensity.	123
Figure 54. TNF-depletion in vivo.....	124
Figure 55. TNF stimulation in vitro.	126
Figure 56. Competitive bone marrow chimeras.....	128
Figure 57. T cells in competitive BM chimeras.....	129
Figure 58. Genotype fractions in the bone marrow chimeras.....	130
Figure 59. Ratio of B and T cells in bone marrow chimeras.....	131
Figure 60. CD8 T cell expansion.....	132
Figure 61. CD8 ⁺ T cell depletion.....	133
Figure 62. Whole T cell depletion.....	135
Figure 63. B and plasmacytic cells expand in T cell-deficient B-BclxL ^{tg} -A20 mice.....	137
Figure 64. Immune cell composition in spleens of T cell deficient B-BclxL ^{tg} -A20 mice.....	138
Figure 65. Lack of autoimmune manifestations in T cell-deficient B-BclxL ^{tg} -A20 mice.....	139
Figure 66. Lethality and lymphoproliferation in CD3 $\epsilon^{\Delta\Delta}$ B-BclxL ^{tg} -A20 mice.....	140
Figure 67. Marker expression on B cells from CD3 $\epsilon^{\Delta\Delta}$ mice.....	143
Figure 68. Lymphoma type and clonality.....	145

Supplementary figures

Supplementary Figure 1. Genotype ratio in newborn mice with B cell specific A20-deficiency and BclxL ^{tg} expression.....	157
Supplementary Figure 2. Survival of PC-like iGB cells.....	157
Supplementary Figure 3. Serum cytokine concentration in individual mice.....	158
Supplementary Figure 4. Thrombus stability.....	159
Supplementary Figure 5. Lethality and lymphoproliferation in CD3 $\epsilon^{\Delta\Delta}$ B-A20 mice.....	160
Supplementary Figure 6. Marker expression on B cells from CD3 $\epsilon^{\Delta\Delta}$ B-BclxL ^{tg} -A20 mice.....	161
Supplementary Figure 7. Variability of Fas expression of B cells from different mice.....	161

LIST OF TABLES

Table 1: Mouse strains used for this project.....	33
Table 2: Genotyping PCR reaction setup for A20, AIDCre, CD19Cre, Cy1Cre and MyD88.....	33
Table 3: Genotyping PCR reaction setup for E μ -BclxL.....	34
Table 4: Genotyping PCR reaction setup for CD3 ϵ	34
Table 5: Genotyping PCR reaction setup for Nur77 ^{GFP}	34
Table 6: PCR program for A20, AIDCre, E μ -BclxL, CD19Cre and Cy1Cre.....	34
Table 7: PCR program for CD3 ϵ	34
Table 8: PCR program for MyD88.....	35
Table 9: PCR program for Nur77 ^{GFP}	35
Table 10. Genotyping PCR primers and product sizes.....	35
Table 11. Buffers and media.....	36
Table 12. Flow cytometry antibodies.....	38
Table 13. Isotype ELISA kits.....	42
Table 14. Autoantibody ELISA kits.....	43
Table 15. Antibody mixture used for the MACS-based depletion of B and T cells.....	49
Table 16. Antibody mixture used for the MACS-based purification of B cells.....	50